THE INVESTIGATION OF PHASE SYNCHRONIZATION IN THE CORTEX DURING A FATIGUING MUSCLE CONTRACTION USING EEG

Devin Roy Bosanquet

Department of Human Biology

University of Cape Town

Submitted to the Faculty of Health Sciences at the University of Cape Town in partial fulfilment of the requirement for the degree of Master of Science in Medicine in Biomedical Engineering.

March 2005

DECLARATION

I, ... DEVIN ROY BOSWORTH ....., hereby declare that this dissertation is my own, original work. It has not been submitted before for any degree or examination at any other University.

Signed: ..... Signed by candidate

Date: ..... 15 MARCH 2005

ACKNOWLEDGMENTS

I would like to thank the following people for their contribution to this project:

Lester John, my primary supervisor, for his assistance, guidance and support and the many hours spent proof reading this document.

Alan "Zig" St Clair Gibson, my co-supervisor, for his assistance, guidance and support and the many hours spent proof reading this document.

Dr. R. Sreenivasan, my original supervisor for his initial guidance and support.

Lize van der Merwe, Biostatistics Unit, Medical Research Council, for her advice on the ANOVA test procedure.

Christopher Vaughan and all my colleagues past and present involved in biomedical engineering and the EEG/Brain group who have knowingly or unknowingly provided guidance and support.

Peter Koeppen, Stephen Schrire and my friends and family for their encouragement and support.

SUMMARY

BACKGROUND: Phase synchronization, defined as the adjustment of the rhythms of oscillating objects (such as a population of neurons) due to their weak interaction, is calculated from EEG signals measured during an exercise-until-fatigue trial. The purpose was to elucidate the brain's role in exercise fatigue, as there is evidence that indicates that the brain has a major role in regulating the work rate in exercise. The exact mechanisms behind this process are unclear but endogenous processes like prior experience, planning and motivation as well as the integration of sensory information may play a role. To demonstrate the brain's role in exercise fatigue, phase synchronization between different EEG electrode locations was measured, as phase synchronization may indicate if the areas of the brain beneath EEG electrodes are interacting.

METHODOLOGY: EEG was measured from an exercise-until-fatigue trial where subjects performed an isometric contraction of the quadriceps muscle until fatigued. The EEG was also measured for the same subjects during a relaxed eyes-closed and eyes-open state, which served as baseline levels of phase synchronization. Therefore there were three conditions in the trial - eyes-closed, eyes-open and exercise-until-fatigue. The trials were all divided into 6 epochs. Phase synchronization coefficients (which provide a measure of phase synchronization) between 2701 electrode pairs for 8 subjects were calculated for each condition at each epoch and at four frequency bands, theta (4-7Hz), alpha (7-13Hz), beta (13-30Hz) and gamma (30-50Hz). Two methods of processing the coefficients for comparisons were performed. The first method involved displaying the smallest (representing desynchronization) and largest (representing synchronization) values of the differentiated phase synchronization coefficients on head maps for each frequency band. Head maps are 2-dimensional representations of the EEG electrode locations on the scalp. The second method involved performing a series of ANOVA statistical tests that performed comparisons of the phase synchronization coefficients and

differentiated phase synchronization coefficients between the different conditions, epochs and 3 groupings of electrode combination pairs. The 3 groupings consisted of prefrontal-motor electrode combinations, frontal-motor electrode combinations and all the electrode combinations. Post-hoc analysis was performed using Tukey's HSD test.

RESULTS: The head maps for the alpha band indicated that there was strong alpha band phase desynchronization followed by strong phase synchronization at the 3^{rd} and 4^{th} epoch transition respectively. The ANOVA tests indicated that there was an interaction between areas and condition in the beta band ($P < 0.05$). Post hoc analysis revealed that prefrontal-motor differentiated beta phase synchronization was significantly lower than the all areas differentiated beta phase synchronization ($P < 0.000$) in the exercise-until-fatigue condition only. Further analysis revealed that prefrontal-motor differentiated beta phase synchronization was nearly statistically significantly less than the all areas differentiated beta phase synchronization at the final epoch transition in the exercise-until-fatigue condition only ($P = 0.07$).

CONCLUSIONS: The investigation showed that clear changes occur in the brain (specifically phase synchronization) in exercise and the progression to fatigue. It was shown that these brain changes occur in the frequency bands alpha and beta. Alpha rhythms are primarily involved in internally directed attention tasks, inhibition of sensory information and cognitive performance. Beta rhythms index arousal and external attention and have been linked to states of emotional intensity. Thus the frequency bands involved associate various cognitive states that are probably of relevance to the process of fatigue.

TABLE OF CONTENTS

LIST OF FIGURES

LIST OF TABLES

LIST OF SYMBOLS

$\tilde{\rho}$	Phase synchronization coefficient
$\Delta\tilde{\rho}$	Differentiated phase synchronization coefficient
$\Delta\tilde{\rho}_{incb}$	Differentiated phase synchronization coefficient where i is a particular epoch transition, a particular channel combination n, condition c and band b
$\Delta\tilde{\rho}_{icb}$	Differentiated phase synchronization coefficient where i is an epoch transition, for a particular condition c and band b grouped by channel combination
$\tilde{\rho}_{\theta}$	Theta band phase synchronization coefficient
$\Delta\tilde{\rho}_{\theta}$	Differentiated theta band phase synchronization coefficient
$\tilde{\rho}_{\alpha}$	Alpha band phase synchronization coefficient
$\Delta\tilde{\rho}_{\alpha}$	Differentiated alpha band phase synchronization coefficient
$\tilde{\rho}_{\beta}$	Beta band phase synchronization coefficient
$\Delta\tilde{\rho}_{\beta}$	Differentiated beta band phase synchronization coefficient
$\tilde{\rho}_{\gamma}$	Gamma band phase synchronization coefficient
$\Delta\tilde{\rho}_{\gamma}$	Differentiated gamma band phase synchronization coefficient
$\overline{\tilde{\rho}}$	Mean phase synchronization coefficient determined by averaging over all channel combinations and subjects grouped by epoch, condition and frequency band
$\overline{\Delta\tilde{\rho}}$	Mean differentiated phase synchronization coefficient determined by averaging over all channel combinations and subjects grouped by epoch transition, condition and frequency band
$\overline{\lvert\Delta\tilde{\rho}\rvert}$	Mean of the absolute values of the differentiated phase synchronization coefficient determined by averaging the absolute values over all channel combinations and subjects grouped by epoch

transition, condition and frequency band

$\overline{\overline{|\Delta\tilde{\rho}|}}$ Mean of $|\Delta\bar{\tilde{\rho}}|$ averaged over epoch transitions grouped by condition and frequency band

$\bar{\bar{\tilde{\rho}}}$ Mean of $\bar{\tilde{\rho}}$ averaged over epochs grouped by condition and frequency band

$\Delta\bar{\bar{\tilde{\rho}}}$ Mean of $\Delta\bar{\tilde{\rho}}$ averaged over epoch transitions grouped by condition and frequency band

1. INTRODUCTION

Synchronous interaction between rhythmic activities, processes and systems can be seen in our everyday environment as well as in different phenomena in biology, physics and economics. Examples include the timing of breathing with the strokes in swimming and the cooperation of muscle fibres to produce rhythmic muscle contractions in the heart. In both examples, synchrony is indeed essential to the proper functioning of the system and would otherwise result in some kind of system failure.

Synchronization occurs when rhythmic or oscillatory systems, through some kind of interaction, adjust their behaviours relative to one another so as to attain a state where they work in unison [1]. A key feature of synchronization is that phase relations must be consistent. Phase is defined here as a particular stage in a repetitive process or phenomenon [2]. So when two processes are synchronized the events at different stages in their respective cycles occur at the same time or occur with the same time delay relative to one another, on every cycle. In the swimming example, the inhalation stage of the breathing cycle must occur at roughly the same stage of the stroke cycle for effective swimming. If the phase difference between the cycles deviates too much inhalation would be happening at the stage of the stroke cycle where the head is under water, leading to 'system failure'.

One can also suggest that if two or more systems display phase synchrony they are part of the same functioning system, or that the one system influences the other, or both systems are influenced by another system [3]. If one were to measure the output of 2 systems and calculate their phases at any instant in time and the difference between them was constant or roughly constant (as would be the case in a non-linear system), the two systems would be functioning synchronously and may somehow be connected.

There is evidence in the literature to support phase synchronization as a means of integrating various processing units in the brain, which inherently display rhythmic or oscillatory behaviour, to achieve a single unified outcome [4]-[10]. The processing of sensory information has traditionally been seen as a bottom up or feedforward process, where information is serially processed from 'lower' to 'higher' areas in the brain hierarchy [4] [5]. This has been well studied in the visual system where different anatomical areas in the brain are adapted for a particular specialized function [4]. There is also evidence to support top-down or feedback processing, where endogenous activity like memory, expectation and attention plays a crucial role in how this sensory information is processed [5][8]. Thus extrinsic sensory information is modulated to 'fit in' with intrinsic endogenous activity and phase synchrony has been proposed as a means to achieve this.

Perception, memory and perhaps consciousness have been suggested to result from the synchronous activity of distributed processing units at various levels of the brain hierarchy [4][5][6]. The oscillatory processing units controlling these functions would be linked or coupled dynamically where the precise timing of their oscillations relative to one another would be not be incidental but rather be of vital significance to the functioning of the system.

The brain processes discussed above are becoming of interest to the study of fatigue in exercise. The cause of fatigue in exercise is a well-researched topic and several theories have been developed to explain the mechanisms contributing to fatigue. Studies have revealed that there is no one single cause of fatigue, but that fatigue is caused by various factors that may originate centrally or peripherally [11]. The peripheral origins of fatigue refer to factors in the periphery of the body that may cause fatigue [12]. The central origins of fatigue refer to factors in the brain that may cause fatigue [12].

In the central fatigue model, the brain plays a major role in regulating the work rate [13]. It has been shown that peripheral factors are not the sole cause of exercise fatigue and that exercise must be constrained by processes occurring in the brain [14][15][16]. The exact mechanisms are unknown but endogenous activity such as prior experience, planning and pacing, arousal, motivation and drive may modulate

the array of sensory information coming in from the periphery and determine levels of muscle recruitment in exercise.

It is still not well known which endogenous factors, if any, modulate sensory information during fatigue, whether the sensation of fatigue itself is physiologically significant or a mere by product of brain regulation, and which brain structures are involved in the control of work output during fatigue [11]-[17].

This study aims to answer some of these questions by providing some insight into the cortical dynamics during fatigue. Specifically, phase synchronization is investigated to determine which regions of the brain form part of the same functioning system and display coherent, dependent behaviour over a large scale during a fatiguing muscle contraction. This is evaluated by means of the electroencephalogram (EEG). Data collected from each EEG electrode represents the electrical activity of the cortex underlying it. Thus phase synchrony between two EEG channels is indicative of communication between the underlying structures or of a functional relationship between the underlying structures [3].

This study presupposes that fatigue due to exercise has a central component and that neuroscience methods (EEG) can potentially elucidate the some of the unknowns in this apparently complex process. The outcome of this study will not only provide insight into the processes of fatigue due to exercise but also will contribute to the body of knowledge of basic brain function and perhaps lead to a slightly greater understanding of how the brain works.

Much of what we know about neurological anatomical specialization has come from studies using functional Magnetic Resonance Imaging (fMRI) and Positron Emission Tomography (PET). These imaging studies have provided neurophysiological correlations to many low level neurological processes as well as high level psychological functions like language and philosophical thought [18]. This is mainly due to the high spatial resolution of the images these methods produce, whereas the spatial resolution in EEG is relatively poor.

PET and fMRI imaging techniques may have high spatial resolution, but have poor temporal capacity while and EEG carries the advantage of being capable of recording activity in time scales in the millisecond range. This is important because it has been shown that the timing of neuronal activity is in the millisecond range [6][7][8]. EEG analysis has much to offer regarding the dynamics of brain function and may be more suitable for the analysis of how different regions of the cortex interact. In fact the spatial resolution of EEG electrodes provides a natural averaging which lends itself to analysis at spatial scales of centimetres instead of micrometers [19]. This together with its fine temporal resolution makes it an important and unique tool for the further understanding of brain functionality.

Most published studies that employ EEG processing involve either amplitude analysis (for example the power spectrum) or correlation analysis (for example coherence). Increased amplitude or power in an EEG channel is associated with an increase in the local synchrony of the underlying neurons whereas increased correlation, coherence or phase consistency is associated with an increase in long-range synchrony [10]. The conventional EEG analysis involves examining specific frequency ranges. There are two main reasons for this. Firstly, even from the early days of EEG analysis, certain psychological states have been associated with rhythmic activity of certain frequency bands [6]. For example EEG rhythms in the 7-13 Hz range, denoted *alpha* rhythms have been classically associated with a relaxed state [6] while more recently, rhythms in the 30-50 Hz range, denoted *gamma* rhythms, have been associated with cognitive processing [9]. Secondly, phase synchrony is a narrow band phenomena and it only makes sense to speak of phase synchrony between signals that are oscillating at the same or nearly the same frequency, or at integer multiples of that frequency [1][3][21].

In this study the phase consistency between EEG recordings taken during a fatiguing exercise trial is quantified to determine levels of long-range synchrony. This is done at four physiologically significant frequency bands. The fatiguing trial consists of 20 subjects performing a voluntary isometric contraction of the quadriceps muscle at 20% of maximal voluntary capacity until exhaustion. EEG measurements from 128 locations on the scalp were taken during the trial and also during a period where the subject was asked to sit in an eyes closed and then eyes open relaxed state. This

allows the cortical dynamics of fatiguing exercise to be compared to two 'neutral' states, eyes closed and eyes open at rest.

There are no known published studies investigating cortical synchrony during exercise fatigue. In fact there are few studies involving EEG and exercise fatigue in general.

The outline for the rest of this dissertation is as follows. In the Chapter 2 central fatigue is discuss in more detail and linked to different concepts in neuroscience such as top-down processing and flow of neuronal information. In Chapter 3 concepts in EEG recording and analysis are defined and developed, including current ideas about the electrophysiological functioning of the brain. In the final chapter of the literature review, Chapter 4, brain rhythms and the principles of the phase synchronization is outlined. The methodology used in this investigation is described in Chapter 5 followed by the results and discussion in Chapter 6 and conclusions discussed in Chapter 7.

2. EXERCISE FATIGUE AND THE BRAIN

Fatigue is defined as an acute impairment in performance, resulting in the increased sense of effort while performing a task and the eventual failure to sustain performance [11]. A more concise definition by Gandevia [23] specific to exercise states that muscle fatigue is a reduction of maximal voluntary muscle force due to exercise.

In this section, the theory of the brain's role in exercise fatigue is outlined. Unknowns about the process are highlighted and the investigation of phase synchronization in the brain is discussed as a means for possibly elucidating the process. For a general review of exercise fatigue please see Appendix A.

2.1 Peripheral Versus Central Fatigue

Traditionally researchers have seen the cause of fatigue during exercise as a result of limitations in physiological systems in the periphery of the body (outside the central nervous system) [11][13]. Examples include changes in the cardio-respiratory system, the maximal oxygen uptake in cells (VO_{2max}), lack of adequate fuel sources, alterations of pH levels and inadequate ATP production in the cells [15][16].

No study has found any single peripheral physiological factor to be the cause of fatigue and there is growing evidence that the central nervous system (CNS) plays the major role in the onset of fatigue. Noakes et al [13] argue that current theories explaining fatigue as a result of changes occurring in the skeletal muscle alone (the peripheral model) cannot adequately explain most forms of exercise fatigue. For example it has been found that motor unit conscription is never maximal even during a maximal voluntary contraction – there is always a reserve capacity [13][23][26]. Studies using transcranial magnetic stimulation (TMS), where an electro-magnetic placed on the scalp is used to stimulate the cortex, have shown twitch like increases

in the force output of the apparently completely fatigued muscle [24]. In their review of the use of the twitch interpolation technique, Shield and Zhou [26] reveal that the latest techniques indicate that muscle recruitment is never fully activated. Furthermore the peripheral model predicts a 'catastrophic' system failure from the depletion or accumulation of metabolites in the muscle tissue that results in exhaustion, but this does not happen [13]. In their analysis of the theories that predict failure in intracellular homeostasis as the cause of fatigue, Noakes and St Clair Gibson [25] conclude that there is little published evidence to support peripheral factors as the direct cause of fatigue.

2.2 Evidence of a 'Central Governor'

Instead Noakes et al [13] suggest that a 'central governor', which resides in the CNS, is responsible for the reduction of motor power output. This governor integrates the sensory information coming in from the periphery and regulates the recruitment of muscle fibres such that homeostasis is maintained and a metabolic catastrophe is always avoided. This would be an unconscious process and the manifestation being the conscious sensation of fatigue [13]. Figure 2-1 is a schematic representation of this model.

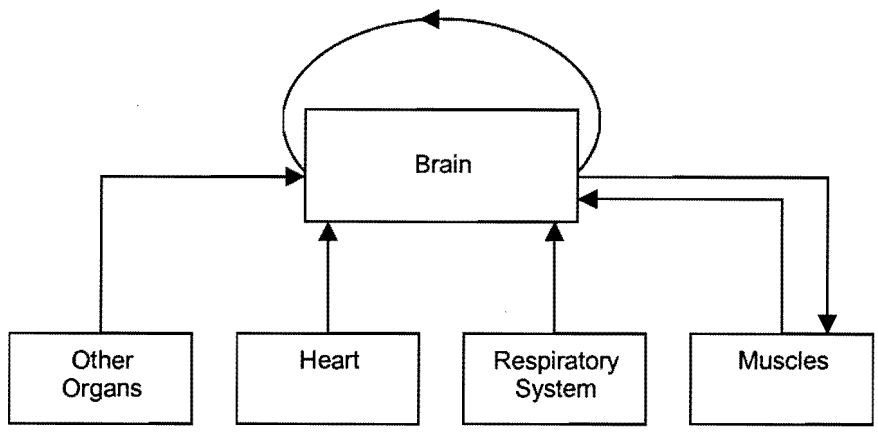

Figure 2-1: Hypothetical model of the 'cental-governor', adapted from Kayser [16].

Evidence for such a governor and central fatigue as a whole include observations in the study of peripheral fatigue and fatigue trials in general, fatigue trials conducted under specific conditions such as exercise in the heat and studies involving TMS and twitch interpolation.

Tucker et al [37] compare the effects of self-paced exercise in hot versus cool conditions. They show there is a reduction in power output in the hot condition, even though the core temperatures, heart rates and ratings of perceived exertion (RPE) are similar in both conditions. Their study shows that there appears to be pre-emptive activity to prevent an abnormal increase in the core body temperature in exercise in the heat [37].

Other studies involving exercise in hot environments indicate that reduced motor drive from the CNS (central fatigue) is a cause for the inability to sustain exercise in the heat [39][38]. In their study Nybo et al [38] tested their hypothesis that the Rating of Perceived Exertion (RPE) is correlated to changes in brain electrical activity (measured using the EEG) and not muscle electrical activity (measured using the EMG) in exercise with hyperthermia. They found EEG activity over the frontal cortex to be the best predictor of RPE, while there was no correlation between RPE and EMG activity. Furthermore, there were no differences in the EMG in exercise in the heat and the controls concluding that hyperthermia does not affect the activation pattern of the muscles [38]. In further work conducted by Nybo et al [39] they show strong correlations between certain EEG parameters and increases in core body temperature. They speculate that the reduced ability to sustain exercise in the heat is a safety mechanism to prevent high core and brain temperatures. This agrees with the findings of Tucker et al [37] and Noakes' 'central governor' theory [14].

Hypoxia is a deficiency in the amount of oxygen reaching body tissues, while hyperoxia is an excess of oxygen reaching body tissues. Noakes et al [14] review data of exercise performance during acute hypoxia and hyperoxia. In the classical theory of peripheral fatigue the heart would be a 'slave' to the body and thus, during hypoxia, the heart rate would increase to maintain muscle oxygenation [14]. Instead they find that during hypoxia there is a reduction in peak cardiovascular function with no primary alteration in myocardial function. They conclude that the data supports a

model where there is central regulation of skeletal muscle recruitment such that the supply of oxygen to the brain, heart and perhaps the respiratory muscles is not compromised [14].

Techniques involving TMS (that stimulate the motor cortex) and twitch interpolation allow the degree of voluntary activation of muscle fibres (central fatigue) to be quantified. It has been found that in most cases muscle fibres are never fully activated even in well-trained, motivated and non-fatigued subjects [24]. In their study Todd et al [41] measure the voluntary activation of fresh and fatigued muscle by stimulating the muscle by means of TMS. They conclude that TMS can be used to quantify voluntary activation of muscles and the technique reveals when extra output is available from the motor cortex.

2.3 The Functional Significance of Fatigue

2.3.1 Fatigue as a Conscious Sensation

Fatigue has been defined above as an acute impairment in performance, resulting in the increased sense of effort to perform a task and the eventual failure to sustain performance [11]. Although the above definition is useful in exercise physiology studies it should be noted that humans experience fatigue as a sensation or an emotion as opposed to a process [17]. As pointed out by Kayser [16] a conscious decision starts any voluntary exercise bout and a conscious decision is made based on the perception of effort, and other sensations such as pain, to stop exercising. It has been shown that there is a mutual interaction between cognitive function and central mechanisms driving motor behaviour during fatigue [51]. Exercise fatigue involves conscious sensations, emotions and cognitive decision-making processes.

It is unknown at this stage where the conscious feeling of fatigue arises or how it is derived from the underlying physiological process [17]. In their review [17] St Clair Gibson and colleagues examine different aspects of the conscious perception of fatigue. They begin by building on the theory of consciousness that suggests consciousness is a result of activity in brain structures. The conscious sensation of

fatigue arises when physiological changes in the body due to physical activity would induce changes in brain activity. This altered brain activity would then cause an awareness of the physiological change. The sensation of fatigue encompasses the conscious perception of changes in the body function such as breathing and heart rate, the sensation of muscle activity, endogenous activity such as motivation, memory of prior experience and decision-making processes [17]. Fatigue may also be likened to emotional states such as anger and fear and may be mental representations of the physiological changes which characterise these emotions [17] or representations of particular states of arousal [15].

2.3.2 The 'Purpose' of Fatigue Central Fatigue Models

Is there a functional significance of the sensation of fatigue? Fatigue as emotion could serve to alter an individual's behaviour or environment or allow an individual to describe their internal state [15]. Emotions allow an individual to cope successfully in environments that may be potentially dangerous or advantageous [50]. St Clair Gibson and colleagues present an article where they discuss the teleological aspect of fatigue in three models of fatigue [15]. The teleological aspect of fatigue in the three models shall be discussed below.

The first model that they discuss is the *peripheral-fatigue* model which has been discussed above. Here the causes of fatigue are metabolic factors and occur in the muscle; examples include depleted glycogen stores and anaerobiosis. In the peripheral fatigue model the sensation of fatigue serves no necessary function, as the peripheral factors themselves limit exercise. The only purpose of the conscious sensation of fatigue would be to bring to conscious awareness that some metabolic set point has been reached.

The second model that is discussed is the *central-teleoanticipation* model. Ulmer presented a series of experiments that showed for an optimal adjustment of the metabolic rate in heavy exercise, a feedback control system must exist that takes into account the planned finishing point [52]. Ulmer termed this *teleoanticipation*. Hampson and colleagues [53] developed this idea further in their work on sensory

cues and how these affect perceived exertion in exercise. They conclude that changes in perceived exertion results from afferent input from various sources such as the heart and muscles and that this allows for the exercise to be regulated such that it can be completed within the metabolic limits of the body. This directly corresponds to the 'central governor' theory outlined by Noakes and colleagues as discussed in reference [13] and [14].

The teleoanticipatory mechanism would be responsible for regulating exercise intensity despite metabolic substrate reserves by subconscious mental processing and the outcome of this would be the conscious sensation of fatigue [15]. St Clair Gibson and colleagues point out that the conscious sensation of fatigue serves no teleological purpose in the central-teleoanticipation model, and like the peripheral fatigue model may serve to give conscious awareness to the underlying mechanisms [15].

Finally St Clair Gibson and colleagues [15] discuss the *cognitive-discussion* model. Here the conscious sensation of fatigue, through cognitive processes, plays an active role in modulating exercise intensity. Cognition processes involve taking in information from the environment or internally and holding it in memory long enough to process it and includes attention, perception, memory and learning, language and visual spatial perception [54]. This model would build up the central-teleoanticipation model, where sensory information being integrated in the subconscious would be presented to the consciousness as the sensation of fatigue. Here the individual may engage in 'self-talk' or an internal discussion integrating memory of prior exercise activity. Prior experience would determine the setpoint of fatigue. Control signals from cognitive processes (the consciousness) would then be sent to the subconscious area responsible for the teleoanticipatory efferent commands, where power output to the muscles would be regulated. Thus the sensation of fatigue has some degree of control over the teleoanticipatory subconscious processes within certain confines.

The authors further suggest that perception of effort and perception of fatigue may in fact be different entities as has been shown in their work where athletes are deceived about exercise intensity [15]. They postulate that perception of exercise

intensity would be related to subconscious teleoanticipatory processes while perception of fatigue would be used by the conscious processes to actively set the degree of exercise intensity by way of the teleoanticipatory subconscious processes as described above.

2.4 Brain Structures Involved in Exercise and Fatigue

It is unclear what brain structures are involved in the process of fatigue in any of the presented models outlined above. However it is known that the frontal cortex may have a role in the generation of RPE and that the motor cortex has a role in muscle activation (see Section 2.2). It has been proposed that the brain integrates various afferent input as well as internal input, such as motivation and memory, leading to fatigue, and thus suggests that various structures across the brain may be involved [15].

In their work on the changes in brain metabolism under various exercise conditions Dalsgaard et al provide evidence that as intensity of exercise increases or sensory stimulation is increased more areas of the brain become activated [49]. Liu and colleagues conclude from their fMRI study on fatiguing submaximal muscle contractions that the brain increases its activity to sustain a fatiguing contraction and to possibly process additional sensory information [56]. They find an increase in the fMRI signals in the ipsilateral sensorimotor cortex, prefrontal cortex, cingulate gyrus, supplementary motor area and cerebellum.

Williamson et al [57] show by means of single-photon-emission computed tomography (SPECT) that the insular cortex is activated by exercise and that the magnitude of activation varies with the intensity of exercise. They find that changes in the regional cerebral blood flow (rCBF) in the right insular cortex are correlated to individual changes in blood pressure and RPE during exercise. The insular cortex is involved in the integration of sensory and visceral information and plays a role in cardiovascular regulation [57]. They also show that the activation of the insular cortex is related to central command and perceived exertion in combination with muscle afferent input.

Cardiovascular response to exercise is a result of the integration of efferent motor command and afferent input from the working muscles [58]. To test structures thought to be involved in central modulation of cardiovascular responses Williamson et al [58] conduct a trial where they hypnotically manipulated sense of effort. Sense of effort was thought to be derived from corollary discharge of central command [11] that would involve areas of the motor and premotor cortex, supplementary motor cortex, basal ganglia and cerebellum [17] but there is evidence that sense of effort resides 'upstream' of the motor cortex [36]. Williamson and colleagues showed that hypnotic manipulation of sense of effort could alter patterns of brain activation and induce cardiovascular changes [58]. They proposed that the insular cortex, thalamus and anterior cingulate cortex are important for integrating sense of effort and creating a response. They also demonstrated that an induced increase in sense of effort leads to an increase in blood pressure and heart rate, yet an induced reduction of sense of effort does not have a reciprocal effect.

The anterior cingulate cortex (ACC) is thought to be involved in a range of autonomic responses, and the cognitive interpretation of ACC activity has been the focus of some research [18]. The ACC has been implicated in conflict processing and response selection and damage to the ACC contributes to decreased motivational performance and blunts emotional response to pain [18]. Further work by Williamson and colleagues demonstrates that activity in the insular cortex and the ACC are related to central command itself and independent of blood pressure elevation [59].

Looking at fatigue as an emotional state, brain areas of significance would be the orbitofrontal cortex, ACC and insular cortex [17]. The amygdala and the ventromedial prefrontal cortex act as interfaces between the processing of emotionally significant stimuli and structures responsible for the execution of the emotional response, which reside in the hypothalamus, basal forebrain and brainstem [50]. Thus these areas could also be of significance during fatigue.

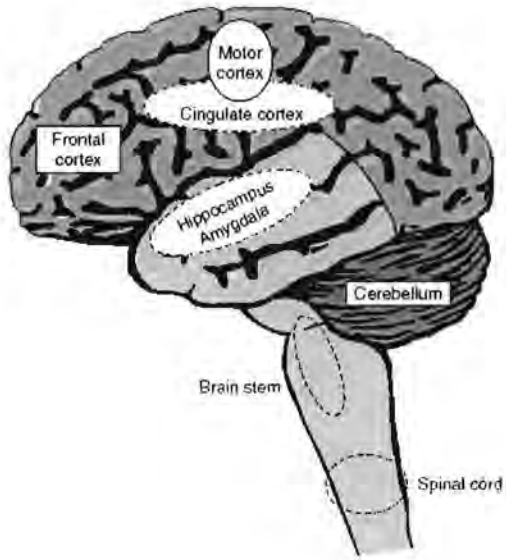

Figure 2-2: Brain regions involved in the sensation of fatigue from St Clair Gibson et al [17].

The prefrontal cortex is involved in memory formation and decision-making processes as well as goal orientated behaviour [60]. St Clair Gibson and colleagues [17] have suggested that the prefrontal cortex may be involved in the conscious perception of fatigue while Liu and colleagues [56] have shown an increase in activity in this area in a fatiguing muscle contraction. The areas that may be involved in the conscious sensation of fatigue are shown in Figure 2-2 above. The process of thought has not been described in the physical sense and has not been localised to any particular brain region, the sensation fatigue may occur in the same manner yet to be determined [15]. Instead fatigue as a sensation or a process, like most complex cognitive processes may be derived from many areas activated at any one moment in time and integrated by other mechanism like phase synchrony [17]. This is referred to as the 'binding problem' and involves the large-scale integration of distributed processing units [4]. Phase synchrony is the most likely candidate for large-scale integration. This has not been looked at previously in exercise or fatigue.

2.5 The Basis for a Study on Central Fatigue

The literature review presented above provides a basis for this investigation. Traditionally exercise fatigue has been attributed to peripheral factors like substrate depletion and metabolic changes in the fatiguing muscle. It has emerged that central factors contribute to fatigue evident in studies looking at exercise in the heat and hypoxia, using techniques like twitch interpolation and TMS, investigating sense of effort and analysing brain chemistry and metabolism during fatiguing exercise.

The concept of a 'central-governor' that controls exercise intensity was introduced. Two models of exercise fatigue that incorporate the principle of the central-governor were presented: the central-teleoanticipatory and the cognitive-discussion models. Here the concept of fatigue as a conscious sensation or emotion was developed and its teleological significance was discussed in the context of the models of fatigue above.

There is a complex interplay between decision-making processes, motivation, cognition, sense of effort, central drive, other bodily sensations and the sensation or emotion of fatigue in a fatiguing exercise that ultimately leads to exhaustion and the failure to sustain exercise. Many areas of the brain can be involved in this process including areas involved in the sense of effort: the motor cortex and premotor cortex, insular cortex, thalamus and anterior cingulate cortex (ACC); areas involved in emotion: the orbitofrontal cortex, ACC, insular cortex, amygdala, ventromedial prefrontal cortex, hypothalamus, basal forebrain and brainstem; areas involved in planning, decision making, motivation and memory activation: the prefrontal cortex and the ACC; and finally areas involved with motor efferent output, autonomic control and afferent sensory information must somehow play a role. Thus many areas distributed across the brain need to be investigated. In this study many areas of the brain are investigated and a specific focus is placed on the relationship between the motor cortex and the pre-frontal cortex. Since the motor cortex is directly functionally related to the frontal motor cortex, naturally being an important part of the brain residing 'upstream' of the motor cortex, the relationship between the motor cortex and frontal cortex is also specifically investigated.

It has been proposed that the brain integrates various processing units in a dynamic spatio-temporal manner and this is how cognition, thought and perhaps even consciousness is derived. This is referred to as the 'binding problem' and it involves issues of *how* the brain integrates various small-scale processing units in a large-scale dynamic spatio-temporal pattern. The favoured mechanism is phase synchronization. It is likely that the process of fatigue falls into this category and that the process or sensation of fatigue cannot be linked to single structures but is a result of a dynamic spatio-temporal 'orchestra' of different processing units. In this investigation the EEG is used to calculate phase synchronization between different areas of the brain. The EEG is measured at different locations on the scalp and phase synchronization between these points will be calculated and analysed (the EEG will be discussed in greater detail in the following chapter), with a specific focus on the phase synchronization between prefrontal and motor areas and frontal and motor areas. Figure 2-3 shows the different positions of the EEG electrodes and the grouping of the electrodes into prefrontal, frontal and motor areas in this investigation.

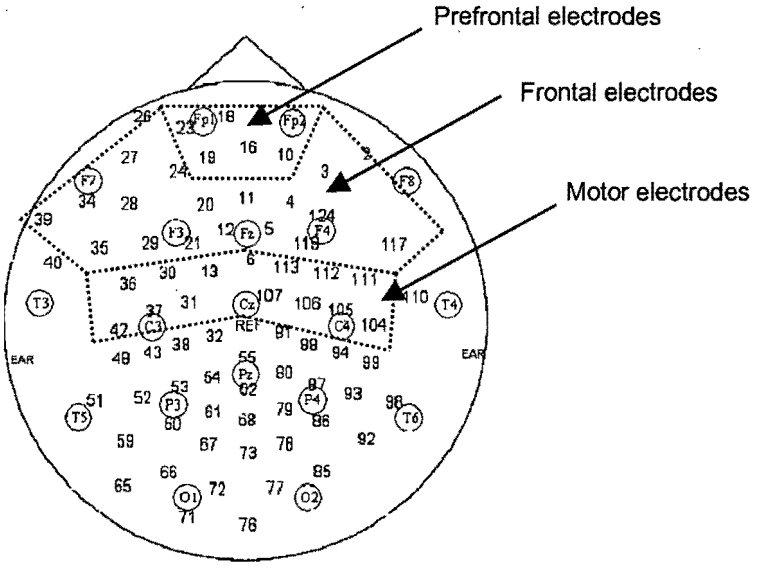

Figure 2-3 The 2 dimensional positions of various EEG electrodes and the groupings of various electrodes into prefrontal, frontal and motor areas on the surface of a schematic diagram of the head. The numbers refer to EGI GSN-128 electrode positions, and the symbols enclosed in circles refer to the international 10-20 system of electrode positions.

There has been no work done describing any exercise process or fatigue in this manner. In the following chapters the concept of 'binding problem', large-scale integration and phase synchrony shall be developed and methods to quantify these mechanism shall be provided and explained.

3. EEG AND THE ELECTROPHYSIOLOGY OF THE BRAIN

In this study EEG will be used as the means for the investigation of phase synchronization in exercise fatigue. A brief overview of the use of EEG in neuroscience shall be discussed. Since EEG is a measure of the brains electrical activity, important aspects of the electrophysiology of the brain shall also be discussed. The EEG in this investigation was analysed for phase synchronization. For a review of other analysis methods used in research involving EEG, please see Appendix B.

3.1 Theoretical Background and Important Concepts

3.1.1 The Generation of Voltages on the Scalp

EEG is the measurement of electrical activity on the surface of the scalp due to the electrical activity of the brain [19]. The cause of this electrical activity is the synchronous action of neurons acting as ionic current sources or generators in the brain, where the ionic current is generated by biochemical processes [61]. Neurons communicate with each other by the generation of action potentials and synaptic transmission of these action potentials, producing fluctuating or oscillating ionic currents in time scales of milliseconds [62]. To generate a potential field on the scalp the action of a certain quantity or population of neurons needs to be synchronised, so individual neurons collectively produce large enough currents by superposition [63].

Populations of neurons are organized into functional units by dynamic reciprocal connections between each other [63]. These functional units vary size from several neurons to over 10^7 and in spatial scales from 1μm to over 2cm [4]. Brain function such as vision, motor control or consciousness is believed to be the result of the global integration (large spatial scale activity) of local functional units (small to

medium spatial scale activity) that are distributed across different regions of the brain [4] [64].

The contribution to scalp potential is thought mainly to represent the electrical current oscillations from the surface of the cortex [21]. The cells found on the surface of the cortex of pyramidal cells that tend to line up in a columnar fashion. A number of these cells, typically 10^6, have strong reciprocal connections and tend to act synchronously [4]. This arrangement of neurons is referred to as a cortical macrocolumn, and occupies a few square millimetres of cortical surface [63]. Macrocolumns act as the basic source or generators of electrical current in the brain, representing the average electrical activity of the neurons of which they are composed [19].

While it is thought that the contribution to scalp potential is mainly due to the cortex, deeper brain structures also contribute to scalp potential. Evidence of this is can be seen in the auditory evoked potential. The auditory evoked potential is readily observed on the EEG recordings and represents electrical activity of auditory neural pathways, which involve deep brain structures such as the brainstem and thalamus [65]. For simplicity, in this project it will be assumed that the brains electrical activity, as measured by surface EEG, is mainly derived from the cortex so that any reference to cortical electrical activity in the text actually refers to the brain activity generally, which may also involve deeper brain structures.

Cortical macrocolumns form an important functional unit in the context of scalp recorded EEG, as their surface area is only slightly less than the lower limit of spatial resolution of the EEG recording electrode, which is the order of 1cm [19] (ignoring volume conduction effects which will be discussed below). Scalp EEG represents the synchrony or the coherence of a number of cortical macrocolums. Nunez [19] demonstrated that if the activities of only 1% of the cortical macrocolums in a given area are coherent, their relative contribution to scalp potential is 30 times greater than the contribution by the other 99% of neurons whose activity is incoherent.

3.1.2 The Spatial Resolution of the EEG

To better understand how voltages are produced on the scalp, researchers have developed models that outline the theory behind the phenomenon. The head volume conductor model says that current sources within a finite conducting medium, i.e. brain tissue, would produce volume currents within the medium and produce potential differences on the surface of the cortex [66]. The current sources are dipoles that consist of a current source generating the current, and a current sink where the generated current returns [66]. The potential measured on the surface of the cortex spreads through the skull and scalp and can then be measured by EEG electrodes. The resistivity of the skull is estimated to be 80 times greater than brain tissue, resulting in severe spatial filtering of the potential on the cortex [21]. This and other effects including the effect of the separation distances of the electrodes from the brain, cause a severe limitation in the spatial resolution of the potential measured on the scalp [19]. The voltage measured by a particular electrode is the spatial average of voltages over several square centimetres of cortex [20].

The theme of spatial scales and spatial resolution is central to current EEG analysis. The raw potential measured by an EEG electrode has complicated origins. The result of any analysis of EEG recorded data must be considered in the context of the above theory to be meaningful and useful.

3.1.3 EEG Signal Processing

The usefulness of EEG analysis would come from associating patterns in the EEG signal to specific physiological or clinical brain states [19] or by quantifying the EEG signal in some manner that could result in data being correlated to specific brain states or functionality [22]. That is one goal in the signal processing of EEG and the goal in this project. To begin analysing EEG data, some of the known characteristics must first be understood and taken into consideration. In the next section of the literature review the characteristics of the EEG signal are described.

3.2 Characteristics of the EEG

3.2.1 Signal Processing Characteristics of the EEG

A proper study of cognition or brain state, such as fatigue involves the study of changing spatiotemporal patterns of neuronal firing that culminate in potential measurable on the scalp [19]. The source of EEG signal generation has been discussed above. The focus has been on issues regarding spatial scale and spatial resolution. The dynamic behaviour of the theoretical dipoles determines the time series signal measured by the scalp EEG electrode. EEG data will be recorded and analysed over a length of time, therefore the characteristics of the time evolution of scalp potential must be understood. Evidence suggests that most dipole sources are distributed over large areas of cortex, and that these sources move around, i.e. their activity is not constant over space and time and the EEG signal is thus generally regarded as nonstationary [19].

EEG signals are unpredictable. With the present techniques available, one cannot predict the future value of the signal based on present values. The EEG signal can be described as a realization of a random or stochastic process, although biophysical processes underlying EEG generation are not necessarily, and are unlikely to be random [22]. A deterministic process on the other hand is one whose behaviour is governed by a set of liner or non-linear mathematical equations and whose future values can be predicted [67]. The output of a deterministic system can generally be classified as either being in state of equilibrium, periodic, quasiperiodic or chaotic [68]. The goal of much current research is to classify the time series behaviour of EEG signals and to attempt to describe it mathematically in order to further understand the underlying processes and to predict outcomes of certain inputs. Researchers are very far from this goal as the underlying processes generating EEG are complex and not well understood.

However, a lot of research has been done attempting to classify the EEG time series as non-linear deterministic chaos. Chaos is a class of dynamic behaviour that is very sensitive to initial conditions, the outcome of which is determined by non-linear equations [68]. Although deterministic, chaotic systems exhibit apparently random

behaviour, even in simple systems with few degrees of freedom [68]. Much work has been done to apply theories of chaos and other non-linear systems theory to EEG [70] [71].

3.2.2 Morphology of the EEG

When an EEG time series is viewed, it appears as noisy, random and/or pseudo-periodic (see Figure 3-1), its morphology often being dependant on brain state or function at a particular instant in time and the position of the electrode on the scalp. The first rhythms in EEG to be noticed by visual inspection by early researchers were rhythms in the 8-13 Hz range known as *alpha* waves. EEG clinicians today still investigate EEG traces and look for specific rhythms, like alpha rhythms, that should be present at specific age ranges under various conditions [21]. The EEG signal in fact varies greatly in amplitude and frequency with the frequency content often being found in preferred ranges that may have some physiological meaning or may be associated to a particular brain states. These frequency ranges are: Delta (0.1 – 3.5 Hz); Theta (4 – 7 Hz); Alpha (7 – 13 Hz); Beta (13 – 30 Hz) and Gamma (30 – 100 Hz) (these frequency ranges are not exactly fixed and other researchers may use slightly different frequency ranges) [74]. A detailed discussion on these brain rhythms is presented in Chapter 4.

The presence of a large value or a peak in a certain frequency range (when looking at the signal in the frequency domain as discussed below) indicates that a group of neurons are oscillating at the same frequency with a common phase [10]. If these synchronous bursts are triggered by a specific stimulus they are called *induced* synchronization and if these synchronous bursts are phase locked to stimulus onset they are called *evoked* synchronization [10]. Evoked synchronization can be considered as a reorganization of the phase of the ongoing EEG signals and have a fixed time delay from stimulus onset [75]. Induced synchronization that reflects a decrease in the synchrony of the underlying neurons is referred to as event-related desynchronization (ERD) while an increase in synchrony of the underlying neurons is referred to as event-related synchronization (ERS) [75]. Studies have shown that

both ERD and ERS can occur concomitantly in different frequency bands for a particular task such as finger movement or mental arithmetic.

The term synchronization as discussed here (with respect to ERS and ERD) is not the same as that applied to this investigation. With respect to ERS and ERD, synchronization refers to the activity of neurons whereby their activity is timed such that the electrical potentials of individual neurons locally add up to collectively produce a large potential. Here the phase and amplitudes relationships between individual neurons are important. With respect to this investigation synchronization has a specific mathematical description as outlined in Section 4.4 to follow, and although they are related concepts there are some important differences. The term synchronization is often used loosely in the literature, depending on the author and the context.

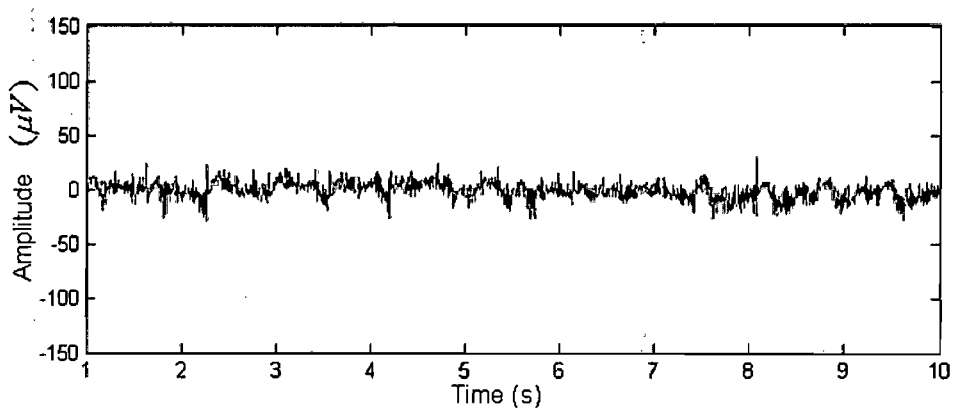

Figure 3-1: EEG Recorded during a fatigue trial.

3.3 Important Aspects of EEG Analysis

To apply any mathematical techniques or theory to real world EEG data some knowledge of the limitations and violation of assumptions must be stated and possibly corrected for. The first and most widely reported issue is one of stationarity, discussed above. Because the EEG time series is constantly changing it is customary to subdivide the waveform into epochs in which the signal can be considered more or less stationary with time invariant properties [22]. The length of such an epoch can be several seconds, but normally falls in the 5 – 10 second range.

Another important issue is noise. Noise is introduced to the EEG recording from the environment, instruments and electrodes [62]. A sophisticated EEG measuring system should take measures to reduce these. Physiological artefacts introduced into the EEG signal are more challenging to correct for. These include the electrical activity of the facial muscles and skin and the movement of the eyes [62]. Noisy data remains a problem in EEG analysis. This is especially an important factor for trials involving physical exercise.

It has been described above how the potentials measured on the scalp result from dipole current sources within the brain that conduct current to the surface by the head volume conductor (brain, skull bone etc.), and the conduction through the skull and other tissues affect the spatial resolution of EEG. This effect, and the fact that the voltages on the scalp are measured by electrodes referenced to a common electrode on the scalp influence results obtained in EEG analysis, such as coherence, where spurious coherence is obtained simply from volume conduction effects [21]. The effects of volume conduction and the reference electrode are largely removed by applying high-resolution algorithms to the EEG data [21]. These high-resolution algorithms also increase spatial resolution considerably [19][21].

Several high-resolution algorithms exist and they are based on models of the head, finite element analysis, the surface Laplacian or a combination of these. The surface Laplacian applied to EEG was introduced by Hjorth [85], where he used the Laplace operator to estimate the orthogonal or radial current at a particular point on the scalp.

The operator acts as a spatial filter, attenuating contributions to radial current from distant sources [20]. The technique has since being refined with several solutions that provide improved results. Due to the limited number of electrodes, the Laplacian can only be calculated using data at discrete points in space. Interpolation techniques can solve this, with techniques specifically developed for EEG analysis by Perrin et al. such as *surface spline interpolation* [86] and *spherical spline interpolation* [87][88]. These techniques provide an enhanced measure of radial current densities that take into account head geometry. Extensive studies involving simulations to test the validity of the *spherical spline Laplacian* have been conducted by Law et al. [89] and Nunez et al [20][21].

The spline-Laplacian techniques, and high resolution EEG in general are not without their assumptions and associated problems [20][21]. Srinivasan et al. [90] and others [21] point out that raw EEG and high resolution EEG are sensitive to different spatial scales and recommend using both in parallel.

Figure 3-2 below, taken from Nunez et al [21] shows the difference between spatially filtered data, using the *Dura Image* algorithm and raw data, the left column showing magnitude and the right column showing the phase distribution. The improvement in spatial resolution is clearly apparent.

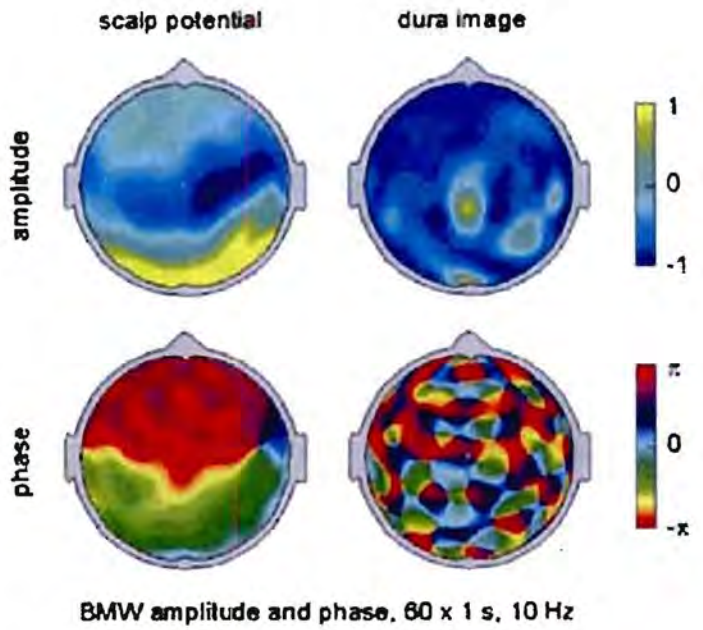

Figure 3-2: Diagram showing amplitude and phase distributions between raw data and dura image (spatially filtered) data, taken from reference [21].

4. BRAIN RHYTHMS AND CORTICAL SYNCHRONIZATION

The EEG is characterised by rhythms of various frequencies that have been shown to be physiologically relevant. The generation of these rhythms is discussed and the role of these rhythms in cognition is reviewed. Cortical synchronization is discussed in the context of rhythmic brain activity. Finally the theory of phase synchronization is presented. Additional rhythms and studies involving phase synchronization in neuroscience are outlined in Appendix C.

4.1 The Rhythmic Oscillatory Behaviour of Neurons

Physiological rhythmic behaviour is evident in many biological systems such as the beating of the heart and the release of hormones regulating growth [7]. The EEG itself reflects the rhythmic oscillatory behaviour of neurons that oscillate in defined frequency ranges, as discussed in the previous chapter. Bodily rhythms interact with each other and a noisy external environment and are kept in range by complex feedback systems, while abnormal rhythms are indicative of abnormal physiological processes and disease [7]. In the EEG these abnormal rhythms can be seen in epilepsy, anaesthesia and coma. The physiological significance of the complex rhythms seen in the EEG remains mostly unexplained but many psycho-physiological experiments have demonstrated functional correlations between cognitive and motor tasks and rhythms in certain frequency ranges. The interaction between different neurological rhythms and their underlying anatomical generation is even less well known. The empirical evidence suggests that brain rhythms reflect basic modes of dynamical organization in the brain [91]. Psycho-physiological experiments and other reviews regarding EEG rhythms will be discussed in the next section.

4.1.1 The Generation of Complex Rhythms in the Cortex

In their review of resonance in cells Hutcheon et al [91] discuss the role of a neuron's intrinsic resonance in the generation of cortical network oscillations. They state that the characteristic frequency ranges in brain rhythms arises from the coupling of oscillatory subunits, each of which possesses a frequency preference determined from its inherent characteristics. Individual neurons have been shown to display resonance that enable them to generate spontaneous oscillations or act as physiological band pass or notch filters enabling them to respond selectively to input [91].

A particular area of the cortex may display varying oscillatory behaviour depending on brain state and the particular task at hand. For example an area of cortex may display beta/gamma oscillations in a visual task and alpha activity in a relaxed eyes closed state [75]. Several rhythms can also coexist in the same brain structures and interact with each other [6].

Neuronal networks display oscillations with frequencies ranging between 0.05Hz to 500Hz [6]. In the case of low frequency oscillations there are more neurons recruited in the oscillatory process than in the case of high frequency oscillations where the oscillations tend to be more spatially restricted [75]. This may be due to neuronal network architecture and the limited speed of axon conductance and synaptic delays in the neuronal network [6]. Thus slower wave oscillations like delta, theta and alpha tend to involve large neuronal populations while beta and gamma band activity involve smaller neuronal populations.

The role of different brain rhythms in various cognitive tasks will be discussed below. Interpretation of brain rhythms should be done with caution with the knowledge that brain processes generating these rhythms are at best not well understood. However the experiments conducted have shed some light on the functional significance of dynamic brain oscillations. The important aspects of the brain rhythms shall be discussed below.

Alpha desynchronization does not always occur in isolation but is sometimes accompanied by alpha synchronization in neighbouring cortical areas; this is termed "focal ERD/surround ERS" [97]. This behaviour has been observed in motor tasks and may be the effect of selective attention where certain areas of the brain are inhibited so that information processing in those areas is reduced and processing in the focal area is facilitated [97]. Cooper and colleagues test the inhibition hypothesis of alpha ERD [92]. In particular they compare the effects of internally directed attention as well as externally directed attention on alpha ERD. They suggested that the role of alpha synchronization is in rejecting incoming sensory information in internally directed tasks such as mental imagery. The inhibitory process may serve to increase the signal to noise ratio in the cortex involved in attentional processing and this may be controlled by thalamo-cortical circuits and the reticular nucleus [92].

4.1.3 Beta Rhythms and Gamma Rhythms

Beta and gamma rhythms have been associated with attention, perception and cognition [98]. Activity in these bands has been observed following intense mental activity and sensory stimulation [99]. These high frequency oscillations have smaller amplitudes than alpha and other lower frequency rhythms. The faster oscillating cell assemblies culminating in beta and gamma rhythms also recruit less neurons than slower alpha rhythms.

There is no integrated theory describing the functional relevance of beta rhythms in the brain, but instead there are several studies describing beta rhythms in various motor, memory, attentional and other cognitive tasks. The Beta rhythms are often categorised as beta1 (12-20Hz) and beta2 (20-30Hz) and may have different functional characteristics.

Fast wave activity such as beta and gamma rhythms are considered to be an index of cortical arousal, which is the state of physiological reactivity of an organism [102]. This can be deduced from observations that beta activity is reduced during sleep onset and during repetitive tasks when states of arousal or attention are reduced.

Fast wave activity such as beta and gamma rhythms are considered to be an index of cortical arousal, which is the state of physiological reactivity of an organism [102]. This can be deduced from observations that beta activity is reduced during sleep onset and during repetitive tasks when states of arousal or attention are reduced. Further evidence that beta band activity is involved in attention and arousal come from studies using biofeedback training that aim to alter beta rhythms. The exact mechanisms behind beta activity is not well understood except that an increase in beta activity, often along with alpha desynchronization, has been shown to reflect cortical activation [103].

It has been found that a sub group of individuals suffering from attention deficit hyperactivity disorder (ADHD) and attention deficit disorder (ADD) have abnormally low beta activity [103]. Biofeedback training involving beta rhythms has been shown to increase attention by raising cortical excitation in under-aroused ADHD and ADD subjects [103].

There exists evidence that beta rhythms are activated in emotional states. In their study of the relationship between cortical activation and intensity of emotional arousal, Foster and colleagues found that there is increased cortical activation in the temporal and frontal regions as emotional intensity increases and this is reflected by increased amplitude across the beta frequency range [106]. Ray and Cole also found evidence of beta activation in the temporal lobes during positive and negative emotional tasks [107].

Many studies have linked gamma activity to sensory processing, the binding of sensory information and sensorimotor integration with the speed of gamma oscillations adequate for the coupling and synchronization of spatially separated cell assemblies [75]. There are several effects of gamma activity on neuronal networks with respect to the processing of sensory information. Firstly gamma band oscillations may act as precise "gates" that determine what afferent input is to be regarded or discarded and secondly two separate oscillating areas may synchronize their oscillations and there is evidence to suggest that this may cause long lasting changes in synaptic strengths between neuronal networks that may be important for learning and memory formation [99]. It has been found that beta oscillations occur

following the latter type of activity. Experimental data has demonstrated that evoked gamma rhythms in response to auditory and visual stimuli are often followed by beta rhythms and gamma rhythms of a different frequency and this may reflect hierarchical use of oscillation frequencies analogous to the specialization different anatomical areas (primary and association areas) in sensory processing [98].

It has been suggested that gamma activity represents the "building blocks" of electrical activity of the brain and may represent a universal code of Central Nervous System (CNS) communication [108]. Gamma rhythms are possibly employed to a greater degree in local processing whereas beta rhythms are used for higher-level interactions [98]. This hypothesis is consistent with experimental data.

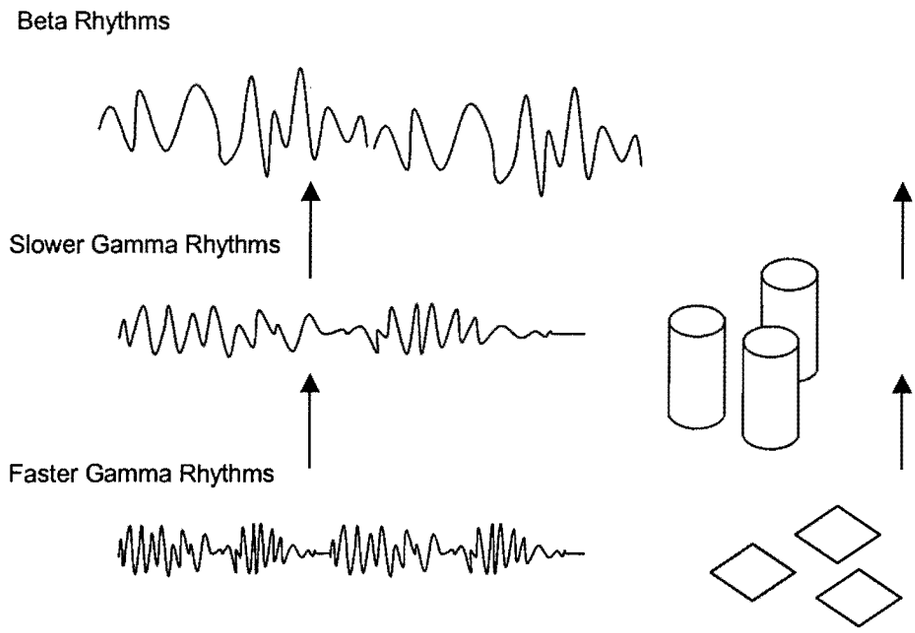

Figure 4-1: The diagram illustrates the hierarchical use of gamma and beta frequencies in the brain. The frequencies of gamma are used for fast local processing in individual neurons and cortical subunits, whereas beta processing is used across larger brain structures.

4.1.4 Delta and Theta Rhythms

Historically slow wave brain activity like delta (0-4 Hz) and theta (4-7Hz) rhythms have been associated with deep sleep, anaesthesia and coma (delta) and sleep and childhood EEG rhythms (theta). More recently delta and theta rhythms have been linked to cognitive processing, learning and memory formation. Delta and theta coherence has been observed in experiments involving the consolidation of newly learnt information for long-term memory storage during sleep. Molle and colleagues [109] investigated the coherence of brain rhythms from delta to beta during the learning of word pairs and during subsequent sleep. During the learning task, the investigators found an increase in coherence across the cortex in all bands, while during subsequent sleep periods, an increase in coherence was found in slow brain waves. They also demonstrate that there is increased coherence in the gamma band during the positive cycles of the slow brain waves. Their study provides important evidence that slow wave activity modulates the temporal behaviour of faster rhythms, which have been linked to information processing.

Delta and theta oscillations have been found to be the primary components of certain event related potentials (ERPs) linked to cognitive processes. It is hypothesized that ERPs are a superposition of transient oscillatory responses of cortical networks with response characteristics unique to the task conditions [110]. In their investigation involving the analysis of ERPs during specific cognitive tasks in healthy subjects, Karakas et al [110] describe the ERPs measured as being mainly composed of delta oscillations with an "interplay" of theta oscillations. They postulate that this delta response to cognitive processing results from distributed neural networks across the brain and that delta responses represent cognitive efforts, specifically being involved in the mediation between signal detection and decision making and may even be a marker of level of consciousness. These ideas are contradictory to the traditional notion of delta being a marker of reduced consciousness, as delta rhythms are the dominant rhythms found during deep sleep, anaesthesia and coma.

The association of theta activity to an array of complex cognitive processes such as alertness, attention, working memory, encoding and retrieval processes has been well established [112]. It has been shown that alpha and theta work in opposite ways in many cognitive processes. Where there is alpha desynchronization, theta synchronization has been observed and visa versa. Theta synchronization has been observed in studies involving episodic memory and encoding of new information. Klimesch and colleagues have conducted several experiments that show that theta synchronization indexes successful encoding of new information [113].

4.1.5 The Brain Rhythms Investigated in this Study

All the brain rhythms of relevance to this investigation are shown in Table 4-1 with the reason why they will form part of the investigation.

Rhythm	Reason for investigating
Theta	Related to alertness, attention, working memory, encoding and retrieval processes.
Alpha	Related to cognitive performance, working memory and internally directed attention.
Beta	Related to attention, perception, cognition and cortical arousal.
Gamma	Related to attention, perception, cognition and processing of sensory information.

Table 4-1: Table showing the brains rhythms relevant to this investigation and the reason why they form part of this investigation.

4.2 The Function of Neuronal Oscillations

Neuronal oscillations clearly characterize the working brain at various temporal and spatial scales. Researchers have linked brain rhythms to various cognitive tasks although this remains largely incomplete and the research at this stage only provides a small clue towards understanding how cognition arises from the working of neuronal circuits and oscillations. A complete theory describing how cognitive functions such as learning, memory and attention, emotion and even consciousness arise from the behaviour of billions of neurons is still far from being realised although some progress has been made from the evidence provided by many studies.

Understanding how the brain achieves cognition through neuronal activity including oscillations may help understand how the brain controls and responds to the process of fatigue. Pertinent questions to be considered are what are the neural mechanisms that select and coordinate distributed brain activity to achieve the unified outcome called cognition [4], are these neural mechanisms common to all cognitive functions [64], and what are the functions of brain oscillations and whether they are linked to information processing. Any theory describing the mechanisms of the global integration of local functioning neuronal units must accommodate and explain the role of oscillations in neuronal populations [64]. Such a theory is slowly being developed and indeed holds the role of neuronal oscillations at its core [4][6].

Detailed studies have shown that neuronal function has been endowed with complex dynamics and has the ability to resonate and oscillate at various frequencies, and this may suggest that the precise timing of their activity within a greater network may represent information processing [6]. Networks of similar frequency characteristics may be distributed across the brain allowing for signal transmission across large distances [108] where oscillations of a particular frequency would facilitate the transfer of one kind of information and not another kind associated with another frequency [115].

The most profound function of neuronal oscillators may be their ability to synchronize with each other over short or long distances creating dynamic functional networks in an energy efficient manner [6]. This concept forms the core of the latest theories

explaining how the brain integrates distributed local functioning units to achieve unified outcomes and will be discussed in the following section.

4.3 The Binding Phenomenon and Oscillatory Synchrony

It has been well established that the brain is functionally and anatomically specialized. The problem of how the brain integrates these local areas of specialization that is required for complex tasks is known as the *binding problem* or *large-scale integration problem.* It has been hypothesized that information in the brain is held and processed in flexible cell assemblies. Neural assemblies as defined by Varela et al are distributed local networks of neurons linked temporarily by dynamic reciprocal connections - specific neuronal assemblies are thought to underlie the operation of every cognitive act [4]. The mechanism by which transient networks can be formed even over large distances is unclear, but oscillatory synchrony as the likely candidate is the most favoured by researchers. Figure 4-2 illustrates the dynamic linking of neurons to form transient neuronal assemblies.

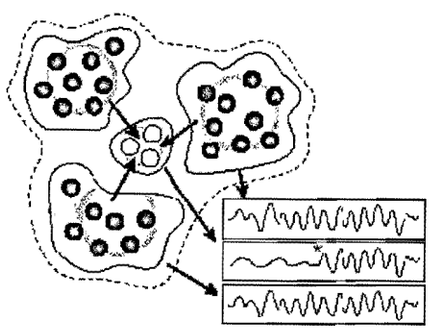

Figure 4-2: A schematic diagram illustrating how a group of neurons dynamically link through oscillatory synchrony. The group of grey neurons couple with the white neurons (center), dynamically creating an oscillating unit. The white neurons change the frequency of their oscillation to that of the coupled system. This is achieved through synchronization. Diagram taken from Engel et al [5].

Oscillatory synchrony occurs when the rhythms of two or more oscillatory systems coincide. More specifically synchronization is the adjustment of rhythms of oscillating objects due to their weak interaction [116]. There is a large body of mathematics devoted to the study of synchronization. The phenomenon of synchronization and the methods used to detect synchrony between two signals will be detailed below. The detection of synchrony between two systems indicates that they form part of the same functioning system and this concept has formed the basis of many studies involving the brain. The exact definition of synchronization, how it works in the brain and how it is measured will be detailed in the following sections.

4.4 Phase Synchronization

Synchronization was first observed by the 17th century mathematician, physicist and astronomer Christiaan Huygens. Huygens, in his quest to create accurate clocks discovered that two pendulum clocks hanging on the same beam adjusted their oscillations such that their rhythms coincided perfectly. This was due to the fact that the beam transmitted each clocks rhythm allowing minute changes in the parameters that determine each clocks oscillatory frequency. The clocks influenced each other's rhythm due to coupling through the beam.

The discussion that follows is based on the extensive work of Pikovsky, Rosenblum, Kurths, Tass and others in the field on non-linear dynamics [80][81][82][116]. The concept of synchronization may have different meanings in various scientific fields, but here it refers to the adjustment of rhythms of oscillating objects (such as a population of neurons) due to their weak interaction [116].

4.4.1 Self-Sustained Oscillators and Entrainment

To achieve synchronization between two oscillators the oscillating objects must have the following characteristics [116]:

- Each oscillator must be an autonomous system – it must have its own energy source such that when it is isolated the oscillator will continue to generate the same rhythms until its energy source runs out.
- The oscillations depend on system parameters and not on the initial conditions of the system.
- The oscillation is stable to small perturbations.

Brain oscillators belong to this class of oscillators [6]. Self-sustained oscillators have the ability to synchronize their rhythms even if the interaction is weak, such as the imperceptible vibrations in the beam connecting Huygen's clocks. This is an important concept in neuroscience because it makes synchronization an energy efficient mechanism for the creation of dynamic neuronal assemblies. When two oscillators synchronize they start off at different frequencies of oscillation, even if the frequencies are close. After synchronization the frequency of oscillation will be the same. This is known as *frequency entrainment* or *frequency locking* [116] (see Figure 4-3).

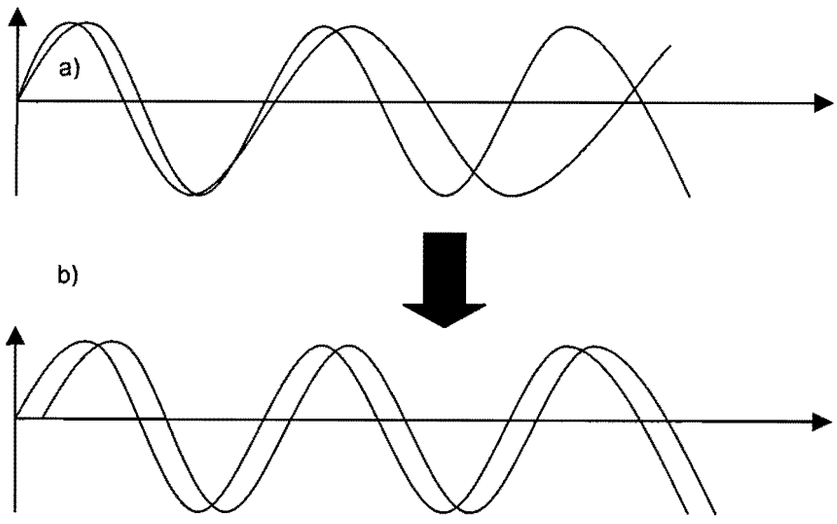

Figure 4-3: Diagrams illustrating frequency entrainment. The first two oscillators in (a) oscillate as different frequencies but when they synchronize oscillate as a common frequency at some phase difference, as seen in (b).

Synchronization of two oscillators depends on two factors [116]: coupling strength and frequency mismatch. Coupling strength describes how strong the interaction between the oscillators is. In the brain this may be the strength of the synaptic connections between populations of oscillating neurons. Frequency mismatch refers to how much the frequencies of the oscillators differ. The bigger the difference, the harder it is to synchronize the oscillators (the stronger the coupling strength must be). There will be a point where the frequency mismatch will be too large and the oscillators will not be able to synchronize.

4.4.2 The Phase Relationship of Synchronized Oscillators

Phase is defined in this discussion as a particular stage in a repetitive process or phenomenon [2]. The phase of an oscillator is a quantity that increases by 2π within one oscillatory cycle and unambiguously determines the state of the oscillator within a cycle [116]. The phase gains a value of 2π every period and since this represents the same state of an oscillation it is sometimes convenient to 'wrap' the phase back to 0 after every 2π increment.

When two oscillators synchronize, the frequency of their oscillations change, and they achieve frequency locking. There will be some degree of phase difference between the oscillators, one may lead the other in the position of the cycle. If frequency locking is achieved this phase difference will always remain constant and this is known as *phase locking*. Frequency locking and phase locking have been achieved in Figure 4-3 b.

4.4.3 Synchronization in Chaotic Oscillators

Brain oscillators can exhibit complex dynamics and even the simplest models of how neurons oscillate and interact with each other display enormous complexity [7]. Brain oscillators may exhibit chaotic dynamics, and together with the knowledge that brain oscillators interact in a noisy environment, the mathematical treatment of brain oscillators, or more specifically the output measured from these oscillators as measured by the EEG, require specific mathematical treatment.

Systems that exhibit complex or chaotic behaviour, like brain oscillators, are also able to undergo synchronization. Chaotic motion means that the long term behaviour of the system cannot be predicted even if the system parameters remain constant and there is no noise – the unpredictability results ironically from the deterministic dynamics of the system [116]. The amplitudes of the chaotic signal appear random and the system may be nearly periodic but is governed by a set of differential equations. Such systems may become synchronized in a similar way to periodic oscillators, except one cannot speak of frequency locking, as the systems generally don't have a fixed frequency of oscillation. Instead one can calculate the mean frequency over a sufficient length of time for the signals and for synchronized chaotic oscillators their mean frequencies should be equal although their amplitudes will remain uncorrelated.

In the case of synchronization in periodic oscillators phase locking is a key feature where there is a constant difference between the phase angles of the oscillators. In chaotic oscillators synchronization is also characterized by phase locking, and synchronization in chaotic systems is referred to as phase synchronization. Phase synchronization is characterized by phase locking (with or without frequency locking) with the amplitudes of the two oscillators remaining uncorrelated.

The detection of phase locking is thus indicative of phase synchronization and this principle is applied in the techniques derived from the theoretical study of phase synchronization of chaotic oscillators by Rosenblum et al [81] and their application to

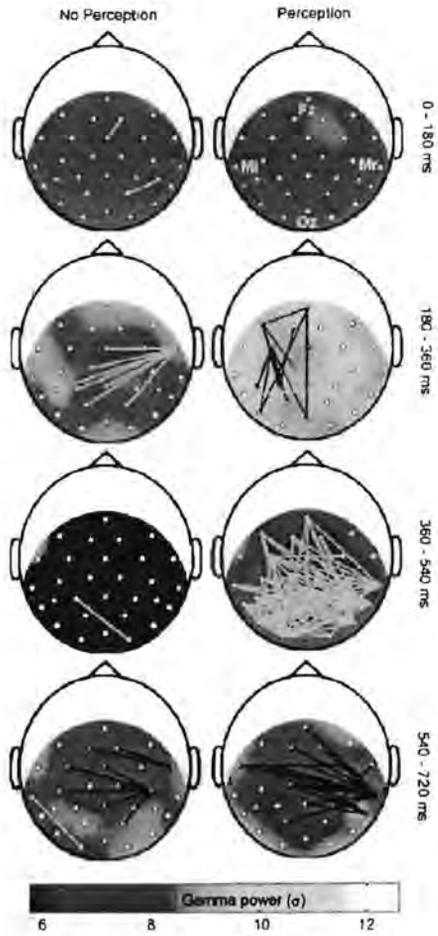

Figure 4-4: Head maps showing phase synchronization between 2 electrode locations on a 2-dimensional representation of the scalp. Dark lines represent increased phase synchronization, while light lines represent decreased phase synchronization. Figure taken from Rodriguez et al. [76] and is discussed in more detail in Appendix C.

5. DESCRIPTION OF THE PROJECT AND METHODOLOGY

5.1 The Aim of the Study

In the literature review of exercise fatigue and the brain two models of exercise fatigue that incorporate the principle of the central-governor were presented: the central-teleoanticipatory and the cognitive-discussion models. In these models the concept of fatigue as a conscious sensation or emotion was introduced and other aspects of the brain's role in regulating the work rate in the muscles were discussed. Endogenous activity such as prior experience, planning and pacing, arousal and motivation may modulate the array of sensory information coming in from the periphery and together determine levels of muscle recruitment in exercise.

The conscious perception of exercise and the accompanying process of fatigue are thus hypothesized to be a collection of known cognitive processes and perhaps a collection of unique cognitive process specific to it. There are many unanswered questions about this hypothesis including what areas of the brain are involved and how the process progresses with time, and the aim of this study is to answer some of these questions.

In this study the EEG was used as a tool to investigate the process of exercise fatigue. What is evident from the EEG is that the brain's activity is rhythmic and oscillatory, with the rhythms falling into distinct frequency bands. These rhythms have been widely studied and linked to many different cognitive functions as shown in the literature review.

The oscillatory behaviour of the brain may be linked not only to the processing of information on a local scale, but also to the formation of dynamic neuronal assemblies that cover large areas of the cortex, that are thought to underlie every cognitive act. Phase synchronization is indicative of the linkage of separate

oscillating groups of neurons that form complex networks dynamically (known as 'brain binding').

Investigating the phase synchronization characteristics in the EEG in specific frequency bands may answer some of the questions raised regarding fatigue as a collection of cognitive processes, since phase synchronization is thought to underlie all cognitive function. A description of the phase synchronization characteristics is hypothetically an indirect investigation of how different areas of the brain form dynamic networks and thus communicate with each other. Applying this to the process of exercise until fatigue may point to specific areas involved in fatigue, may give a better understanding to the time course of fatigue and most importantly provide a general description of what is happening in the brain during fatigue.

Thus the aim of this project is to investigate phase synchronization across different areas of the brain in order to elucidate the brains role in exercise fatigue.

5.2 Outline of the Project

5.2.1 Proposed Solution

The aim of this project, described above, was met by quantifying phase synchronization characteristics in physiologically relevant frequency bands calculated from EEG recordings taken during an exercise-until-fatigue trial and compared to that of baseline eyes-closed and eyes-open states. Dense array EEG recording equipment was selected to provide high-spatial sampling across the scalp.

The exercise-until-fatigue trial[1] was designed to minimalize the movement of the upper body or the use of the upper body muscles especially near the head. This was in order to reduce EEG artefact and errors. The exercise chosen was a submaximal isometric contraction of the quadriceps muscle where the subject was strapped down. In this experiment the subjects were their own controls with EEG recordings also

[1] The exercise-until-fatigue trial was carried out by Yolande Harley and colleagues [118].

also taken during a relaxed eyes-closed and eyes-open state. The subjects reached fatigue when they were unable to continue with their muscle contraction.

Once the EEG recordings were collected phase synchronization was calculated to provide information about its characteristics across the time span of the exercise trial (and baseline levels) and for different areas of the cortex[2]. These phase synchronization values were graphically presented and then statistically analysed to determine if exercise, and more importantly fatigue due to exercise, is related to a change in phase synchronization in different regions of the cortex or across the time span of exercise compared to baseline levels.

Changes in phase synchronization levels between two cortical sites are indicative of changes in neuronal cell communication between those cortical sites. A decrease or increase in phase synchronization during fatiguing exercise would indicate what areas of the cortex that are being dynamically linked or unlinked, and would also indicate during what periods of the process these dynamic links are being formed or broken. In this project the above-described process was visualized by plotting changes in phase synchronization on head maps allowing the location of these changes to be viewed. Head maps are 2-dimensional plots representing the surface of the scalp, where the relative positions of the electrodes on the scalp can be seen. Figure 5-6 is an example.

The phase synchronization calculations and the subsequent visualization and statistical analysis provided a means to answer specific questions about the time course of fatigue and what areas were involved. Building upon existing knowledge of the characteristics of cortical rhythms in various cognitive tasks a description of what is happening in the brain during exercise fatigue was built up hopefully leading to a better understanding of the brain's role in exercise fatigue.

---

[2] The electrical activity measured at an electrode location may represent activity from the entire brain, including deep structures although it is mostly thought to represent the underlying cortex and thus the term cortex will be used. Please see section 3.1.1 of the text for further details.

5.2.2 Spatial and Temporal Resolution Considerations

The biggest challenge posed by this kind of analysis of the EEG over the time period under consideration is the large amount of information generated that needs to be 'made sense of'. Indeed the brain processes that are occurring for the duration of the exercise trial are extremely complex, with changes in brain state occurring at millisecond time intervals over periods of several minutes over the entire cortex consisting of billions of information processing units. For scientists to begin to understand the process averaging and collapsing of these large data sets is essential.

The first process of averaging occurs naturally by the skull and other tissues when the neural currents pass from the brain to the scalp (see Section 3.1.2). This averaging causes much spatial information to be lost and methods to correct for this spatial information loss are applied. The second process of averaging involves the measurement of voltages on the scalp. Here the electrodes average the voltage to about one cm^3 of scalp area, due to the physical size of the electrode in contact with the scalp. The number of electrodes used will also determine the amount of spatial information available. The number of channels available with the given equipment will improve spatial sampling thus spatial resolution indirectly. The use of high resolution EEG equipment in this project greatly improves spatial resolution alongside the use of spatial filtering algorithms.

EEG has high temporal resolution making it an invaluable tool for measuring phase synchronization. Changes in phase synchronization values can be calculated at time scales of milliseconds, which correlate to the same time frames that these changes are occurring in the brain. In this project the limitation on temporal resolution is dependant on computational time and the quantity of data that needs to be interpreted. Furthermore since fatigue in this project is a process that takes a few hundred seconds it may not be useful to describe what is happening at the millisecond range, but instead at a time frame that matches the process more closely. The information also needs to be visually presented in a manner that allows for comparison and is conducive to understanding the dynamics of the process. Too

much data can be a hindrance and its generation computationally costly so suitable time averaging was carefully considered.

5.2.3 Outline of the Methodology

Once issues of spatial and temporal resolution had been considered appropriate methods were employed for the analysis of EEG. The methodology of the experiment and the analysis is outlined below. The methodology may be conceptually categorised into four parts: data collection, data pre-processing, data processing and data post-processing (Figure 5-2).

The first step was to acquire the data from a carefully planned exercise-until-fatigue trial [118]. Twenty-five subjects were selected. The EEG was recorded for the duration of a muscle contraction that ultimately resulted in fatigue and the inability to sustain the contraction. EEG was also recorded for the same subjects during a relaxed eyes-open and eyes-closed state. The three states - relaxed eyes-open, eyes-closed and exercise-until-fatigue (with eyes open) are described as the three trial conditions (Figure 5-1). The data was inspected for errors and artefact and data that were not suitable for analysis was discarded. This was done on a per subject and per channel basis.

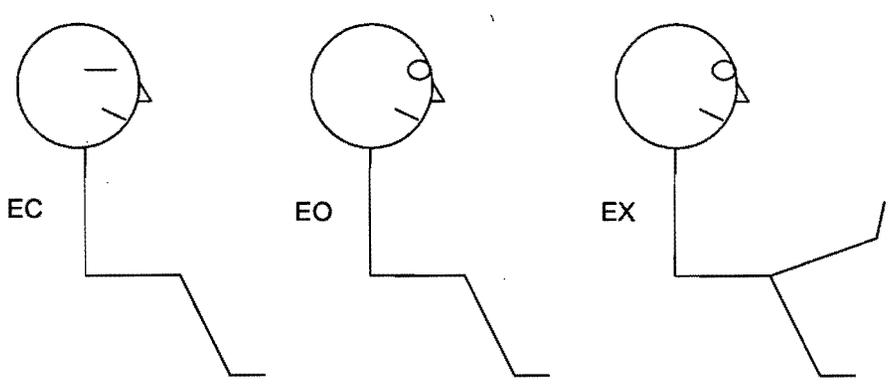

Figure 5-1: Schematic representation of the 3 conditions: eyes-closed (EC), eyes-open (EO) and exercise-until-fatigue (EX).

Once valid data was collected the second part of the methodology involved data pre-processing. Data was spatially filtered to enhance spatial resolution. The spatially filtered data was then filtered into the frequency bands of interest, namely theta, alpha, beta and gamma bands. The data from the subjects that were selected for analysis had a varied length depending on the time taken to reach fatigue. The data records of each subject were divided into epochs of equal length. The number of epochs per subject was chosen to be a constant value and thus allowed data of different lengths to be averaged and compared. Epoch lengths varied from subject to subject but were constant for a particular subject and condition.

Once pre-processing was completed processing of the data began. Algorithms to quantify phase synchronization were applied to each epoch, for each channel combination pair, each frequency band, each condition and each subject. The outcome is a phase synchronization coefficient that varies between 0 and 1 for each epoch.

Post processing involved processing and averaging the coefficients in various ways which were presented graphically, on head maps (see Figure 5-6) and analysed statistically. Custom software was written by this author (see Figure 5-16) to display head maps showing changes in phase synchronization that occur spatially and temporally. Statistical analysis was applied to determine if phase synchronization had changed between conditions, certain areas of the brain, and across time for each frequency band. The results of the post-processing provided a description of phase synchronization characteristics during exercise-until fatigue compared to the eyes-closed and eyes-open resting states.

An outline of the methodology is described in Figure 5-2. The details of each step of data analysis shall be described in the following sections.

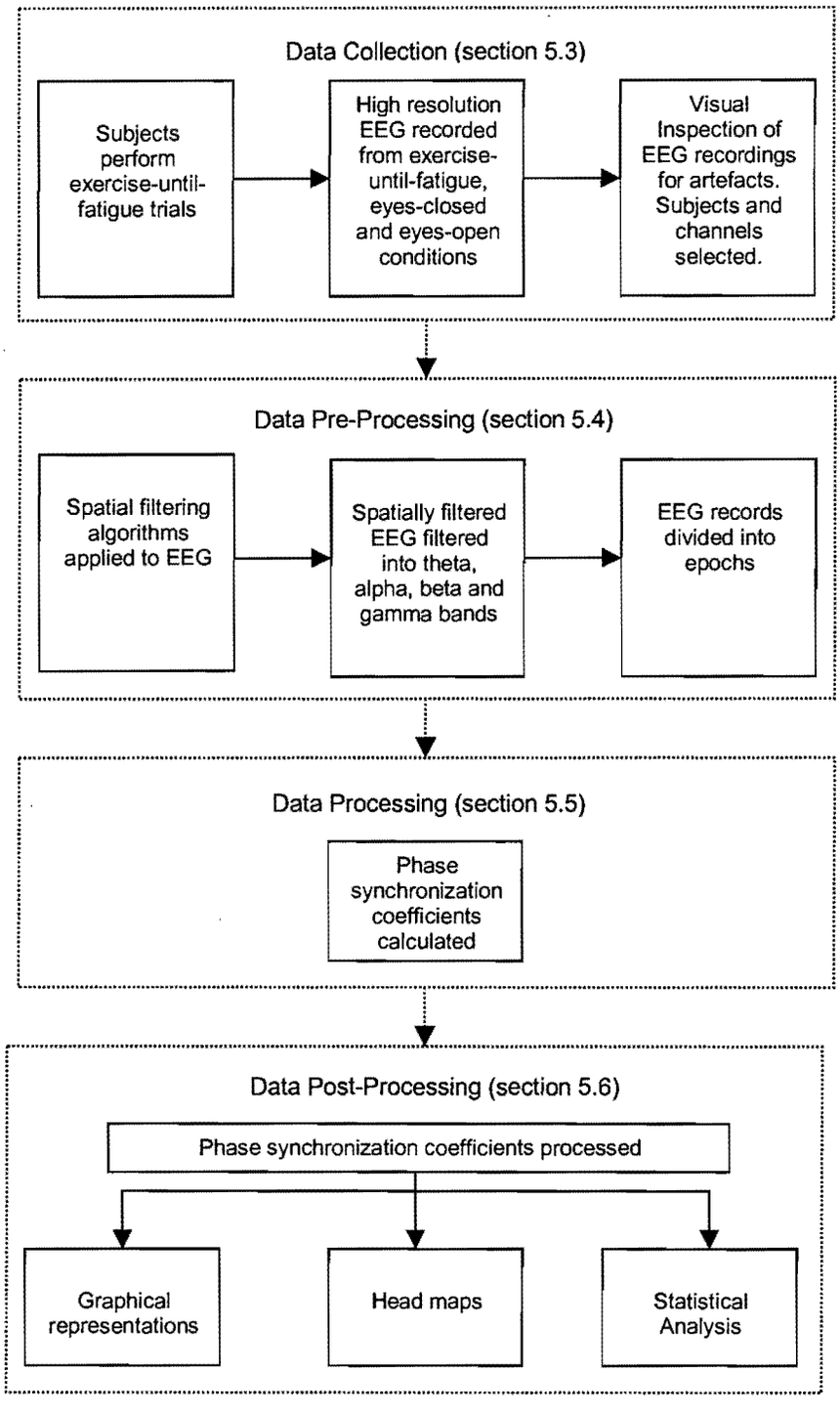

Figure 5-2: Outline of the methodology.

5.3 Data Collection

Data Collection involved the design of the experiment, the methods of measuring the EEG and the validation and selection of the EEG recordings. Each step is detailed below.

5.3.1 The Fatigue Trial

The fatigue trial was carried out as part of a study conducted by Yolande Harley and colleagues [118] and the description of the trial is from reference [118]. Twenty-five healthy subjects participated in the exercise-until-fatigue trial with the subjects having a range of physical activity levels. Initially six data sets where excluded due to errors or artefact while the remaining 19 data sets were retained for further detailed review. After a second round of close investigation, only data from eight of the subjects (5 male and 3 female) was determined to be suitable for analysis due to data artefact. The remaining subjects had a mean age of 28 ± 7.4 years. The study was approved by the Ethics and Research Committee of the University of Cape Town [119].

The trial involved a seated subject performing an isometric contraction (a contraction where the muscle length does not change) of the right quadriceps muscle, by extending the right knee. The use of an isometric contraction as opposed to dynamic exercise greatly restricts movement. The subjects were seated with the hip in 90° flexion, arms folded and strapped down for stability, with their eyes open. The subject's upper body was thus kept as stationary as possible throughout the trial.

Firstly as a warm up the subjects were requested to contract their quadriceps for 4s at 50% of their subjective maximum, twice at 70% and again at 90% of maximum respectively. The subjects were then asked to perform a maximum voluntary

contraction of the quadriceps muscle, where a subject contracted his or her muscle using the greatest possible force he or she was capable. An isokinetic dynamometer (Kin-Com, Chattanooga Group Inc., USA) was used to measure this force and displayed on a computer monitor. This force output level, called the maximal voluntary contraction served as a basis for the individual subjects maximal force capacity.

Before the commencement of the actual trial and after a rest period, EEG recordings were taken of the subjects in both a relaxed eyes closed state and a relaxed eyes open state. The recordings lasted approximately 2 minutes each per subject and serve as a baseline for the analysis of the EEG data collected during the trial.

The trial required that the subjects contract the quadriceps muscle at 20% of their own maximal voluntary capacity until exhaustion. The subject was able to sustain this particular level of contraction by observing and hence maintaining the output of the dynamometer. The subject maintained the force until he or she was unable to continue to do so, i.e. until the subjective point of fatigue was reached.

The EEG of each subject was recorded during the trial. The trial was designed to minimise the impact that exercise induced artefact would have on the EEG recordings. Dynamic exercise would obviously be impractical for EEG measurement, as would a maximal contraction because of the tendency to use the upper body thus contaminating the EEG signals with EMG artefact as well as causing the EEG electrodes to shift. Despite efforts to keep the subjects still, EEG electrodes did move and EMG artefact was introduced – this was particularly evident in the final stages of trials. This resulted in the data of only 8 out of 25 subjects being suitable for further analysis.

5.3.2 EEG Measurement

A dense array EEG system, the Geodesic System 200 [120] (see Figure 5-3), was used for EEG recordings. The system has 128 recording channels and a reference channel, allowing for high spatial sampling of scalp EEG recordings.

Figure 5-3: Photograph of Geodesic EEG System 200 connected to a subject, picture obtained from [121].

The system consists of three modules, the Geodesic Sensor Net 200, Net Amps 200 and Net Station 2.0. The Geodesic Sensor Net 200 is an electrode array with electrodes placed within a tense framework that fits like a cap on the scalp, with a single inter-electrode distance. The Net Amps 200 is an amplifier and analogue to digital converter, and Net Station is the data acquisition software.

The EEG signals were recorded at a sampling frequency 200Hz, with the electrode at the vertex of the head used as a reference. The data was filtered online with a bandpass filter with frequency cut-offs at 0.1 and 70Hz and was saved in a Matlab [122] file format for further offline processing.

Figure 5-4: A photograph of a seated subject before the exercise trial. Photograph provided courtesy of Yolande Harley.

5.3.3 Data Validation

The data was visualized and inspected using EMSE [123]. The data was transformed into ASCII format for input into EMSE. Using EMSE, the data is easily inspected at various amplitudes and time scales and makes identifying artefact across many channels convenient.

Initially the data from 19 subjects was inspected. It was determined early that the outer ring of electrodes was mostly contaminated with artefact and was thus discarded. Most subject's data had several contaminated channels so it was impossible to keep all the remaining channels for all the subjects. A process of elimination took place where each subject's data was inspected and bad channels marked on a map. The maps were inspected and subjects with the least amount of bad channels retained. The subset of maps was collated and bad channels found in any individual map were discarded. The process resulted in the retention of data from 8 subjects and 74 out of 128 channels per person. A relatively large proportion

of data was thus discarded but the nature of the experiment is such that contamination of channels is difficult to avoid while the integrity of EEG measurements must be maintained for confidence in the analysis and the eventual outcome of the experiment. An example of the output from EMSE used for the selection process is shown in Figure 5-5 a and b. Figure 5-5 a shows clean data taken from a subject in a relaxed eyes close state. Alpha rhythms are clearly present. Figure 5-5 b shows corrupt data from the same subject during the exercise trial.

a

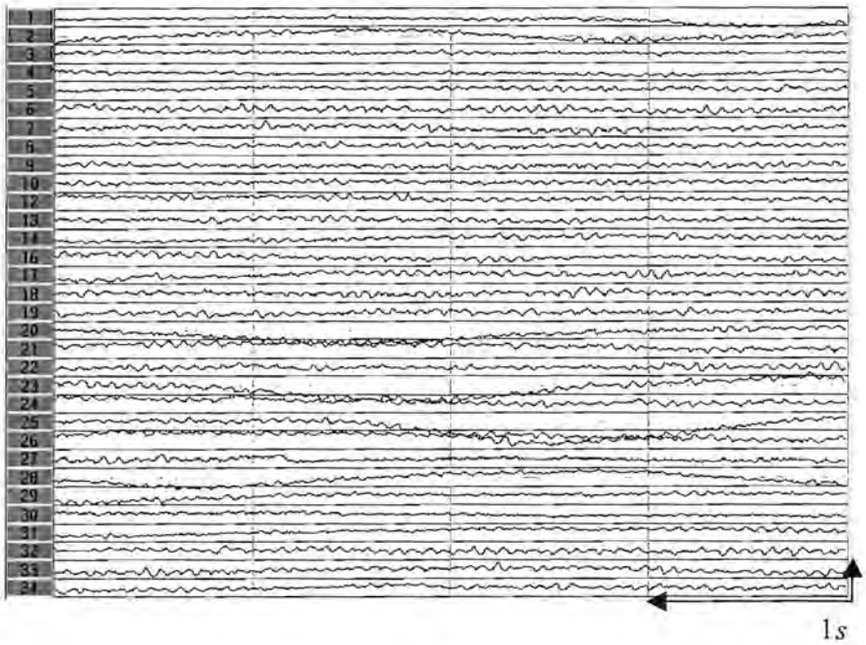

b

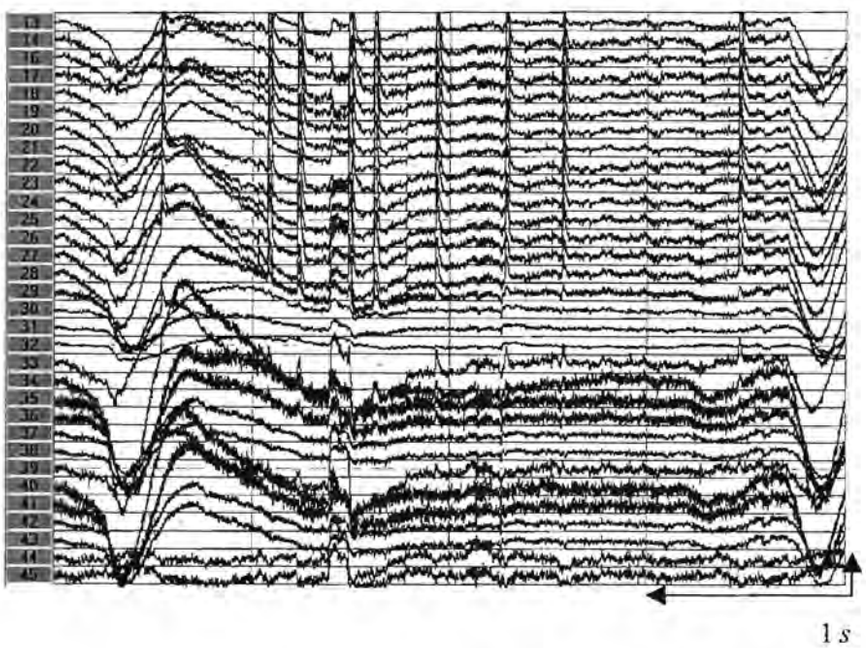

Figure 5-5: Clean EEG traces of a subject in a relaxed eyes closed state (a) and corrupt EEG traces of the same subject during the exercise trial (b).

A map representing all the channel positions on the scalp is shown in Figure 5-6 a. Figure 5-6 b shows channel positions that were retained for analysis. Most of the channels that were rejected formed part of the outer ring of electrodes or were electrodes located over the temporalis muscle. Presumably the action of this muscle caused movement of electrodes over this region, as well as introducing excessive EMG artefact. Interestingly this effect was worse towards the end of the trial where the subjects reached fatigue and perhaps recruited upper body muscles for joint stabilization.

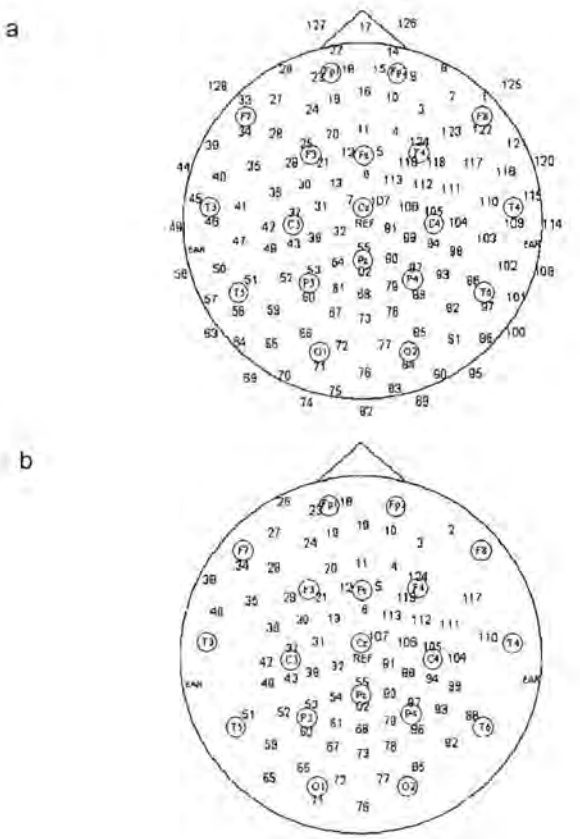

Figure 5-6: Head map showing all the channel positions on the scalp (a) and head map showing the channels selected for further processing (b). Most of the channels rejected formed part of the outer ring of electrodes or were electrodes located over the temporalis muscle. The International 10-20 system of electrodes, indicated by the symbols enclosed in a circle, are superimposed for reference purposes (see Appendix E for a description of the international 10-20 system).

The list of rejected channels was: 1; 7; 8; 9; 14; 15; 17; 22; 25; 26; 33; 41; 44; 45; 46; 47; 49; 50; 56; 57; 58; 63; 64; 69; 70; 74; 75; 82; 83; 84; 89; 90; 91; 95; 96; 97; 100; 101; 102; 103; 108; 109; 114; 115; 116; 118; 120; 121; 122; 123; 125; 126; 127; 128.

5.4 Data Pre-processing

Pre-processing involved filtering the data and dividing it into appropriate epochs. Filtering of the data involved applying algorithms for spatial enhancement and temporal filtering into the theta, alpha, beta and gamma bands.

5.4.1 Spatial Enhancement

As outlined in the literature review there is a need for the spatial enhancement of the EEG. One technique for spatial enhancement is the surface Laplacian operator and was introduced by Hjorth [85]. When neuronal current passes throught the skull and the scalp, the tangential components become smeared due to the low conductivity of the skull and scalp (see Figure 5-7). The Laplace operator is used to estimate the orthogonal or radial current at a particular point on the scalp that doesn't suffer as much from the averaging effects of the skull and the scalp (see Section 3.1.2 for further details).

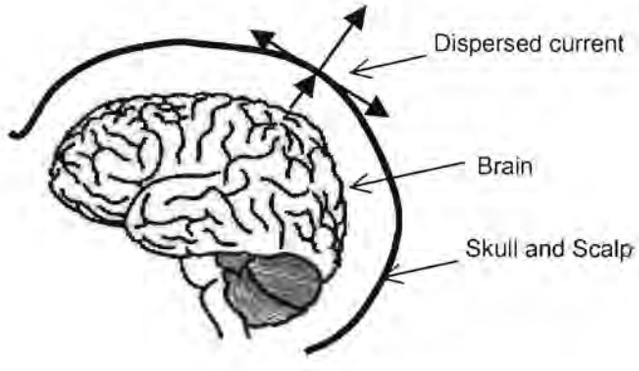

Figure 5-7: The effects of the skull and scalp on neuronal current.

When the Laplace operator is applied to a two dimensional function in the tangent plane it is zero at most locations except where the function is spreading radially in the tangent plane [117] (see Figure 5-7). Thus the orthogonal current is given by

$$i_{xy} = -\frac{1}{r} \cdot \left(\frac{\partial^2}{\partial x^2} + \frac{\partial^2}{\partial y^2} \right) v_{xy}, \qquad (5\text{-}1)$$

where r is a constant that represents the resistivity of the skull and other tissues and v_{xy} is the potential measured at an instance of time. The negative sign indicates that the current is directed outward from the volume.

The successful implementation of the Laplacian operator requires accurate spline interpolation of the voltage between the electrode positions. Spherical spline interpolation developed by Perrin et al, as outlined in [87][88], is a well tested method that has a neat mathematical solution for the calculation of the Laplacian operator on the spherical splines. The concept of interpolation is shown in Figure 5-8, where the voltage values of the electrode positions (shown by dots on the diagram) are used to determine (interpolate) voltage values at all points between the electrode positions (shown as various shades of grey).

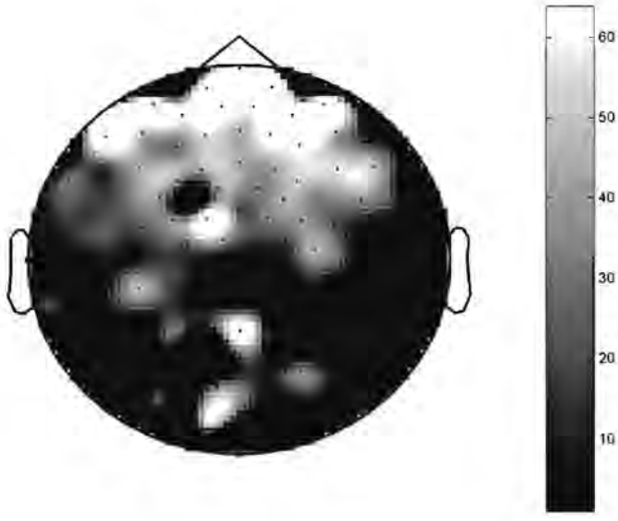

Figure 5-8: Illustration of interpolation, values are in μV .

The method involves firstly projecting the three-dimensional coordinates of the Geodesic sensor net electrode array placed on a dummy head onto a sphere. Of course the dummy head is just an approximation to the real coordinates of the electrodes placed on each subject with the actual coordinates of each subject being unavailable. Once projected onto a sphere the spherical spline can be defined from a set of projected coordinates and measured voltages.

Let $V(\mathbf{r})$ be the potential at an arbitrary point $\mathbf{r}$ where $\mathbf{r}_i$ is the position and z_i is the voltage of electrode i, as shown in Figure 5-9, then the spherical spline is defined by

$$V(\mathbf{r}) = c_0 + \sum_{i=1}^{74} c_i g_m(\cos(\hat{r} \cdot \hat{r}_i)), \qquad (5\text{-}2)$$

where coefficients $(c_0, \ldots, c_{74})$ are obtained from the following

$$GC + Tc_0 = Z \qquad (5\text{-}3)$$

$$T'C = 0, \qquad (5\text{-}4)$$

where

$$T' = (1,\ 1,\ \ldots, 1)\ , \tag{5-5}$$

$$C' = (c_1, c_2, \ldots, c_{74}), \tag{5-6}$$

$$Z' = (z_1, z_2, \ldots, z_{74}), \tag{5-7}$$

$$G = g_m(\cos(\hat{r}_i \cdot \hat{r}_j)) \tag{5-8}$$

and where $\cos(\hat{r}_i \cdot \hat{r}_j)$ denotes the angle between electrode projections $\mathbf{r}_i$ and $\mathbf{r}_j$.

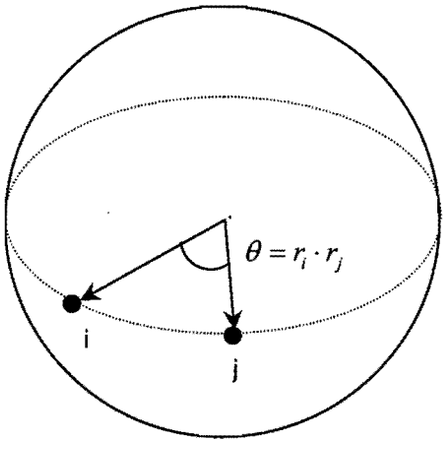

Figure 5-9: Electrode positions projected onto a sphere. $\cos(\hat{r}_i \cdot \hat{r}_j)$ is the angle θ between electrode positions i and j.

The function $g_m(x)$ is defined as the sum of the following series:

$$g_m(x) = \frac{1}{4\pi} \sum_{n=1}^{\infty} \frac{2n+1}{n^m (n+1)^m} P_n(x) \tag{5-9}$$

where $P_n(x)$ is the n[th] degree Legendre polynomial (see Appendix F for further details):

$$P_n(x)=\frac{1}{2^n n!}\left[\frac{d^n}{dx}\left(x^2-1\right)^n\right]. \qquad (5\text{-}10)$$

Once the data has been interpolated the Laplace operator may be applied to the spherical spline function to obtain an expression proportional to the orthogonal currents. This process is made simple by the fact that the Laplacian of the Legendre polynomial is a multiple of the same polynomial:

$$\Delta P_n = -n(n+1)P_n, \qquad (5\text{-}11)$$

and $g_m(x)$, truncated to *N* terms, can be replaced with

$$h_m(x)=\frac{1}{4\pi}\sum_{n=1}^{N}\frac{2n+1}{n^{m-1}(n+1)^{m-1}}P_n(x) \qquad (5\text{-}12)$$

The value m can be thought of as the order of interpolation and emphasises low order polynomials [143], and higher values cause the sum to converge more rapidly. The surface Laplacian was calculated with $m=4$ and $N=7$ which gives an accuracy for $h_m(x)$ of 10^{-6}, with these values being obtained from simulations conducted Perrin et al [87][88]. The solution is implemented in Matlab [122]. See Appendix I for the Matlab program.

5.4.2 Filtering into Frequency bands

Once the data has been spatially filtered as outlined above it can then be filtered into the four frequency bands of interest.

A digital implementation of a sixth order Butterworth filter was chosen to filter the data as it has the most monotonicity in the pass bands, although it sacrifices steepness in rolloff (please see Appendix G for details on the Butterworth filter). For

EEG analysis steepness in rolloff is not critical while the least amount of distortion in the passbands is desirable.

The operation on sample m of data $\mathbf{x}$ by the filtering operation is represented by the recursive time domain difference equations with output $\mathbf{y}$:

$$y(m) = b(1)x(m) + z_1(m-1) \quad (5\text{-}13)$$

$$z_1 = b(2)x(m) + z_2(m-1) - a(2)y(m) \quad (5\text{-}14)$$

$$\vdots = \quad \vdots \quad \vdots \quad \vdots$$

$$z_{n-2} = b(n-1)x(m) + z_{n-1}(m-1) - a(n-1)y(m) \quad (5\text{-}15)$$

$$z_{n-1} = b(n)x(m) - a(n)y(m) \quad (5\text{-}16)$$

where $n-1$ is the filter order. The filter coefficients $a(2...n)$ and $b(1...n)$ are determined by the filter design, in this case a Butterworth filter. The filter is implemented as well as designed in Matlab [122].

5.4.3 Windowing

The length of each subject's data set for the exercise trial is determined by the individual's time to reach fatigue and obviously varies from subject to subject. The shortest time taken to reach fatigue form the selected subjects was 135s and the longest time to fatigue was 307s. Using these values as a guide a suitable epoch length was determined.

EEG recordings remain approximately stationary for up to 10 seconds (see Section 3.3 for a discussion on stationarity). That determined the upper limit for the epoch length. A manageable number of epochs per subject in terms of computational time and ease of presentation and visualization was initially determined to be 50. The length of the epochs thus ranged from 2.7s to 6.14s for the exercise condition. The eyes-open and eyes-closed records varied slightly in length between subjects. For

the eyes closed condition the range was 2.2s to 2.7s and for the eyes open condition the range was 2s to 2.5s.

5.5 Data Processing

This section shows how the data was processed – i.e. which algorithms were applied to the pre-processed data. The method to calculate phase synchronization is developed, the validation of the method as applied to a theoretical system (the Rossler system) is described, the method to calculate the phase synchronization coefficients are presented and its application to the pre-processed data discussed.

5.5.1 Method to Calculate Phase Synchronization

The method used to calculate phase synchronization between oscillating systems is based on the work of Tass and colleagues [80] and Rosenblum and colleagues [81] (see Section 4.4 for a review of the theory of phase synchronization).

Generalized phase locking is defined mathematically as

$$\left| \varphi_{n,m}(t) \right| < const , \qquad (5\text{-}17)$$

where

$$\varphi_{n,m}(t) = n\phi_1(t) - m\phi_2(t) , \qquad (5\text{-}18)$$

n and m are some integers and will be restricted to $n = m = 1$, $\phi_{1,2}$ are the phases of the two oscillators. Both $\varphi_{n,m}$ and $\phi_{1,2}$ are defined on the whole real line and not just on the circle $[-\pi, \pi]$. In simple cases equation 5-18 is equivalent to frequency locking where

$$\Omega_1 = \Omega_2 \qquad (5\text{-}19)$$

and

$$\Omega_{1,2} = \left\langle \dot{\phi}_{1,2} \right\rangle \tag{5-20}$$

Ω is the frequency of the oscillator and brackets represent time averaging.

In the presence of strong noise or when the systems display chaotic dynamics the detection of phase locking becomes non trivial and the question of synchronization becomes ambiguous and can only be answered in the statistical sense [80]. The condition of frequency locking may not be achieved. Synchronization of noisy and/or chaotic systems can be understood by observing preferred values of the generalized phase difference of the oscillators by looking at the distribution of the *cyclic relative phase* defined as

$$\Psi_{n,m} = \varphi_{n,m} \bmod 2\pi \tag{5-21}$$

This distribution can be statistically quantified and provides a useful 'measure' of phase synchronization. Strong noise (whether external noise or deterministic noise) can introduce rapid jumps in the relative phases of the oscillators. In this case frequency locking will not be achieved and $\varphi_{n,m}(t)$ will exhibit a random-walk-like motion [81]. Phase locking will be determined if there are preferred values for $\Psi_{n,m}$ or peaks in the distribution of $\Psi_{n,m}$.

The first step in calculating $\Psi_{n,m}$ was to determine the phases of the oscillators. This was achieved using the analytic signal $\psi(t)$ which is a complex function of time where the instantaneous amplitude $A(t)$ and phase $\phi(t)$ of a signal $s(t)$ can be determined. It is defined as

$$\psi(t) = s(t) + j\tilde{s}(t) = A(t)e^{j\phi(t)} \tag{5-22}$$

where $\tilde{s}(t)$ is the Hilbert transform of $s(t)$

$$\tilde{s}(t) = \pi^{-1} PV \int_{-\infty}^{\infty} \frac{s(\tau)}{t-\tau} d\tau \qquad (5\text{-}23)$$

where PV means that the integral is taken in the sense of the Cauchy principal value. The Hilbert transform may be considered as a convolution of the functions $s(t)$ and $1/\pi t$. The Fourier transform of $\tilde{s}(t)$ is thus the product of the Fourier transforms of $s(t)$ and $1/\pi t$. Therefore the Hilbert transform of $s(t)$ may be represented as a filter operation by an ideal filter with an amplitude response of unity and a phase response a constant $\pi/2$ lag at all frequencies [81].

5.5.2 Verification of Phase Synchronization – Application to Rossler System

To verify the methods discussed above, they were applied to a well known system of chaotic oscillators, as is performed in reference [80] and [81]. The parameters of the system could then be adjusted and the resulting changes in phase synchronization observed. The Rossler oscillator was selected as it is a relatively simple example of a three dimensional chaotic oscillator used as a model in nonlinear dynamics. The system used for the verification of the methodology of phase synchronization calculations consists of two coupled Rossler oscillators and is represented as the following set of differential equations:

$$\dot{x}_1 = -\omega_1 y_1 - z_1 + C(x_2 - x_1), \qquad (5\text{-}24)$$

$$\dot{y}_1 = \omega_1 x_1 + 0.15 y_1, \qquad (5\text{-}25)$$

$$\dot{z}_1 = 0.2 + z_1(x_1 - 10). \qquad (5\text{-}26)$$

$$\dot{x}_2 = -\omega_2 y_2 - z_2 + C(x_1 - x_2), \qquad (5\text{-}27)$$

$$\dot{y}_2 = \omega_2 x_2 + 0.15 y_2 \qquad (5\text{-}28)$$

$$\dot{z}_2 = 0.2 + z_2(x_2 - 10). \qquad (5\text{-}29)$$

where x_i, y_i and z_i are the 3 dimensions of each system and '$\dot{x}$' represents $\frac{dx}{dt}$.

The system parameters C and $\omega_{1,2} = 1 \pm \Delta\omega$ represent strength of coupling and frequency mismatch respectively which were concepts discussed in Section 4.4. For a fixed frequency mismatch, C can be varied such that the phases of the two oscillators rotate with different velocities to a state where the phase difference does not grow with time.

The solution to the system represented by equations 5-24 to 5-29 is achieved by a numerical integration method implemented in Matlab [122]. Matlab was also used to implement all the phase synchronization algorithms. Three solutions were investigated with a frequency mismatch $\Delta\omega$ of 0.015 and with $C = 0.005$ representing no phase synchronization, $C = 0.012$ representing near phase synchronization, and $C = 0.04$ representing phase synchronization (these values were determined by trial and error for purposes of demonstration and testing, but were initially based on values given in reference [80] and [81]). Figure 5-10, Figure 5-11 and Figure 5-12 shows the output of variable y_1 and y_2 with $C = 0.005$, $C = 0.012$ and $C = 0.04$ respectively. The amplitudes of Figure 5-10 and Figure 5-11 are chaotic and uncorrelated and by observing the peaks of the output variables y_1 and y_2 in each time series very carefully it can be seen that there is a frequency mismatch. The amplitudes in Figure 5-12 remain chaotic and uncorrelated, but the coincidence of peaks with a small constant lag indicates frequency locking.

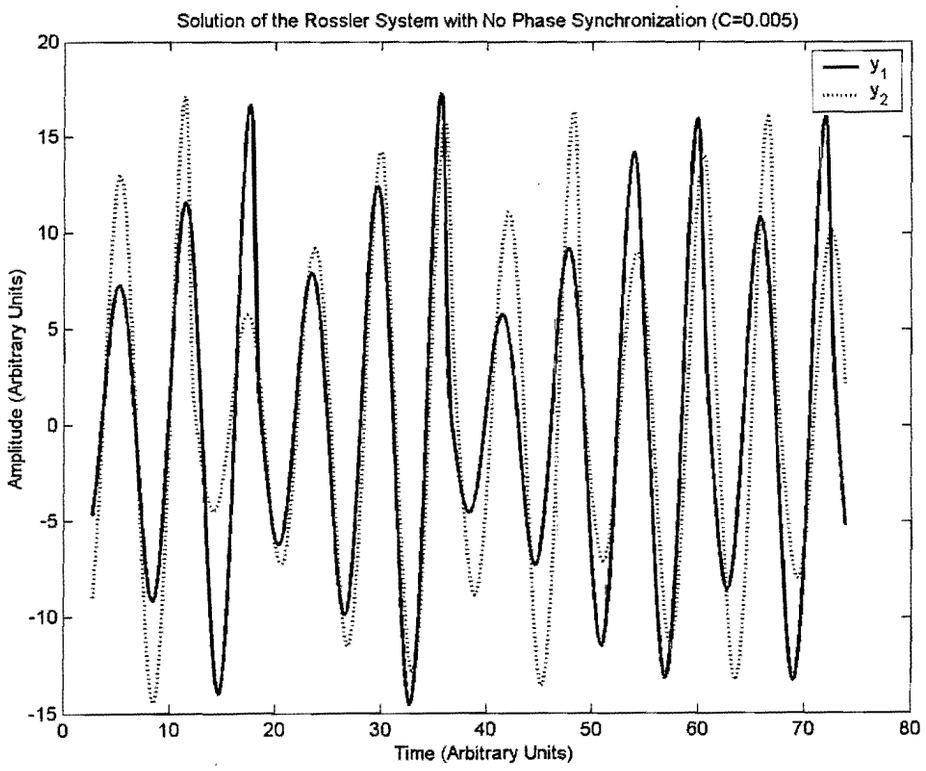

Figure 5-10: The solution to the unsynchronized Rossler system showing the output variables y_1 and y_2 with $C = 0.005$.

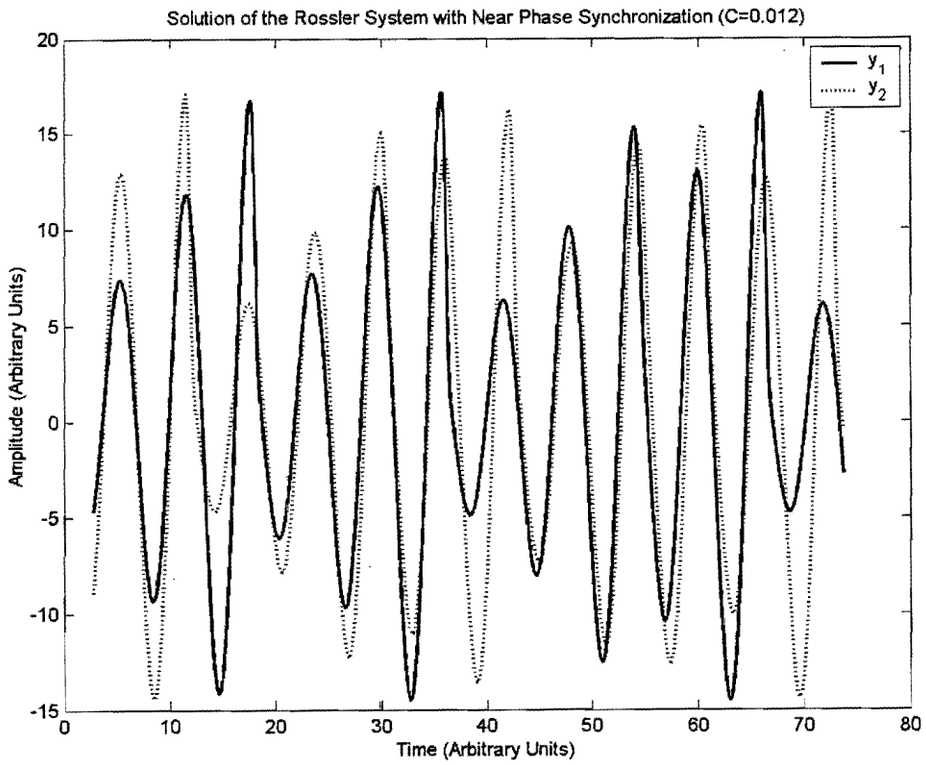

Figure 5-11: The solution to the near synchronized Rossler system showing the output variables y_1 and y_2 with $C = 0.012$.

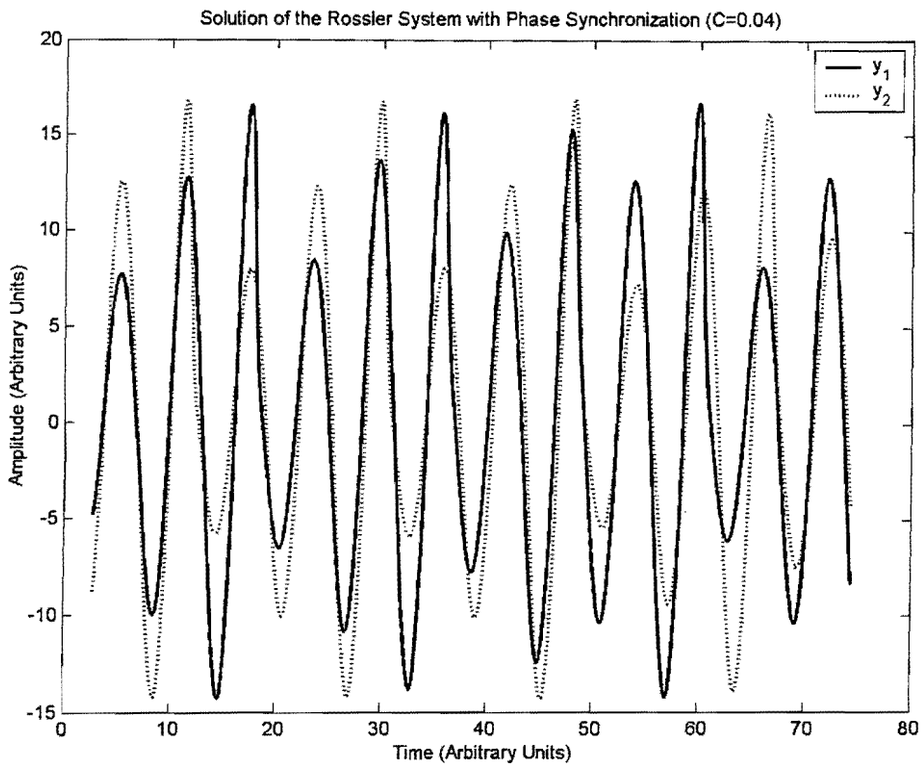

Figure 5-12: The solution to the synchronised Rossler system showing the output variables y_1 and y_2 with $C = 0.04$.

Next the generalized phase differences, $\varphi_{1,1}(t)$, of the three solutions are plotted to give an idea of the degree of phase locking. Figure 5-13 is a plot of $\varphi_{1,1}(t)$ for the three solutions with $C = 0.005$ (curve 1), $C = 0.012$ (curve 2) and $C = 0.04$ (curve 3). Curve 1 shows the phase difference increasing over time; clearly there is no phase locking and thus no synchronization. Curve 2 shows typical behaviour of a near phase locking condition (near synchronization); the curve starts off quite flat with a sudden period of increasing phase difference, then levelling off again. Curve 3 shows how the phase difference fluctuates around some constant value; phase locking and thus phase synchronization is achieved here.

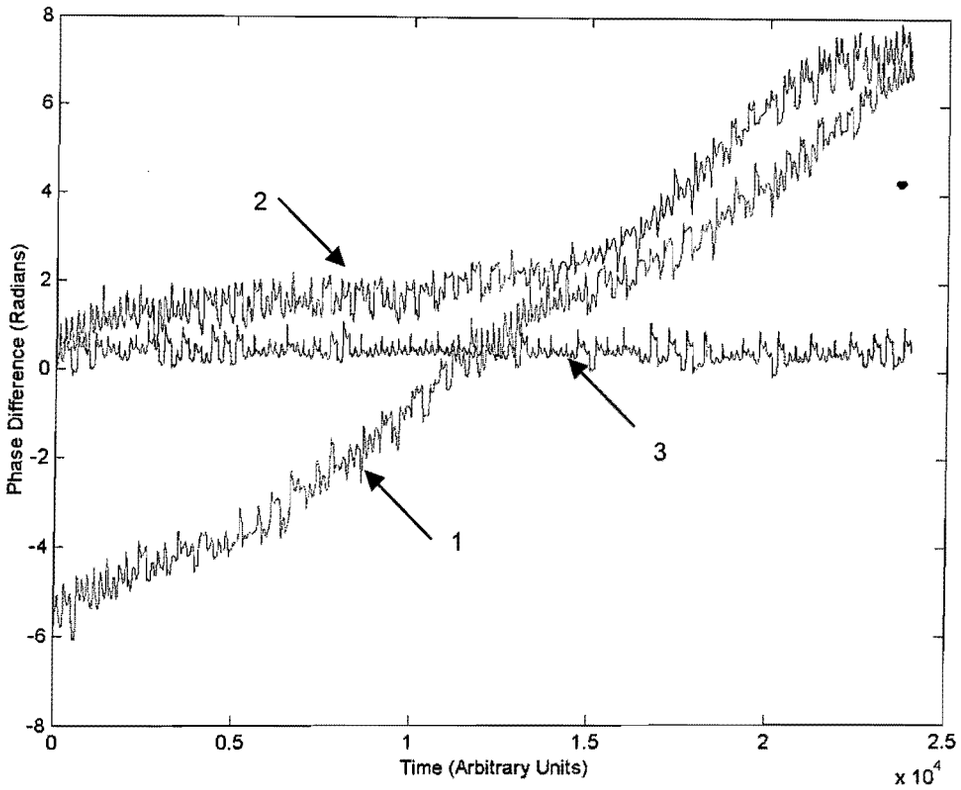

Figure 5-13: The phase difference between the output variables y_1 and y_2 of the Rossler system with $C = 0.005$ (curve 1), $C = 0.012$ (curve 2) and $C = 0.04$ (curve 3).

The distribution of the cyclic relative phase $\Psi_{1,1}$ for the three solutions $C = 0.005$, $C = 0.012$ and $C = 0.04$ is shown in Figure 5-14. Phase synchronization is demonstrated by the fact that there is a clearly a sharp peak in the distribution of $\Psi_{1,1}$ in Figure 5-14 c, while there is no clear value for a preferred value of phase difference in Figure 5-14 a. Figure 5-14 b shows a slight peak, indicating near phase synchronization, although this is not nearly as sharp as the phase synchronization case (Figure 5-14 c).

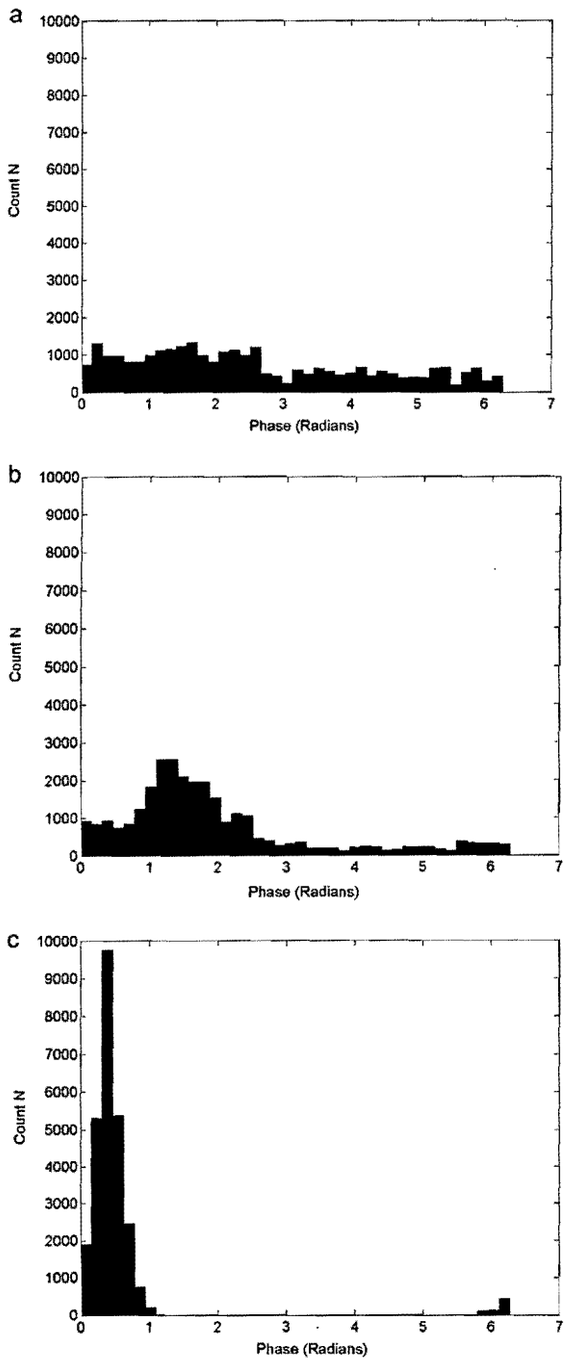

Figure 5-14: The distribution of the cyclic relative phase $\Psi_{1,1}$ between the output variables y_1 and y_2 of the Rossler system with $C = 0.005$ (a), $C = 0.012$ (b) and $C = 0.04$ (c).

5.5.3 The Phase Synchronization Coefficient

To quantify the deviation of the relative cyclic phase $\Psi_{1,1}$ from a uniform distribution the method developed by Tass et al [80] based on Shannon entropy was applied to the test data above as well as to the EEG. Their method is outlined below:

A phase synchronization coefficient

$$\tilde{\rho}_{n,m} = \left(S_{\max} - S\right) / S_{\max} \tag{5-30}$$

is defined where

$$S = -\sum_{k=1}^{N} p_k \ln p_k \tag{5-31}$$

is the entropy of the distribution of $\Psi_{n,m}$,

$$S_{\max} = \ln N \tag{5-32}$$

and N is the number of bins in the distribution. This results in a normalized value representing the degree of phase synchronization, where $\tilde{\rho}_{n,m} = 0$ corresponds to a flat distribution of $\Psi_{n,m}$ and no phase synchronization and $\tilde{\rho}_{n,m} = 1$ corresponds to a sharp peak in the distribution of $\Psi_{n,m}$ and perfect phase synchronization. Equation 5-30 applied to the Rossler system above for $C = 0.005$, $C = 0.012$ and $C = 0.04$ yields a value of $\tilde{\rho}_{1,1}$= 0.1146 (no synchronization), 0.2958 (near synchronization) and 0.4980 (synchronization) respectively. Since $\tilde{\rho}$ was calculated on chaotic (but noise free) data, it was not expected to be near the value of perfect synchronization achieved in perfectly linear systems. The value of $\tilde{\rho} = 0.4980$ is far from 1 but it was clearly larger than 0.1146 (no synchronization). The difference between 0.2958 and

0.4980 may be less distinct, and with noise added to the system (not done for this example), the distinction between these values may be more blurred. The phase synchronization coefficients may make sense only when compared to other values or are statistically analysed, as discussed in the next section.

5.5.4 Calculation The Phase Synchronization Coefficient on the Data

Phase synchronization coefficients were calculated to determine phase synchronization between all electrode sites in a particular condition (exercise-fatigue, eyes-closed and eyes-open), band (theta, alpha, beta and gamma) and subject. This was done on a per epoch basis (50 epochs per channel for each condition, band and subject). Since there were 74 channels used the number of channel combinations pairs was $\binom{74}{2} = 2701$. Matlab [122] was used to implement all the phase synchronization algorithms (see Appendix I for the program). Levels of phase synchronization between different areas of the cortex during the progression of the exercise trial were then compared to the baseline eyes closed and eyes open conditions. Furthermore phase synchronization across time was analysed and changes in phase synchronization was calculated between epochs. The methods involved in this analysis will be discussed in the next section.

Since there is no value of $\tilde{\rho}$ that determines a threshold of synchronization it is necessary to compute $\tilde{\rho}$ on noise or surrogate data for the purpose of comparison and then use appropriate statistical techniques (statistical methods used in this project will be outlined in the following sections) to determine significant levels of phase synchronization. EMSE [123] was used to generate surrogate EEG data. The surrogate data was then spatially filtered and band-pass filtered in exactly the same way as the trial data. Phase synchronization coefficients were calculated in the same manner as the trial data except that coefficients were calculated between random epochs and not epochs that corresponded in time. These coefficients served as baseline levels where no phase synchronization can be assumed. The results of this analysis will be presented in the following chapter.

5.6 Data Post-Processing

Data post-processing involved the display of coefficients in various graphical presentations, shown in the following chapter. Further processing of the coefficients is discussed here and involves the display of phase synchronization data on head maps and the statistical analysis of the phase synchronization coefficients and the differentiated phase synchronization coefficients.

5.6.1 Displaying Phase Synchronization Data on Head Maps

Custom software was written to display phase synchronization data on head maps (see Figure 5-16). This software is presented and then the methodology of displaying phase synchronization data on head maps is discussed.

5.6.1.1 Custom Software for Visualizing Phase Synchronization Data

Head maps provide an opportunity to view the phase synchronization between two points (i.e. electrode locations) in two-dimensions, and a series of head maps may indicate how phase synchronization between two points changes in time. The basic template used is shown in Figure 5-6 and shows all the channel positions. Custom software was required to read the phase synchronization data output from Matlab [122] and display it on a series of head map templates with the ability to average a variable number of epochs per head map.

The software was written by this author in Microsoft Visual C++ 6.0 for Microsoft Windows [124] and is called PSViewer. The PSViewer not only produced the final head maps selected for presentation, but was used in viewing, organizing and averaging the large amount of data produced by the Matlab scripts through a graphical user interface. For example, 2701 phase synchronization values make little sense unless they can be viewed on a head map, indicating where the

synchronization is occurring, with an appropriate threshold (determined statistically) so that only relevant levels of synchronization are shown.

PSViewer was designed with three main functions:

1. Read input data in Matlab format and display links between electrodes that are phase synchronized. The threshold level that determines phase synchronization and the number of epochs to average per head map are input by the user. There is the option to display electrode number and nearest neighbour electrode synchronization. The purpose here was to the view the data for individual subjects or the average of the subjects with various thresholds and time averaging both for testing the statistical methods and for general graphical presentation of phase synchronization.

2. Read a list of electrode combinations to display phase synchronization links for those channels. Here the threshold that determines a phase synchronization link is specified in the input file. This function only plots a single head map. There is an option to specify actual channels to ignore and phase synchronization links for that channel to any other is not plotted. The purpose here was to view phase synchronization between electrode pairs after more sophisticated statistical tests were performed in Matlab, to view phase synchronization links restricted to specific areas of the cortex and channels, and for general graphical presentation of phase synchronization.

3. Run general test utilities important for testing and verification of the software itself and the output of the Matlab scripts. Utilities include converting between row numbers representing channel recordings and the corresponding real channel value, finding the channel numbers given the combination pair number and displaying data values given channel numbers or position in an array.

Typical output head maps from PSViewer look like that in Figure 5-15. Each line connects the approximate channel position mapped onto a plane that has a value of phase synchronization over a certain threshold.

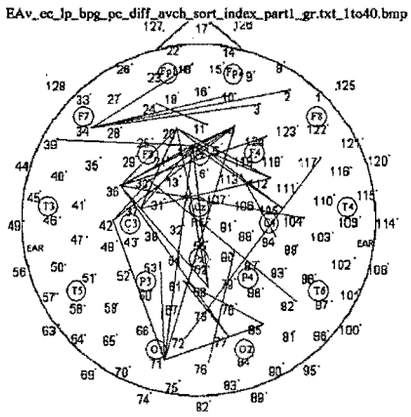

Figure 5-15: An arbitrary output head map from PSViewer with lines indicating phase synchronization. A line is plotted when the value of the phase synchronization coefficient is above a certain threshold determined statistically.

A screenshot of PSViewer is shown in Figure 5-16 below. In addition to the above mentioned features, it contains a scrollable window that displays messages indicating various actions, allowing a user to keep track of operations performed.

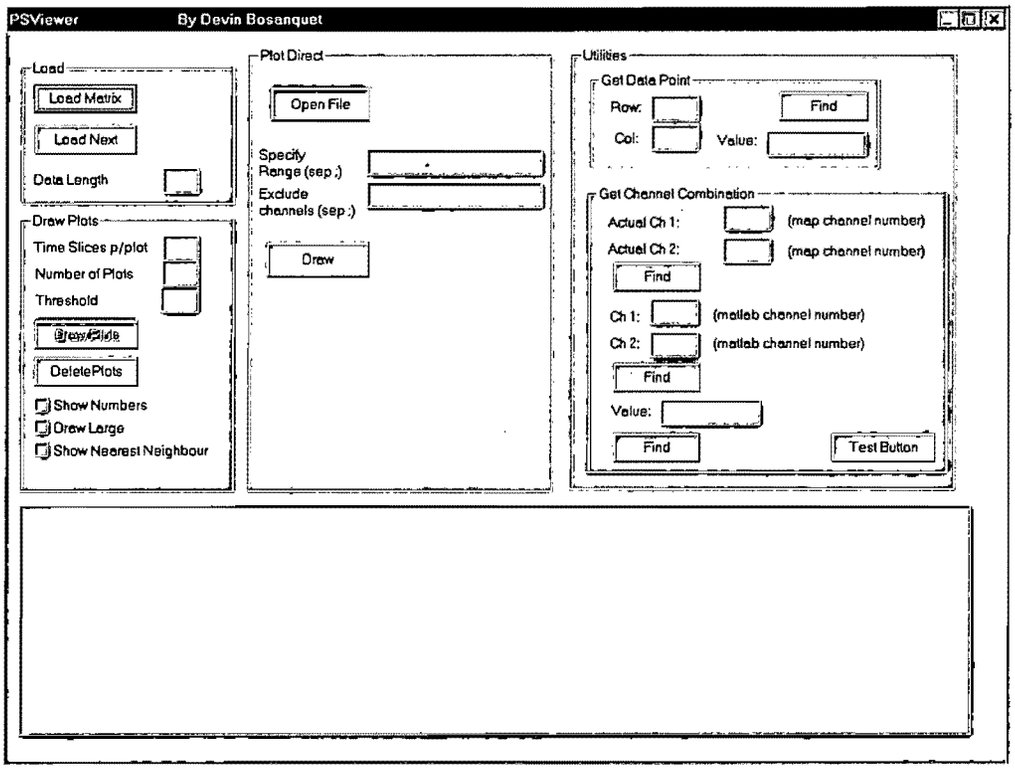

Figure 5-16: Screenshot of the PSViewer software.

5.6.1.2 Processing and Display of Coefficients

PSViewer was used to investigate individual subjects' and average-over-subject's phase synchronization data for the different conditions and bands. The data was inspected at each epoch and for various epoch averages. It was determined that the phase synchronization coefficients needed to be collapsed further (from 50 epochs) and averaged such that they represented six epochs during the course of a particular recording. This value was chosen because of practical display reasons.

The 50 phase synchronization coefficients representing the 50 epochs were averaged down to 6 epochs by averaging every 8 coefficients to a single coefficient. Since 6 by 8 is 48, the two coefficients that remained were included in the final set, such that the 6^{th} averaged coefficient was an average of the final 10 instead of the final 8 epochs.

Furthermore the *change* in the phase synchronization coefficients between these six time frames were calculated and gave a more powerful indication of the time course of phase synchronization (i.e. the phase synchronization coefficients were differentiated). This allowed small changes in synchronization to be observed, that otherwise may not be noticed if the changes are small in relation to the mean value. Both values are useful and provide complimentary information about cortical dynamics during the different conditions. The phase synchronization coefficients of the shifted surrogate data were also differentiated. The concept is outlined in Figure 5-17.

The differentiated phase synchronization coefficients, $\Delta\tilde{\rho}$, were calculated by simply subtracting the value of the phase synchronization coefficient at each epoch from its preceding epoch. This resulted in 5 values of $\Delta\tilde{\rho}$, representing the time course of $\Delta\tilde{\rho}$, per subject and channel combination for each condition and frequency band.

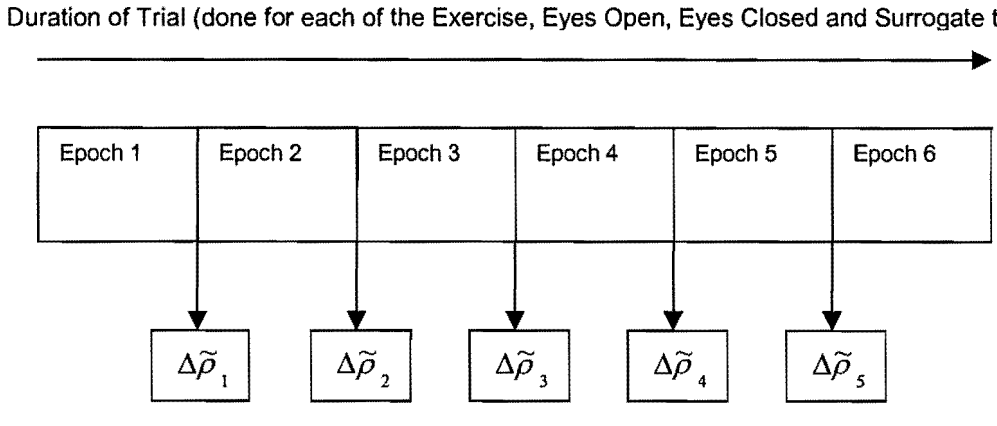

Figure 5-17: The division of trials into epochs and the corresponding $\Delta\tilde{\rho}$ values.

After a period of trial and error experimentation (using PSViewer) with various methods of averaging both the phase synchronization coefficients and differentiated phase synchronization coefficients the following procedure was followed. The aim of

the process was to see which particular channel combinations displayed the greatest increases or decreases in phase synchronization and whether these increases or decreases were stronger for a particular condition such as exercise-until-fatigue, performed separately for each frequency band theta, alpha, beta and gamma. The process is described below and outlined in Figure 5-18.

The $\Delta\tilde{\rho}$ values were averaged over subjects and all the subject-averaged $\Delta\tilde{\rho}$ values were pooled together for each frequency band. Thus all subject-averaged $\Delta\tilde{\rho}$ values for each condition, channel combination and epoch transition formed a single pool, and there was a pool of subject-averaged $\Delta\tilde{\rho}$ values for the theta, alpha, beta and gamma bands. The subject-averaged $\Delta\tilde{\rho}$ values in each pool were then ranked. The highest 0.5% and the lowest 0.5% of the ranked values were retained and plotted on head maps. The highest 0.5% represents phase synchronization (all these values were positive) and the lowest 0.5% represents phase desynchronization (all these values were negative).

The retained subject-averaged $\Delta\tilde{\rho}$ values correlated to a particular condition, channel combination and epoch transition. Each retained subject-averaged $\Delta\tilde{\rho}$ value was plotted on a head map that indicated its position on the map (a line drawn between 2 channel locations representing a channel combination). There were 5 head maps representing the time course of $\Delta\tilde{\rho}$, per condition and frequency band forming a single graphical unit referred to as a head map series. Each retained $\Delta\tilde{\rho}$ value was plotted on a head map that corresponded to its correct epoch transition number and condition. The process resulted in 24 head map series, one synchronization map and one desynchronization head map series per condition and frequency band combination. The aim was determine where the highest and lowest subject-averaged $\Delta\tilde{\rho}$ values fell with respect to epoch transition and condition for each frequency band. The methodology is outlined below:

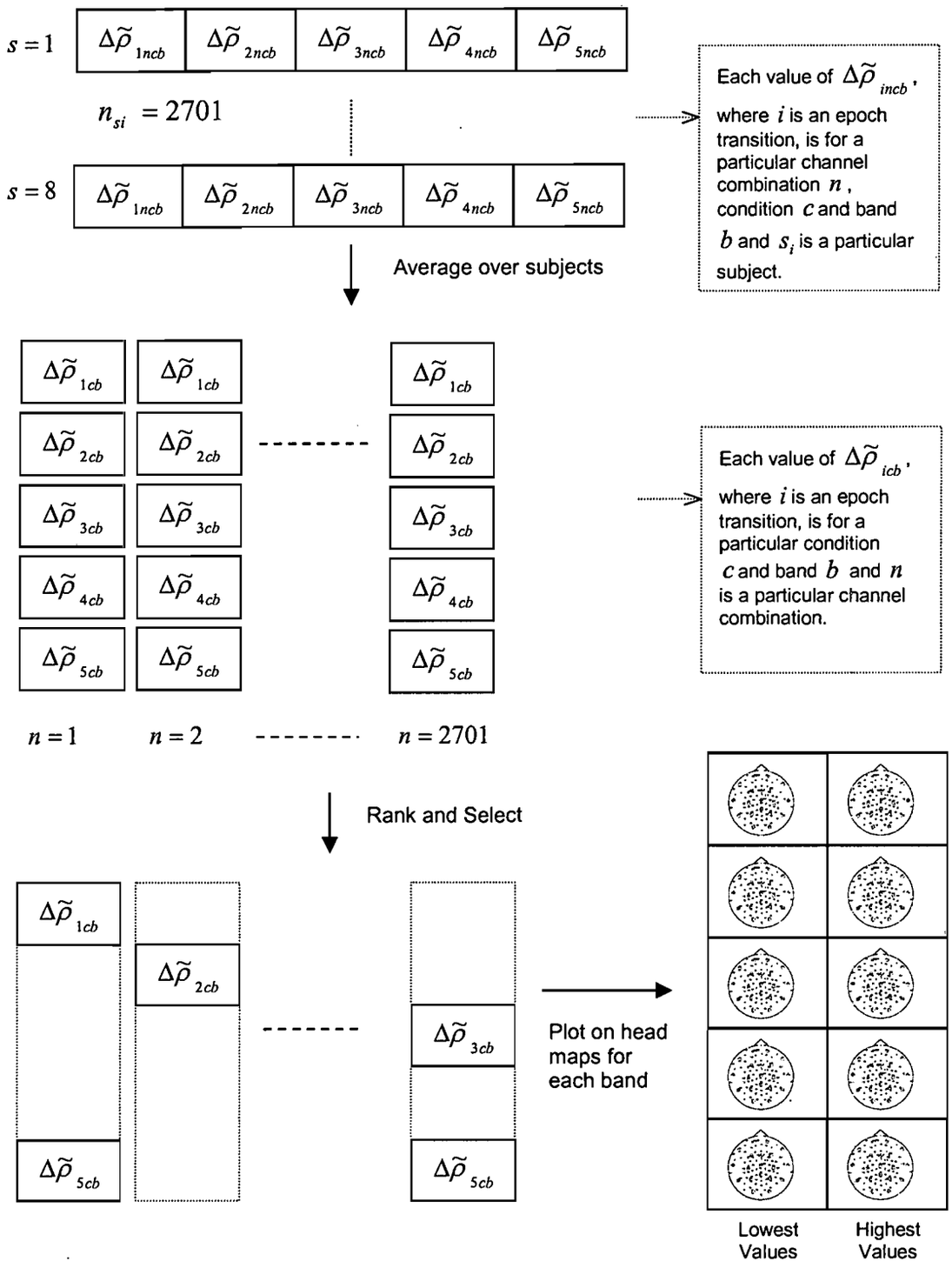

Figure 5-18: Outline of the methodology for plotting highest and lowest ranked values of $\Delta\tilde{\rho}$.

5.6.2 Statistical Analysis

In this project, statistical analysis was used to compare the phase synchronization coefficients $\tilde{\rho}$ for 6 epochs and the differentiated phase synchronization coefficients $\Delta\tilde{\rho}$ for 5 epoch transitions at various conditions and brain areas (the 50 original coefficients of each subject, condition and frequency band were collapsed to 6 coefficients and differentiated as described in Section 5.6.1.2). The particular statistical tests employed will be discussed and test hypotheses that represent comparisons will be detailed. Please see Appendix H for a more detailed discussion on hypothesis testing.

5.6.2.1 The Statistical Tests

The particular statistical test used in this project was largely determined by the experimental design and the purpose of the test. In this experiment the subjects were their own controls; each subject's EEG was recorded for the eyes closed, eyes open (baseline levels) and exercise-until-fatigue condition and the EEG recordings were further divided into bands, channel pairs and time and all represent different *treatments*. The purpose of the test here is to determine differences in the levels of both $\tilde{\rho}$ and $\Delta\tilde{\rho}$ for the different treatments.

A repeated measures analysis of variance (ANOVA) test was appropriate for the experimental design. This was because ANOVA tests for differences in means and makes adjustments for the fact that the same subjects were measured repeatedly (the subjects were there own controls) (please see Appendix H for more details on the ANOVA test). It was used here to test the means of the various *factors* for differences and to test the *interaction* between factors (the null hypothesis would state that there are no differences due to a particular factor and no interaction). A factor is an independent variable that has different levels (categories) that are adjusted and may result in changes in the dependent variable. In this case the

independent variables were the treatments (condition, areas and time (epochs)), while the dependent variables are $\tilde{\rho}$ and $\Delta\tilde{\rho}$. The test is used to determine if the different factors representing treatments (like the exercise condition at the sixth epoch) have an effect on the values of $\tilde{\rho}$ and $\Delta\tilde{\rho}$ compared to another treatment (like the eyes-open condition at the sixth epoch) and to test if the factors interact. Individual factors may not have any effect on $\tilde{\rho}$ and $\Delta\tilde{\rho}$ on their own but together may have an effect. An example of this may be that exercise (a particular category of the condition factor) has no effect on $\tilde{\rho}$ (over all categories of the time factor), but may effect $\tilde{\rho}$ at the sixth epoch (a particular category of the time factor). The interaction in this example is a particular category of the condition factor, exercise and a particular category of the time factor, the sixth epoch. ANOVA makes use of the *F* statistic to give a *P* value that is used to fail to reject or reject the null hypothesis.

There are several assumptions about the dependent variable that must be met. Firstly the dependent variable must be normally distributed and display equality of variance across the groups. These assumptions may be somewhat relaxed when the sample size is large and equal which is the case here. Also a transformation may be applied to the data to correct for these problems. Secondly the assumption of *compound symmetry* must be met. Due to the fact that multiple measurements from the same people are being compared, a correlation between measurements is introduced [125]. Compound symmetry is met when the correlations between measurements and the variances across the measurements are the same.

When the condition of compound symmetry is not met the degrees of freedom in the *F* statistic may be adjusted by a certain value, epsilon, that makes the test more stringent and reduces the chances of a type I error [125]. Epsilon is calculated on the basis of how far the condition of compound symmetry has been violated. Different methods exist to calculate the epsilon correction factor and include Greenhouse-Geisser, Huynh-Feldt (least conservative), and lower bound (most conservative).

5.6.2.2 The Test Hypotheses

Repeated measures ANOVA was applied to determine differences in both $\tilde{\rho}$ and $\Delta\tilde{\rho}$ for the different treatments and to determine interaction between treatments. The different treatments are the factors in the ANOVA test, and all these factors are within-subjects factors as they are applied to all the subjects.

The different treatments provided a varied assessment of how the exercise-until-fatigue condition affected both $\tilde{\rho}$ and $\Delta\tilde{\rho}$. The treatments involved include the three physiological conditions (eyes open, eyes closed, exercise-until-fatigue, referred to simply as the *conditions*), the four EEG frequency bands (theta, alpha, beta and gamma, referred to simply as the *bands*), the 6 epochs and 5 epoch transitions (referred to as *time*) and particular groupings of channel combinations that form particular cortical area groupings (referred to simply as the *areas*). The particular groupings of channel combinations was done such that 3 groups were formed – channel combinations from all the electrode pairs (all areas pairs), channel combinations from the electrodes over the frontal cortical area to the electrodes over the motor cortical area (frontal-motor pairs) and channel combinations from the electrodes over the prefrontal cortical area to the electrodes over the motor cortical area (prefrontal-motor pairs). This is shown in Figure 5-19.

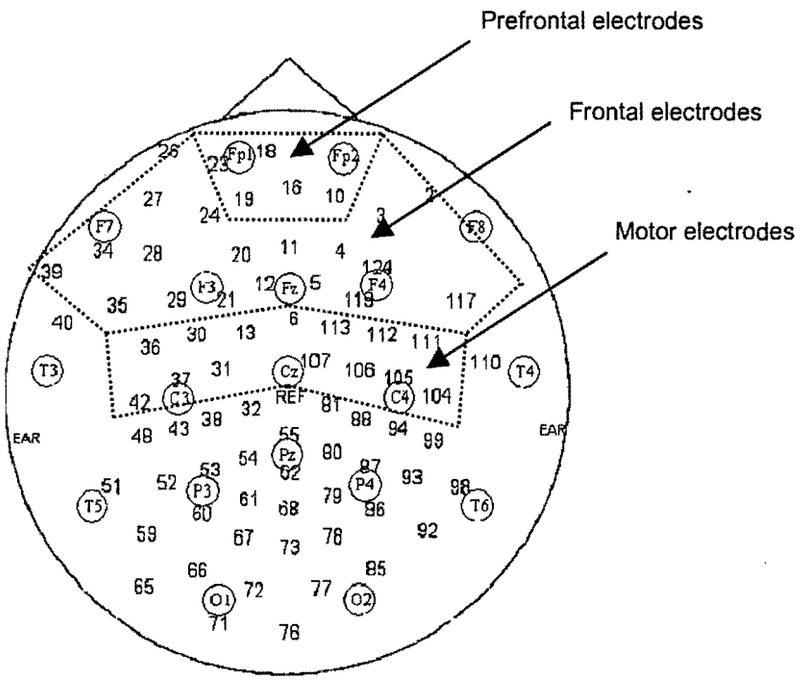

Figure 5-19: Diagram showing the position of the prefrontal electrodes, the frontal electrodes and the motor electrodes.

Each treatment has a level associated with it representing the different measurements, for example there are 3 levels of conditions representing eyes-closed, eyes-open and exercise-until-fatigue. Table 5-1 below details the levels of the various treatments that were applied.

Treatment	Levels ($\tilde{\rho}$)	Levels ($\Delta\tilde{\rho}$)	Description
Physiological Condition	3	3	Eyes closed, eyes open, exercise-until fatigue.
EEG Frequency Bands	4	4	Theta, alpha, beta, gamma
Time	6	5	Epochs (for $\tilde{\rho}$) or transition between epochs (for $\Delta\tilde{\rho}$)
Cortical Areas	3	3	All areas pairs, frontal-motor pairs, prefrontal-motor pairs

Table 5-1: A Description of the levels associated with a treatment.

Four ANOVA tests were performed for each of the four frequency bands. The details of the tests are shown in the table below, with the levels of each treatment shown in brackets:

	Test 1	Test 2	Test 3	Test 4
Dep. Variable	$\tilde{\rho}$	$\tilde{\rho}$	$\Delta\tilde{\rho}$	$\Delta\tilde{\rho}$
Factor 1	Condition (3)	Condition (3)	Condition (3)	Condition (3)
Factor 2	Time (6)	Areas (3)	Time (5)	Areas (3)

Table 5-2: Details of the four ANOVA tests. These tests were repeated for each frequency band.

Test 1 and Test 3 tested the means of $\tilde{\rho}$ and $\Delta\tilde{\rho}$ respectively for differences that would indicate a relationship to any of the levels of condition and time. The hypothesis here is that there is a relationship between levels of condition or time and $\tilde{\rho}$ and $\Delta\tilde{\rho}$. The two treatments, condition and time were looked at independently.

The different levels of condition were first compared irrespective of time. This provides some interesting information on the differences between the conditions on average. The different levels of time are then compared irrespective of whether the condition is eyes closed or exercise-until-fatigue for instance. This isn't of any particular interest in this project but what is of importance is the interaction between the levels of time and condition. Changes in the means of $\tilde{\rho}$ and $\Delta\tilde{\rho}$ due to the levels of time (changes across time) are of great interest if they occur at a certain condition (for example exercise-until-fatigue). The ANOVA tests test for this interaction. The hypotheses being tested in test 1 and 3 are summarized in the Table 5-3.

	Hypothesis	**Relevance**	**Comment**
1	Condition affects $\tilde{\rho}$ or $\Delta\tilde{\rho}$	Yes	Determines if exercise-until-fatigue has a different effect to eyes closed or eyes open conditions.
2	Time affects $\tilde{\rho}$ or $\Delta\tilde{\rho}$	No	The effect of time on its own is irrelevant unless seen in the context of separate conditions. This test needs to be performed to test for the third hypothesis.
3	The interaction of condition and time and affects $\tilde{\rho}$ or $\Delta\tilde{\rho}$	High	This provides the most information because changes in time during the exercise-until-fatigue condition could point to fatigue specific effects.

Table 5-3: Table describing the hypotheses that will be tested in Test 1 and Test 3.

Test 2 and Test 4 tested the means of $\tilde{\rho}$ and $\Delta\tilde{\rho}$ respectively for differences that would indicate a relationship to any of the levels of condition and areas. The test for effects of the conditions is the same as in test 1 and 3. Like time, the effect of areas

(differences between areas) is tested for all the conditions combined. This provides interesting information in the general sense but is not very relevant to the questions raised in this project. What is of importance in these tests is the interaction between areas and conditions. For example frontal-motor pairs may have greater $\tilde{\rho}$ values due to exercise-until-fatigue only. The hypotheses being tested in test 2 and 4 are summarized in Table 5-4.

	Hypothesis	**Relevance**	**Comment**
1	Condition affects $\tilde{\rho}$ or $\Delta\tilde{\rho}$	Yes	Determines if exercise-until-fatigue has a different effect to eyes closed or eyes open conditions.
2	Areas affects $\tilde{\rho}$ or $\Delta\tilde{\rho}$	Slight	The 'effects' of areas is a way of describing how values of $\tilde{\rho}$ or $\Delta\tilde{\rho}$ differ between areas. May be interesting in the general sense but more relevant when in the context of separate conditions. This test needs to be performed to test for the third hypothesis.
3	The interaction of condition and areas affects $\tilde{\rho}$ or $\Delta\tilde{\rho}$	High	This provides the most information because changes in areas because of the exercise-until-fatigue condition could point to fatigue specific effects.

Table 5-4: Table describing the hypotheses that will be tested in Test 2 and Test 4.

5.6.2.3 The Methodology of the ANOVA test procedure

The repeated ANOVA test has been discussed and the different hypotheses to be tested have been detailed. This section describes the testing procedure that was followed. The process is outlined in Figure 5-20 and is explained below.

Firstly the $\tilde{\rho}$ values where inspected for the assumption of being normally distributed. The $\tilde{\rho}$ values were not normally distributed but were skewed. A transformation was applied to all the $\tilde{\rho}$ values to correct for this. The transformation that was applied was the inverse hyperbolic tangent function ($\tanh^{-1}$). ANOVA is robust for reasonable violations in the assumption of normal distribution of the dependant variable and equality of variance across the groups [125].

Next the $\tilde{\rho}$ values that represent phase synchronization coefficients for 50 epochs per subject, electrode combination, frequency band and condition were collapsed in into six epochs. The differentiated coefficients $\Delta\tilde{\rho}$ between the 6 epochs were calculated providing 5 values of $\Delta\tilde{\rho}$ per subject, electrode combination, frequency band and condition. These values were then averaged for the areas treatment. The $\Delta\tilde{\rho}$ values were suitably normally distributed. The values of $\tilde{\rho}$ and $\Delta\tilde{\rho}$ were used to calculate the average of all the 2701 pairs, the prefrontal-motor pairs and the frontal-motor pairs. The data was then ready for the four ANOVA tests to be performed. The four tests were performed per frequency band. The statistical software package Statistica [126] was used to perform the ANOVA tests and the related statistical tests and calculations discussed below.

As part of the ANOVA tests the assumption of compound symmetry was tested. The test used is Mauchly's test of sphericity. If this test is significant the assumption of compound symmetry has not been met. The values of $\tilde{\rho}$ and $\Delta\tilde{\rho}$ for all the tests failed the test for sphericity and thus epsilon correction had to be applied. Of the three methods discussed above Greenhouse-Geisser was used as the method for epsilon correction as it is relatively conservative but not as conservative as the lower bound test. This provides an adjusted *F* statistic and *P* value that may be used to fail to reject or reject the null hypothesis.

Finally post-hoc analysis was performed where the mean value of the levels of each treatment are compared to each other. This is useful because the ANOVA test merely indicates if a particular treatment has an effect on the dependant variable or not. If a treatment has more than two levels it may not be clear which level or levels of the treatment are having the effect. For instance the ANOVA test may indicate that the levels of condition are having a significant effect on $\tilde{\rho}$. This information is of little use unless it can be shown that particular levels such as exercise-until-fatigue the cause of this effect. In the case of time having an effect, it also indicates which epoch or epochs are having the effect. A specific kind of test is used for post-hoc analysis: the Tukey HSD test. The Tukey HSD test is a multiple comparison procedure that tests for the null hypothesis that all possible treatment pairs have the same mean and is a relatively stringent test [127].

The outcome of the 16 tests is a set of probability values that can be used to judge whether a particular hypothesis is true. The comparisons of the means of the levels of each treatment provide further details about the effect. The outcome of the statistical tests will be discussed in the following chapter.

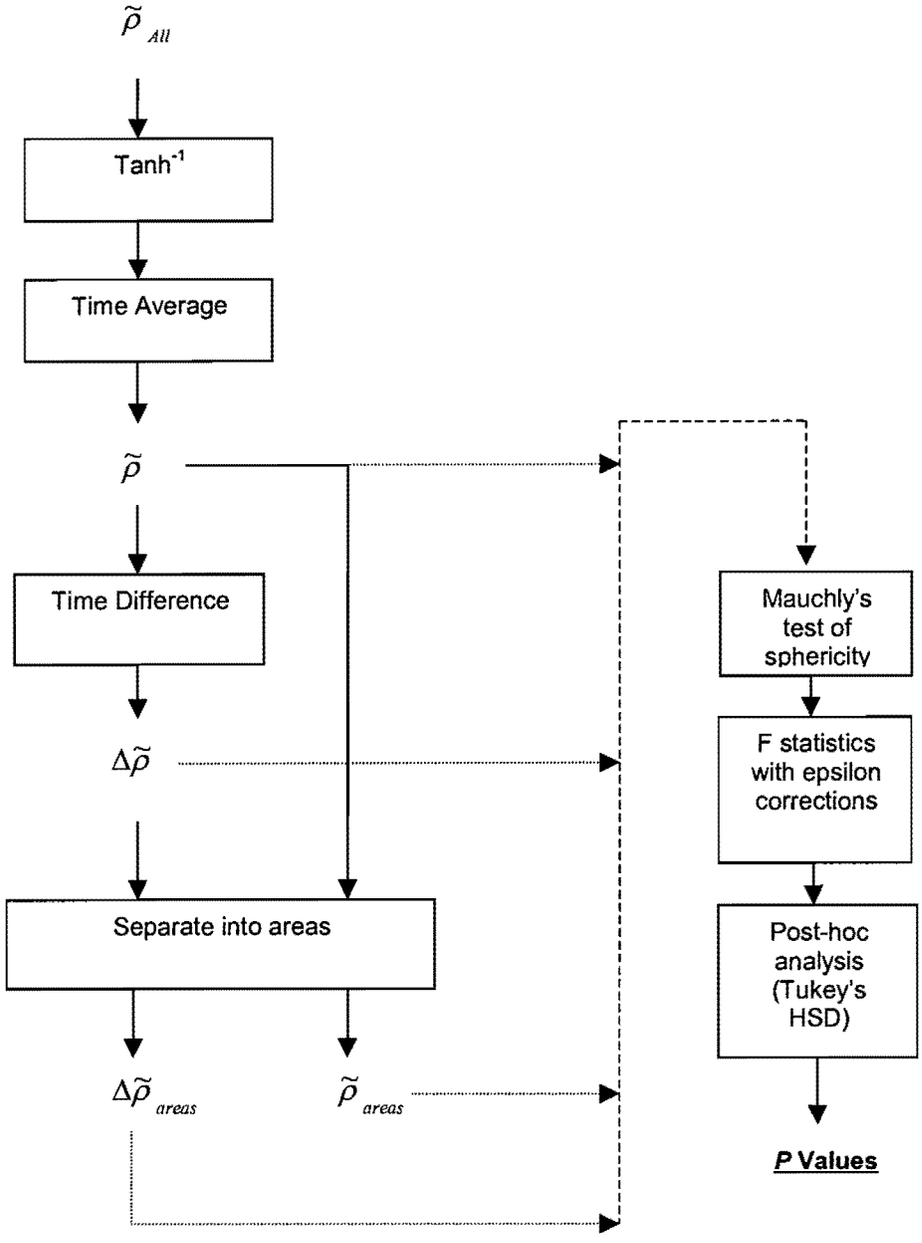

Figure 5-20: Outline of the methodology of the ANOVA test procedure.

5.6.3 Comparison Between the Head Map and ANOVA Methodology

The two methods of processing the phase synchronization coefficients, the use of head maps and statistical comparisons using ANOVA, offer different ways of extracting information from the data sets obtained from the exercise-until-fatigue trial. The two methods analysed the phase synchronization coefficients differently and were not necessarily directly comparable. The methodology for plotting head maps (see Section 5.6.1.2) involved the selection of 0.5% of the smallest and 0.5% of greatest values of $\Delta\tilde{\rho}$. For example, looking at an arbitrary sample distribution of $\Delta\tilde{\rho}$ in Figure 5-21, the methodology used for plotting head maps would have involved selecting the values lying in the shaded area of the distribution (representing 0.5% of the smallest and 0.5% of greatest values of $\Delta\tilde{\rho}$), whereas the methodology of the ANOVA tests (see Section 5.6.2.3) would have involved looking at every value in the distribution as shown in Figure 5-22.

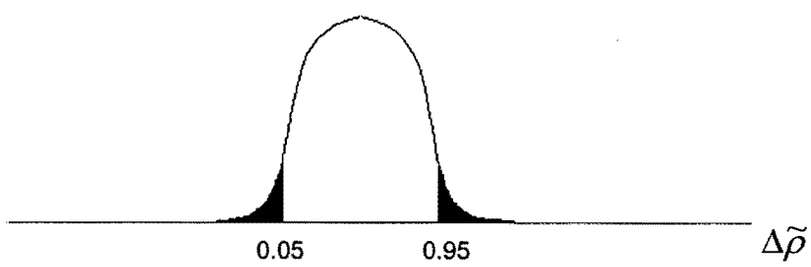

Figure 5-21: The distribution of an arbitrary sample of differentiated phase synchronization coefficients $\Delta\tilde{\rho}$, showing the 0.5% of the smallest and 0.5% of greatest values used in displaying the head maps.

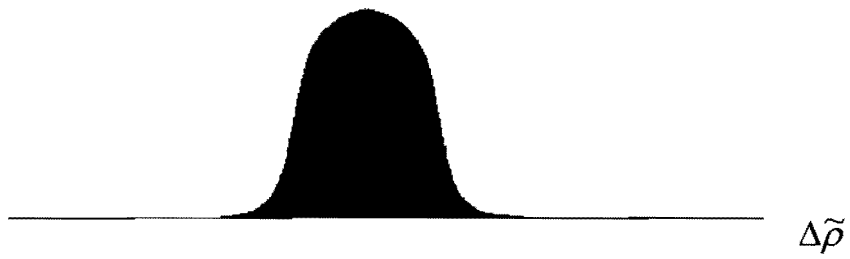

Figure 5-22: The distribution of an arbitrary sample of differentiated phase synchronization coefficients $\Delta\tilde{\rho}$ showing that all the values are used in the ANOVA tests.

So if a head map representing alpha phase synchronization indicates that the highest values of $\Delta\tilde{\rho}$ occur at the 5th epoch transition for the exercise-until-fatigue condition, this may not necessarily reflect in the corresponding ANOVA test comparing the levels of the condition and time factor. This is because the ANOVA test takes into account all the values, not just 0.5% of the smallest and 0.5% of greatest. The 0.5% of the smallest and 0.5% of greatest values of $\Delta\tilde{\rho}$ may not be 'extreme enough' to influence the total mean and variance of the $\Delta\tilde{\rho}$ sample distributions, which are calculated from many more numbers.

Similarly, a significant result in an ANOVA test, such as the $\Delta\tilde{\rho}$ of the prefrontal-motor pairs being significantly higher than the all-areas pairs for the exercise-until-fatigue condition, may not be reflected in the head maps. This may be because the values of the $\Delta\tilde{\rho}$ of the prefrontal-motor pairs are on average higher than the all areas pairs, but all the extremely high values of $\Delta\tilde{\rho}$ happen to coincidently form part of the all areas pairs group only and not the prefrontal-motor pairs group, and that the all areas pairs group also contains many low values of $\Delta\tilde{\rho}$ bringing down its average considerably.

6. RESULTS AND DISCUSSION

Phase synchronization coefficients were calculated for the eyes-open at rest, eyes-closed at rest and exercise-until-fatigue conditions for each of the eight subjects, 50 epochs, 2701 channel combinations and the frequency bands theta, alpha, beta and gamma, as well as for surrogate data which was processed in the same way as the trial data. The coefficients were processed and analysed in various ways as discussed in the methodology (Chapter 5). This chapter is a presentation of the outcome of that analysis and a presentation of the coefficients as well as a discussion and interpretation of the outcome of the analysis.

Firstly the distribution and time course of the coefficients and the differentiated coefficients are presented and discussed (Section 6.1). Then the head maps are presented (Section 6.2.1) and discussed (Section 6.2.2) and finally the results of the statistical analysis is shown and discussed (Section 6.3.1 to 6.3.9). A brief discussion of the results forms part of each presentation and a more thorough discussion and interpretation of the results and the investigation as a whole follows the presentation of all the data (Section 6.4 and 6.5).

6.1 Distribution and Time-Course of the Phase Synchronization Coefficients

Figures 6-1 – 6-5 illustrate the general characteristics of the phase synchronization coefficients $\tilde{p}$ for each of the eyes-closed, eyes-open and exercise-until-fatigue conditions and the shifted surrogate data. The data here shows general trends in the values of the coefficients for each of the conditions and the shifted surrogate data. The data here provides an opportunity for some elementary comparisons to be made based on visual inspection, as well as providing a basis for further refined comparisons which follow in the next sections.

Five figures are presented here; Figure 6-1 and Figure 6-2 show the distribution of all the phase synchronization coefficients $\tilde{\rho}$ and all the differentiated phase synchronization coefficients $\Delta\tilde{\rho}$ respectively for all channel combinations, subjects and frequency bands for each of the conditions and the shifted surrogate data; Figure 6-3 and Figure 6-4 show the time course of the mean phase synchronization coefficients $\bar{\tilde{\rho}}$ and the mean differentiated phase synchronization coefficients $\Delta\bar{\tilde{\rho}}$ respectively for each of the conditions and the shifted surrogate data. The mean $\bar{\tilde{\rho}}$ for each of the 50 epochs was determined by averaging over all channel combinations, subjects and frequency bands for each of the conditions and the shifted surrogate data. The mean $\Delta\bar{\tilde{\rho}}$ for each of the 50 epochs was determined by averaging over all channel combinations, subjects and frequency bands for each of the conditions and the shifted surrogate data. Figure 6-5 is similar to Figure 6-4 except it shows the time course of the mean of the absolute values of the differentiated phase synchronization coefficients $\left|\Delta\bar{\tilde{\rho}}\right|$, for each of the 50 epochs for all channel combinations, subjects and frequency bands for each of the conditions and the shifted surrogate data.

[6.1.1] The distribution of the phase synchronization coefficients $\tilde{\rho}$ for the different conditions is shown in Figure 6-1 a – c, and for the shifted surrogate data in Figure 6-1 d. Comparing the distributions of the 3 conditions (a-c) to the distribution of the shifted surrogate data (d), the distributions of the 3 conditions has a long upper tail and the distributions of the 3 conditions are flatter indicating that the values of $\tilde{\rho}$ are more spread out. This should be expected, as $\tilde{\rho}$ for the 3 conditions, which represent coupling between cortical sites[3] for the 3 conditions, will vary between 0 and 1 depending on the strength of coupling. The $\tilde{\rho}$ values of the shifted surrogate data also produce a type of distribution to be expected. In this case, $\tilde{\rho}$ was calculated between epochs in the (random) surrogate data that did not coincide with time. Thus no phase synchronization is expected, other than that calculated by chance coincidences of phase relationships. This value is low ($\bar{\bar{\tilde{\rho}}}$ = 0.06) with most

[3] It could also represent coupling between deep brain structures. Please see Section 3.1.1 for a discussion on this matter.

of the values being distributed near this value i.e. the data has a low variance. These graphs clearly indicate that $\tilde{\rho}$ calculated from the trial data represent real phase synchronization between cortical sites while that calculated from the shifted surrogate data represent chance or random background phase synchronization and provides confidence in the phase synchronization calculation technique.

Comparing the distributions of $\tilde{\rho}$ of the 3 conditions (a-c) to each other it can be seen that the peaks of the distributions for the eyes-closed (a) and eye-open condition (b) are similar but in the distribution for the exercise-until-fatigue condition (c) the peak is found at a lower value, indicating on average $\tilde{\rho}$ for the exercise-until-fatigue condition has a lower value. This further indicates that for the exercise-until-fatigue condition the average strength of coupling between cortical sites is less than that of the eyes-closed and eye-open conditions.

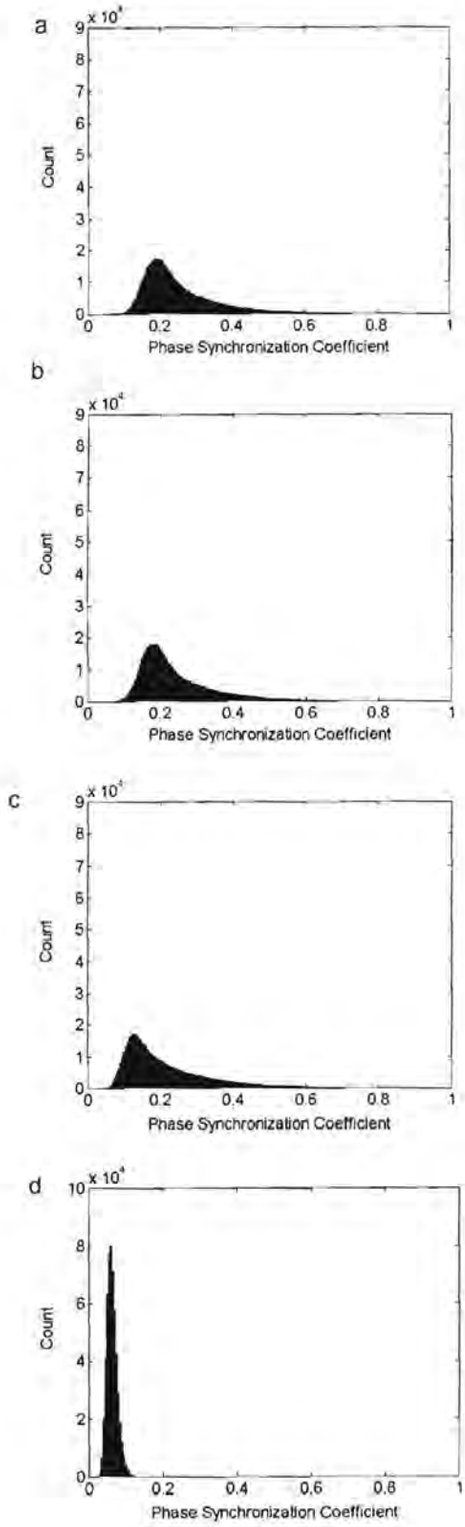

Figure 6-1: The distribution of the phase synchronization coefficients $\tilde{\rho}$. The distribution is shown for $\tilde{\rho}$ for all 50 epochs, channel combinations, subjects and frequency bands in the eyes-closed (a), eyes-open (b) and exercise-until fatigue (c) conditions, and shifted surrogate data (d).

[6.1.2] The distribution of the differentiated phase synchronization coefficients $\Delta\tilde{\rho}$ for the different conditions is shown in Figure 6-2 a – c, and for the shifted surrogate data in Figure 6-2 d. Here all the distributions are approximately normal, indicating that there are approximately equal numbers of positive and negative $\Delta\tilde{\rho}$ values. In fact for the shifted surrogate data this is almost exactly the case with 50% of the values falling below and above zero. For the eyes-open condition 49% of the values are positive and 51% negative, for the eye-closed condition 50% of the values are positive and 50% negative and for the exercise-until-fatigue condition 52% of the values are positive and 48% negative, so there is a slight tendency for phase synchronization to be increasing across time for the exercise-until-fatigue condition.

Comparing the distributions of the 3 conditions Figure 6-2 a-c to each other it can be seen that the peaks of the distributions for the eyes-closed (a) and eye-open condition (b) are similar but in the distribution of the exercise-until-fatigue condition (c) the peak is not as sharp although the difference is quite small. This indicates that there is slightly greater variance in $\Delta\tilde{\rho}$ in the exercise-until-fatigue condition, indicating that phase synchronization in the exercise-until-fatigue condition shows more variability.

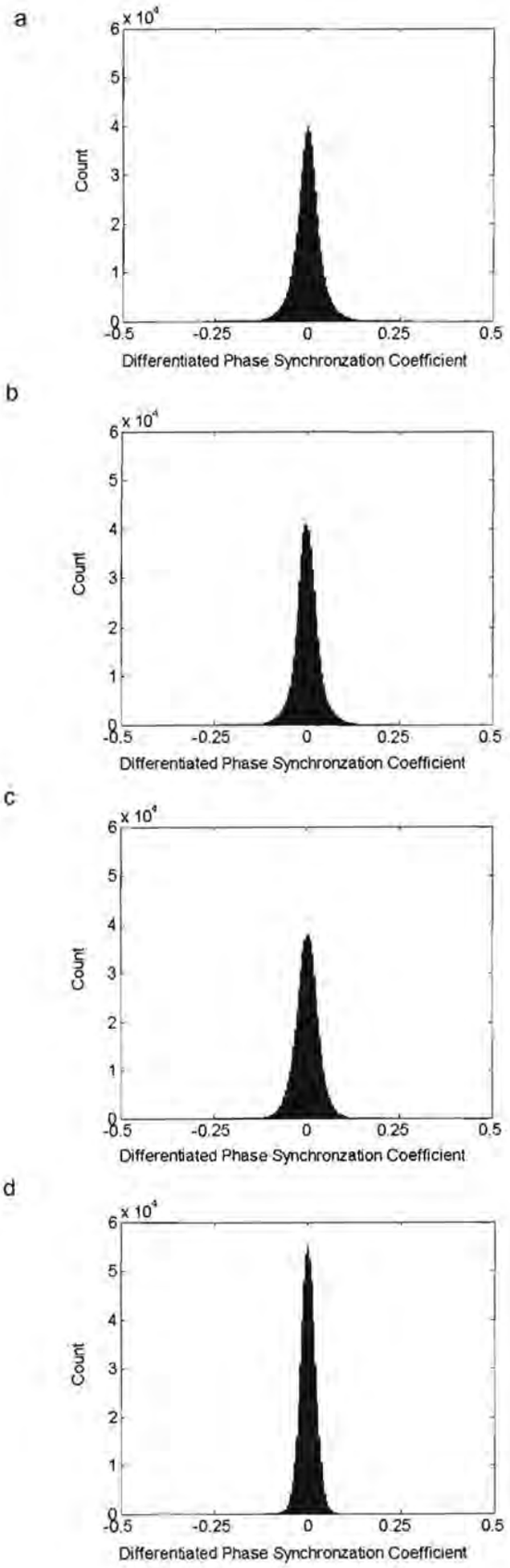

Figure 6-2: The distribution of the differentiated phase synchronization coefficients $\Delta\tilde{\rho}$. The distribution is shown for $\Delta\tilde{\rho}$ for all 49 epoch transitions, channel combinations, subjects and frequency bands in the eyes-closed (a), eyes-open (b) and exercise-until fatigue (c) conditions, and shifted surrogate data (d).

[6.1.3] The same values shown in the distributions in Figure 6-1 and Figure 6-2 are plotted in time in Figure 6-3 and Figure 6-4 respectively. The values of $\tilde{\rho}$ and $\Delta\tilde{\rho}$ are averaged across channel combinations, subjects and frequency bands per epoch for each condition respectively and are represented by $\bar{\tilde{\rho}}$ and $\Delta\bar{\tilde{\rho}}$ respectively. The absolute values of $\Delta\tilde{\rho}$ were also plotted in Figure 6-5 and are represented by $\overline{|\Delta\tilde{\rho}|}$.

Figure 6-3 a – c is the plot of $\bar{\tilde{\rho}}$ for each condition. For each of these plots there is a superimposed plot of $\bar{\tilde{\rho}}$ for the shifted surrogate data. Figure 6-4 a – c are plots of $\Delta\bar{\tilde{\rho}}$ for each condition. Figure 6-4 d – f is a plot of $\Delta\bar{\tilde{\rho}}$ for the shifted surrogate data. Figure 6-5 a – c are plots of the absolute values of the differentiated phase synchronization coefficients for each condition. Figure 6-5 d – f is a plot of the absolute values of the differentiated phase synchronization coefficients for shifted surrogate data. Figure 6-4 and Figure 6-5 are plots of the same data except in the latter case the $\overline{|\Delta\tilde{\rho}|}$ values are plotted. This is done for comparison purposes and is discussed below.

Comparing the plots of $\bar{\tilde{\rho}}$ for the 3 conditions (Figure 6-3 a – c) to the superimposed plot of $\bar{\tilde{\rho}}$ for shifted surrogate data the smaller mean and standard deviation of the shifted surrogate data is clearly visible and is agreement with the observations made in the distributions of these values in Figure 6-1 d. The slightly smaller mean for the exercise-until-fatigue data ($\bar{\tilde{\rho}}$ = 0.22 for exercise-until-fatigue compared to $\bar{\tilde{\rho}}$ = 0.26 for eyes-closed and $\bar{\tilde{\rho}}$ = 0.25 for eyes-open) is also apparent in Figure 6-3 c and is in agreement with the graphs of the distribution (Figure 6-1 c).

What is noteworthy in Figure 6-3 a – c is the time course of $\bar{\tilde{\rho}}$; on average the values of $\bar{\tilde{\rho}}$ tend to remain fairly constant throughout the trials although the values are not nearly as static as those seen in the superimposed shifted surrogate data. Looking at the exercise-until-fatigue condition (Figure 6-3 c) on average there are no obvious changes across time that could be a marker of fatigue.

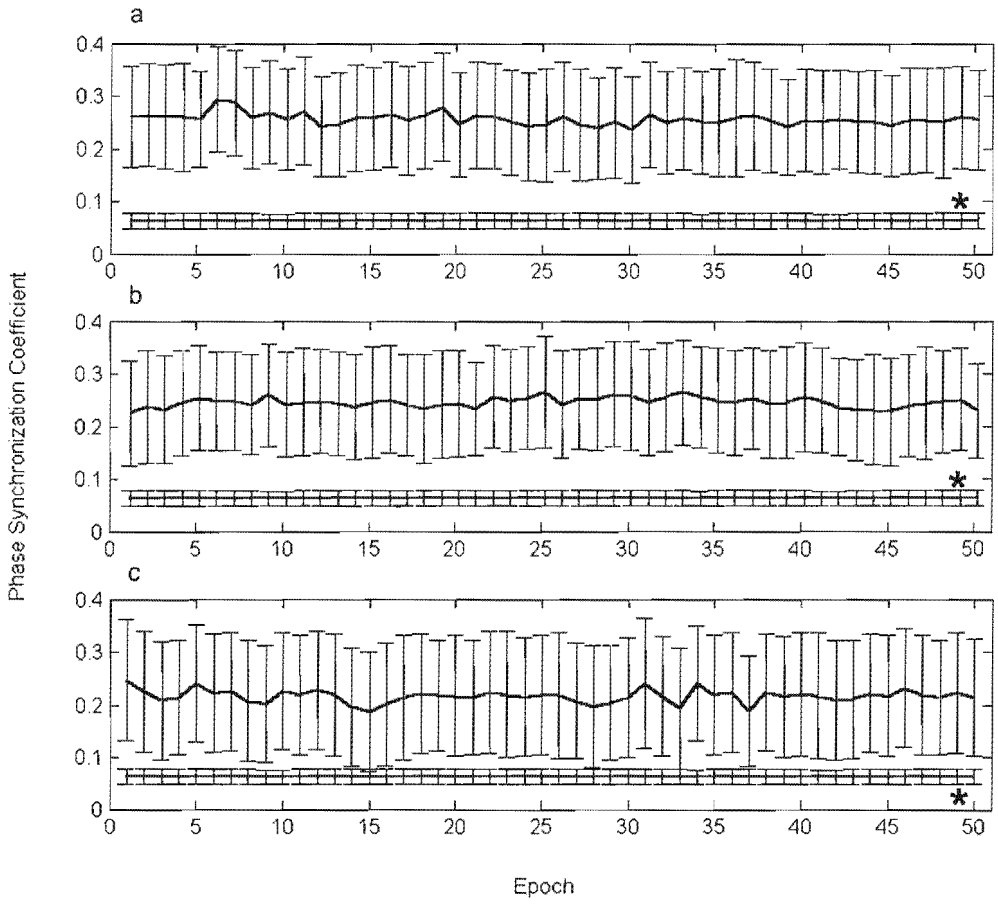

Figure 6-3: The time course of the mean phase synchronization coefficients $\overline{\overline{\rho}}$. The plots show $\overline{\overline{\rho}}$ of the 50 epochs for all channel combinations, subjects and frequency bands of the exercise-until-fatigue (a) ($\overline{\overline{\rho}}$ = 0.22), eyes-closed (b) ($\overline{\overline{\rho}}$ = 0.26) and eyes-open (c) ($\overline{\overline{\rho}}$ = 0.25) conditions. On each graph (a) – (c), 50 values of the $\overline{\overline{\rho}}$ of the shifted surrogate data are superimposed ($\overline{\overline{\rho}}$ = 0.06) as indicated by the asterisks (*). The error bars indicate the standard error.

[6.1.4] The plots of $\Delta\bar{\bar{\bar{\rho}}}$ of the three conditions (Figure 6-4 a – c) show greater variability in their means and standard deviations. The $\Delta\bar{\bar{\rho}}$ of the shifted surrogate data show very little variability in its mean and standard deviation as expected from randomised data (Figure 6-4 d – f). The $\Delta\bar{\bar{\bar{\rho}}}$ values are also of the order of 10 times smaller than the $\bar{\bar{\rho}}$ values. The $\Delta\bar{\bar{\bar{\rho}}}$ values of the shifted surrogate case are close to zero which should also be expected, as on average, there should be no change in the level of random background phase synchronization ($\Delta\bar{\bar{\bar{\rho}}}$ = -0.0000049). This provides confidence in the phase synchronization calculation technique. The values of the mean and standard deviation are however comparable (they look quite similar) between the conditions and shifted surrogates. However the mean of the surrogate data ($\Delta\bar{\bar{\bar{\rho}}}$ = -0.0000049) is in the order of 100 times smaller than $\Delta\bar{\bar{\bar{\rho}}}$ for the three conditions ($\Delta\bar{\bar{\bar{\rho}}}$ = 0.00018, -0.00010 and 0.00068 for the eyes-open, eyes-closed and exercise-until-fatigue conditions respectively). To highlight absolute differences between the conditions and the shifted surrogates, the absolute values of $\Delta\bar{\bar{\rho}}$ were taken before averaging and then plotted in the same way. This is shown in Figure 6-5 a – f. Only the positive values of the standard error were plotted. This was to highlight the peaks and troughs of the time course of $\overline{|\Delta\tilde{\rho}|}$.

Looking at Figure 6-5 a – c and Figure 6-5 d – f the variability of the means and standard deviations of the three conditions is accentuated compared to those of the shifted surrogates. The values of the data for the 3 conditions (Figure 6-5 a – c) have peaks that move about a similar mean ($\overline{\overline{|\Delta\tilde{\rho}|}}$ = 0.025, 0.024 and 0.024 respectively for eyes-closed, eyes-open and exercise-until-fatigue). The mean $\overline{\overline{|\Delta\tilde{\rho}|}}$ of the shifted surrogates is 0.016. Peaks in the plots are indicative of increased and/or decreased phase synchronization between epochs. Both the exercise-until-fatigue (Figure 6-5 c) and eyes-closed (Figure 6-5 a) have many peaks compared to the relatively static eyes-open condition (Figure 6-5 b). The peaks occurring in the exercise-until- fatigue (Figure 6-5 c) condition between epochs 30 and 40 may be a marker of the fatigue process, but compared to similarity in values of the peaks in the eyes-closed (Figure 6-5 a) condition a simple inspection cannot provide any evidence of an obvious marker of fatigue.

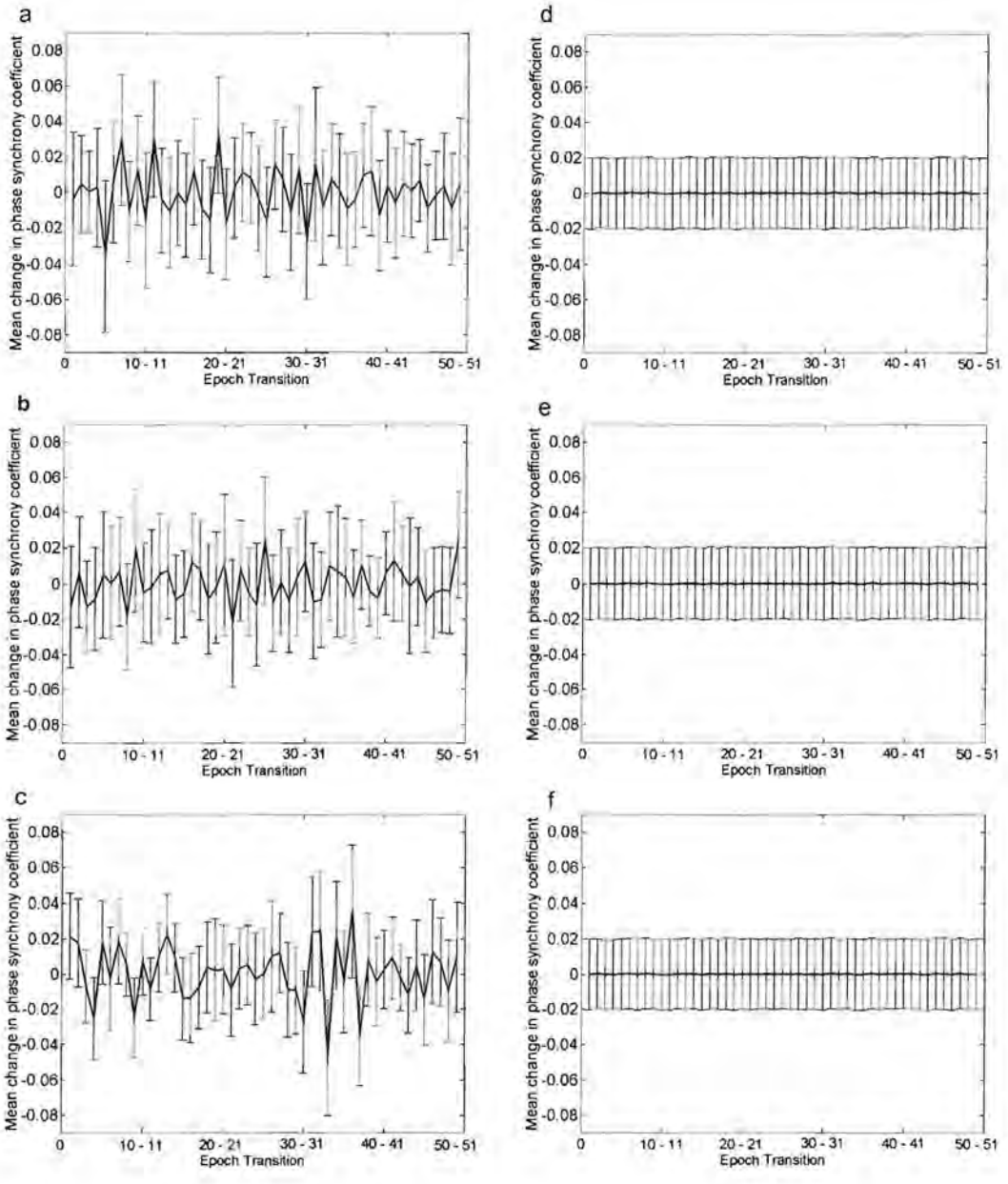

Figure 6-4: The time course of the mean differentiated phase synchronization coefficients $\Delta\tilde{\tilde{\rho}}$ at each epoch transition; values of $\Delta\tilde{\tilde{\rho}}$ between shifted surrogate data epochs (identical graphs d,e,f). The plots a – c show $\Delta\tilde{\tilde{\rho}}$ for each of the 49 epoch transitions for all channel combinations, subjects and frequency bands of the eyes-closed (a) ($\Delta\tilde{\tilde{\rho}}$ = 0.00018), eyes-open (b) ($\Delta\tilde{\tilde{\rho}}$ = -0.00010) and exercise-until-fatigue (c) ($\Delta\tilde{\tilde{\rho}}$ = 0.00068) conditions. Alongside each graph a – c, is a plot $\Delta\tilde{\tilde{\rho}}$ between shifted surrogate data epochs (d – f) ($\Delta\tilde{\tilde{\rho}}$ = -0.0000049) (repeated for the purpose of comparison). The error bars indicate the standard error.

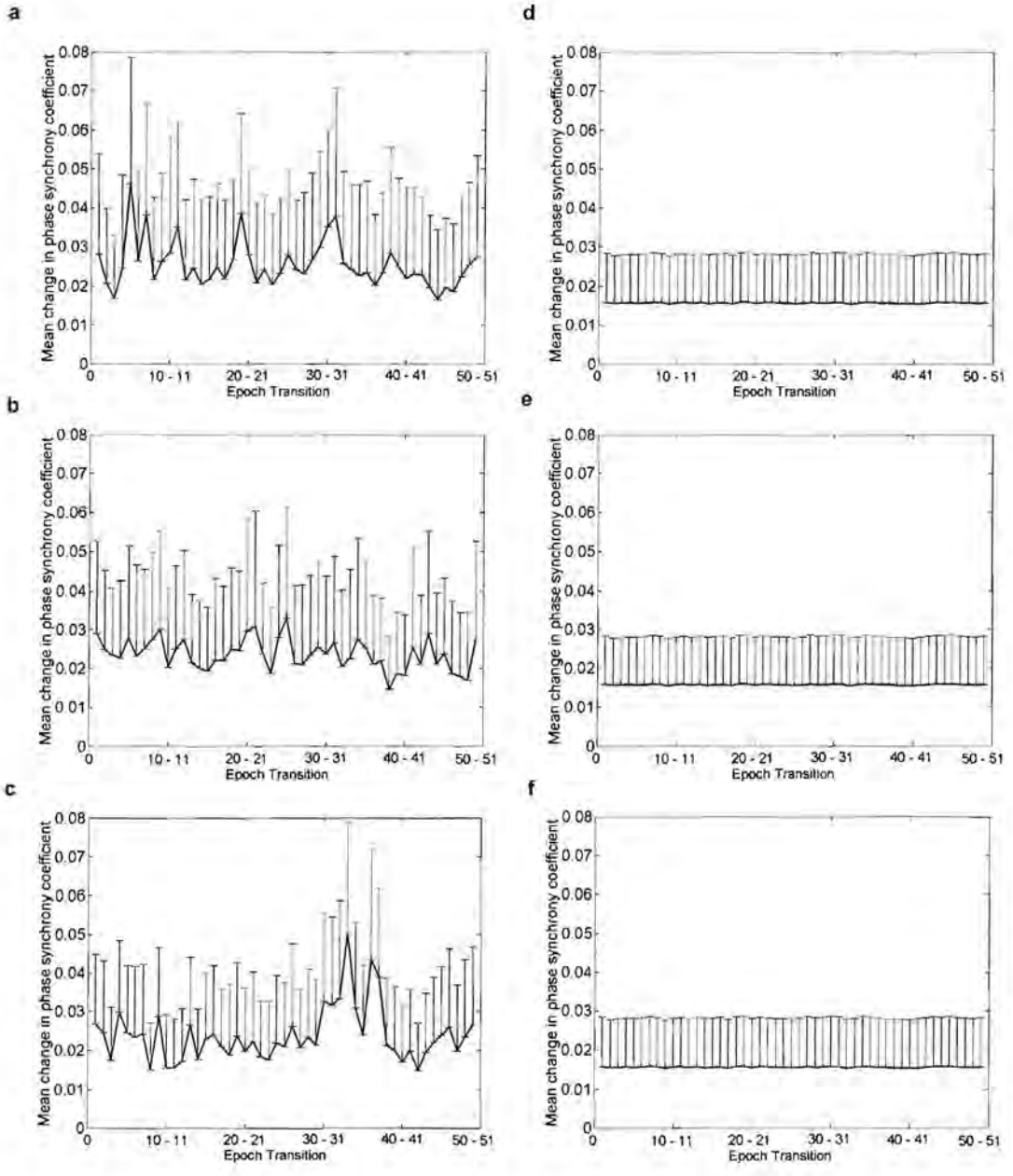

Figure 6-5: The time course of the absolute values of the differentiated phase synchronization coefficients $\overline{|\Delta\tilde{\rho}|}$ between epochs; $\overline{|\Delta\tilde{\rho}|}$ between shifted surrogate data epochs (identical graphs d,e,f). The plots a – c show $\overline{|\Delta\tilde{\rho}|}$ for each of the 49 epoch transitions for all channel combinations, subjects and frequency bands of the eyes-closed (a) ($\overline{\overline{|\Delta\tilde{\rho}|}}$ = 0.025), eyes-open (b) ($\overline{\overline{|\Delta\tilde{\rho}|}}$ = 0.023) and exercise-until-fatigue (c) ($\overline{\overline{|\Delta\tilde{\rho}|}}$ = 0.024) conditions. Alongside each graph a – c, is a plot of $\overline{|\Delta\tilde{\rho}|}$ between shifted surrogate data epochs (d – f) ($\overline{\overline{|\Delta\tilde{\rho}|}}$ = 0.016) (repeated for the purpose of comparison). The error bars indicate the standard error and only positive values are shown for clarity.

The following points provide qualitative summary of the data presented in Figure 6-1 to Figure 6-5:

- The phase synchronization of the shifted surrogates has a small mean and standard deviation and indicates a value of phase synchronization for chance synchronization.
- The $\Delta\tilde{\rho}$ of the shifted surrogates has a constant mean of nearly zero and a small constant standard deviation.
- The above points provide confidence in the phase synchronization calculation technique
- For the exercise-until-fatigue condition phase synchronization is less than that of the eyes-closed and eye-open conditions.
- Looking at phase synchronization in the exercise-until-fatigue condition on average there are no obvious changes across time that could be a marker of fatigue.
- Looking at differentiated phase synchronization in the exercise-until-fatigue condition on average there are no changes across time that could be a clear marker of fatigue although peaks between epochs 30 and 40 could point to some effect.

The data shown here provides a basis for further analysis and discussion for the data produced by the ANOVA tests and the head maps.

6.2 Head Maps

The 5 values of the differentiated phase synchronization coefficients $\Delta\tilde{\rho}$, representing the time course $\Delta\tilde{\rho}$, for all channel combinations averaged over subjects for a particular band were ranked and the highest 0.5% and the lowest 0.5% of the ranked values were retained and plotted on head map series. Please see Section 5.6.1.2 for the detailed procedure that was followed for plotting head maps.

Only the alpha head maps will be presented here, as they are the only set of maps ones showing remarkable patterns. The head maps for theta, beta and gamma are shown in Appendix J. The first set of head maps to be presented show alpha phase synchronization for the exercise-until-fatigue, eyes-closed and eyes-open conditions. Firstly the exercise-until-fatigue condition is shown next to the eyes-closed condition (Figure 6-6), and then the exercise-until-fatigue condition is shown next to the eyes-open condition (Figure 6-7). The second set of head maps to be presented show alpha phase desynchronization for the exercise-until-fatigue, eyes-closed and eyes-open conditions. The exercise-until-fatigue condition is shown next to the eyes-closed condition (Figure 6-8), and then the exercise-until-fatigue condition is shown next to the eyes-open condition (Figure 6-9). Finally phase desynchronization and phase synchronization for the exercise-until-fatigue condition is shown in Figure 6-10.

6.2.1 Alpha Synchronization and Desynchronization Maps

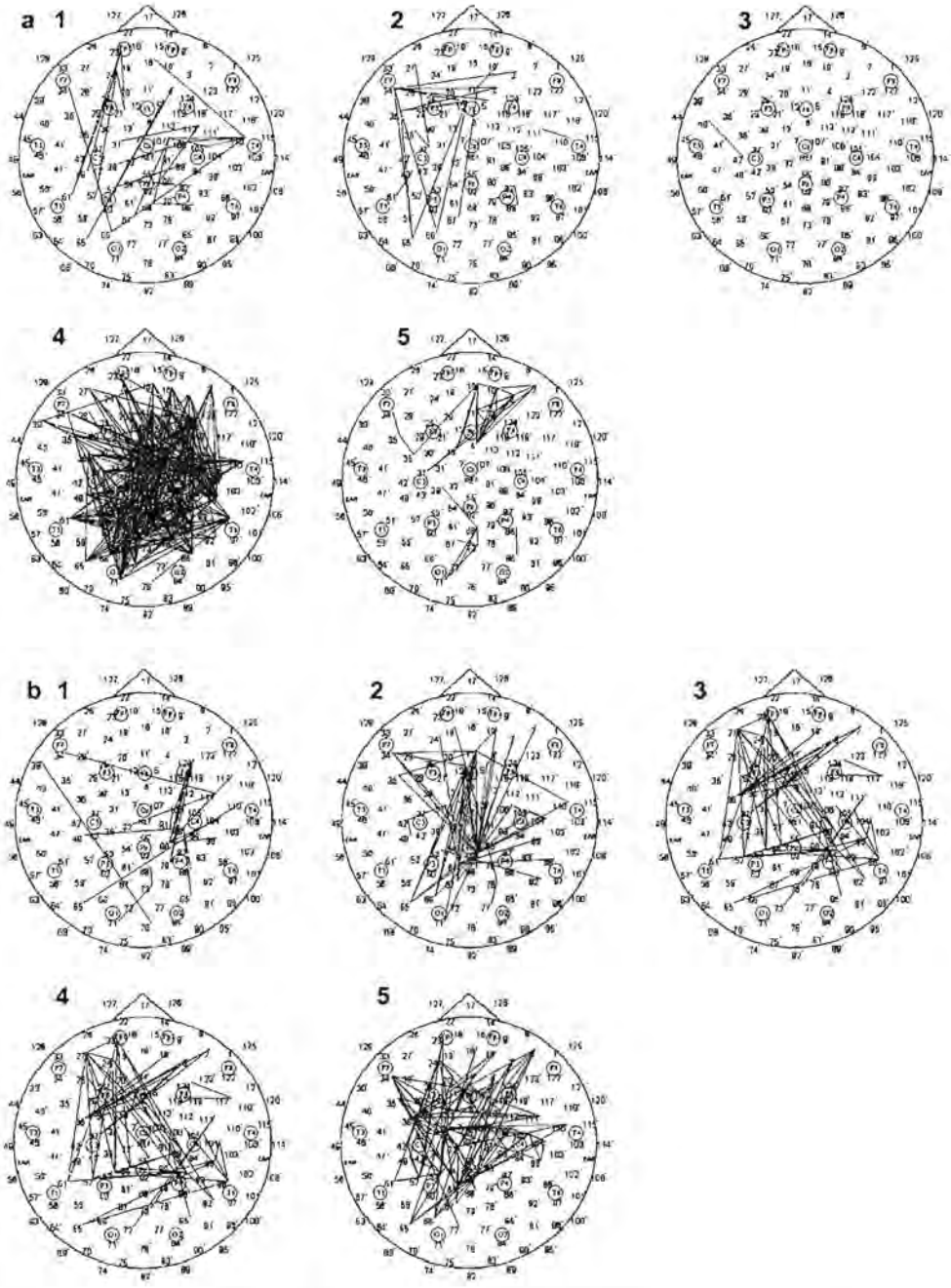

Figure 6-6: Alpha phase synchronization for the exercise-until-fatigue (a) and the eyes-closed condition (b) for each epoch transition 1-5 (indicated on each head map). Note that a line indicates a $\Delta\widetilde{\rho}_{\alpha}$ value above a certain threshold. Please see Section 5.6.1.2 and Figure 5-18 for a description of how the threshold value was determined.

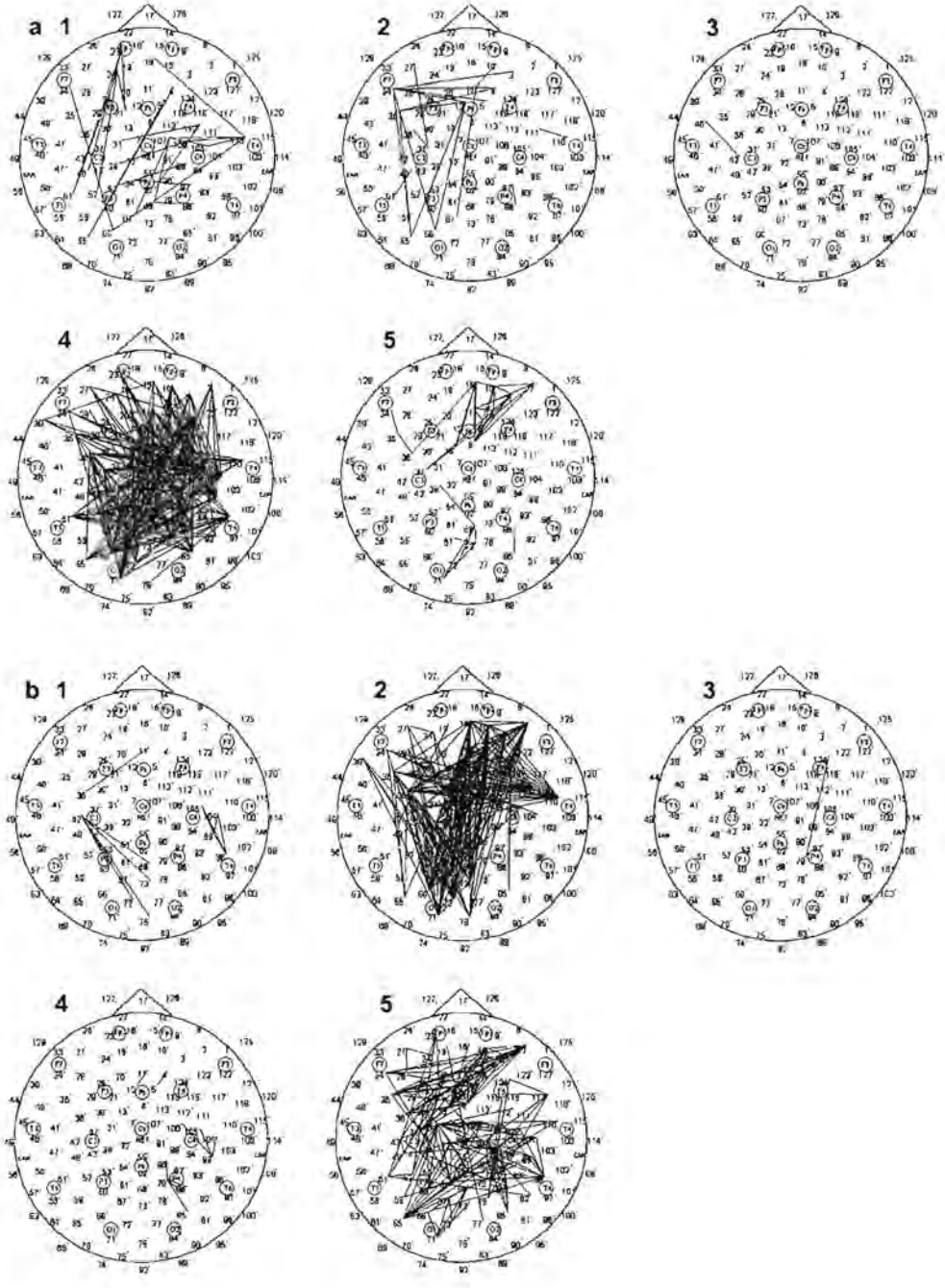

Figure 6-7: Alpha phase synchronization for the exercise-until-fatigue (a) and the eyes-open condition (b) for each epoch transition 1-5 (indicated on each head map). Note that a line indicates a $\Delta\tilde{\rho}_{\alpha}$ value above a certain threshold. Please see Section 5.6.1.2 and Figure 5-18 for a description of how the threshold value was determined.

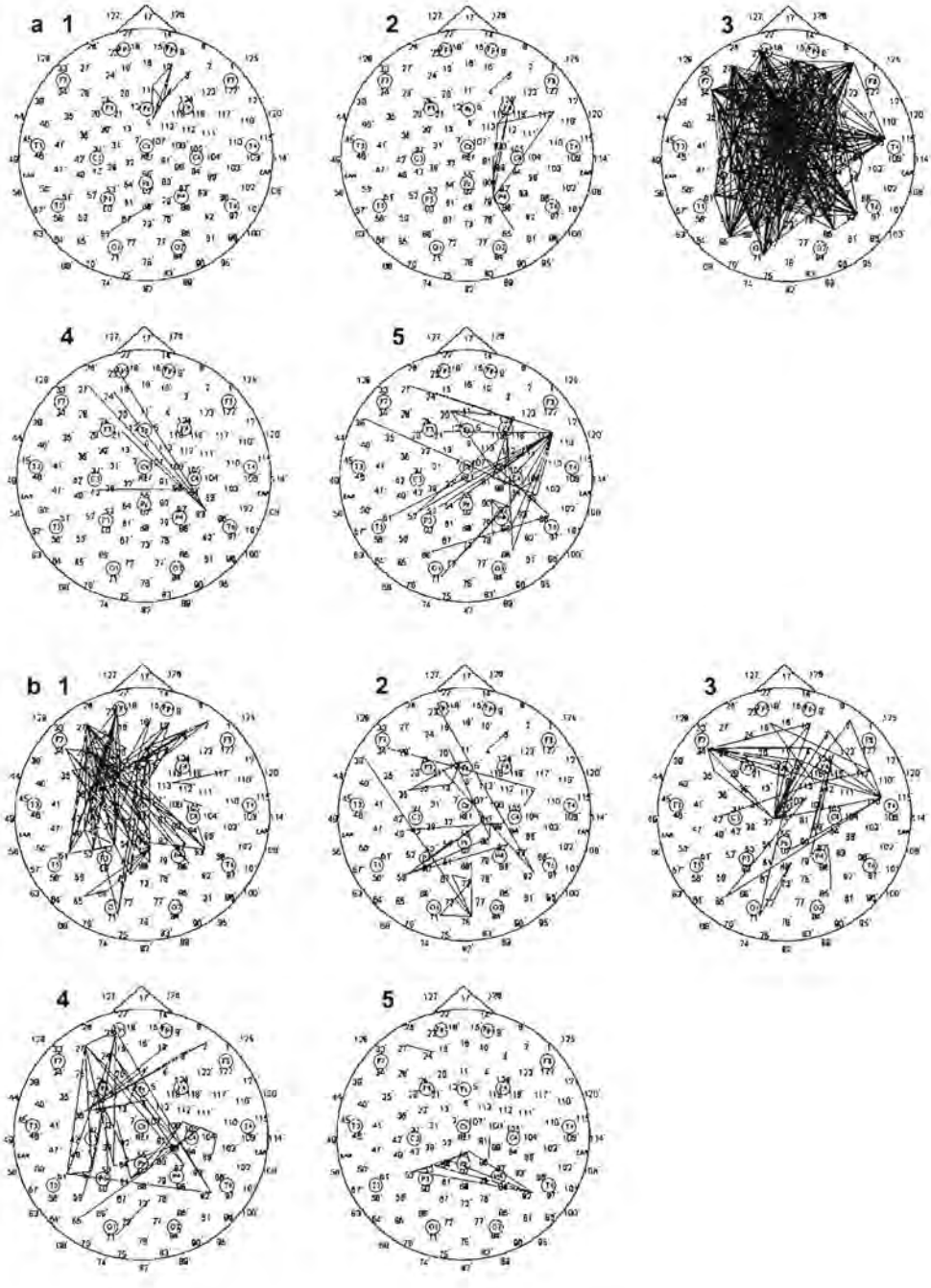

Figure 6-8: Alpha phase desynchronization for the exercise-until-fatigue (a) and the eyes-closed condition (b) for each epoch transition 1-5 (indicated on each head map). Note that a line indicates a $\Delta\widetilde{\rho}_{\alpha}$ value below a certain threshold. Please see Section 5.6.1.2 and Figure 5-18 for a description of how the threshold value was determined.

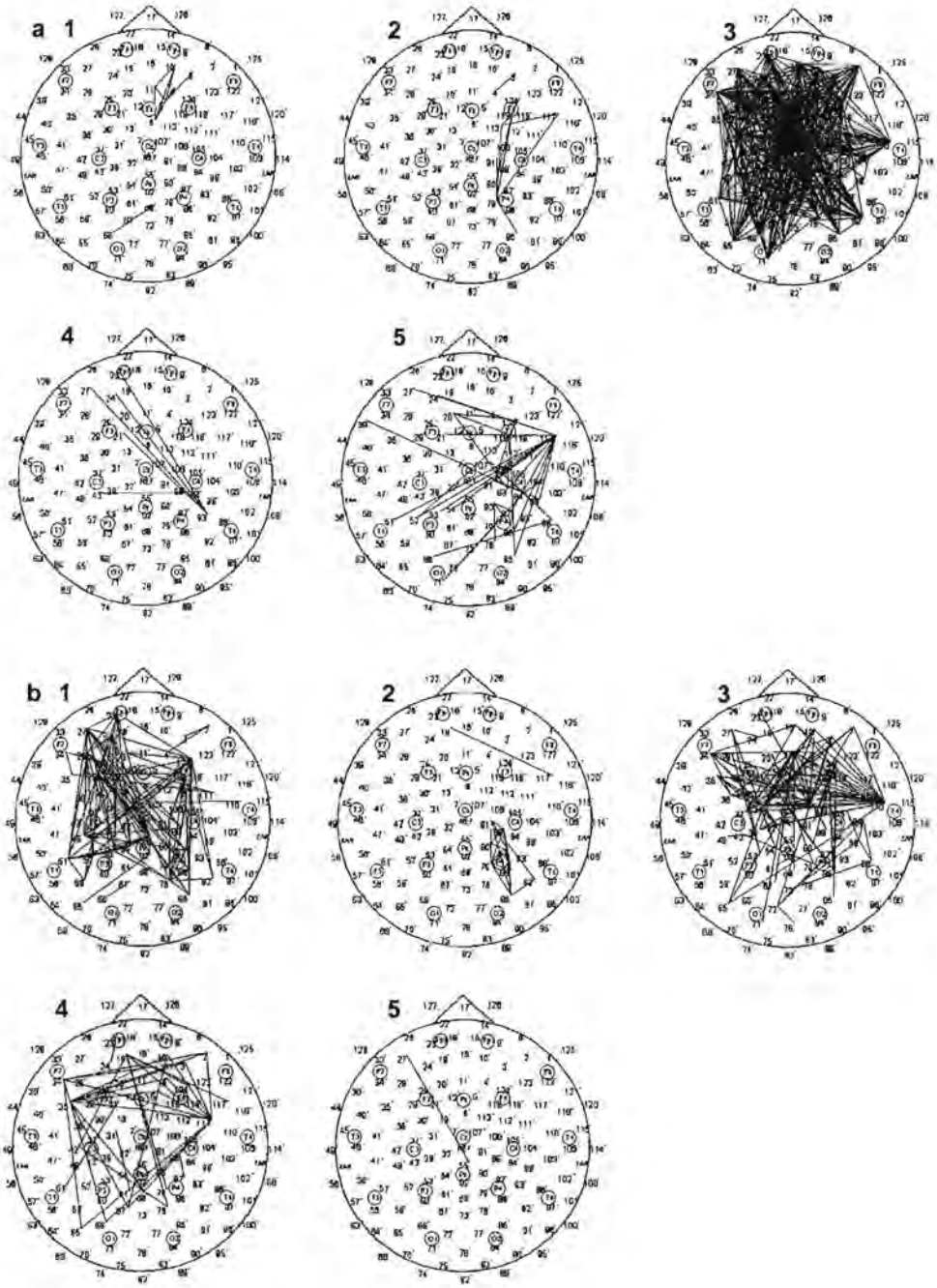

Figure 6-9: Alpha phase desynchronization for the exercise-until-fatigue (a) and the eyes-open condition (b) for each epoch transition 1-5 (indicated on each head map). Note that a line indicates a $\Delta\widetilde{\rho}_{\alpha}$ value below a certain threshold. Please see Section 5.6.1.2 and Figure 5-18 for a description of how the threshold value was determined.

6.2.2 Discussion: Alpha Synchronization and Desynchronization

The maps provide a way of observing where the greatest amount of synchronization and desynchronization is occurring in time and space and under what condition. What is clear is that there is strong synchronization or desynchronization at almost all time points and all conditions. Some time frames display more of this phenomenon than others. This is an interesting phenomenon and indicates that at any time there is active coupling and decoupling in the cortex of healthy awake individuals. There are no known published studies to date describing cortical phase synchronization patterns for either exercise or relaxed eyes-closed or eye-open states in this manner.

What is particularly noteworthy is the massive desynchronization pattern at epoch transition 3 (Figure 6-10 a no. 3) followed by a massive synchronization pattern at epoch transition 4 (Figure 6-10 b no. 4) in the exercise-until-fatigue condition. This pattern is absent from all epochs in the other conditions. The desynchronization pattern observed in Figure 6-10 a (no. 3) shows the participation of many electrode combination pairs across the entire cortex. The synchronization pattern that follows (Figure 6-10 b no. 4) seems to recruit less electrode pairs although it is still widespread across the cortex. Further interpretations of the data presented here will be discussed in the general discussion, after presentation of the ANOVA test results.

6.3 ANOVA Results and Plots of Factor Means

The results of the sixteen ANOVA tests with supporting graphics are presented in this section. Four kinds of tests were performed, for each of the four frequency band treatments. Tests 1 and 2 were applied to the phase synchronization coefficients $\tilde{\rho}$ and tests 3 and 4 were applied to the differentiated phase synchronization coefficients $\Delta\tilde{\rho}$. The tests are summarized in Table 5-2.

Test 1 and Test 3 tested the means of $\tilde{\rho}$ and $\Delta\tilde{\rho}$ respectively for a relationship with the different levels of the condition and time (independently) and for an interaction between the levels of time and condition. There are three levels of condition for both

tests (exercise-until-fatigue, eyes-closed and eyes-open) and 6 levels of time for test 1 (6 epochs) and 5 levels of time for Test 2 (5 transitions between epochs). Details of Test 1 and Test 3 are described in Table 5-3.

Test 2 and Test 4 tested the means of $\widetilde{\rho}$ and $\Delta\widetilde{\rho}$ respectively for a relationship with the different levels of the condition and areas (independently) and for an interaction between the levels of time and areas. There are three levels of condition for both tests (exercise-until-fatigue, eyes-closed and eyes-open) and 3 levels for areas (all pairs, frontal-motor pairs and prefrontal-motor pairs). Details of Tests 2 and Test 4 are described in Table 5-4.

The outcome of each test for each factor being compared is the *F* statistic and *P* value. For each test, three methods of epsilon correction were applied thus there are three values for *F* and *P*. *P* values were chosen to be significant below 0.05, a standard level of significance in most scientific literature.

The outcome of each of the 16 tests will be presented below if there are any significant differences found for any factor or interaction only. The results of each test will be discussed after its presentation. The results of all the tests can be found in Appendix J.

6.3.1 ANOVA Results of Test 1 (Condition, Time): All Bands

The outcome for Test 1 for all the frequency bands produced no significant results. The results of the tests are shown in Appendix J.

6.3.2 ANOVA Results of Test 2 (Condition, Areas): Theta Band

The result of Test 2 for the theta band is shown in Table 6-1. The factors were condition and areas and the dependant variable was the theta phase synchronization $\widetilde{\rho}_{\theta}$.

Factor	Epsilon Correction	F Statistic	P Value
Condition	Greenhouse-Geisser	2.276	0.166
Areas	Greenhouse-Geisser	56.892	0.000
Condition * Areas (Interaction)	Greenhouse-Geisser	1.577	0.249

Table 6-1: For the theta band, the output of ANOVA Test 2 (condition, areas).

The results of the test show that condition alone did not significantly affect $\tilde{\rho}_\theta$. Areas did affect $\tilde{\rho}_\theta$. The interaction between areas and condition was not significant.

6.3.3 ANOVA Results of Test 2 (Condition, Areas): Alpha Band

The result of Test 2 for the alpha band is shown in Table 6-2. The factors were condition and areas and the dependant variable was alpha phase synchronization $\tilde{\rho}_\alpha$.

Factor	Epsilon Correction	F Statistic	P Value
Condition	Greenhouse-Geisser	1.542	0.255
Areas	Greenhouse-Geisser	9.414	0.009
Condition * Areas (Interaction)	Greenhouse-Geisser	4.419	0.054

Table 6-2: For the alpha band, the output of ANOVA Test 2 (condition, areas).

The results of the test show that condition alone did not significantly affect $\tilde{\rho}_\alpha$. Areas did affect $\tilde{\rho}_\alpha$. The interaction between areas and condition is not significant.

6.3.4 ANOVA Results of Test 2 (Condition, Areas): Beta Band

The result of Test 2 for the beta band is shown in Table 6-3. The factors were condition and areas and the dependant variable was beta phase synchronization $\tilde{\rho}_{\beta}$.

Factor	Epsilon Correction	F Statistic	P Value
Condition	Greenhouse-Geisser	0.573	0.486
Areas	Greenhouse-Geisser	7.925	0.008
Condition * Areas (Interaction)	Greenhouse-Geisser	0.889	0.407

Table 6-3: For the beta band, the output of ANOVA Test 2 (condition, areas).

The results of the test show that condition alone did not significantly affect $\tilde{\rho}_{\beta}$. Areas did affect $\tilde{\rho}_{\beta}$. The interaction between areas and condition is not significant.

6.3.5 ANOVA Results of Test 2 (Condition, Areas): Gamma Band

The outcome for Test 2 for the gamma bands produced no significant results. The results of the tests are shown in Appendix J.

6.3.6 ANOVA Results of Test 3 (Condition, Time): All Bands

The outcome for Test 3 for all the frequency bands produced no significant results. The results of the tests are shown in Appendix J.

6.3.7 ANOVA Results of Test 4 (Condition, Areas): Beta Band

The result of Test 4 for the beta band is shown in Table 6-4. The factors were condition and areas and the dependant variable was the beta differentiated phase synchronization coefficient $\Delta\tilde{\rho}_{\beta}$.

Factor	Epsilon Correction	F Statistic	P Value
Condition	Greenhouse-Geisser	1.254	0.310
Areas	Greenhouse-Geisser	5.696	0.037
Condition * Areas (Interaction)	Greenhouse-Geisser	3.999	0.032

Table 6-4: For the beta band, the output of ANOVA Test 4 (condition, areas).

The results of the test show that condition alone did not significantly affect $\Delta\widetilde{\rho}_{\beta}$. Areas did affect $\Delta\widetilde{\rho}_{\beta}$. The interaction between areas and condition was also significant. The condition or conditions that are affecting the areas factor can be determined qualitatively by looking at a plot of the means of the levels of the factors shown below in Figure 6-11.

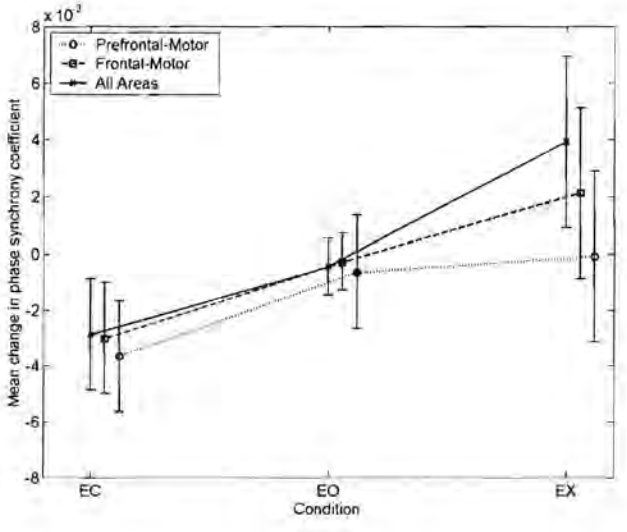

Figure 6-11: For the beta band for each level of each factor in Test 4 (condition, areas), plot of the means of the differentiated phase synchronization coefficients $\Delta\widetilde{\rho}_{\beta}$. The y-axis represents the differentiated phase synchronization coefficients and x-axis represents the conditions where EC stands for eyes-closed, EO stands for eyes-open and EX stands for exercise-until-fatigue. There are three plots, one for each area identified on the legend. The markers representing the means of a particular condition and area are shifted on the x-axis for readability. The error bar represents the standard deviation from the mean.

Figure 6-11 shows that the means of the three levels of areas for the eyes-closed condition and the eyes-open condition and the tangents of the curves connecting points of the same level of area shown in the figure are almost the same. However for the exercise-until-fatigue condition the means are in different positions relative to one another. The mean of frontal-motor pairs has decreased relative to the all areas pairs and the mean of the prefrontal-motor pairs has decreased relative to both the frontal-motor pairs and the all areas pairs. The inverse may also be true: the mean of the all areas pairs may have increased relative to both the frontal-motor pairs and prefrontal-motor pairs, and frontal-motor pairs may have increased relative to the prefrontal-motor pairs. Either way there is an interaction between the prefrontal-motor pair level and frontal-motor pairs and the exercise-until-fatigue condition.

The post-hoc test (the Tukey HSD test) provides a method to compare the means of each factor combination. The test compares each mean of a particular condition-areas combination pair, to every other combination pair and provides a P-value to indicate if the means are the same or not (Please see Appendix H for a description of P-values). For instance, the all areas pairs for exercise-until fatigue was compared to the prefrontal-motor pairs for the eyes-open condition. The purpose of this test is to quantify the above qualitative discussion by providing P-values to indicate the relationship between the factors. Therefore not all the comparisons provided by the Tukey HSD test are relevant to this discussion. Comparisons that are relevant to this discussion are the relationship between the means of the frontal-motor pairs and prefrontal-motor pairs to the all areas pairs, and how these relationships change for each condition. The relevant comparisons provided by the Tukey HSD test are shown in Table 6-5 below. The full table of comparisons can be found as an Excel spreadsheet in the data CD provided with this document.

Condition	Area Combination	P-value
Eyes-closed	All Areas to Frontal-motor	1.000
	All Areas to Prefrontal-motor	0.976
Eyes-open	All Areas to Frontal-motor	1.000
	All Areas to Prefrontal-motor	1.000
Exercise-until-fatigue	All Areas to Frontal-motor	0.290
	All Areas to Prefrontal-motor	0.000

Table 6-5: For the beta band, the result of the Tukey HSD test for certain area combinations for the eyes-closed, eyes-open and exercise-until-fatigue conditions. The values shown are the P-values that indicate if the means are from the same population.

Table 6-5 shows that the means of the frontal-motor and prefrontal-motor pairs do not differ from the all areas pairs for both the eyes-close and eyes-open condition (all comparisons have a P-value equal to 1.000 or close to 1.000). However the means of the frontal-motor and prefrontal-motor pairs do differ from the all areas pairs for the exercise-until-fatigue condition. The difference between the means of the frontal-motor pairs and all areas pairs for the exercise-until-fatigue condition did not differ significantly ($P = 0.290$) but the difference between the means of the prefrontal-motor pairs and all areas pairs for the exercise-until-fatigue condition are significantly different ($P < 0.000$). Thus the exercise-until-fatigue condition affects the means of the prefrontal-motor pairs relative to the all areas pairs significantly.

The effect of exercise on $\Delta\tilde{\rho}_\beta$ for each area level as described above was investigated further. Figure 6-11 represents $\Delta\tilde{\rho}_\beta$ values that are averaged over time. To see possible affects related to time, the values of $\Delta\tilde{\rho}_\beta$ before time averaging were plotted for the eyes-closed condition (Figure 6-12 a), the eyes-open condition (Figure 6-12 b) and the exercise-until-fatigue condition (Figure 6-12 c) for the 3 area levels. The purpose here was to see what the effect of the exercise-until-fatigue condition is on the different area groups between the 5 epoch transitions, and not just the average of the 5 epoch transitions. This may point to effects that occur at later time periods that may possibly be related to fatigue.

Looking at the time course of $\Delta\tilde{\rho}_{\beta}$ for the exercise-until-fatigue condition (Figure 6-12 c), the 3 areas have means that seem qualitatively different at the 1st and the 5th epoch transition, while for the rest of the epoch transitions the means seem very similar. In the 1st transition all the values lie in the negative range. This indicates reduced phase synchronization between the first and second epochs, and then the values increase so that there is on average no phase synchronization change for the 2nd and 3rd transition. In the 4th transition, phase synchronization increases slightly. In the final epoch transition, between epoch 5 and 6, the 3 levels of the areas factor show different phase synchronization changes. The all areas pairs tend to remain as they were, with a slight increase in phase synchronization. The frontal-motor pairs tend to show a decrease in phase synchronization differentiation, to a level where phase synchronization did not change and prefrontal-motor pairs tend to show a decrease in phase synchronization differentiation, to a level where phase synchronization is negative again.

Looking at the eyes-closed condition (Figure 6-12 a), the 3 levels of the areas factor have means that seem qualitatively different at the 1st epoch transition as well, similar to the exercise-until-fatigue condition but they remain at qualitatively similar levels throughout the trial and in the eyes-open condition (*Figure* 6-12 b) they were all qualitatively similar throughout the entire trial. What is also of significance is that the values remain mostly near zero for epoch transition 2 to 5 in the eyes-closed condition. This indicates that for all the levels of areas the change in $\Delta\tilde{\rho}_{\beta}$ in the cortex does not change on average across time in the eyes-closed condition (apart from the initial decrease at the 1st epoch transition). In the eyes-open condition (Figure 6-12 b) there is slightly more variability in $\Delta\tilde{\rho}_{\beta}$ (increases and decreases in $\Delta\tilde{\rho}_{\beta}$) but not much difference between the levels of areas. In the exercise-until-fatigue condition (Figure 6-12 c) there were slight differences between the levels of areas in $\Delta\tilde{\rho}_{\beta}$, but as the trial progresses these values increase and become similar, until the final epoch transition as described above.

a

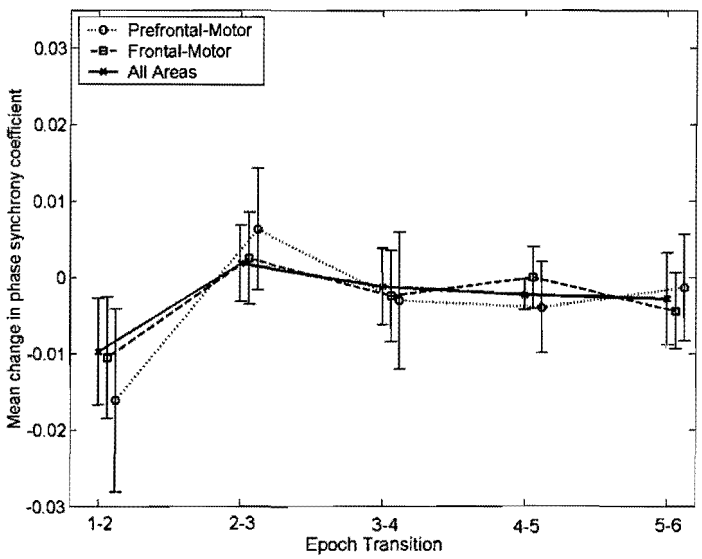
Prefrontal-Motor
Frontal-Motor
All Areas
Mean change in phase synchrony coefficient
0.03
0.02
0.01
0
-0.01
-0.02
-0.03
1-2
2-3
3-4
4-5
5-6
Epoch Transition

b

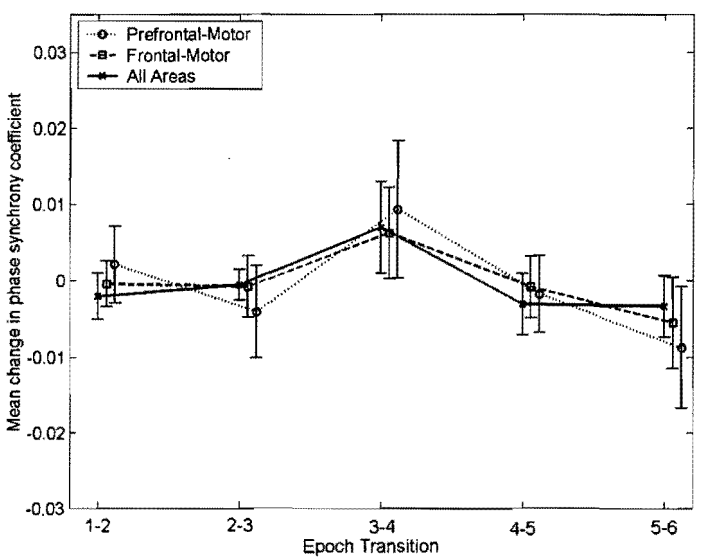
Prefrontal-Motor
Frontal-Motor
All Areas
Mean change in phase synchrony coefficient
0.03
0.02
0.01
0
-0.01
-0.02
-0.03
1-2
2-3
3-4
4-5
5-6
Epoch Transition

c

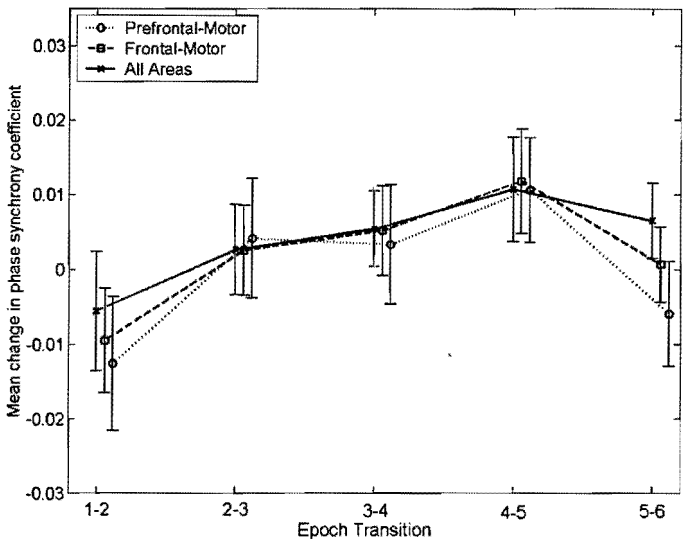

Figure 6-12: For the beta band, for the eyes-closed condition (a) the eyes-open condition (b) and the exercise-until-fatigue condition (c), for each epoch transition (1-5), for the 3 areas of the areas factor in Test 4 (condition, areas), the mean and standard error of the differentiated phase synchronization coefficients $\Delta\widetilde{\rho}_{\beta}$. The y-axis represents $\Delta\widetilde{\rho}_{\beta}$ and x-axis represents epoch transitions. There are three plots on each graph (a) – (c), one for each area identified on the legend. The markers representing the means of a particular condition and area are shifted on the x-axis for readability. The error bar represents the standard deviation from the mean.

To statistically verify the above qualitative discussion, the Tukey HSD post-hoc test was performed. Since the current analysis separates the three conditions, areas as well as the five epoch transitions a the Tukey HSD test looks at all the factors in a single test (3 factors). The test compares every possible combination of conditions, areas as well as the five epoch transitions. This results in 990 comparisons, of which only a small number are of relevance (there are 45 means from 3 conditions by 3 areas by 5 epoch transitions, and $\binom{45}{2} = 990$). The entire table is presented as an Excel spreadsheet in the data CD provided with this document. Comparisons of interest are shown in Table 6-6, Table 6-7 and Table 6-8. With respect to the discussion above the comparisons of interest are the relationships between the means of the frontal-motor pairs and prefrontal-motor pairs to the all areas pairs, and how these relationships change for each epoch transition for each condition.

Eyes-closed condition		
Epoch Transition	**Combination**	**P-value**
1	All Areas to Frontal-motor	1
	All Areas to Prefrontal-motor	1
2	All Areas to Frontal-motor	1
	All Areas to Prefrontal-motor	1
3	All Areas to Frontal-motor	1
	All Areas to Prefrontal-motor	1
4	All Areas to Frontal-motor	1
	All Areas to Prefrontal-motor	1
5	All Areas to Frontal-motor	1
	All Areas to Prefrontal-motor	1

Table 6-6: For the beta band, the result of the Tukey HSD test for certain factor combinations (epoch transitions, areas) for the eyes-close condition. The values shown are the P-values that indicate if the means are from the same population.

Eyes-open condition		
Epoch Transition	**Combination**	**P-value**
1	All Areas to Frontal-motor	1
	All Areas to Prefrontal-motor	1
2	All Areas to Frontal-motor	1
	All Areas to Prefrontal-motor	1
3	All Areas to Frontal-motor	1
	All Areas to Prefrontal-motor	1
4	All Areas to Frontal-motor	1
	All Areas to Prefrontal-motor	1
5	All Areas to Frontal-motor	1
	All Areas to Prefrontal-motor	1

Table 6-7: For the beta band, the result of the Tukey HSD test for certain factor combinations (epoch transitions, areas) for the eyes-open condition. The values shown are the P-values that indicate if the means are from the same population.

Exercise-until-fatigue condition		
Epoch Transition	**Combination**	**P-value**
1	All Areas to Frontal-motor	1
	All Areas to Prefrontal-motor	0.997
2	All Areas to Frontal-motor	1
	All Areas to Prefrontal-motor	1
3	All Areas to Frontal-motor	1
	All Areas to Prefrontal-motor	1
4	All Areas to Frontal-motor	1
	All Areas to Prefrontal-motor	1
5	All Areas to Frontal-motor	1
	All Areas to Prefrontal-motor	0.07

Table 6-8: For the beta band, the result of the Tukey HSD test for certain factor combinations (epoch transitions, areas) for the exercise-until-fatigue condition. The values shown are the P-values that indicate if the means are from the same population.

Table 6-6 clearly shows that the means of the frontal-motor and prefrontal-motor pairs do not differ from the all areas pairs for every epoch transition for the eye-closed condition as expected. Table 6-7 clearly shows that the means of the frontal-motor and prefrontal-motor pairs do not differ from the all areas pairs for every epoch transition for the eye-open condition also to be expected. Table 6-8 shows that that the means of the frontal-motor and prefrontal-motor pairs do not differ from the all areas pairs for every epoch transition for the exercise-until-fatigue condition, except the final epoch transition. At the final epoch transition, the prefrontal-motor pairs clearly differ from the all areas pairs, although this is not significant at the 0.05 level. One would expect that there should be some change in the P-value at the final epoch transition between the frontal-motor pairs and the all areas pairs according to the qualitative analysis presented above, but this is not the case according to the Tukey HSD test.

6.3.8 ANOVA Results of Test 4 (Condition, Areas): Alpha, Theta and Gamma Band

The outcome for Test 3 for all the frequency bands produced no significant results. The results of the tests are shown in Appendix J.

6.3.9 Comparison of Head Maps with ANOVA Results

The methods used to display head maps and the methods used in the ANOVA tests are different and did not necessarily correspond (see Section 5.6.3 for a discussion on comparing the results of the two methods). However a brief comparison shall be made here for completeness.

The alpha phase desynchronization and synchronization observed in 3rd and 4th epoch transition respectively (Figure 6-10 a no. 3 and Figure 6-10 b no. 4) did not reflect in the corresponding ANOVA test (ANOVA Test 3 for the alpha band, presented in Appendix J). Figure 6-13 is a plot of the means at each epoch transition for the 3 levels of areas, for the exercise-until-fatigue condition, similar to Figure 6-12 c but for the alpha band. This was a representation of the corresponding ANOVA test. The mean $\Delta\tilde{\rho}_{\alpha}$ (all areas) at epoch transition 3 in Figure 6-13 is lower than epoch transition 4 as expected (corresponding to Figure 6-10 a no. 3 and Figure 6-10 b no. 4). The mean $\Delta\tilde{\rho}_{\alpha}$ (all areas) at epoch transition 4 had the highest positive value, as expected as this corresponds to the massive synchronization observed in Figure 6-10 b no. 4. However, the mean $\Delta\tilde{\rho}_{\alpha}$ (all areas) at epoch transition 3 had a mean close to zero and was not the lowest mean (the first epoch transition had the lowest and a negative mean). This does not correspond to Figure 6-10 a no. 3 (and no. 1). The reason for this is that the Figure 6-10 a represents only 0.5% of the smallest values of $\Delta\tilde{\rho}_{\alpha}$. Figure 6-10 a no.3 indicates that epoch transition 3 had most of the smallest values but its average (representing many more numbers) is still greater and not smaller than epoch transition 1.

For the beta band, the head maps (shown in appendix J) show no patterns that would correspond to the results discussed in Section 6.3.7. The reasons for this are discussed in Section 5.6.3.

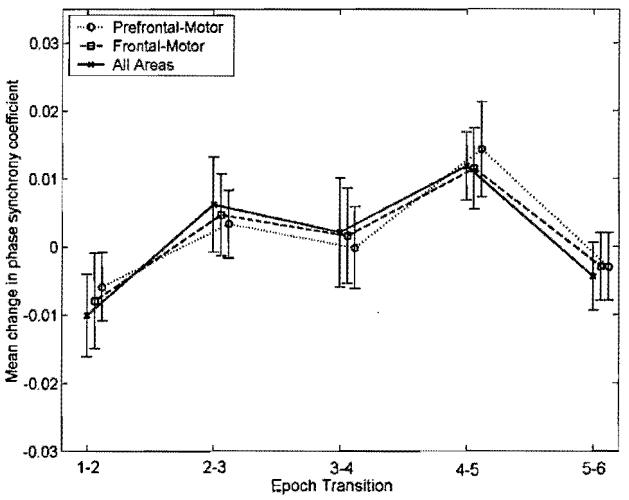

Figure 6-13: For the alpha band, for the eyes-closed condition (a) the eyes-open condition (b) and the exercise-until-fatigue condition (c), for each epoch transition (1-5), for the 3 areas of the areas factor in Test 4 (condition, areas), the mean and standard error of the differentiated phase synchronization coefficients $\Delta\tilde{\rho}_{\alpha}$. The y-axis represents $\Delta\tilde{\rho}_{\alpha}$ and x-axis represents epoch transitions. There are three plots on each graph (a) – (c), one for each area identified on the legend. The markers representing the means of a particular condition and area are shifted on the x-axis for readability. The error bar represents the standard deviation from the mean.

6.4 General Discussion on the Results

The aim of this project was to elucidate the brain processes controlling central fatigue by investigating the electrical activity of the brain during the fatiguing process and comparing it to 'baseline' eyes-closed and eyes-open states. In particular phase synchronization between different brain areas in specific frequency bands of physiological significance was investigated, as phase synchronization is thought to be the means of dynamic communication between different parts of the brain. The

outcome of this analysis has been presented above and involves a description of phase synchronization across the brain and across the time taken to reach fatigue.

The time changes of phase synchronization occur in the millisecond range and upwards. Because of the large amount of data to be analysed, up to a few hundred seconds per subject, channel combination, condition and frequency band, time averaging was essential. Although this invariably results in a loss of information, it allows a complex process to be described in a simpler manner and facilitates the use of a few graphs and statistics to describe the complex process. The result of this analysis may then point to effects that can be later investigated in more detail. This is particularly true in this experiment, where the analysis of the averaged numbers pointed to specific effects under certain treatments and not others.

6.4.1 Overview of the Phase Synchronization Coefficients

The phase synchronization coefficients, which are a calculation of the level of phase synchronization, are not a perfect calculation of phase synchronization. The complexity of calculating phase synchronization in a complex, chaotic and noisy environment like the scalp has been described in the literature review and requires a method based on statistics. There is no predetermined value that can be chosen as a threshold for phase synchronization and phase synchronization values are a better indicator when compared with baseline levels or when the values are statistically analysed and compared to control processes. This has been the primary approach in processing the phase synchronization values in this investigation.

In the first section, in the presentation of the results, the phase synchronization coefficients $\tilde{\rho}$ and the differentiated phase synchronization coefficients $\Delta\tilde{\rho}$ of the 3 conditions as well as the shifted surrogate data were presented as distributions and as time series. The results show that $\tilde{\rho}$ of the trial data were clearly from a different population to that of the shifted surrogates, which represent phase synchronization based on pure chance or artefact due to temporal or spatial filtering. This value for shifted surrogate data is low, with a near constant mean and variance, whereas the $\tilde{\rho}$ of the trial data had a changing mean and variance. The time course of the $\tilde{\rho}$ values of the 3 conditions, eyes-closed, eyes-open and exercise-until-fatigue,

shows that the conditions were on average somewhat similar, although the values for the exercise-until-fatigue condition had a slightly lower mean. Furthermore there were no obvious differences in the $\tilde{\rho}$ values across time that could have indicated some kind of progression to fatigue.

The results show that $\Delta\tilde{\rho}$ of the trial data had different characteristics to that of the shifted surrogates. The mean values of $\Delta\tilde{\rho}$ of the shifted surrogates was nearly zero with a small deviation which should be expected.

6.4.2 Alpha Phase Synchronization and Desynchronization

The head maps indicated strong alpha band desynchronization between the 3rd and 4th epochs (Figure 6-10a no. 3) followed by strong synchronization between the 4th and 5th epochs (Figure 6-10b no. 4) for many electrode locations across the cortex for the exercise-until-fatigue condition only. These findings may be a marker of the progression to fatigue. As discussed in the literature review (Section 3.2.2) alpha ERD and ERS, which is a measure of local synchronization or desynchronization, is important in cognitive tasks and the degree of alpha ERS and ERD has been linked to levels of cognitive performance. Alpha activity has been shown to be important in working memory, in internally directed attention tasks and in the inhibition of sensory information (Section 4.1.2). The increase in task complexity of internally directed attention tasks is related to an observed increase in alpha activity (Section 4.1.2).

Although alpha ERS and ERD is not being directly measured here, alpha phase synchronization changes, over many areas of the brain, may be linked to the inhibition of sensory information and an increase in internally directed attention during the progression of fatigue. In the progression of fatigue it is expected that a subject would start focussing on overcoming fatigue or implement some pacing strategies or otherwise engage in more internal cognitive processes. The changes in

alpha phase synchronization observed across many electrode pairs could be a marker of this process and could possibly be related to alpha ERS and ERD.

There may be variations in the way the subjects' brain's processed the sensory information coming in from the body that signal peripheral changes in homeostasis. At some periods this information may be suppressed from the consciousness, while at other times it may be part of complex cognitive processes. Alpha phase synchronization could possibly be a marker of this inhibition of sensory information. As exercise progresses, more information signalling peripheral fatigue would transmitted to the brain for processing and would require the brain to respond somehow. If a greater amount of sensory inhibition is required by the brain in order to override fatigue, this could possibly be reflected in the enhanced changes of alpha phase synchronization. Of course this is only one suggested hypothesis.

It is interesting to note that the changes in alpha phase synchronization occurred across many areas of the brain indicating multiple areas are involved in some kind of 'orchestra', and that there is clearly a period of desynchronization followed by synchronization. In terms of dynamic network formation desynchronization is the uncoupling of brain areas (or weakening of coupling) that were once phase synchronized to form a unified system. The period of strong desynchronization over many electrode pairs is thus an indication that many areas of the brain that at some stage formed part of a stable system (perhaps when the brain was at a 'baseline' level similar to eyes-closed or eyes-open) have 'disconnected' and are involved in forming new large scale networks or in local processing in response to the demands of increasing fatigue. Many seconds later (about 20s for most subjects) the next stage on average involved strong synchronization, but involving not as many sites as the desynchronization pattern. This may be indicative of new network formation or increases in the strength of coupling between cortical sites. At the final stage of fatigue synchronization and desynchronization patterns seem to go back to baseline levels.

Perhaps the pattern described above is the outward manifestation of different stages of cognition or brain processes directly involved in the process of fatigue – whether it be the control of motor output to the muscles by conscious and unconscious

processes, the sensation and emotion of fatigue itself or the interaction of motivation, planning, control of sensory information and various memory processes such as episodic, working and long term memory. Alpha activity has been shown to be directly involved in many of the processes mentioned (see Section 4.1.2 for a review of alpha activity).

A comment should be made on the strong synchronization and desynchronization found at the 'baseline' levels of the eyes-closed and eyes-open condition. Since the activity of the brain is ongoing, and during 'baseline' states there is consciousness and an intact cognitive ability it should be expected that there would indeed be strong synchronization and desynchronization at certain times and at certain sites. But exercise and the progression of fatigue are more 'intense' states where the brain is obviously involved in more specific processing with far more sensory and endogenous activity being present and perhaps the emergence of the synchronization and desynchronization patterns during the exercise-until fatigue condition is indicative of this.

6.4.3 Prefrontal-Motor and Frontal-Motor Phase Beta Desynchronization

The discussion has so far revolved around the patterns of alpha synchronization and desynchronization observed in the head maps. Its been shown above that exercise increases phase desynchronization in the beta band for prefrontal-motor pairs as well as frontal-motor pairs, compared to the all areas pairs (Table 6-5, Table 6-8, Figure 6-11 and Figure 6-12). This is indeed an interesting effect and deserves some interpretation.

The prefrontal cortex is involved in planning, motivation, goal orientated behaviour, and decision-making [65]. These processes may be directly relevant to exercise and fatigue (see Section 2.3.1 and 2.4 of the literature review). The frontal cortex is mainly involved in the preparation for movement, contains circuits for the activation of muscles for specific movements, and orienting the body for movement [65]. The frontal cortex is activated for imagined or rehearsed movement, even if no muscle activation occurs [65]. The motor cortex is directly involved in muscle activation [65].

Thus increased desynchronization between prefrontal-motor pairs and frontal-motor pairs indicates that strength of beta band coupling between these areas is decreasing or they are being uncoupled. It is seen directly in the decrease in $\Delta\tilde{\rho}$ where it occurs between the 1st and 2nd epoch transition and particularly in the 5th and final epoch transition (Figure 6-12 c) where it is almost statistically significant for the prefrontal-motor pairs (P = 0.07, Table 6-8). This desynchronization effect suggests that although coupling strength between these areas may be both increasing and decreasing at different times, on average it is decreasing and therefore there is less cooperation, communication and dependence between the prefrontal area and motor area pairs and to a lesser degree the frontal area and motor area pairs.

The prefrontal-motor area, that is known to be linked with planning, motivation, goal orientated behaviour and decision-making [65] has an overall reduced cooperation with the motor area involved in direct activation of muscles [65]. The effect is the strongest (and statistically significant) between the penultimate and the final epochs of the exercise trial in the beta band. This could indicate that the reduction in beta band communication between these brain areas play a role in the onset of fatigue or is somehow a marker of the fatigue process.

Increased beta band activity is considered to be an index of cortical arousal, which is the state of physiological reactivity of an organism, and attention as well as being activated in emotional states (see Section 4.1.3 for a review of beta band activity). Perhaps the reduced beta band phase synchronization between the pre-frontal cortex and the motor cortex is an index of reduced cortical arousal and decreased attention due to inputs from other parts of the brain involved in the homeostatic control of bodily functions that are being activated from peripheral changes occurring in the body due to sustained exercise. Or perhaps it is the prefrontal cortex itself that is the main component of the 'central-governor' and that this area utilizes the beta band to control motor output by directly modulating the activity of the motor cortex, and that in fatigue this control is reduced.

The supplementary motor area and premotor area, both the major constituents of the frontal cortex facilitate planned movement [65] and is activated by imagined movement [65]. The relative decrease (i.e. with respect to the all areas pairs) in beta phase synchronization between the frontal area and motor area provides some evidence that there is reduced drive to the muscles (Figure 6-11), although this effect is not statistically significant (Table 6-5). This effect is to be expected as the frontal motor areas contain circuits for specific movements and would directly communicate with the motor cortex [65], and motor drive has been shown to be reduced during exercise fatigue (see Section 2.2 of the literature review). The occurrence of a decrease in beta phase synchronization of both frontal-motor and prefrontal-motor pairs is interesting because of the possible direct modulating effect (or lack of it) of the prefrontal cortex on the motor cortex. It should also be noted that the decrease in beta phase synchronization of prefrontal-motor pairs is stronger and than that of the frontal-motor pairs (and statistically significant, Table 6-5) perhaps indicating some overriding process of the prefrontal cortex or that the prefrontal cortex has a more pronounced effect.

The first phase of eyes-closed and exercise follow a very similar pattern in the beta band phase synchronization differentiation. It is not clear why this would be the case, but it may be due to the fact that the eyes-closed measurements were taken after the warm up exercises (see Section 5.3.1 for a description of the trial), and the effects of that, being similar to the exercise trial in the early stages, are being observed. Another reason may be that it is the effect of some cognitive processing that is occurring in the eyes-closed state, perhaps in anticipation of the forth-coming trial including maybe imagined movement, imagined fatigue or some pre-emptive strategy being played out in the minds of the subjects. It could also be the effect of reduced attention and arousal found in both conditions. In any case, the phase synchronization differentiation for all 3 areas stabilize to nearly zero, indicating that phase synchronization remains constant.

Continuing with the progression of beta band phase synchronization in the exercise-until-fatigue condition, it was observed that at the 2^{nd} to 4^{th} epoch transition $\Delta\tilde{\rho}_{\beta}$ increased gradually from initially negative values to positive values and the

means of the 3 areas remain similar (Figure 6-12c). This increasing phase synchronization indicates a progressively stronger communication between all electrode sites, with the frontal-motor and prefrontal-motor pairs increasing at the same rate as the all areas pairs. Perhaps therefore there is an increasingly stronger drive to the motor cortex from the frontal and prefrontal cortices and this is due to the motivation and desire to overcome increasing fatigue.

The sudden change in phase synchronization of frontal-motor and prefrontal-motor pairs that follows in the 5th epoch transition could be indicative of a disruption in this process (Figure 6-12 c). Perhaps the prefrontal and frontal cortices themselves are being driven by the 'central-governor' to in turn reduce their drive to the motor cortex, despite the best efforts of the subjects to overcome fatigue. Or maybe some activity originating in the prefrontal cortex, such as a strong emotional state or an unconscious desire to reduce power output to the muscles is actively reducing motor output drive by influencing both the frontal cortex and motor cortex. It could even reflect the subjects' voluntary decision to reduce drive to the muscles because of unbearable sense of effort or other sensations. Since prefrontal activity is associated with conscious decision making processes, the data presented here brings the notions of conscious control of fatigue and the functionality of the sensation of fatigue to the fore.

There are many examples where activity in a particular band is reduced and is concomitantly accompanied by an increase in activity by another band (see Section 4.1 of the literature review). This could be the case here, where the reduction in beta phase synchronization in the final stages of the exercise trail may be linked to increased activity in other bands not observed in the data presented. Furthermore the beta phase synchronization changes observed here should not be viewed as being isolated from the alpha desynchronization and synchronization patterns discussed above. In the exercise-until-fatigue condition it is interesting to note that at the 3rd epoch transition where strong alpha phase desynchronization occurs on a massive spatial scale (Figure 6-10 a no. 3), beta phase synchronization is quite stable (Figure 6-12 c), and at the 4th epoch transition where strong alpha phase synchronization occurs (Figure 6-10 b no. 4), beta phase synchronization is

increasing (Figure 6-12 c). At the final epoch transition alpha phase synchronization is quite stable (Figure 6-10 a no. 5 and Figure 6-10 b no. 5) whereas beta phase synchronization displays the specific changes described above (Figure 6-12 c).

6.4.4 Changes in Theta and Gamma Bands

No significant results were observed in the data presented here for both the theta and gamma band. Since activity in both of these bands has been shown to be linked to cognition (see Section 4.1.3 and 4.1.4 of the literature review), the difference between activity in these bands between the conditions may simply not differ significantly. Another more probable reason is the methodology employed here is not sensitive to the differences that would otherwise have been observed. In particular the use of such a wide band pass filter for gamma isolation may have been the reason for lack of observable phase synchronization differences. The band chosen was 20Hz wide, and since phase synchronization is a narrow band phenomenon (even if the bands are integer multiples of each other, they should still be quite narrow) the wide band probably violates the requirement beyond which the method used here is able to be adequately robust.

6.5 General Discussion on the Investigation

The description of phase synchronization in this investigation is rather basic and provides just a starting point for a more thorough investigation, nevertheless the results provide evidence that there are specific changes in brain communication during the progression of fatigue and give a condensed overview of a very complex phenomenon.

To begin a more thorough analysis of phase synchronization alternative methods need to be derived to deal with the large amount of data generated from trials without loosing critical information. This is the biggest challenge with this kind of analysis. Perhaps a more focused analysis needs to be performed, investigating a particular aspect of the process with greater detail or an investigation with the aims

of improving the methods of analysis. For example, an investigator could focus on looking at the changes in phase synchronization for small time windows of maybe a couple hundred milliseconds for a band in the alpha range. An investigator could then determine through a systematic process of averaging the best time window length to use that outputs data in manageable quantities without sacrificing important information. Phase synchronization between other cortical areas should be investigated and not be restricted to only frontal-motor and prefrontal-motor pairs.

There are a few other criticisms of this investigation that should be briefly discussed. Firstly is the use of variable window lengths. Because it took each subject different times to reach fatigue, epoch lengths had to be of variable length to do any kind of averaging across subjects. This may have an effect on phase synchronization coefficients calculated. Perhaps an alternative method of averaging across subjects needs to be investigated, where equal epoch lengths can be used. Furthermore the lengths of the eyes-closed and eyes-open trials were different to the exercise trials. A method to make them more comparable needs to be developed. One proposed solution may be to have the subjects' individual trials the same length, so the length of the eyes-open and eyes-closed trial would be the same length of the exercise trial for each subject.

Not only is a variable window length problematic, but the choice of window length. The selection of window length is related to the problem of stationarity. Ideally window lengths should be as small as possible (with the limit being the time resolution obtainable after filtering), since an assumed sationarity of 10s may not hold for the exercise-until-fatigue trial. Since the stationarity of the EEG recordings are unknown, a more thorough method should be developed to determine the largest window length that fulfils the stationarity requirement.

In this investigation, the smaller window lengths that represent 1/50 of the trial lengths were then further averaged into window lengths representing 1/6 of the trial lengths. It could be argued that this simply represents phase synchronization calculated using larger (possibly non-stationary) windows. To determine the effect on the phase synchronization coefficient on window of different sizes, a simulation using the Rossler systems in Section 5.2.2 was performed and shown in Appendix L. The

outcome of that simulation shows that the mean value of the phase synchronization coefficients tends to increase with smaller time windows, and this seemed to occur to a greater degree for non-synchronous systems. However the phase synchronization coefficients showed great variability at all window lengths (provided the window lengths were small enough to create several epochs from the total length). It could indicate that at first glance there is little to gain by using window lengths of 1/50 versus 1/6, and that the only issue here is stationarity, but it also indicates that the issue of window lengths is complicated and deserves a thorough analysis.

A related issue is one of measurement variability. Repeating the trials several times could reduce the variability in the phase synchronization coefficients by using the average of the trials as is done in ERD, ERS and coherence trials [75].

The next issue is the large quantity of data rejected due to artefact and the possible contamination of retained data sets with artefact. This is an ongoing problem with EEG analysis in general and one that deserves a more thorough review, particularly here with the EEG measured during exercise. EMG artefact in particular may cause spurious detection of phase synchronization. A means to detect this needs to be investigated.

The use of spherical spline interpolation and the surface Laplacian to improve spatial resolution may have introduced errors by either introducing false phase synchronization or more probably hiding phase synchronization where it exists. Since the technique emphasises the radial component of the voltage radiating from a point on the scalp, any tangential components that exhibit phase synchronization to another point on the scalp may be lost. The extent of this effect needs to be investigated. Although the technique is widely used in EEG research, alternative methods are available such as those that make use of finite element analysis based on MRI data providing the 3-dimensional structure of the head.

Next is the issue of the widths of the frequency bands used in the calculation of phase synchronization coefficients. The width of the frequency bands chosen in this investigation needs to be reviewed. Frequency bands were selected based on traditional frequency band lengths used in EEG research. Smaller bands of equal

lengths may be more appropriate based on the theory of phase synchronization (narrow bands of about 2Hz [76][141]). This may be the reason for finding no effect in the gamma frequency band in this investigation. The delta frequency band should also be investigated. Furthermore, frequency band selection should be considered on an individual subject basis, as Individual Peak Frequency should be considered as discussed in reference [75].

Furthermore phase synchronization across frequency bands should be investigated, as there is evidence of synchronization between narrow band signals of different frequencies, such as those found in the beta and alpha range. This of course must be investigated in the context of the appropriate theoretical considerations of phase synchronization. Another kind of analysis that could provide further information is *direction of coupling* where a particular system is identified as the slave or driving system. This theory has been developed but has yet to be applied to EEG analysis. The investigation of phase synchronization could also be performed concomitantly with investigations of supporting method like ERS, ERD, spectral analysis, coherence and bicoherence.

Since this study involved both motor and cognitive brain processes, a methodology that would attempt to discern the two processes should be investigated. As a starting point, since the exercise was performed with a one sided leg contraction, the differences in hemispheres should be investigated, in a similar way to how the different areas was determined. Since movement creates specific changes in ipsi-lateral and contra-lateral brain areas [100][75], these could have been used to help differentiate between motor and cognitive effects. Other methods could be devised to help understand the endogenous and sensory processing effects during exercise, such as the use concomitant use of Rate of Perceived Exertion (RPE), heart rates, EMG and body temperature measurements for example.

Related to EEG hemispheric differences is handedness. In the fatigue trial, the handedness of the subject was not considered and this could affect the EEG patterns. The subjects had mixed handedness (see Appendix D) and this source of variance should perhaps be eliminated or its effects investigated (see reference [100]).

The final issue to be discussed is the ANOVA test procedure. Firstly was the use of 2-way ANOVA. Two-way ANOVA was sufficient for the analysis initially, but in order to perform the post-hoc analysis that involved all 3 factors together, 3-way ANOVA needed to be performed.

Secondly, the prefrontal-motor pairs and the frontal-motor pairs were compared to the all areas pairs. The use of every electrode combination pair to form the all areas pairs allowed effects for the entire head to be observed and quantified. Since the all areas pairs also includes the prefrontal-motor pairs and the frontal-motor pairs, there will be some distortion of the results of the ANOVA, since all the levels of the factors of the ANOVA are not completely independent. The number of prefrontal-motor pairs and the frontal-motor pairs is small in comparison to the number of the all areas pairs. Thus it was expected that the effect of the overlapping of values would be small. All the ANOVA tests performed in this investigation were therefore repeated, with the prefrontal-motor pairs and the frontal-motor pairs not being included in all areas pairs (thus the all areas pairs were completely independent). This also allowed 3-way ANOVA to be employed instead of the initial 2-way ANOVA. The results of these tests are in electronic form (Excel format) and can be found in the data CD provided with this document. The results show very little difference between the original ANOVA tests and the tests performed with a completely independent all areas pairs group. Significant results remain significant, and non-significant results remain non-significant across all tests.

7. CONCLUSIONS AND RECOMMENDATIONS

The aims of the project were primarily to elucidate the brains role in the process of exercise fatigue by looking at how different areas of the brain communicate through phase synchronization. Specific questions like how the process progresses in time and what areas are involved were raised. More generally there is little hard evidence to support certain models of fatigue involving cognition, like the *cognitive-discussion* model where the conscious sensation of fatigue, through cognitive processes, plays an active role in modulating exercise intensity (see Section 2.3 of the literature review). By providing an overview of phase synchronization during an exercise-until-fatigue trial, it was hoped that some of the specific and general questions could at least be partly answered.

The alpha band and beta band phase synchronization patterns that occur during the exercise-until-fatigue condition provide a first step in describing the progression to fatigue. This data cannot be compared to other studies, as there are no known published studies to date that describe the progression of fatigue in this manner.

The findings have met the aims of the project by firstly showing that clear changes occur in the brain (specifically phase synchronization) in exercise and the progression to fatigue. It was shown that these brain changes occur in the frequency bands alpha and beta. Alpha rhythms are primarily involved in internally directed attention tasks, inhibition of sensory information and cognitive performance (see Section 4.1.2 of the literature review). Beta rhythms index arousal and external attention and have been linked to states of emotional intensity (see Section 4.1.3 of the literature review). Thus the frequency bands involved associate various cognitive states that are probably of relevance to the process of fatigue.

Phase synchronization activity in these bands show distinct activity at different periods in the progression of exercise fatigue. It appears as if the progression to fatigue has 3 components; first there are non specific changes followed by an intermediate stage characterized by strong alpha desynchronization (Figure 6-10a no. 3) followed by synchronization (Figure 6-10b no. 4), and fairly stable beta synchronization (Figure 6-12c), then followed by a final stage characterized by unchanging alpha synchronization (Figure 6-10a no. 5 and Figure 6-10b no. 5), and reduced beta synchronization in the frontal-motor areas and beta desynchronization in the prefrontal-motor areas (Figure 6-12c).

In particular the beta phase synchronization of prefrontal-motor and frontal-motor areas show their own specific patterns in the final stages of the progression of exercise fatigue. This directly links cognitive processes like planning, motivation, and decision-making as well as emotion to motor output. Of course in reality the process may be very complex and one can only hypothesize as to the causality of the relationship.

Thus specific changes in brain activity at specific time periods have been demonstrated, as well as changes in particular areas at the final stages of exercise, possibly linked to the process of fatigue. The results show that there may indeed be evidence that cognitive function may play a role in the process of fatigue, and that further neurological studies (including studies involving EEG and phase synchronization) may provide further supporting evidence for the hypotheses concerning the brains role and the role of cognition in exercise fatigue.

The following recommendations are made:

- Find appropriate averaging methods and methods of dealing with data of different lengths (including control trials of different lengths)
- Investigate phase synchronization with finer time resolution
- Investigate appropriate window lengths
- Investigate window lengths with respect to stationarity requirements

- Investigate appropriate ways of reducing or correcting for EEG artefact and investigate the effects of possible artefact
- Specifically investigate and compare phase synchronization between more cortical areas
- Select smaller bands (about 2Hz) for filtering data, covering all bands from 0.1-100Hz
- Investigate other methods of spatial resolution of EEG data
- Employ supporting methods such as direction of coupling, ERS and ERS, spectral analysis, coherence and bicoherence that will supplement phase synchronization data
- Devise methods to differentiate between motor and cognitive effects, including differences in the 2 brain hemispheres

8. REFERENCES

[1] Mosekilde E., Maistrenko Y. and Postnov D. Chaotic synchronization: applications to living systems. World Scientific, River Edge, NJ, 2002.

[2] Winfree A. The Geometry of Biological Time. Springer-Verlag, New York, 1980.

[3] Rosenblum, M. G., Pikovsky, A. S., Kurths, J., Schäfer, C., and Tass, P. A. Phase synchronization: From theory to data analysis. In Moss, F. and Gielen, S., Ed. , Neuro-informatics, vol. 4 of Handbook of Biological Physics, pp. 279-321. Elsevier. (2001).

[4] Varela F., Lachaux J.P., Rodriguez E. and Martinerie J. The brainweb: phase synchronization and large-scale integration. *Nature Reviews Neuroscience,* 2 (4):229-239, Apr. 2001.

[5] Engel A.K., Fries P. and Singer W. Dynamic Predictions: Oscillations And Synchrony In Top-Down Processing. *Nature Reviews Neuroscience,* 2 704-716, 2001.

[6] Buzsáki G. and Draguhn A. Neuronal Oscillations in Cortical Networks. *Science*, 304: 1926-1929, 2004

[7] Glass L. Synchronization and Rhythmic processes in physiology. *Nature* 410: 277-284, 2001.

[8] Salinas E. and Sejnowski T.J. Correlated Neuronal Activity and the Flow of Neural Information. *Nature Reviews Neuroscience,* 2: 539-549, 2001.

[9] Hopfield J.J. and Brody C.D. What is a moment? Transient synchrony as a collective mechanism for spatiotemporal integration. *Proceedings of the National Academy of Sciences of the USA* 98(3): 1282-1287, 2001.

[10] Lutz A., Lachaux J., Martinerie J. and Varela F.J. Guiding the study of brain dynamics by using first person data: Synchrony patterns correlate with ongoing conscious states during a simple visual task. *Proceedings of the National Academy of Sciences of the USA* 99(3): 1586-1591, 2002.

[11] Enoka R.M., Stuart D.G. Neurobiology of Muscle Fatigue. *Journal of Applied Physiology*, 72(5): 1631 - 1648, 1992.

[12] Davies J.M. Central and Peripheral Factors in Fatigue. *Journal of Sports Science* 13: S49 -S53, 1995.

[13] Noakes T.D., St Clair Gibson A. and Lambert E.V. From catastrophe to complexity: a novel model of integrative central neural regulation of effort and fatigue during exercise in humans. *British Journal of Sports Medicine* 38: 511-514, 2004

[14] Noakes T.D., Peltonen J.E. and Rusko H.K. Evidence that a central governor regulates exercise performance during acute hypoxia and hyperoxia. *The Journal of Experimental Biology* 204: 3225-3234, 2001.

[15] St Clair Gibson A., Lambert E.V., Lambert M.I., Hampson D.B. and Noakes T.D. Exercise and Fatigue-control Mechanisms. *International SportMed Journal* 2(3): 1-14, 2001.

[16] Kayser B. Exercise starts and ends in the brain. *European Journal of Applied Physiology* 90: 411-419, 2003.

[17] St Clair Gibson A., Baden D.A., Lambert M.I., Lambert E.V., Harley Y.X.R., Hampson D., Russell V.A. and Noakes T.D. The Conscious Perception of the Sensation of Fatigue. *Sports Medicine* 33(3): 167-176, 2003.

[18] Critchley H.D. The human cortex responds to an interoceptive challenge. *Proceedings of the National Academy of Sciences of the USA* 101(17): 6333-6334, 2004.

[19] Nunez P.L. Neocortical Dynamics and Human EEG Rhythms, Oxford University Press, 1995.

[20] Nunez P.L. and Pilgreen K.L. The Spline Laplacian in Clinical Neurophysiology: A Method to Improve EEG Spatial Resolution. Journal of Clinical Neurophysiology, 8(4):397-413, 1991.

[21] Nunez P.L., Wingeier B.M. and Silberstein R.B. Spatial-Temporal Structures of Human Alpha Rhythms: Theory, Microcurrent Sources, Multiscale Measurements, and Global Binding of Local Networks. *Human Brain Mapping*, 13 (2): 125-164, 2001.

[22] Lopes da Silva F. EEG Analysis: Theory and Practice in Electroencephalography: Basic Principles, Clinical Applications, and Related Fields, Third Edition. Baltimore, Williams and Wilkins 1097-1118, 1993.

[23] Gandevia S.C. Spinal and Supraspinal Factors in Human Muscle Fatigue. *Physiological Reviews* 81(4): 1725-1789, 2001.

[24] Gandevia S.C., Enoka R.M., McComas A.J., Stuart D.G. and Thomas C.K. Neurobiology of Muscle Fatigue: Advances and Issues, in *Fatigue*, Plenum Press, New York, 1995.

[25] Noakes T.D. and St Clair Gibson A. Logical limitations to the "catastrophe" models of fatigue during exercise in humans. *British Journal of Sports Medicine* 38(5): 648-649, 2004.

[26] Shield A. and Zhou S. Assessing voluntary muscle activation with the twitch interpolation technique. *Sports Medicine* 34(4): 253-267, 2004.

[27] Millet G.Y and Lepers R. Alterations of neuromuscular function after prolonged running, cycling and skiing exercises. *Sports Medicine* 34(2): 105-116, 2004.

[28] Bigland-Ritchie B, Rice CL, Garland SJ and Walsh ML. Task-dependent factors in fatigue of human voluntary contractions. *Advances in Experimental Medicine and Biology* 384: 361-380, 1995.

[29] Garland S.J. and Gossen E.R. The muscular wisdom hypothesis in human muscle fatigue. *Exercise Sport Science Review* 30(1): 45-49, 2002.

[30] St Clair Gibson A., Lambert M.L. and Noakes T.D. Neural control of force output during maximal and submaximal exercise. *Sports Medicine* 31(9): 637-650, 2001.

[31] Utter A.C., Kang J. and Robertson R.J. Perceived Exertion, *www.acsm.org*, American College of Sports Medicine. August 2001.

[32] Shigematsu R., Ueno L.M., Nakagaichi M., Nho H. and Tanaka K. Rate of perceived exertion as a tool to monitor cycling exercise intensity in older adults. *Journal of Aging Physical Activity*. 12(1): 3-9, 2004.

[33] Hampson D.B., St Clair Gibson A., Lambert M.I., Dugas J.P., Lambert E.V. and Noakes T.D. Deception and perceived exertion during high-intensity running bouts. *Percept Motor Skills* 98(3): 1027-1038, 2004.

[34] Impellizzeri F.M., Rampinini E., Coutts A.J., Sassi A. and Marcora S.M. Use of RPE-based training load in soccer. *Medicine and Science in Sports and Exercise* 36(6): 1042-1047, 2004.

[35] Utter A.C., Kang J., Nieman D.C., Dumke C.L., McAnulty S.R., Vinci D.M. and McAnulty L.S. Carbohydrate supplementation and perceived exertion during prolonged running. *Medicine and Science in Sports and Exercise* 36(6): 1036-1041, 2004.

[36] Carson R.G., Riek S. and Shahbazpour N. Central and peripheral mediation of human force sensation following eccentric or concentric contractions. *Journal of Physiology* 539(3): 913-925, 2002.

[37] Tucker R, Rauch L, Harley Y.X.R. and Noakes T.D. Impaired exercise performance in the heat is associated with an anticipatory reduction in skeletal muscle recruitment. *Pflugers Archiv* 448(4): 422, 2004.

[38] Nybo L and Nielsen B. Perceived exertion is associated with an altered brain activity during exercise with progressive hyperthermia. *Journal of Applied Physiology* 91(5): 2017-2023, 2001.

[39] Nielsen B. and Nybo L. Cerebral changes during exercise in the heat. *Sports Medicine* 33(1): 1-11, 2003.

[40] Kayser B., Narici M., Binzoni T., Grassi B. and Cerretelli P. Fatigue and exhaustion in chronic hypobaric hypoxia: influence of

exercising muscle mass. *Journal of Applied Physiology* 76(2): 634-640, 1994.

[41] Todd G., Taylor J.L. and Gandevia S.C. Measurement of voluntary activation of fresh and fatigued human muscles using transcranial magnetic stimulation. *Journal of Physiology* 551(2): 661-671, 2003.

[42] Andersen B., Westlund B. and Krarup C. Failure of activation of spinal motoneurones after muscle fatigue in healthy subjects studied by transcranial magnetic stimulation. *Journal of Physiology* 551(1): 345-356, 2003.

[43] Tergau F., Geese R., Bauer A., Baur S., Paulus W. and Reimers C.D. Motor cortex fatigue in sports measured by transcranial magnetic double stimulation. *Medicine and Science in Sports and Exercise* 32(11): 1942-1948, 2000.

[44] Blomstrand E. Amino Acids and Central Fatigue. *Amino Acids*, 20 (1): 25-34 2001

[45] Davies, J.M. Central and Peripheral Factors in Fatigue. *Journal of Sports Science* (13): S49 –S53, 1995

[46] Pitsiladis Y.P., Strachan A.T., Davidson I. and Maughan R.J. Hyperprolactinaemia during prolonged exercise in the heat: evidence for a centrally mediated component of fatigue in trained cyclists. *Experimental Physiology*, 87 (2): 215-226, 2002.

[47] Dalsgaard MK, Ide K, Cai Y, Quistorff B and Secher NH. The intent to exercise influences the cerebral O(2)/carbohydrate uptake ratio in humans. *Journal of Physiology* 540(2): 681-689, 2002.

[48] Dalsgaard M.K., Quistorff B., Danielsen E.R., Selmer C., Vogelsang T. and Secher NH. A reduced cerebral metabolic ratio in exercise reflects metabolism and not accumulation of lactate within the human brain. *Journal of Physiology* 554(2): 571-578, 2004.

[49] Dalsgaard M.K., Nybo L., Cai Y., and Secher N.H. Cerebral metabolism is influenced by muscle ischaemia during exercise in humans. *Experimental Physiology* 88(2): 297-302, 2003.

[50] Damasio A. Fundamental Feelings. *Nature* 413: 781, 2001.

[51] Lorist M.M., Kernell D., Meijman T.F. and Zijdewind I. Motor fatigue and cognitive task performance in humans. *Journal of Physiology* 545(1): 313-319, 2002.

[52] Ulmer HV. Concept of an extracellular regulation of muscular metabolic rate during heavy exercise in humans by psychophysiological feedback. *Experientia* 52(5): 416-420, 1996.

[53] Hampson DB, St Clair Gibson A, Lambert MI and Noakes TD. The influence of sensory cues on the perception of exertion during exercise and central regulation of exercise performance. *Sports Medicine* 31(13): 935-952, 2001.

[54] Hartley L. Cognitive-communicative abilities following brain injury: a functional approach. Singular Publishing Group, San Diego, California, 1995.

[55] Guadagnolia M.A., Etnyreb B. and Rodriguea M.L. A test of a dual central pattern generator hypothesis for subcortical control of locomotion. *Journal of Electromyography and Kinesiology* 10(4): 241-247, 2000.

[56] Liu J.Z., Shan Z.Y., Zhang L.D., Sahgal V., Brown R.W. and Yue G.H. Human Brain Activation During Sustained and Intermittent Submaximal Fatigue Muscle Contractions: An fMRI Study. *Journal of Neurophysiology* 90: 300-312, 2003.

[57] Williamson J.W., McColl R., Mathews D., Ginsburg M. and Mitchell J.H. Activation of the insular cortex is affected by the intensity of exercise. *Journal of Applied Physiology* 87(3):1213-1219, 1999.

[58] Williamson J.W., McColl R., Mathews D., Mitchell J.H., Raven P.B. and Morgan W.P. hypnotic manipulation of effort sense during dynamic exercise: cardiovascular responses and brain activation. *Journal of Applied Physiology* 90: 1392-1399, 2001.

[59] Williamson J.W., McColl R. and Mathews D. Evidence for central command activation of the human insular cortex during exercise. *Journal of Applied Physiology* 94(5): 1726-1734, 2003.

[60] Miller E.K. The Prefrontal Cortex And Cognitive Control. *Nature Reviews Neuroscience* 1: 59-65, 2000.

[61] Lopes da Silva F., Van Rotterdam A. *Biophysical Aspects of EEG and Magnetencephalogram Generation* in Electroencephalography: Basic Principles, Clinical Applications, and Related Fields, Third Edition. Baltimore, Williams and Wilkins 78-80, 1993.

[62] Duffy F.H., Lyer V.G., Surwillo W.W. *Clinical Encephalography and Topographic Brain Mapping.* New York, Springer-Verlag, 1-6, 97-98, 243 –252, 1989.

[63] Lopes da Silva F. *Dynamics of EEGs as Signals of Neuronal Populations: Models and Theoretical Considerations* in Electroencephalography: Basic Principles, Clinical Applications, and Related Fields, Third Edition. Baltimore, Williams and Wilkins 63-75, 1993.

[64] Bressler S.L. *Understanding Cognition Through Large-Scale Cortical Networks*. Current Directions in Psychological Science, 11(2): 1-4, Apr 2002 (In-Press).

[65] Haines D.E. *Fundamentals of Neuroscience*, 2nd Edition. Churchill Livingstone, 2002.

[66] Koles Z.J. Trends in EEG source localization. *Electroencephalography and clinical Neurophysiology,* 106: 127-137, 1998.

[67] Leon-Garcia A. *Probability and Random Processes for Electrical Engineers*, Second Edition. Addison Wesley, 1994.

[68] Nunez P.L. Non-Linear Phenomena and Chaos in *Neocortical Dynamics and Human EEG Rhythms*, Oxford University Press, 417-472, 1995.

[69] Schreiber T. *Interdisciplinary application of nonlinear time series methods*. Physics Report, Elsevier Science, 308, 1-64, 1999.

[70] Widman G., Schreiber T., Rehberg, B., Hoeft A. and Elger C.E. Quantification of the depth of anesthesia by nonlinear time series analysis of brain electrical activity. *Physical Review E*, 62 (4): 4898 – 4903, 2000.

[71] Sarbadhikari S.N. and Chakrabarty K. Chaos in the brain: a short review alluding to epilepsy, depression, exercise and lateralization. *Medical Engineering and Physics* 23: 445-455, 2001.

[72] Steyn-Ross M. L., Steyn-Ross D. A., Sleigh J. W. and D. T. J. Liley. Theoretical electroencephalogram stationary spectrum for a white noise driven cortex: Evidence for a general anesthetic-induced phase transition. *Physical Review E*, 60 (6): 7299 – 7311, 1999.

[73] Jeong J., Kim M.S. and Kim S.Y. Test for low-dimensional determinism electroencephalograms. *Physical Review E*, 60 (1): 831 – 837, 1999.

[74] Niedermeyer E. *The Normal EEG of the Waking Adult* in Electroencephalography: Basic Principles, Clinical Applications, and Related Fields, Third Edition. Baltimore, Williams and Wilkins 131-146, 1993.

[75] Pfurtscheller G. and Lopes da Silva F.H. Event-related EEG/MEG synchronization and desynchronization: basic principles. *Clinical Neurophysiology* 110: 1842-1857, 1999.

[76] Rodriguez E., George N., Lachaux J.P., Martinerie J., Renault B. and Varela F.J. Perception's shadow: long-distance synchronization of human brain activity. *Nature* 397: 430 – 433, 1999.

[77] Bhattacharya J. and Petsche H. Enhanced phase synchronization in the electroencephalograph γ band for musicians while listening to music. *Physical Review E*, 64 Article No. 012902: 1 – 4, 2001.

[78] Amjad A.M., Halliday D.M., Rosenberg J.R. and Conway B.A. An extended difference of coherence test for comparing and combining several independent coherence estimates: theory and application to the study of motor units and physiological tremor. *Journal of Neuroscience Methods* 73: 69-79, 1997.

[79] Stopfer M., Bhagavan S., Smith B.H. and Laurent G. Impaired odour discrimination on desynchronization of odour-encoding neural assemblies. *Nature* 390: 70 -74, 1997.

[80] Tass P., Rosenblum M.G., Weule J., Kurths J., Pikovsky A.S., Volkmann J., Schnitzler A. and Freund H.J. Detection of *n:m* Phase locking from Noisy Data: Application to Magnetoencephalography. *Physical Review Letters*, 81 (15): 3291 – 3294, 1998.

[81] Rosenblum M.G., Pikovsky A.S. and Kurths J. Phase Synchronization of Chaotic Oscillators. *Physical Review Letters*, 76 (11): 1804 – 1807, 1996.

[82] Rosenblum M.G. Identification of coupling direction: Application to cardiorespiratory interaction. *Physical Review E*, 65, Article No. 041909: 1 – 11, 2002.

[83] Diambra L. and Malta C.P. Nonlinear models for detecting epileptic spikes. *Physical Review E*, 59 (1): 831 – 837, 1999.

[84] Ott E. *Chaos in Dynamical systems*. Cambridge University Press. 1993.

1

[85] Hjorth B.O. An Online Transformation of EEG Scalp Potentials into Orthogonal Source Derivations. *Electroencephalography and Clinical Neurophysiology,* 39:526-530, 1975.

[86] Perrin F., Pernier J., Bertrand O., Giard M.H. and Echallier J.F. Mapping of scalp potentials by surface spline interpolation. *Electroencephalography and clinical Neurophysiology*, 66: 75-81, 1987.

[87] Perrin F., Pernier J., Bertrand O. and Echallier J.F. Spherical splines for scalp potential and current density mapping. *Electroencephalography and clinical Neurophysiology*, 72: 184-187, 1989.

[88] Perrin F., Pernier J., Bertrand O. and Echallier J.F. Corrigenda: EEG 02274, *Electroencephalography and clinical Neurophysiology*, 76: 565, 1990.

[89] Law S.K., Nunez P.L. and Wijesingghe R.S. High-Resolution EEG Using Spline Generated Surface Laplacians on Spherical and Ellipsoidal Surfaces. *IEEE Transactions on Biomedical Engineering*, 40(2) 145-153, 1993.

[90] Srinivasan R., Nunez P.L. and Silberstein R.B. Spatial filtering and neocortical dynamics: estimates of EEG coherence. *IEEE Transactions on Biomedical Engineering*, 45(7): 814-826, Jul. 1998.

[91] Hutcheon B. and Yarom Y. Resonance, oscillation and the intrinsic frequency preferences of neurons. *Trends in Neuroscience* 23(5): 216-222, 2000.

[92] Cooper N.R., Croft R.J., Dominey S.J., Burgess A.P. and Gruzelier JH. Paradox lost? Exploring the role of alpha oscillations during externally vs. internally directed attention and the implications for idling and inhibition hypotheses. *International Journal of Psychophysiology* 47(1): 65-74, 2003.

[93] Klimesch W., Sauseng P. and Gerloff C. Enhancing cognitive performance with repetitive transcranial magnetic stimulation at human individual alpha frequency. *European Journal of Neuroscience* 17(5): 1129-33, 2003.

[94] Jensen O., Gelfand J., Kounios J. and Lisman J.E. Oscillations in the alpha band (9-12 Hz) increase with memory load during retention in a short-term memory task. *Cerebral Cortex* 12(8): 877-82, 2002.

[95] Stam C.J., van Cappellen van Walsum A.M. and Micheloyannis S. Variability of EEG synchronization during a working memory task in healthy subjects. *International Journal of Psychophysiology* 46(1): 53-66, 2002.

[96] Sauseng P, Klimesch W, Gruber W, Doppelmayr M, Stadler W and Schabus M. The interplay between theta and alpha oscillations in the human electroencephalogram reflects the transfer of information between memory systems. *Neuroscience Letters* 324(2): 121-4, 2002.

[97] Pfurtscheller G. Induced oscillations in the alpha band: functional meaning. *Epilepsia* 44(12s): 2-8, 2003.

[98] Kopell N., Ermentrout G.B., Whittington M.A. and Traub R.D. Gamma rhythms and beta rhythms have different synchronization properties. *Proceedings of the National Academy of Sciences of the USA* 97(4): 1867-1872, 2000.

[99] Whittington M.A., Faulkner H.J., Doheny H.C. and Traub R.D. Neuronal fast oscillations as a target site for psychoactive drugs. *Pharmacology and Therapeutics* 86: 171-190, 2000.

[100] Pfurtscheller G. and Andrew C. Event-Related Changes of Band Power and Coherence: Methodology and Interpretation. *Journal of Clinical Neurophysiology* 16(6): 512-519, 1999.

[101] Karrasch M., Laine M., Rapinoja P. and Krause CM. Effects of normal aging on event-related desynchronization/synchronization during a memory task in humans. *Neuroscience Letters* 366(1): 18-23, 2004.

[102] Coull J.T. Neural correlates of attention and arousal: insights from electrophysiology, functional neuroimaging and psychopharmacology. *Progress in Neurobiology* 55: 343-361, 1998.

[103] Egner T. and Gruzelier J.H. EEG biofeedback of low beta band components: frequency-specific effects on variables of attention and event-related brain potentials. *Clinical Neurophysiology*. 115,131-139, 2004.

[104] Egner T and Gruzelier JH. Learned self-regulation of EEG frequency components affects attention and event-related brain potentials in humans. *Neuroreport* 12(18): 4155-9, 2001.

[105] Vazquez Marrufo M., Vaquero E. Cardoso M.J. and Gomez C.M. Temporal evolution of alpha and beta bands during visual spatial attention. *Brain Research: Cognitive Brain Research* 12: 315-320, 2001.

[106] Foster P.S. and Harrisson D.W. The relationship between magnitude of cerebral activation and intensity of emotional arousal. *International Journal of Neuroscience* 112: 1463-1477, 2002.

[107] Ray W.J. and Cole H.W. EEG alpha activity reflects attentional demands and beta activity reflects emotional and cognitive processes. *Science* 228:750-752, 1985.

[108] Basar E., Basar-Eroglu C., Karakas S. and Schurmann M. Brain oscillations in perception and memory. *International Journal of Psychophysiology* 35: 95-124, 2000.

[109] Molle M., Marshall L., Gais S. and Born J. Learning increases human electroencephalographic coherence during subsequent slow sleep oscillations. *Proceedings of the National Academy of Sciences of the USA* 101(38): 13963-13968, 2004.

[110] Karakas S., Erzengina OU. and Basar E. The genesis of human event-related responses explained through the theory of oscillatory neural assemblies. *Neuroscience Letters* 285: 45-48, 2000.

[111] Vogel W, Broverman D.M and Klaiber E.L. EEG and mental abilities. *Electroencephalography Clinical Neurophysiology* 24(2): 166-75, 1968.

[112] Kamarajan C., Porjesz B, Jones K.A., Choi K., Chorlian D.B., Padmanabhapillai A., Rangaswamy M., Stimus A.T. and Begleiter H. The role of brain oscillations as functional correlates of cognitive systems: a study of frontal inhibitory control in alcoholism. *International Journal of Neuroscience* 51: 155-180, 2004.

[113] Klimesch W. EEG alpha and theta oscillations reflect cognitive and memory performance: a review and analysis. *Brain Research Reviews* 29: 169-195, 1999.

[114] Sakowitza O.W, Schurmanna M. and Basar E. Oscillatory frontal theta responses are increased upon bisensory stimulation. *Clinical Neurophysiology* 111: 884-893, 2000.

[115] Knyazev G.G. and Slobodskaya H.R. Personality trait of behavioral inhibition is associated with oscillatory systems

reciprocal relationships. *International Journal of Psychophysiology* 48: 247-261, 2003.

[116] Pikovsky A., Rosenblum M. and Kurths J. *Synchronization: A universal concept in nonlinear sciences*. Cambridge University Press, Cambridge UK, 2001.

[117] Ferree T. and Srinivasan R. *Theory and Calculation of the Scalp Surface Laplacian*. Electrical Geodesics, Inc. Technical Note: 1-6, 2000.

[118] YXR Harley. *Endurance performance: the integrative physiology of resisting fatigue*. PhD Thesis. University of Cape Town, 2004.

[119] Ethics approval number: 069/99 (16 April 1999).

[120] Manufactured by Electrical Geodesics Inc, USA. (EGI). http://www.egi.com

[121] EGI System 200 Technical Manual S-MAN-200-SYSR-007, Electical Geodesics Inc, USA, system200. Pdf downloaded from http://www.egi.com.

[122] http://www.mathworks.com/

[123] http://www.sourcesignal.com/

[124] http://msdn.microsoft.com/visualc/

[125] Munro B.H. *Statistical Methods For Health Care Research* 4th Edition. Lippincott Williams and Wilkins, 2001.

[126] http://www.statsoft.com/

[127] Daniel W.W. *Biostatistics: A foundation for analysis in health sciences* 6th Edition. John Wiley and Sons, Inc. 1995.

[128] http://www.brainmaster.com/generalinfo/electrodeuse/eegbands/1020/1020.html

[129] http://members.aol.com/aduial/1020sys.html

[130] http://faculty.washington.edu/chudler/1020.html

[131] http://www.du.edu/~jcalvert/math/legendre.htm

[132] http://mathworld.wolfram.com/LegendrePolynomial.html

[133] http://zone.ni.com/devzone/conceptd.nsf/webmain/057F9CCC873BA547862568C7006AD36B?opendocument&node=12601_US

[134] http://kwon3d.com/theory/filtering/lpass.html

[135] Tabachnick B.G. and Fidell L.S. Using Multivariate statistics. 4th edition. Allyn and Bacon. Boston, 2001.

[136] Swinscow T.D.V. Statistics at square one. 9th edition. BMJ Publishing group, 1996.

[137] Wonnacott T.H. and Wonnacott R.J. Introductory Statistics 3rd edition. John Wiley and Sons, Inc., 1977.

[138] PSViewer Software, written by this author (Devin Bosanquet). For details on how the software was used please see Section 5.6.1.1.

[139] Muthukumaraswamy S.D. and Johnson B.W. Changes in rolandic mu rhythm during observation of a precision grip. *Psychophysiology* 41: 152–156, 2004.

[140] Arnhold J., Grassberger P., Lehnertz K. and Elger C.E. A robust method for detecting interdependencies: application to intracranially recorded EEG. *Physica D* 134: 419-430, 1999.

[141] Le Van Quyen M, Foucher J, Lachaux J, Rodriguez E, Lutz A, Martinerie J and Varela FJ. Comparison of Hilbert transform and wavelet methods for the analysis of neuronal synchrony. *Journal of Neuroscience Methods* 111(2): 83-98, 2001.

[142] He B, Lian J and Li G. High-resolution EEG: a new realistic geometry spline Laplacian estimation technique. *Clinical Neurophysiology* 112: 845-852, 2001.

[143] Ferree T. *Spline Interpolation of the Scalp EEG*. Electrical Geodesics, Inc. Technical Note: 1-5, 2000.

Appendix A Background on Exercise Fatigue

A.1 Factors Influencing the Onset of Fatigue

In their review on the neurobiology of muscle fatigue [11], Enoka and Stuart outline four themes that emerge in the study of muscle fatigue that shall be discussed here and shall provide a background for the rest of this review.

A.1.1 Task dependency

Here Enoka and Stuart [11] describe the role of task variability in determining the onset of fatigue. Task variability includes type of exercise, type of muscle contraction, duration and intensity of the exercise [11][27]. Bigland-Ritchie provides evidence to support task dependency in fatigue, by comparing studies of different exercise protocols [28].

A.1.2 Force-fatigability relationships

Here Enoka and Stuart [11] indicate that there is a relationship between fatigue and the amount of force generated in the muscle – the greater the force generated by the muscle the more it will fatigue. This suggests that there is a relationship between the level of force generated and the fatiguing mechanism [11].

A.1.3 Muscle Wisdom

There is a tendency for the relaxation rate, firing frequency and motor neuron discharge to decrease as fatigue develops [11]. Enoka and Stuart [11] suggest that this may be an optimisation strategy on behalf of the CNS to ensure force generation is sustained and ensure the economical activation of muscle fibres as well as to reduce fatigue [29]. St Clair Gibson et al [30] suggest this is part of a

neural mechanism that serves to maintain muscle reserve and prevent severe metabolic changes from damaging the contracting muscle.

A.1.4 Sense of Effort

Perception of effort is an important factor in the decision to stop exercising. Ultimately it's the sense of effort or perceived exertion along with other sensations that become intolerable that determine when exercise is volitionally terminated [16]. When sense of effort is compared to the ability to generate a force it has been found that there is an independence of perceived effort and force failure during sustained activity and in fact in certain cases there may be an effort related fatigue but no impairment in the ability to sustain a force [11].

When large forces are being generated any additional force output will result in a disproportionate increase in the perceived exertion. The opposite is true at low force generation where any increase in force output results in only a small increase in perceived effort.

In an attempt to quantify perceived effort or exertion, the Swedish psychologist Gunnar Borg developed a 15-point scale that categorises the subjective feelings of effort, strain, discomfort, and fatigue [31]. The scale starts at level six which represents no exertion. Level nine represents very light exertion; level thirteen 'somewhat hard', level fifteen 'heavy' and level twenty maximal exertion. The Rate of Perceived Exertion (RPE) scale developed by Borg has been shown to be linearly correlated with heart rate and oxygen uptake [31]-[34] and carbohydrate substrate availability [35].

Sense of effort is thought to be derived from corollary discharges or the resultant activity of motor commands from the motor cortex [11]. In their investigation of force sensation in the triceps brachii muscle Carson et al [36] they find that centres 'upstream' of the motor cortex may be involved in sense of effort in eccentric contractions. They hypothesize that sensory information from the

(fatigue) damaged muscle influences the relationship between neural mechanisms responsible for sense of effort and motor cortex output, and that these neural mechanisms reside 'upstream' of the motor cortex.

Hampson et al present further evidence that afferent feedback mediates sense of effort [33]. They tested how RPE would be affected by a deception about the actual intensity of an exercise protocol. It was found that there was no significant differences in the RPE of the deceived group and the control group that had accurate knowledge of the exercise intensity level. This indicates that RPE reflects actual afferent feedback and is not altered by pre-exercise expectation [33].

Appendix B EEG Analysis Methods

This appendix describes different ways the EEG could be analysed for the purpose of associating patterns in the EEG signal to specific physiological or clinical brain states or quantifying the EEG signal in some manner that could result in data being correlated to specific brain states or functionality [22]. Methods discussed in this review are described qualitatively and the mathematical theory is not presented.

B1.1 Absolute Amplitude reporting

Analysis and reporting of absolute amplitude measurements of the EEG waveform, which is in the microvolts (μV) range, is generally avoided in EEG research. Absolute amplitude measurements depend on many variables within the context of taking the EEG readings and repeated measurements would probably have a high variation [74]. It is generally more meaningful to report relative amplitudes such as the amplitude difference between the above mentioned frequency ranges.

B1.2 Statistical and Spectral Analysis

The EEG is an complex time series whose future values cannot be easily predicted from past values. The underlying processes generating scalp voltages are complex with many degrees of freedom. Thus it is often useful to treat the EEG as a random or stochastic process, employing various statistical measures such as mean, variance, covariance, correlation and the cross spectrum. The correlation coefficient gives a measure of the correlation of two signals. Two signals are correlated if the future values of one can be predicted as a function of another [4]. Successive values of EEG time series may be dependant on

previous sample values or sample values at other sites, with or without a time delay between sample values. Measures of dependence or interdependence can be calculated by covariance or correlation functions [22]. These and other methods to detect dependencies will be discussed in the next section.

Power spectral analysis is commonly performed in EEG analysis and gives an indication of the relative strength of a signal at all frequencies components. Methods based on the fast fourier transform (FFT) are usually used to calculate the power spectrum. The fourier transform allows a time series to be decomposed into a sum of sinusoids with a range of frequencies. A function of time that varies slowly has relatively strong sinusoidal components in the low frequency range while a function of time that varies rapidly has relatively strong sinusoidal components in the high frequency range [67]. The various sinusoidal components are weighted and added together and is called the power spectrum [67]. Techniques that compare the power present in two signals are important in EEG analysis and provide a means to quantify the relationship between EEG signals [22]. This technique is well suited for systems displaying rhythmic behaviour [78] and is particularly important for determining the frequency content of the EEG in the context of the frequency ranges discussed above, thus opening the door to a wide range of methods that investigate EEG frequency content.

The presence of a large value or a peak in a certain frequency range indicates that a group of neurons are oscillating at the same frequency with a common phase and thus the power spectrum is a tool for measuring synchronization of neurons locally [10]. The power spectrum may be utilized in studies involving event related synchronization (ERS) and event related desynchronization (ERD) [75].

B1.3 Measurements of Dependency

In the previous section spectral analysis was discussed as a method for measuring cortical synchronization locally (at small scales). The dependence or interdependence of signals measured at two locations can provide much insight into how different areas of the brain cooperate during a cognitive task. Statistical measures such as covariance, cross correlation and cross spectrum analysis can be employed. Correlation techniques have been widely used to investigate dependencies and determine signal pathways in the brain [78]. Coherence is by far the most widely applied method for detecting dependencies between signals measured at different locations on the scalp. More recently developed methods are being employed with success and offer powerful alternatives to traditional methods.

Coherence is applied widely in EEG research and is practically implemented using the fourier transform. Coherence is the correlation coefficient squared across the frequency spectrum, and provides an important measure of functional interactions between oscillating systems and network formation [21].

Coherence between voltages measured at two points in a linear, isolated noise free circuit has the value one, while coherence between voltages measured at two points that are located on non-interacting circuits is zero [21]. Coherence is a measure of phase synchronization. The activity of two signals is synchronous when their rhythms coincide, measurable by the phase relationship between the signals [4]. Coherence is an indirect measure of synchrony in that it measures phase consistency between signals but its value is also dependent on the amplitudes of the signals under consideration [80].

B1.4 Measurements of Phase Synchronization

Recently researchers have started to look beyond dependence between signals and have begun to look at phase synchronization alone as being functionally important for various complex cognitive processes. Varela et al. [4] provide a thorough review on the topic of large-scale integration of local cortical activity, in which they focus on synchronization as means by which this process occurs. Along with new ideas about how the brain processes information and organizes itself, new methods to quantify synchrony beyond coherence have been developed. Some of these methods will be compared and discussed here.

Phase synchronization as measured by coherence has several drawbacks, the most important being that weak phase coupling in the brain may not be detected by current coherence methodologies. Phase coupling achieved in brain oscillators may be weak and will most likely be buried in strong noise. The most profound function of neuronal oscillators may be their ability to synchronize with each other over short or long distances in an energy efficient manner [6], such as weak phase coupling which allows networks to be dynamically created in an energy inexpensive manner. The high amplitude of the background noise will mask the weak interaction, as the coherence methodology is dependent on the signal amplitudes as well as the phase angles. Furthermore the coherence methodology assumes the system generating the signals is a noise free linear system. Of course this assumption may be violated and successful results obtained, but a measurement technique that takes into account non-linearity may be preferable.

The coherence methodology as outlined in reference [100] requires a specific experimental methodology to be carried out, which involves experimental trials to be repeated in order to obtain statistical confidence in the coherence calculations. This may not always be practical, and in the current investigation the trial was not designed for this kind of analysis.

Therefore more suitable methods of calculating phase synchronization were considered.

The analysis of synchronization in science has wide application, including physics, astrophysics, chemistry and economics [140] and as such, many methods have been developed to quantify synchronization including generalized synchronization, mutual information and other methods developed in reference [140]. It was beyond the scope of this investigation to do a thorough comparison of all the methods for quantifying phase synchronization, so the author was guided by popular methods used in high profile publications, provided that the theory was thoroughly developed. Two methods for quantifying phase synchronization are popular in the leading neuroscience publications: the method based on wavelets and the method based on the Hilbert transform [141]. A study published by leading authors in studies of synchronization compared the two methods and determined they were "fundamentally equivalent for the study of neuroelectric signals" [141]. The methods based on the Hilbert transform led to a relatively simple implementation and is based on a solid theoretical framework [1][3][80][81][82] and was thus favoured by the author.

Much of the phase synchronization theory is based on the study of theoretical chaotic oscillators. The methods are based on the concept that the phase of a signal can be separated in the frequency domain independent of the amplitude information. This is unlike coherence where amplitude information is integrated with phase information. These methods allow for the detection of interdependence between weakly interacting systems, not obtainable by other methods [80]. The application of this theory has been shown to be well suited for EEG analysis as it takes into account the noise present in real world EEG signals. Nunez et al. [21] provide a thorough review of coherence and phase synchrony and discuss the characteristics of synchrony and coherence at different temporal and spatial scales.

B1.5 Other Non-Linear Analysis Methods

Analysis measures based on chaos and non-linear systems theory abound in the literature, often with much controversy [69] [70] [83]. This controversy often arises when techniques are applied to EEG data that violate assumptions, although other techniques applied to EEG such as spectral analysis violate some basic assumptions and conditions, such as stationarity [69][83]. Non-linear dynamical methods of analysis include calculating the correlation dimension (not the same measure as correlation coefficient in classical statistics), Lyapunov exponents and Kolmogorov entropy [83]. The theory is outlined in [84], and has widespread applications [69] [84].

Because the EEG is an ever-changing signal whose properties vary with brain-state and function, EEG signals can be modelled to suit a particular physiological state. For example EEG recorded during seizures [83] and anaesthesia [70] [72] can be modelled separately because of their unique characteristics. In their study, Widman et al. [70] applied theories of non-linear dynamics to quantify depth of anaesthesia. The study highlights the use of potentially useful analysis methods without too much consideration of the underlying process generating the signals [70]. Diambra et al. [83] examine the possibility of applying nonlinear prediction methods for detecting epileptic spikes with mixed results. Many examples of nonlinear time series analysis applied to EEG abound in the literature.

B1.6 EEG Preprocessing: Methods for Improving Spatial Resolution

Nunez et al [21] give a thorough review of methods to improve spatial resolution of EEG recordings. There are 2 general approaches to EEG spatial resolution: dura imaging and Scalp surface Laplacian (SL) [21][142]. Dura imaging depends on concentric sphere or finite element modelling of the head [21]. For this

investigation, methods based on head models were out of scope and only methods based on a generic head shape or model were considered. Thus methods involving the SL were selected.

The method was first introduced by Hjorth [85]. The method is simplified by the fact that it does not require knowledge of head conductance or other parameters [142] and is relatively simple to implement in software. There are many sophisticated derivatives of SL that provide more accurate spatial filtering and include the spherical spline Laplacian, ellipsoidal spline Laplacian and realistic geometry spline Laplacian [142]. The difference between these methods is the mathematical model used for the estimation of the surface over which the SL is estimated for potentials, where the methods based on realistic geometry are inherently more difficult [142]. The use of the spherical spline Laplacian as developed by Perrin et al [86][87][88] has gained widespread popularity, as it uses a generic sphere to estimate the shape of the head, which greatly simplifies the SL calculations. This is the method that was selected for this investigation.

Appendix C Additional Brain Rhythms and Studies Involving Phase Synchronization in Neuroscience

Central Mu Rhythms and Central Beta Sensorimotor Rhythms

Several rhythms exist in the cortex that are specific to motor activity. These rhythms exist in the alpha and beta band and their specific characteristics will be briefly discussed.

The sensorimotor cortex produces a rhythm in the 8-13Hz range that is attenuated before and during the execution of movement, and is referred to as Rolandic mu [139]. The desynchronization of Mu rhythms may also occurr in subjects where movement is observed and not executed, and Muthukumaraswamy et al [139] have shown that the pattern of mu rhythm desynchronization is sensitive to the degree of complexity in the movements observed by subjects.

The lower beta band rhythms in the central cortex is also affected by movement in a similar way to mu rhythms described above [75]. Mu rhythm desynchronization begins about 2s prior to movement onset in the contralateral region and becomes bilaterally similar just before movement execution, while beta ERD is more discrete and specific to certain regions of the cortex such as the motor cortex [75]. Mu band Event Related Coherence (ERCoh), which is a measure of phase synchronization, is close to zero between the contralateral and ipsilateral hemispheres in the preparatory period and execution of movement in finger movement tasks, and indicates that the mu generating networks of each hemisphere are linearly independent [100].

Pfurtscheller et al hypothesise that contralateral pre-movement mu desynchronization represents unspecific pre-activation, priming or presetting of motor neurons [75].

Finally, postmovement beta ERS has been reported in studies involving voluntary movement [100]. The beta ERS is found in both sides of the cortex during movement but is stronger over the contralateral representation area and is seen as a dynamic response of the cortex to the termination of movement [100]. Postmovement beta ERS is a robust phenomenon and is consistently seen in most subjects after finger, hand and foot movement [75]. Postmovement beta ERS has the following characteristics: beta ERS is larger with hand movement compared to finger movement; beta ERS is found after imagined movement and the maximum of beta ERS coincides with reduced excitability of motor cortex neurons [75]. Beta ERS as well as beta ERD may be associated with imagining, planning and execution of movement [101].

Studies Involving Phase Synchronization in Neuroscience

There has been much work devoted to the investigation of phase synchrony in the brains of humans and animals, particularly studying the visual system at gamma frequencies [4][6]. A few key studies will be highlighted here. Firstly Stopfer et al [79] demonstrate that odour encoding in honeybees depends on the oscillatory synchronization of projection neurons. This synchronization can be interrupted by the introduction of an antagonist to a certain neurotransmitter receptor. By inducing desynchronization in such a manner, the honeybees were unable to discriminate between similar odourants, but were still able to differentiate between dissimilar odourants. This study shows that oscillatory synchronization of neuronal assemblies is important for fine sensory discrimination in honeybees.

Rodriguez et al. [76] demonstrate that face perception induces a long-distance pattern of synchronization. This was the first study to show the direct participation of synchrony in a cognitive task in humans. This study will be discussed in some detail, as many of the methods employed will form the basis of the current work.

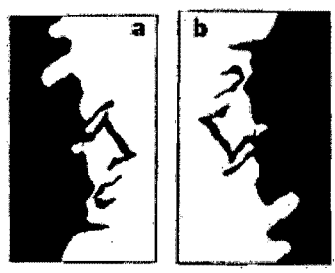

Figure C1: 'Mooney' face and (a) the same 'mooney' face presented upside down (b). Taken from Rodriguez et al. [76].

Ten subjects were shown 'mooney' faces, shown in Figure C-1 a) above. They are easily categorized as faces when presented upright, otherwise remain meaningless shapes as shown in Figure C-1 b). The subjects were presented with either an upright image or upside down image and were asked to press one of two buttons depending if they perceived a face or not during which their EEGs were recorded. The two conditions were analysed for phase synchrony in the gamma band from the EEG data. The perception and no perception condition elicited very different patterns of phase synchrony in the gamma band. The outcome of the analysis is shown in Figure C-2 below. It can be seen that in the perception condition there is an increase in phase synchrony between certain electrode pairs corresponding to perception itself, then followed by desynchronization. In both conditions synchronization is observed again corresponding to the reaction time for button press. What is noteworthy in this study is not only the long distance pattern of synchronization marking perception, but the active desynchronization between cognitive states (perception and motor

activity). This corresponds to the proposal by other researchers that the transition between two cognitive states should be punctuated by the undoing of previous synchronous assemblies to make way for a new ensemble [76].

Finally, Bhattacharya and Petsche investigate the phase synchrony between EEG electrodes in musicians and non-musicians listening to music [77]. They found that phase synchrony was significantly high in musicians while listening to music, across large areas of the cortex. The authors postulate that this is indicative of the musicans ability to host long-term memory representations of music and mediate access to these stored representations.

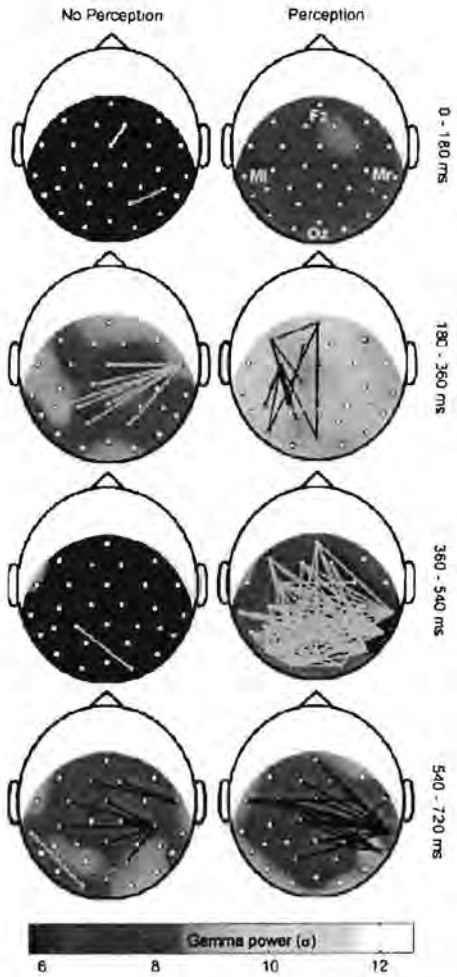

Figure C2: Head maps indicating synchronization and desynchronization. Black lines and green lines represent synchronization and desynchronization respectively. Distinct patterns of synchronization and desynchronization can be observed in the perception condition. Taken from Rodriguez et al. [76].

Appendix D Subject Details

Subject	Gender	Age	Height (cm)	Weight (kg)	Handedness	Net size	
subject1	m	35	177	73	r	m	*
subject2	m	24	167	72.2	r	m	
subject3	m	27	178	68	r	l	*
subject4	m	22	182	85	r	l	*
subject5	m	22	184	68.2	r	m	
subject6	m	22	180	63.5	r	s	*
subject7	m	35	185	101	l	m	
subject8	f	30	167	72	r	m	*
subject9	f	24	164	54	r	s	
subject10	m	32	176	84	r	l	*
subject11	f	25	171	61.5	r	s	*
subject12	f	44	167.5	54	r	s	*
subject13	m	44	171	72.5	l	m	
subject14	m	42	178	66	r	m	*
subject15	f	25	158	57.5	r	m	
subject16	f	31	161	100.8	r	m	
subject17	f	26	152	51.2	r	s	
subject18	m	30	165.4	63.4	r	m	*
subject19	m	24	167	63	l	?	*
subject20	m	29	178.5	93.3	l	m	*
subject21	m	18	175	64.5	r	m	*
subject22	m	18	160	48.4	r	s	*
subject23	m	18	169.5	60.5	r	s	*
subject24	m	18	163	56.5	r	s	*
subject25	m	23	171	65	r	m	*

* = excluded from EEG analysis

Appendix E The International 10-20 System

The international 10-20 system is an internationally recognized system of EEG electrode placement. The electrode placements correspond to the cerebral anatomical regions underlying them. Due to the variation in head size, the electrode positions are specified as a percentage (normally 10% or 20 %) of the circumference of the head relative to anatomical landmarks. Letters are used to label electrode positions, which stand for the underlying cortical region. For example the electrode labelled F3 would be found over the frontal cortex. Figure xx below illustrates the electrode positions, enclosed by circles. Electrodes labelled 'T' cover the temporal lobe, 'F' frontal lobe, 'Fp' frontal polar lobe, 'C' central gyrus, 'P' parietal lobe and 'O' the occipital lobe. The even numbers corrspond to the right hand side, and odd numbers the left hand side. The letter 'z' is used to indicate electrodes in the midline. [128] [129]

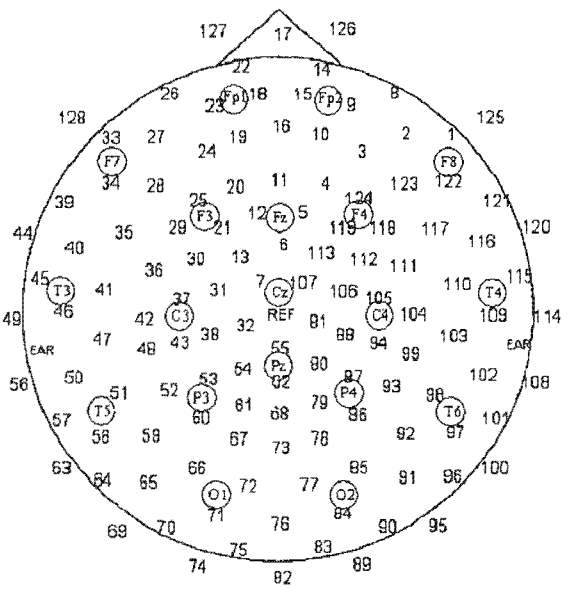

Figure E1: Positions of the international 10-20 system shown in enclosed circles, with the EGI GSN-128 electrode numbers.

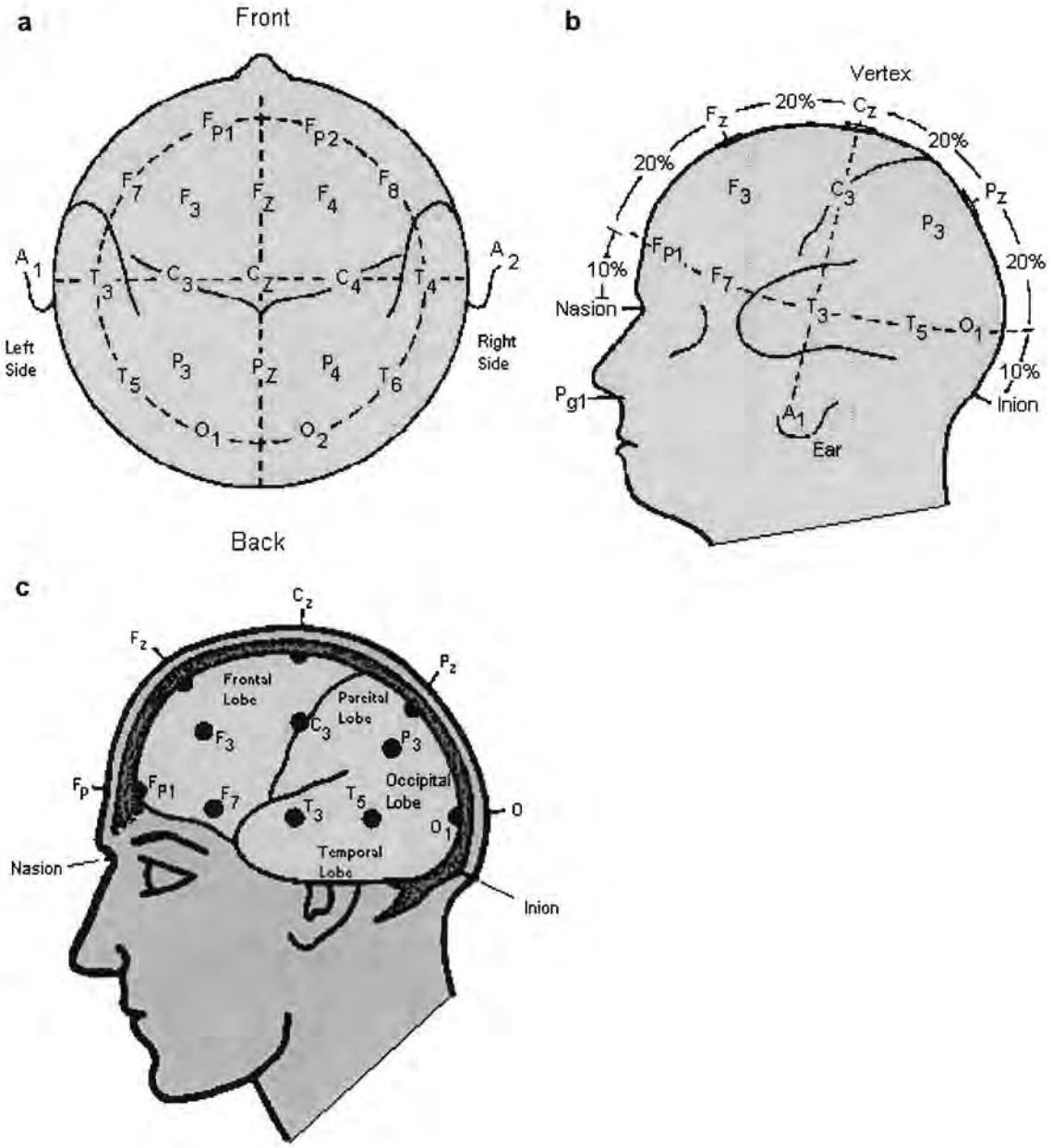

Figure E2: The positions of the international 10-20 system electrodes shown on a head, with the relative distances shown against anatomical landmarks in b). Taken from [130].

Appendix F The Legendre Polynomial

The n^{th} degree Legendre polynomial is given by

$$P_n(x) = \frac{1}{2^n n!}\left[\frac{d^n}{dx}\left(x^2 - 1\right)^n\right] \qquad \text{(F-1)}$$

with the recursive relationship

$$(n+1)P_{n+1}(x) = (2n+1)x\,P_n(x) - P_{n-1}(x) \qquad \text{(F-2)}$$

and since

$$P_n(1) = 1 \text{ and } P_n(-1) = (-1)^n \qquad \text{(F-3)}$$

the values of the polynomials can be calculated, with the first 7 polynomials shown in Figure F-1 below.

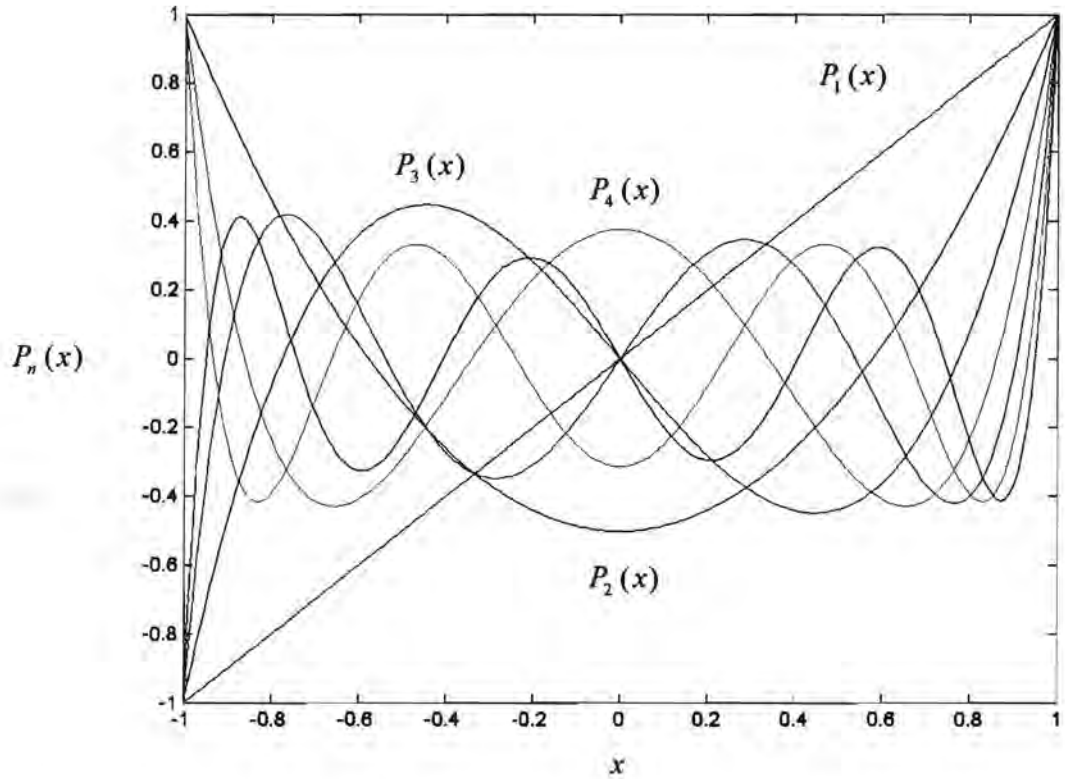

Figure F1: Solution to the first 7 Legendre polynomials.

Please see reference [131] and [132] for more details on the Legendre polynomials.

Appendix G Butterworth Filters

The Butterworth filter is characterized by a smooth response in the passband and a monotonic rolloff from the cutoff frequency. The cutoff frequency is defined as the half power point or 3-dB attenuation. The filter characteristic is also a slow rolloff between the passband and stopband, with the rolloff being steeper as the filter order increases. The response in the passband and stop band approximates an ideal filter – whose response in the pasband is 1 and in the stopband is 0. [133][134]

The operation on sample m of data $\mathbf{x}$ by the filtering operation is represented by the recursive time domain difference equations with output $\mathbf{y}$:

$$
\begin{aligned}
y(m) &= b(1)x(m) + z_1(m-1) \qquad \text{(G-1)} \\
z_1 &= b(2)x(m) + z_2(m-1) - a(2)y(m) \\
\vdots &= \quad \vdots \qquad\qquad \vdots \qquad\qquad \vdots \\
z_{n-2} &= b(n-1)x(m) + z_{n-1}(m-1) - a(n-1)y(m) \\
z_{n-1} &= b(n)x(m) - a(n)y(m)
\end{aligned}
$$

where $n-1$ is the filter order.

The filter transfer function is given as:

$$H(z) = \frac{A(z)}{B(z)} = \frac{b(1) + b(2)z^{-1} + \cdots + b(n+1)z^{-n}}{1 + a(2)z^{-1} + \cdots + a(n+1)z^{-n}} \qquad \text{(G-2)}$$

The frequency response of a sixth order bandpass ARMA (Autoregressive Moving Average) filter with Butterworth characteristics is shown in Figure G-1 below. The sampling frequency is 500Hz with the passband between 50Hz and 250Hz.

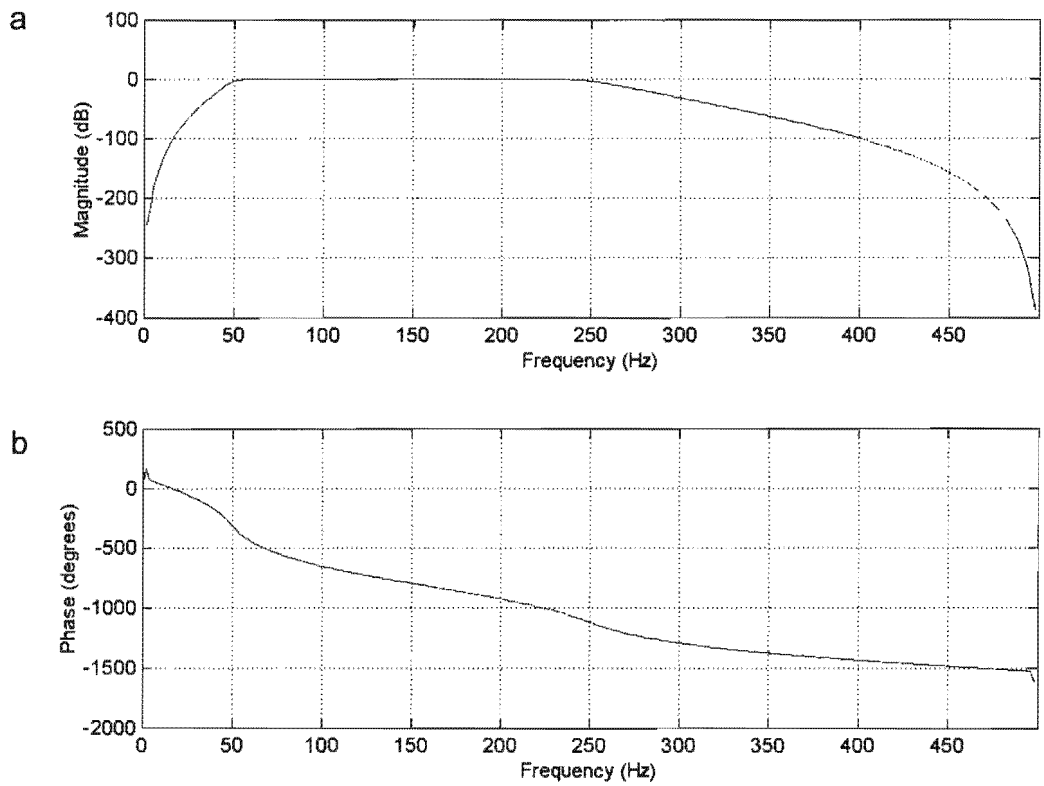

Figure G1: The frequency response of an ARMA Butterworth filter. The magnitude response (a) shows the slow rolloff and smoothness in the passband. The phase response is shown in (b).

Appendix H Hypothesis Testing and the ANOVA test.

H1.1 Hypothesis Testing

To determine if the means of two samples come from the same population or different populations it is necessary to use statistical decision theory. The population mean is usually unknown and the mean of the sample will have a standard error. Thus the means of two samples will likely be different from each other and different from their respective populations. To determine if they come from the same population, the degree of overlap in the range of the means is tested and this forms the basis of testing whether the 2 means form part of the same population or not. [135][136]

Two hypothetical states are set up; one that there is a difference in the means, and another that the means come from the same population. Only one hypothesis represents the truth. If one were to test whether the 2 means came from 2 populations, the null hypothesis, H_0, would state that there is no difference in the means (i.e. they come from the same population) and that any differences are due to chance. The alternative hypothesis, H_1, would state that the means of the samples come from different populations. H_1 is the claim to be proved (that the means are 'different') and H_0 is 'everything else' or no difference. [135][136]

The decision to accept or reject the null hypothesis is based on assessing the standard errors (SE) of the means. A decision is made based on the difference of the means. If the mean of one sample lies outside the range of twice the SE of the difference in means, there is a 1 in 20 chance that that mean comes from the same population. Thus is it far more likely that the mean come from different populations. The chance of rejecting the null hypothesis when it is true is 5%. This is known as a type I error. The probability used for rejecting the null hypothesis by chance, or making a type I error is usually chosen to be 5% or less. The probability that the means of the same population differ by chance is

known as the P-value. A more formal definition of the P-value is the probability of the sample value (say the one sample mean) being as large as the value actually observed, if the H_0 was true. The smaller the P-value, the greater the chance that the means come from different populations. Failing to reject the null hypothesis when it is false is known as a type II error. [135][136]

H1.2 Analysis of variance (ANOVA)

Analysis of variance is a technique used to compare 2 or more sample means. If one were to compare 3 sample means for differences calculated from 5 individual samples each, each mean would differ in value and one would need to use the SE of the means to determine if they are from different populations. If one were to compute the mean of a particular sample several times, that mean would vary due to chance fluctuation of the samples. The question of the means coming from different populations could be answered by comparing the variation of the samples to the variation of all the means. If they are in the same order, then the 3 sample means most likely come from the same population. If the variation of all the means is much larger than the variation of the individual samples, the means are likely to come from different populations. This is illustrated in Figure H-1 below. [137]

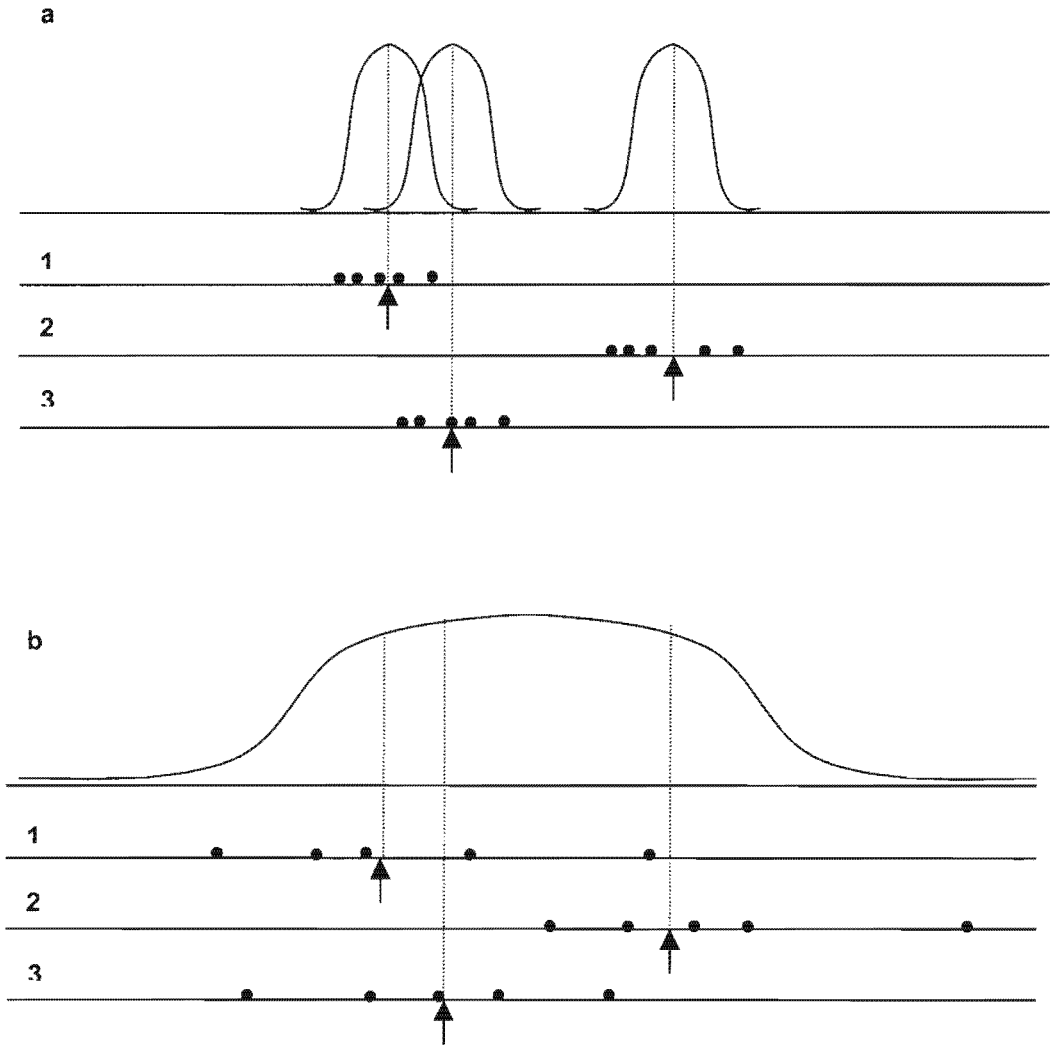

Figure H1: Graphs showing a comparison between 3 means with a small sample variation (a), and large sample variation (b). The means in example (a) are from different populations, while the means in example (b) are from the same population, although the means of each sample 1,2 and 3 are the same for both (a) and (b) respectively. Shaded circles represent individual samples and arrows the sample means. Figure adapted from reference [137].

This forms the basis of a formal test. The null hypothesis H_0 is that the 3 means are equal. The formal test tests for the variation in the sample means relative to

the variation observed within each sample. The variance of the sample mean is given by

$$s_{\bar{X}}^2 = \frac{1}{(r-1)} \sum_{i=1}^{r} \left(\bar{X}_i - \bar{\bar{X}} \right)^2 , \qquad \text{(H-1)}$$

where r is the number of sample means, X_i is the mean of sample i and $\bar{\bar{X}}$ is the mean of the sample means.

The variance of each sample i is given by

$$s_i^2 = \frac{1}{(n-1)} \sum_{j=1}^{n} \left(X_{ij} - \bar{X}_i \right)^2 , \qquad \text{(H-2)}$$

where n is the number of values in sample i, and X_{ij} is particular observation in sample i.

The pooled variance is given by

$$s_p^2 = \frac{1}{r} \sum_{i=1}^{r} s_i^2 . \qquad \text{(H-3)}$$

Now a comparison can be made between the sample means variance $s_{\bar{X}}^2$ and the pooled variance of the samples s_p^2.

A ratio *F* is defined,

$$F = \frac{n s_{\bar{X}}^2}{s_p^2} . \qquad \text{(H-4)}$$

The *F* statistic will be near 1 when the null hypothesis is true, and a large *F* value indicates that the null hypothesis can be rejected. The *F* statistic follows a distribution depending on the degrees of freedom in the numerator $(r-1)$ and denominator $r(n-1)$. A particular value of *F* can be compared to a table of given *F* values and their corresponding P-values to determine if the null hypothesis is to be rejected or not. [137]

Appendix I The Matlbab Program Outline and Selected Matlab Code Listing

The figure below illustrates the relationships of the different processes that are implemented in software. Each group forms a logical process that is implemented as one or more routines and functions written in Matlab. The groups are labelled (a) to (i), where Table I1 contains the file names and locations of routines and functions for each group.

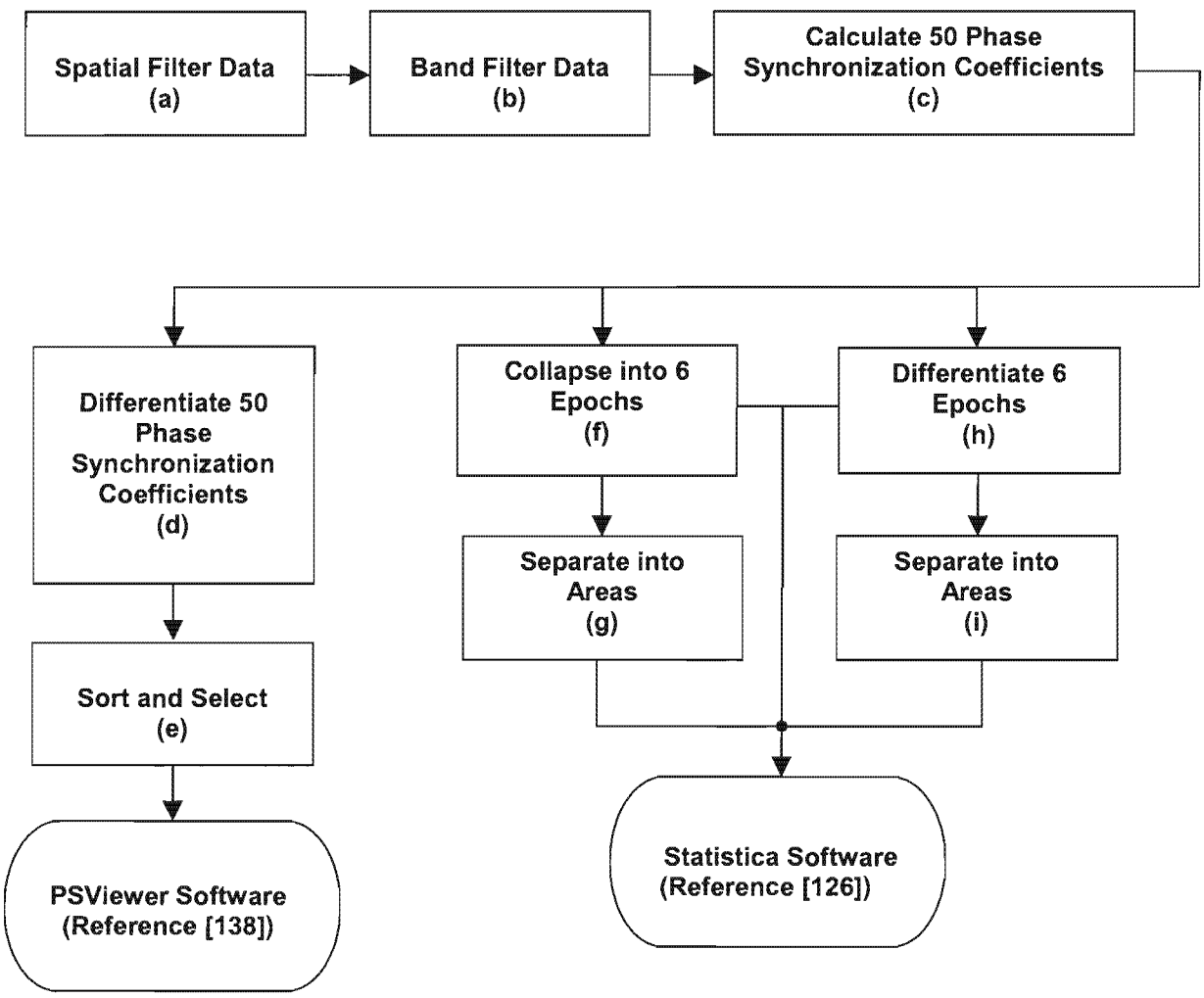

Figure I1: Flowchart showing software components. Labelled items (a) – (i) indicate a functional group of Matlab routines or functions detailed below.

Functional Group	Routine or function file	Location
a	Convert_lap.m	Please see CD
	eeg_lap_sph_spline_2.m	I 1
b	load_lp.m	Please see CD
c	p_synch_ts_lp.m	Please see CD
	PhaseSynchTS_VWL	Please see CD
	PhaseSynchNbyN_TS_VWL	Please see CD
	PhaseSynch	I 2
d,e	determine_hi_lo_range_srpt.m	Please see CD
f	average_across_ch_to_asc.m	Please see CD
g	seperateAreas.m	Please see CD
	get_motor_pfr_values.m	Please see CD
	get_motor_fr_values.m	Please see CD
h,i	seperateAreas_diff.m	Please see CD
	GetDiffAv.m	Please see CD

Table I1: Table showing the file name and location of routines and functions for a functional group.

I 1. Functions For The Calculation of the Spherical Spline and the Surface Laplacian

function [S,Vi] = **eeg_lap_sph_spline**(V,X,Y,Z,Npoints, a0,b0,c0)

% Edited copy of original by Devin Bosanquet
% Original by Darren.Weber@flinders.edu.au

```
% Computations derived from Perrin et al. (1989)
% solve for C = V * Sp' (C = V\Sp; (see "help slash"))
% First calc G, where G is a function of the cosine of
% the angle (theta) between electrode point vectors


% get spherical electrode radius
[r,x,y,z] = elec_fit_sphere(X,Y,Z,a0,b0,c0,50);
A  = [x y z];
S = [x y z];
[NV MV] = size(V);
COS = cosines(A,A);
G  = spheric_spline(COS);
C  = spline_coefficients(G,V); % spline coefficients (Co,C1,...,Cn)
Co  = C(1,:);
Ci  = C(2:end, :);
```

```
    % Obtain interpolated potentials at S (eq.1, Perrin et al., 1989)
    [x,y,z]   = elec_sphere_points(16,Npoints,r);

    % The following calculates voltages for each point for the given co-ords
    for p = 1:length(X)

       B = [X(p) Y(p) Z(p)];
       Cos = cosines(A,B);        %(1xN)
       Gx  = spheric_spline(Cos);  %(1xN)
       Gx = Gx';
       Gx = repmat(Gx, 1,MV);
       CiGx = Ci .* Gx;          %(1xN)

       Vi(p,:) = Co + sum(CiGx);

    end

return


% Solve eq. 3 Perrin et al. (1989)
% g(COS) = 1/4pi * sum[n=1:inf] (( (2*n+1)/(n^m * (n+1)^m) ) * Pn(COS));

function [Gx] = spheric_spline(Cosine)

    m = 4;
    N = 7;    % gives accuracy of 10^-6

    P = legendre(N,Cosine);

   %P = LEGENDRE(N,X) computes the associated Legendre functions
    %of degree N and order m = 0, 1, ..., N, evaluated for each element
    %of X.
    %In general, P has one more dimension than X.
    %Each element P(m+1,i,j,k,...) contains the associated Legendre
    %function of degree N and order m evaluated at X(i,j,k,...).

    ndim = ndims(P);
    switch ndim
    case 2, P = P(2:N+1,:);
    case 3, P = P(2:N+1,:,:);
    case 4, P = P(2:N+1,:,:,:);
    otherwise
    end

    k = (1/4 * pi);

    for n = 1:(N),  Series(n,1) = (2*n + 1) / (n^(m-1) * (n+1)^(m-1));  end

    if min(size(Cosine)) == 1,    Gx      = k * ( Series' * P );
    else
       for i = 1:length(Cosine), Gx(i,:) = k * ( Series' * P(:,:,i) );
       end
    end
return
```

```
function [Gx] = spheric_spline_intrp(Cosine)

   m = 4;
   N = 7;   % gives accuracy of 10^-6

   P = legendre(N,Cosine);
   %P = LEGENDRE(N,X) computes the associated Legendre functions
   %of degree N and order m = 0, 1, ..., N, evaluated for each element
   %of X.
   %In general, P has one more dimension than X.
   %Each element P(m+1,i,j,k,...) contains the associated Legendre
   %function of degree N and order m evaluated at X(i,j,k,...).

   ndim = ndims(P);
   switch ndim
   case 2, P = P(2:N+1,:);
   case 3, P = P(2:N+1,:,:);
   case 4, P = P(2:N+1,:,:,:);
   otherwise
   end

   k = (1/4 * pi);

   for n = 1:(N),  Series(n,1) = (2*n + 1) / (n^m * (n+1)^m);  end

   if min(size(Cosine)) == 1,   Gx     = k * ( Series' * P );
   else
      for i = 1:length(Cosine), Gx(i,:) = k * ( Series' * P(:,:,i) );
      end
   end
  return

% Solve eq. 2 Perrin et al. (1989)
function [C] = spline_coefficients(Gx,V)

   % add ones to first row & column of Gx
   [n m] = size(V);
   tmp =  ones(n,1);
   Gx   = [tmp Gx];
   tmp = [ones(n + 1,1)];
   Gx   = [tmp Gx']';

   Gx(1,1) = 0;
   CoV = [zeros(1,m); V];


   C = Gx\CoV;

return

function [Cos] = cosines(A,B)

   for    a = 1:size(A,1),  Aa = A(a,:); A_len = sqrt( sum(Aa.^2));
      for b = 1:size(B,1),  Bb = B(b,:); B_len = sqrt( sum(Bb.^2));
```

```
        if( Aa == Bb ) Cos(a,b) = 0;
        else           Cos(a,b) = dot(Aa,Bb) / (A_len * B_len);
        end
      end
    end
return


function [Gx] = g(X)
        % Solve Eq. 3 Perrin et al. (1989)
        %
        % g(x) = 1/4pi * (for n=1:inf, sum = sum + ( ( (2*n+1)/(n^m * (n+1)^m) ) * Pn(x) ) );
        %
        % where m is a constant > 1 and Pn(x) is the nth degree Legendre
        % polynomial.  Perrin et al. (1989) evaluated m=1:6 and recommend m=4,
        % for which the first 7 terms of Pn(x) are sufficient to obtain
        % a precision of 10^-6 for g(x) (ie, the above for loop is n=1:7).

  m = 4;
  N = 7;

        % Perrin et al. (1989) recommend tabulation of g(x) for
        % x = linspace(-1,1,2000) to be used as a lookup given actual
        % values for cos(Ei,Ej).
  if isempty(X),
     msg = sprintf('...Cosine matrix empty for g(x).\n');
     error(msg);
  end

  P = legendre(N,X);
  %P = LEGENDRE(N,X) computes the associated Legendre functions
  %of degree N and order m = 0, 1, ..., N, evaluated for each element
  %of X.
  %In general, P has one more dimension than X.
  %Each element P(m+1,i,j,k,...) contains the associated Legendre
  %function of degree N and order m evaluated at X(i,j,k,...).

  for n=1:N, Series(n) = (2*n + 1) / (n^m * (n+1)^m); end

  switch ndims(P)
  case 2,
     P = P(2:N+1,:);
     tmp = ones(N,size(X,1));
     for n=1:N, tmp(n,:) = Series(n) * P(n,:); end
  case 3,
     P = P(2:N+1,:,:);
     tmp = ones(N,size(X,1),size(X,2));
     for n=1:N, tmp(n,:,:) = Series(n) * P(n,:,:); end
  otherwise
  end

  Gx = (1/(4*pi)) * squeeze(sum(tmp));

return
```

I 2. Function for the Calculation of the Phase Synchronization Coefficient

```
function ps = PhaseSynch(x,y,N)
% This function provided courtesy of D.R. R Sreenivasan
DataLen = size(x,2);
h1=hilbert(x);
h2=hilbert(y);
p1 = unwrap(angle(h1), 2*pi);
p2 = unwrap(angle(h2), 2*pi);
dp = p1 - p2;
nb = N;
hi = hist(dp, nb);
S=0.0;
T=0.0;
for k=1:nb,
   p=hi(k)/DataLen;
   T=T+hi(k);
   if(p>0.0)
      S=S+p*log(p);
   end;
   if(p>1)
      bb=1
   end;
end;
S=-S;
Smax=log(nb);
if(Smax == 0)
   S=S;
end
ps = (Smax -S)/Smax;
```

Appendix J-1 Head Maps

J1.1 Plots of Theta Band Differentiated Phase Synchronization Coefficients

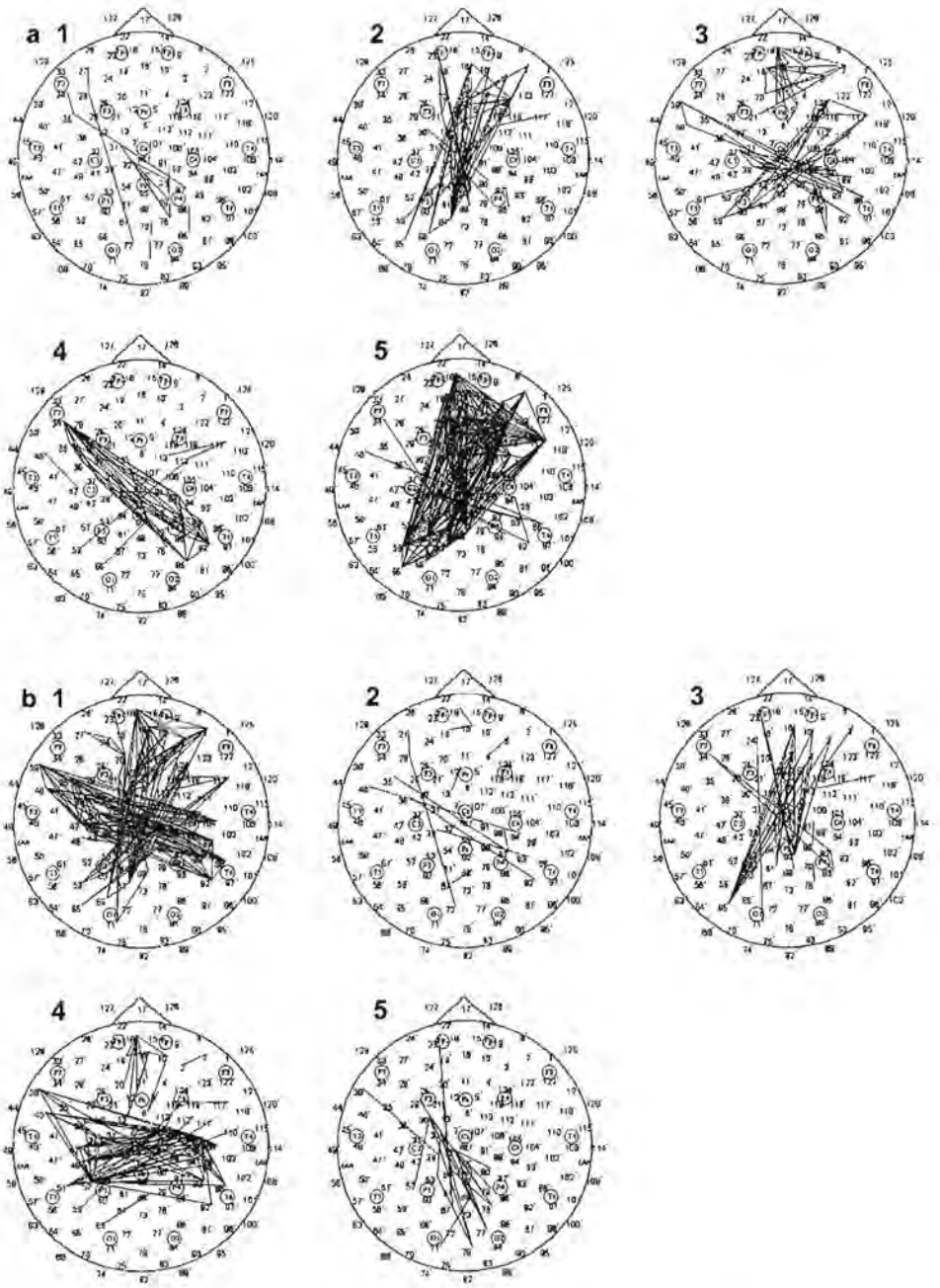

Figure J1: Theta phase synchronization (a) and phase desynchronization (b) for the eyes-closed condition for each epoch change 1-5 (indicated on each head map). Note that a line indicates a $\Delta\bar{\rho}$ value above (synchronization case) or below (desynchronization case) a certain threshold. Please see section 5.6.1.2 and figure 5-18 in the main body for a description of how the threshold value was determined.

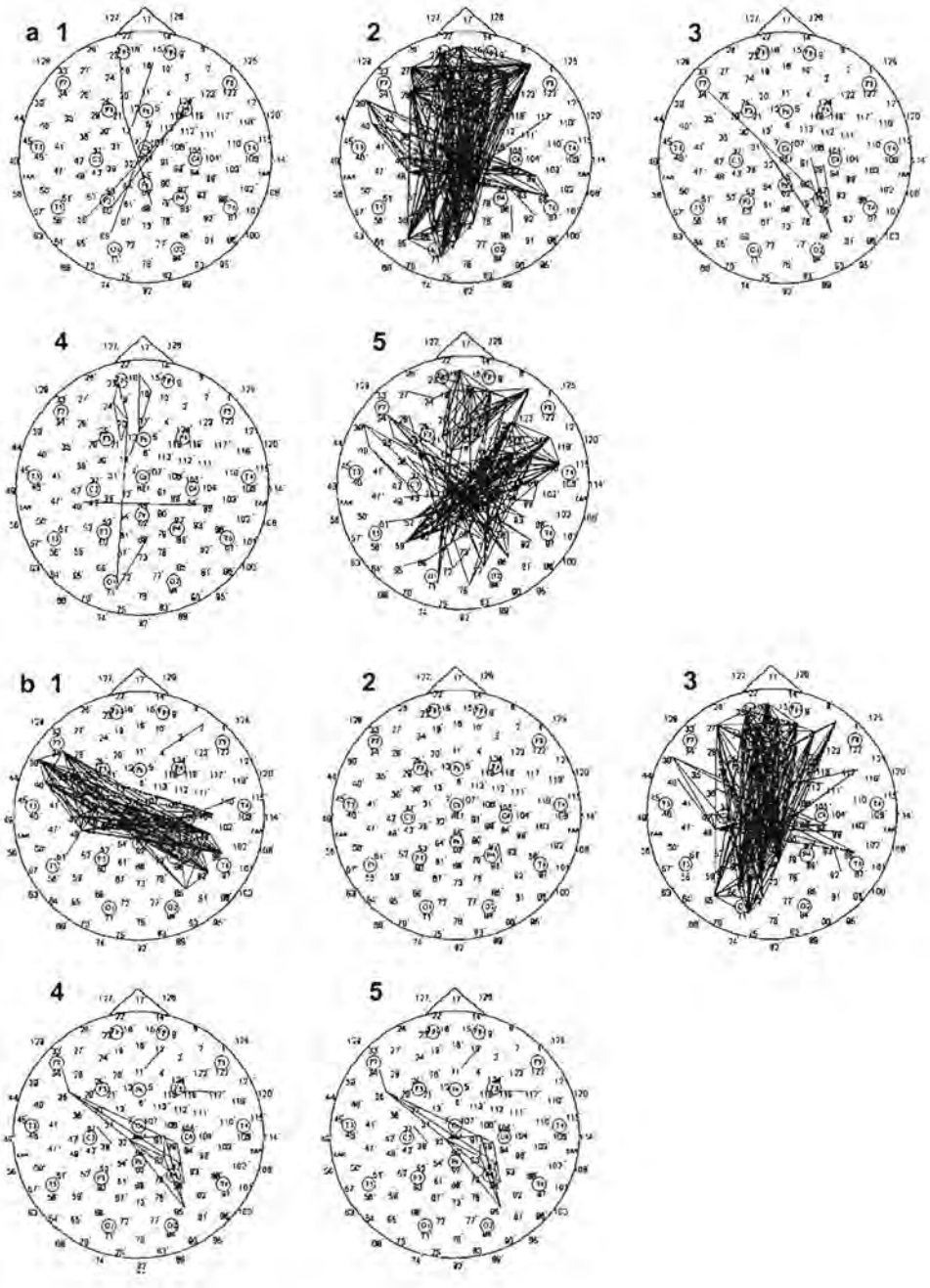

Figure J2: Theta phase synchronization (a) and phase desynchronization (b) for the eyes-open condition for each epoch change 1-5 (indicated on each head map). Note that a line indicates a $\Delta\widetilde{\rho}$ value above (synchronization case) or below (desynchronization case) a certain threshold. Please see section 5.6.1.2 and figure 5-18 in the main body for a description of how the threshold value was determined.

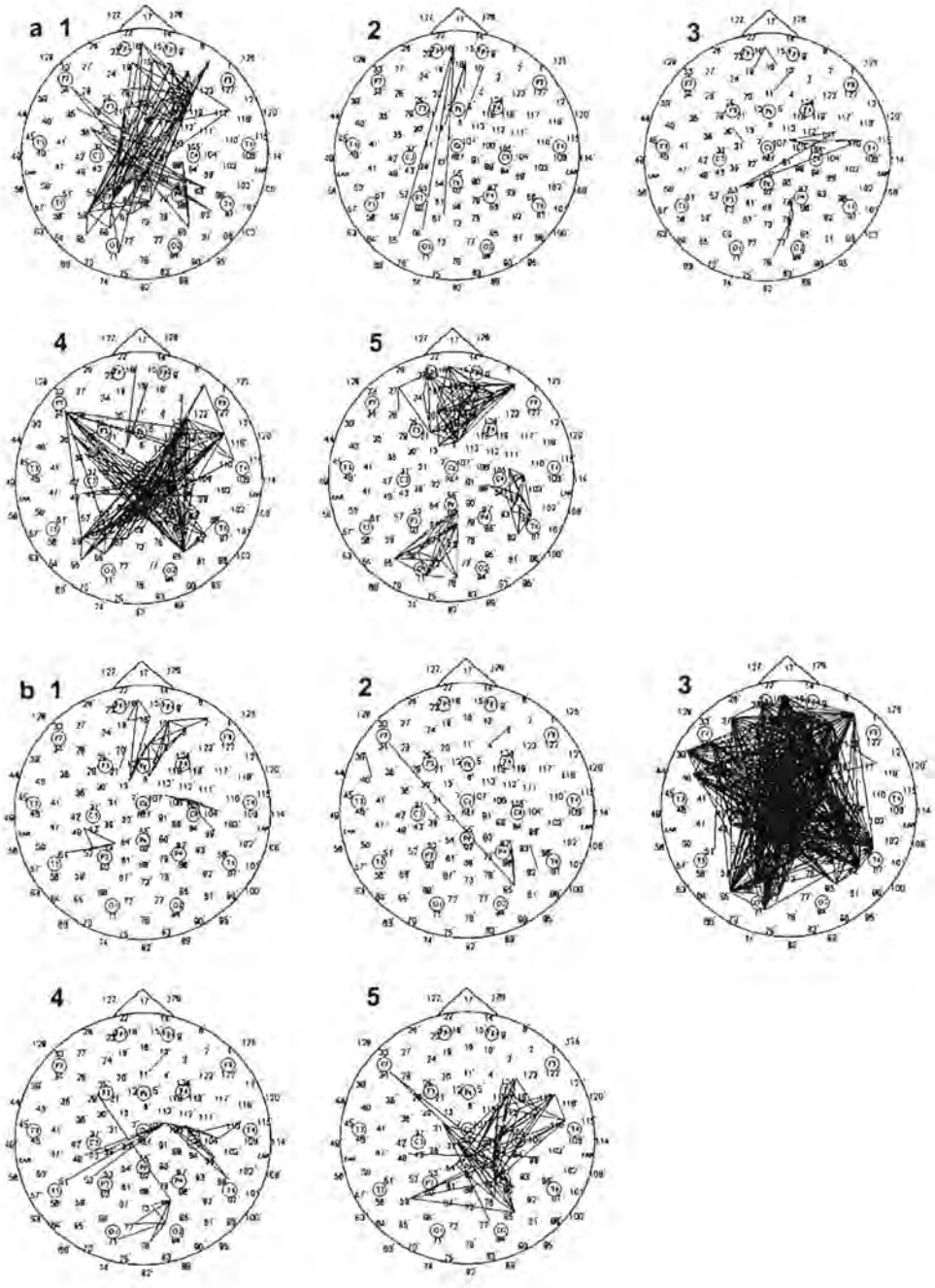

Figure J3: Theta phase synchronization (a) and phase desynchronization (b) for the exercise-until fatigue condition for each epoch change 1-5 (indicated on each head map). Note that a line indicates a $\Delta\tilde{\rho}$ value above (synchronization case) or below (desynchronization case) a certain threshold. Please see section 5.6.1.2 and figure 5-18 in the main body for a description of how the threshold value was determined.

J1.2 Plots of Alpha Band Differentiated Phase Synchronization Coefficients

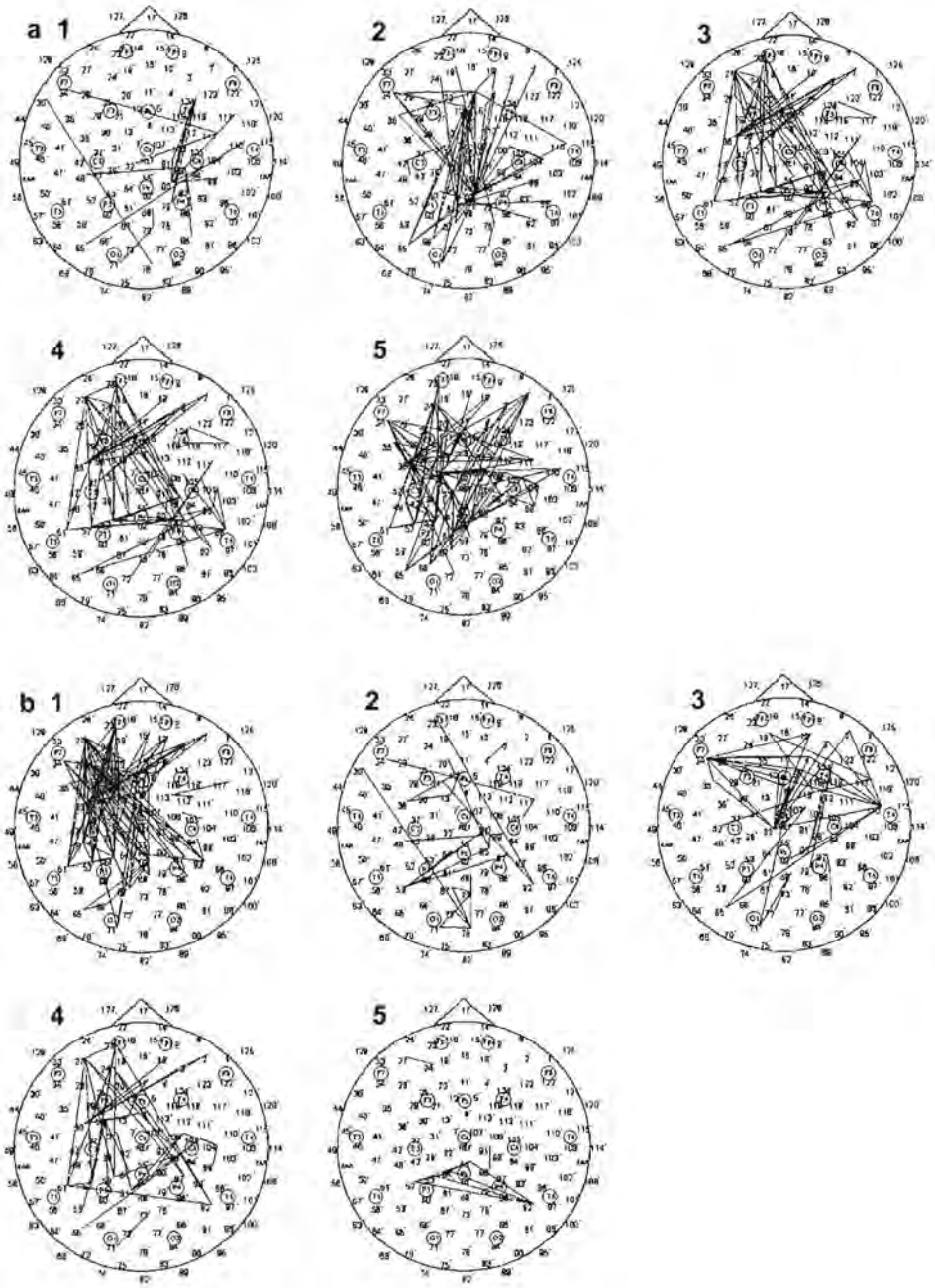

Figure J4: Alpha phase synchronization (a) and phase desynchronization (b) for the eyes-closed condition for each epoch change 1-5 (indicated on each head map). Note that a line indicates a $\Delta\tilde{\rho}$ value above (synchronization case) or below (desynchronization case) a certain threshold. Please see section 5.6.1.2 and figure 5-18 in the main body for a description of how the threshold value was determined.

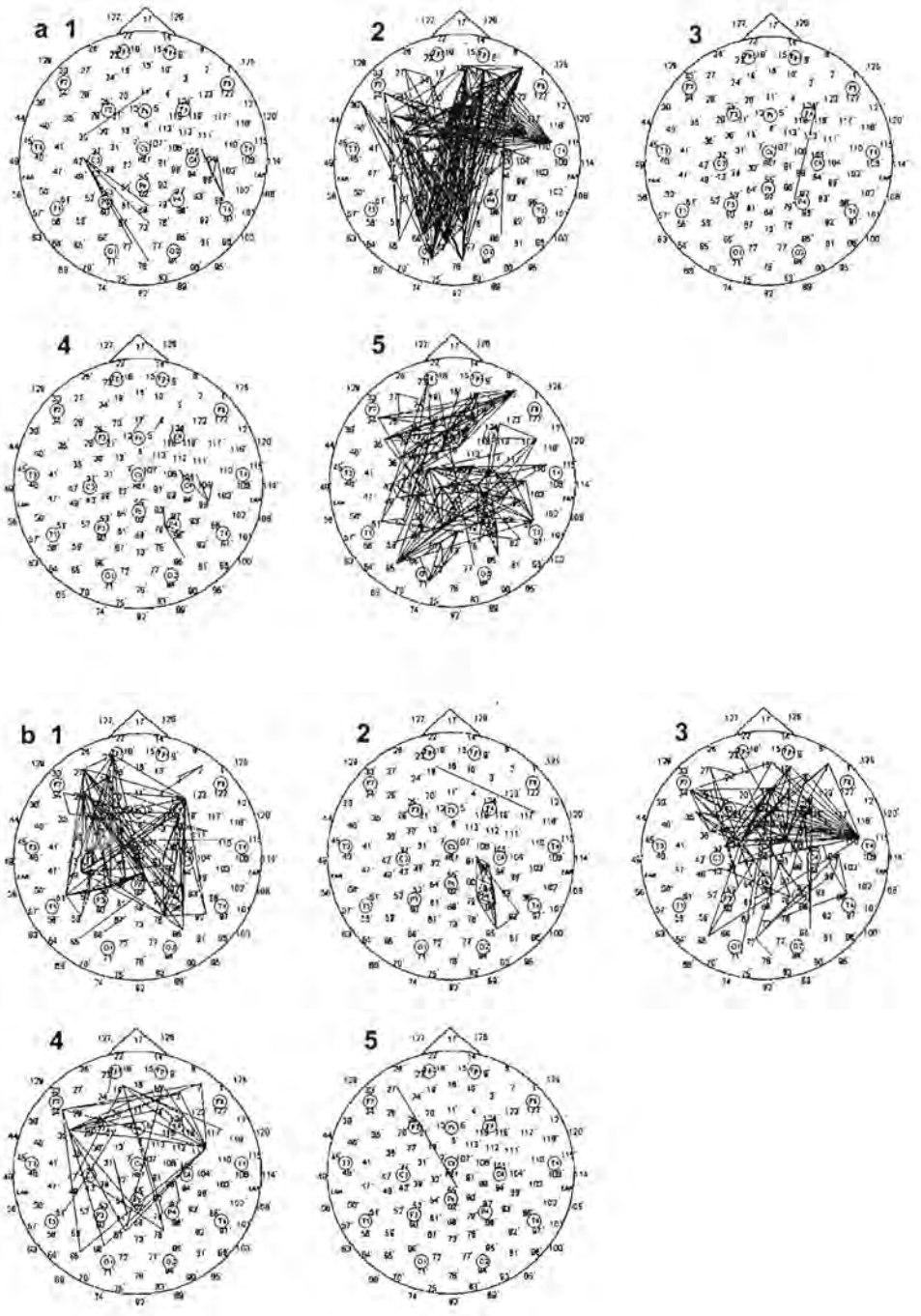

Figure J5: Alpha phase synchronization (a) and phase desynchronization (b) for the eyes-open condition for each epoch change 1-5 (indicated on each head map). Note that a line indicates a $\Delta\tilde{\rho}$ value above (synchronization case) or below (desynchronization case) a certain threshold. Please see section 5.6.1.2 and figure 5-18 in the main body for a description of how the threshold value was determined.

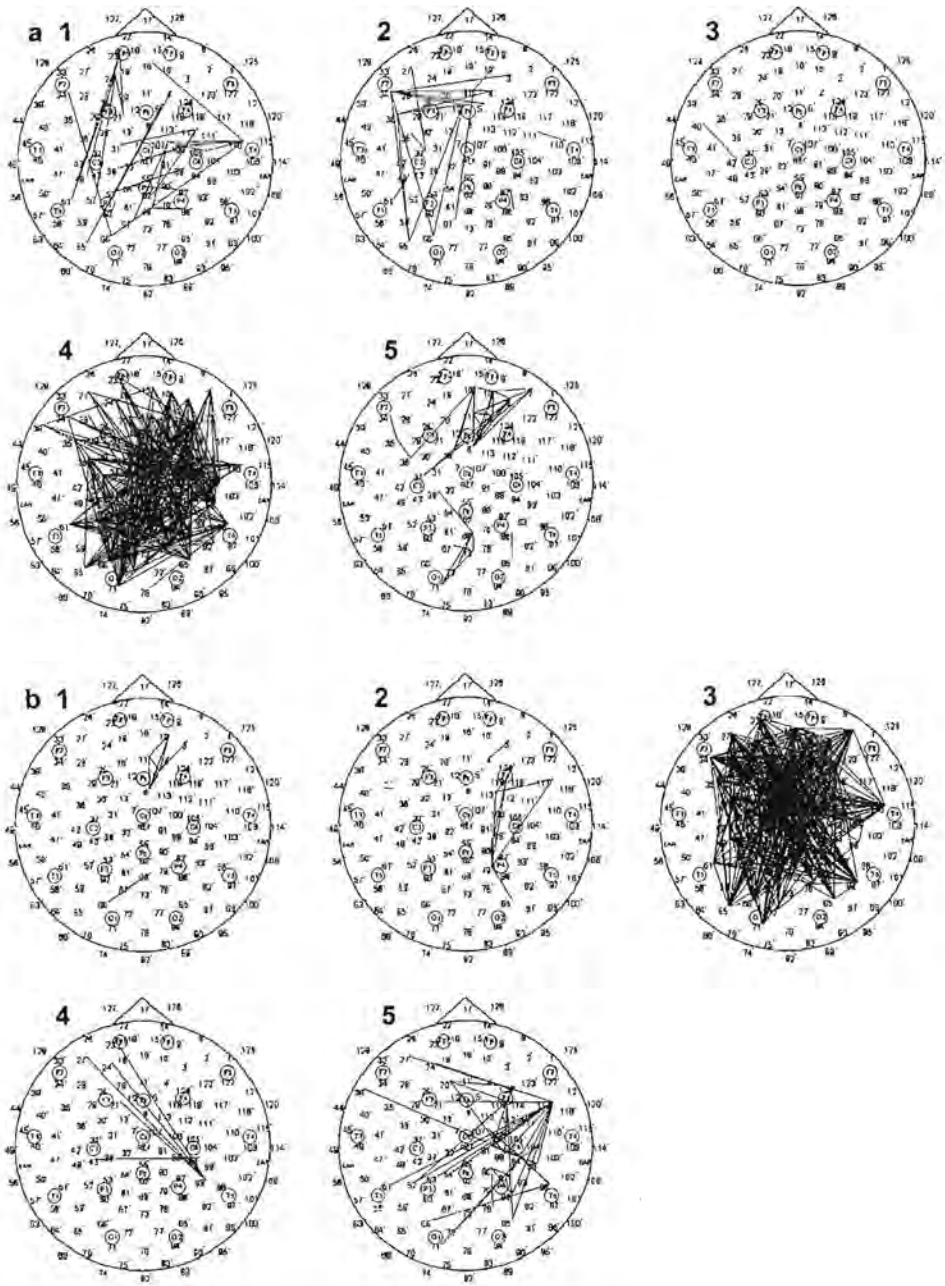

Figure J6: Alpha phase synchronization (a) and phase desynchronization (b) for the exericise-until-fatigue condition for each epoch change 1-5 (indicated on each head map). Note that a line indicates a $\Delta\tilde{\rho}$ value above (synchronization case) or below (desynchronization case) a certain threshold. Please see section 5.6.1.2 and figure 5-18 in the main body for a description of how the threshold value was determined.

J1.3 Plots of Beta Band Differentiated Phase Synchronization Coefficients

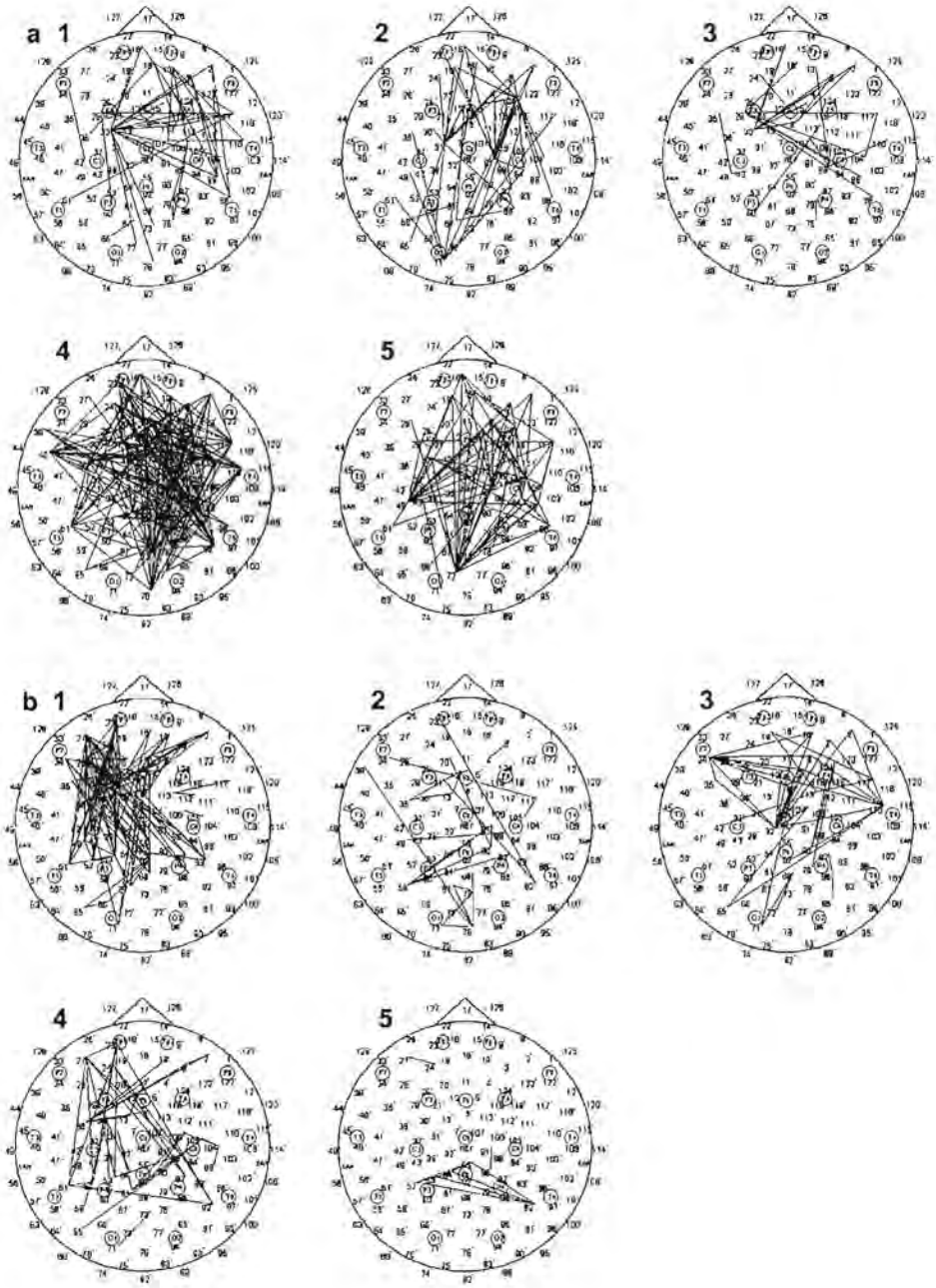

Figure J7: Beta phase synchronization (a) and phase desynchronization (b) for the eyes-closed condition for each epoch change 1-5 (indicated on each head map). Note that a line indicates a $\Delta\tilde{\rho}$ value above (synchronization case) or below (desynchronization case) a certain threshold. Please see section 5.6.1.2 and figure 5-18 in the main body for a description of how the threshold value was determined.

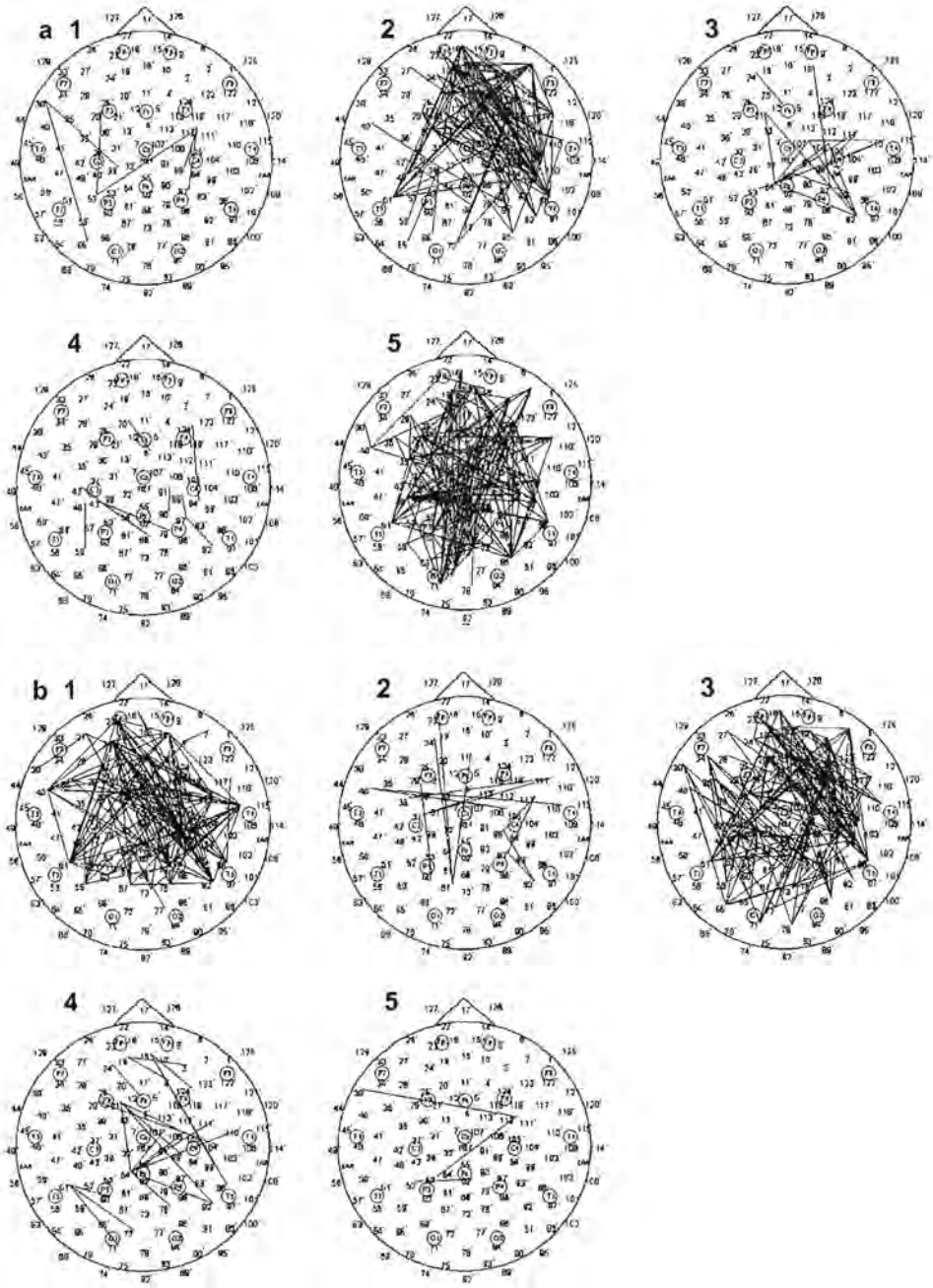

Figure J8: Beta phase synchronization (a) and phase desynchronization (b) for the eyes-open condition for each epoch change 1-5 (indicated on each head map). Note that a line indicates a $\Delta\tilde{\rho}$ value above (synchronization case) or below (desynchronization case) a certain threshold. Please see section 5.6.1.2 and figure 5-18 in the main body for a description of how the threshold value was determined.

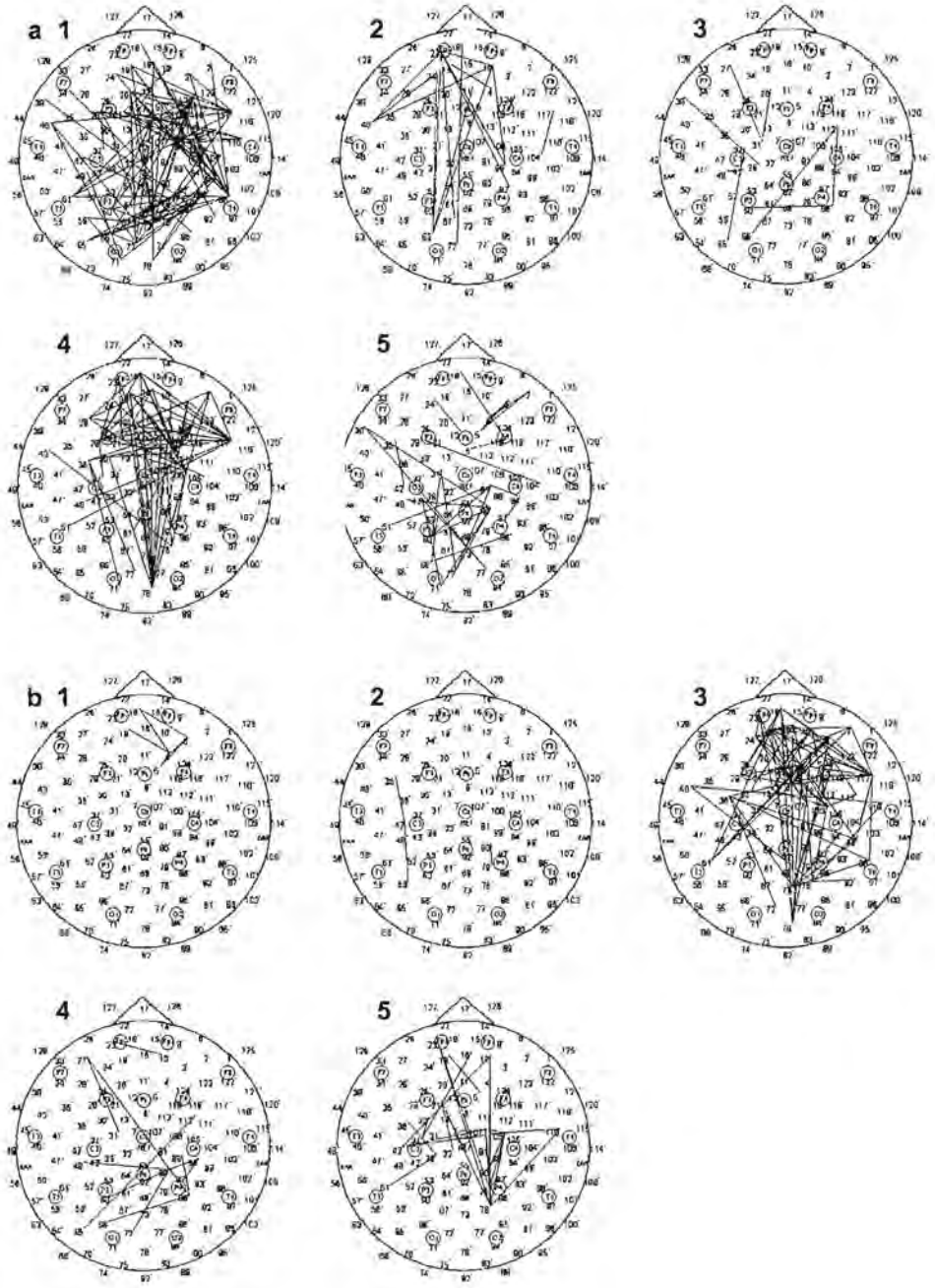

Figure J9: Beta phase synchronization (a) and phase desynchronization (b) for the exercise-until-fatigue condition for each epoch change 1-5 (indicated on each head map). Note that a line indicates a $\Delta\tilde{\rho}$ value above (synchronization case) or below (desynchronization case) a certain threshold. Please see section 5.6.1.2 and figure 5-18 in the main body for a description of how the threshold value was determined.

J1.4 Plots of Gamma Band Differentiated Phase Synchronization Coefficients

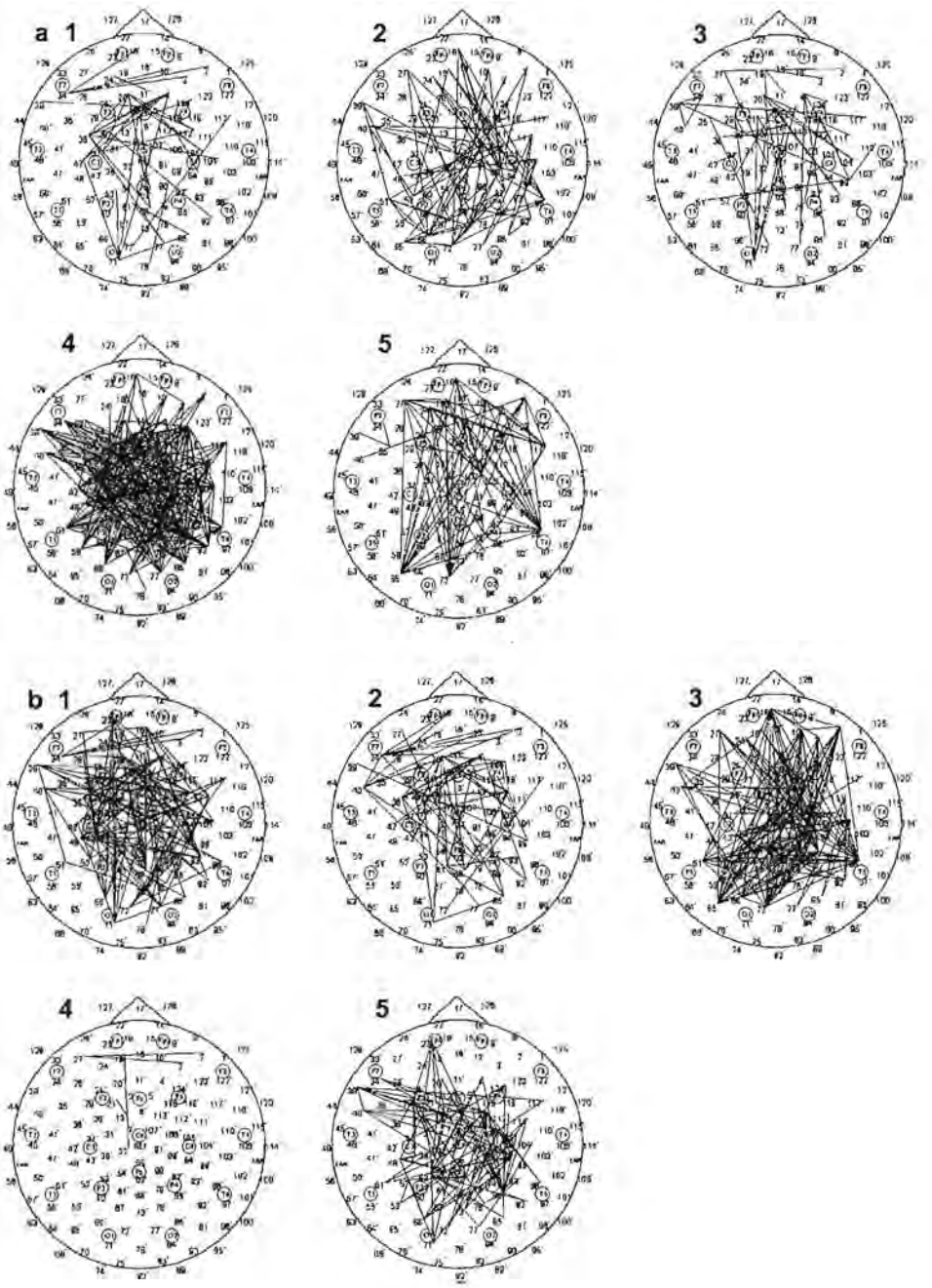

Figure J10: Gamma phase synchronization (a) and phase desynchronization (b) for the eyes-closed condition for each epoch change 1-5 (indicated on each head map). Note that a line indicates a $\Delta\tilde{\rho}$ value above (synchronization case) or below (desynchronization case) a certain threshold. Please see section 5.6.1.2 and figure 5-18 in the main body for a description of how the threshold value was determined.

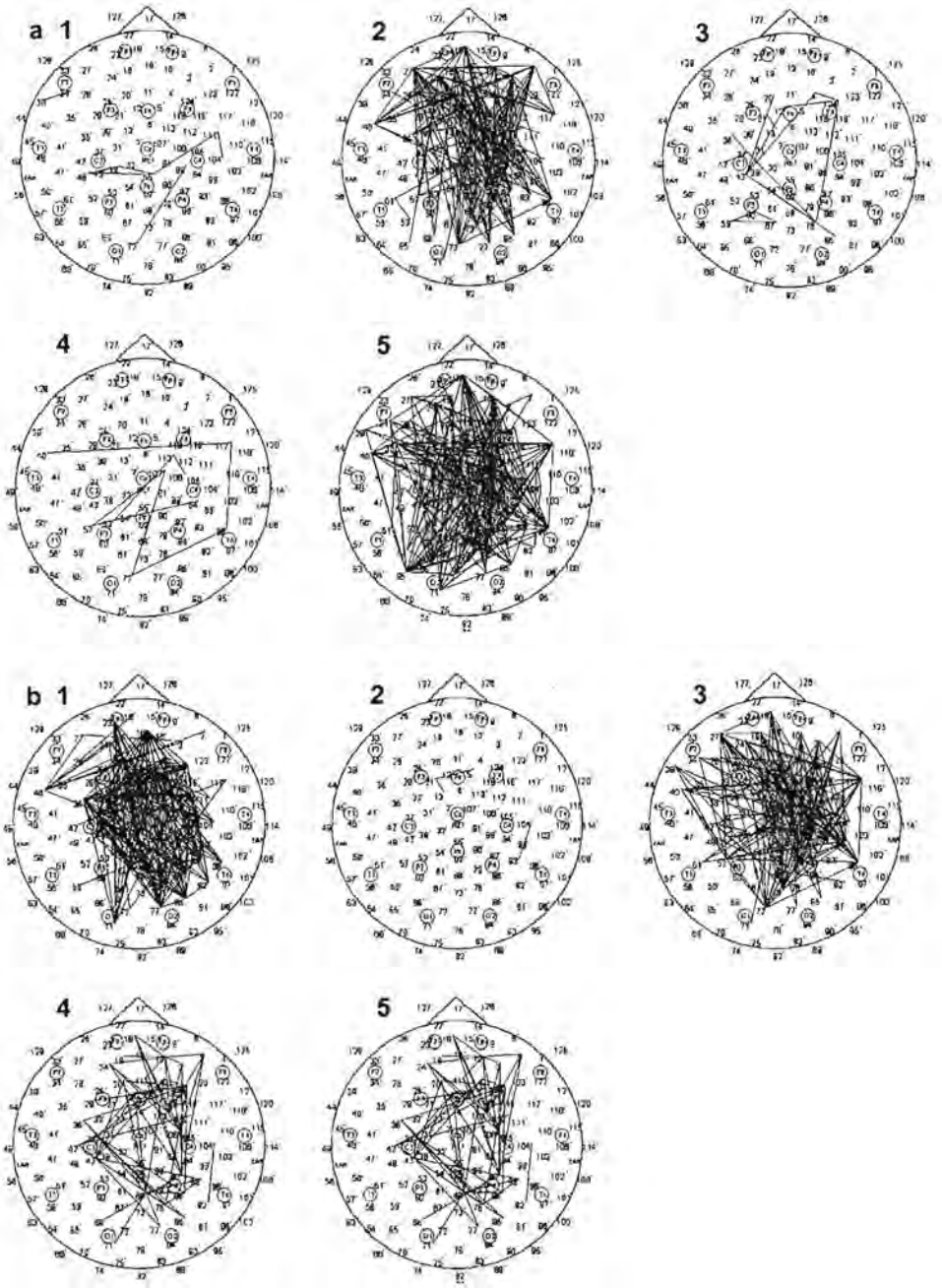

Figure J11: Gamma phase synchronization (a) and phase desynchronization (b) for the eyes-open condition for each epoch change 1-5 (indicated on each head map). Note that a line indicates a $\Delta\tilde{\rho}$ value above (synchronization case) or below (desynchronization case) a certain threshold. Please see section 5.6.1.2 and figure 5-18 in the main body for a description of how the threshold value was determined.

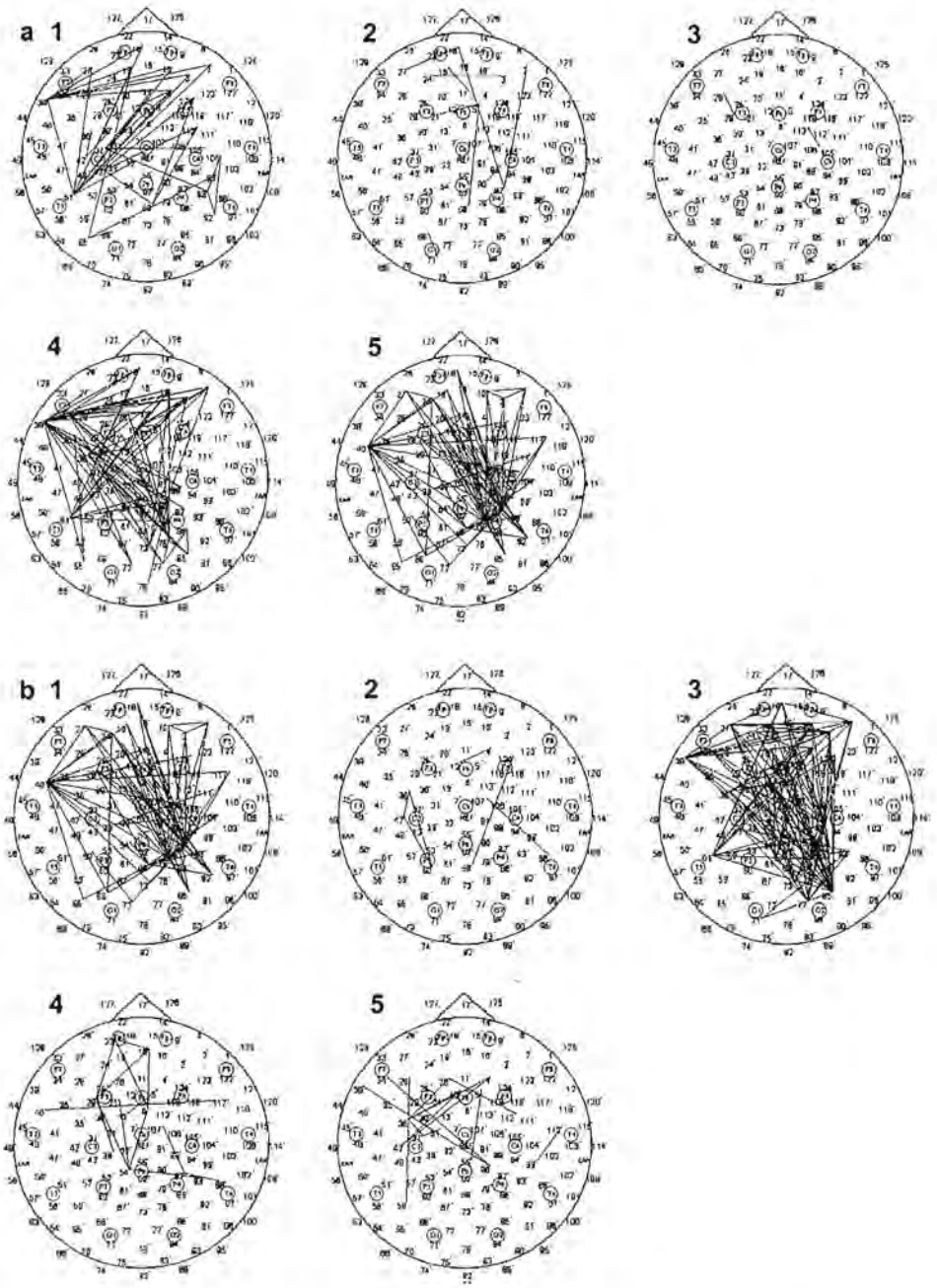

Figure J12: Gamma phase synchronization (a) and phase desynchronization (b) for the exercise-until-fatigue condition for each epoch change 1-5 (indicated on each head map). Note that a line indicates a $\Delta\tilde{\rho}$ value above (synchronization case) or below (desynchronization case) a certain threshold. Please see section 5.6.1.2 and figure 5-18 in the main body for a description of how the threshold value was determined.

Appendix J-2 ANOVA Results

J2.1 Theta Band ANOVA Test 1 (Condition, Time) and Test 2 (Condition, Areas) Results

Factor	Epsilon Correction	F Statistic	P Value
Condition	Greenhouse-Geisser	2.276	0.166
Time	Greenhouse-Geisser	1.080	0.367
Condition * Time (Interaction)	Greenhouse-Geisser	1.749	0.219

Table J1: For the theta band, the output of ANOVA Test 1 (condition, time).

Factor	Epsilon Correction	F Statistic	P Value
Condition	Greenhouse-Geisser	2.276	0.166
Areas	Greenhouse-Geisser	56.892	0.000
Condition * Areas (Interaction)	Greenhouse-Geisser	1.577	0.249

Table J2: For the theta band, output of ANOVA Test 2 (condition, areas).

Condition	Area	Mean	Standard Error
EC	ALL	0.253	0.013
	F-M	0.222	0.016
	PF-M	0.274	0.022
EO	ALL	0.237	0.012
	F-M	0.204	0.014
	PF-M	0.253	0.020
EX	ALL	0.227	0.005
	F-M	0.189	0.005
	PF-M	0.232	0.006

Table J3 For the theta band for each level of each factor in Test 2 (condition, areas), the mean and standard error of the phase synchronization coefficients. The three conditions are represented by EC (eyes-closed), EO (eyes-open) and EX (exercise-until-fatigue). The three areas are represented by ALL (all pairs), F-M (frontal-motor pairs) and PF-M (prefrontal-motor pairs). The values are plotted in the graph below.

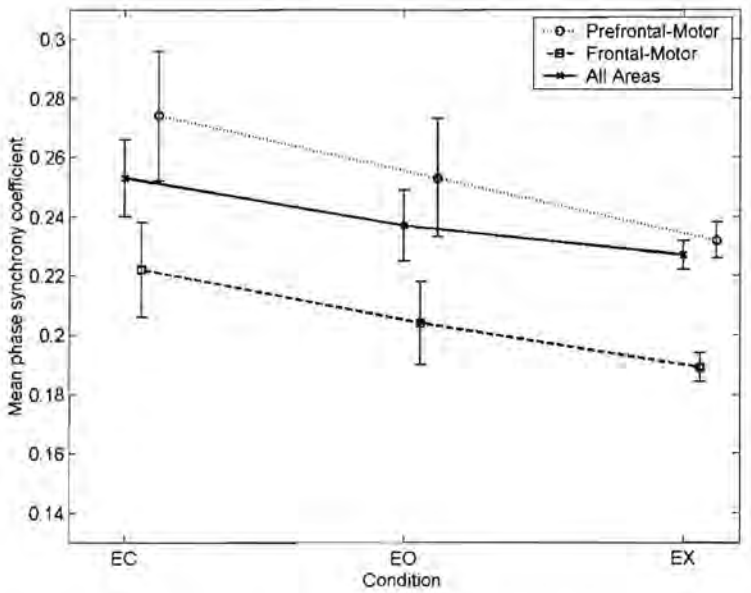

Figure J13: For the theta band for each level of each factor in Test 2 (condition, areas), plot of the means of the phase synchronization coefficients. The y-axis represents the phase synchronization coefficients and x-axis represents conditions where EC stands for eyes-closed, EO stands for eyes-open and EX stands for exercise-until-fatigue. There are three plots, one for each area identified on the legend. The markers representing the means of a particular condition and area are shifted on the x-axis for readability. The error bar represents the standard deviation from the mean.

J2.2 Alpha Band ANOVA Test 1 (Condition, Time) and Test 2 (Condition, Areas) Results

Factor	Epsilon Correction	F Statistic	P Value
Condition	Greenhouse-Geisser	1.542	0.255
Time	Greenhouse-Geisser	0.844	0.447
Condition * Time (Interaction)	Greenhouse-Geisser	1.286	0.307

Table J4: For the alpha band, the output of ANOVA Test 1 (condition, time).

Factor	Epsilon Correction	F Statistic	P Value
Condition	Greenhouse-Geisser	1.542	0.255
Areas	Greenhouse-Geisser	9.414	0.009
Condition * Areas (Interaction)	Greenhouse-Geisser	4.419	0.054

Table J5: For the alpha band, the output of ANOVA Test 2 (condition, areas).

Condition	Area	Mean	Standard Error
EC	ALL	0.223	0.020
	F-M	0.237	0.019
	PF-M	0.238	0.020
EO	ALL	0.207	0.021
	F-M	0.220	0.021
	PF-M	0.217	0.021
EX	ALL	0.195	0.006
	F-M	0.206	0.006
	PF-M	0.196	0.006

Table J6: For the alpha band for each level of each factor in Test 2 (condition, areas), the mean and standard error of the phase synchronization coefficients. The three conditions are represented by EC (eyes-closed), EO (eyes-open) and EX (exercise-until-fatigue). The three areas are represented by ALL (all pairs), F-M (frontal-motor pairs) and PF-M (prefrontal-motor pairs). The values are plotted in the graph below.

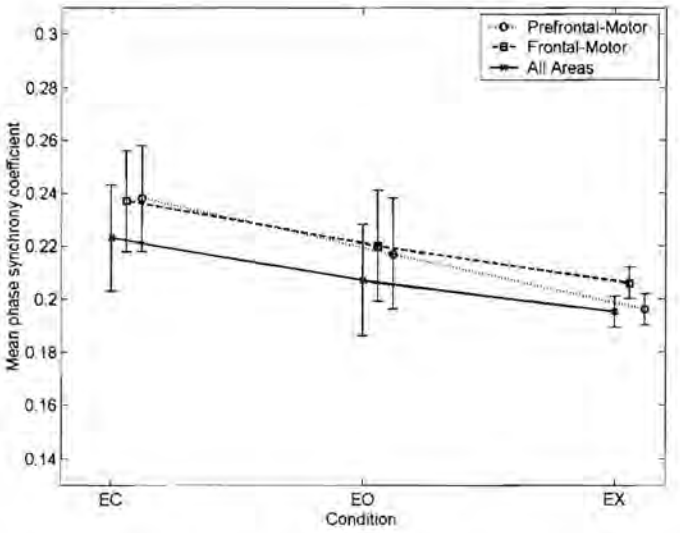

Figure J 14: For the alpha band for each level of each factor in Test 2 (condition, areas), plot of the means of the phase synchronization coefficients. The y-axis represents the phase synchronization coefficients and x-axis represents conditions where EC stands for eyes-closed, EO stands for eyes-open and EX stands for exercise-until-fatigue. There are three plots, one for each area identified on the legend. The markers representing the means of a particular condition and area are shifted on the x-axis for readability. The error bar represents the standard deviation from the mean.

J2.3 Beta Band ANOVA Test 1 (Condition, Time) and Test 2 (Condition, Areas) Results

Factor	Epsilon Correction	F Statistic	P Value
Condition	Greenhouse-Geisser	0.573	0.486
Time	Greenhouse-Geisser	1.227	0.325
Condition * Time (Interaction)	Greenhouse-Geisser	1.313	0.300

Table J7: For the beta band, the output of ANOVA Test 1 (condition, time).

Factor	Epsilon Correction	F Statistic	P Value
Condition	Greenhouse-Geisser	0.573	0.486
Areas	Greenhouse-Geisser	7.925	0.008
Condition * Areas (Interaction)	Greenhouse-Geisser	0.889	0.407

Table J8: For the beta band, the output of ANOVA Test 2 (condition, areas).

Condition	Area	Mean	Standard Error
EC	ALL	0.166	0.012
	F-M	0.170	0.018
	PF-M	0.180	0.017
EO	ALL	0.155	0.015
	F-M	0.160	0.019
	PF-M	0.170	0.017
EX	ALL	0.153	0.007
	F-M	0.151	0.007
	PF-M	0.165	0.006

Table J9: For the beta band for each level of each factor in Test 2 (condition, areas), the mean and standard error of the phase synchronization coefficients. The three conditions are represented by EC (eyes-closed), EO (eyes-open) and EX (exercise-until-fatigue). The three areas are represented by ALL (all pairs), F-M (frontal-motor pairs) and PF-M (prefrontal-motor pairs). The values are plotted in the graph below.

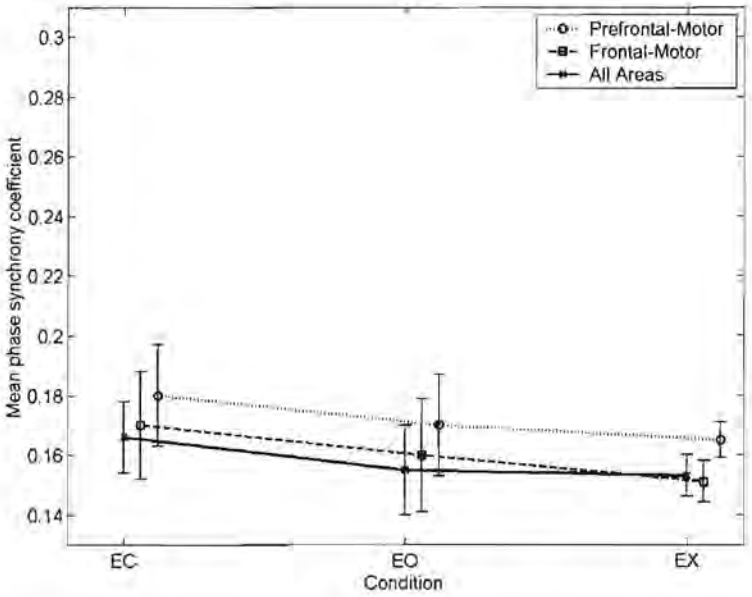

Figure J15: For the beta band for each level of each factor in Test 2 (condition, areas), plot of the means of the phase synchronization coefficients. The y-axis represents the phase synchronization coefficients and x-axis represents conditions where EC stands for eyes-closed, EO stands for eyes-open and EX stands for exercise-until-fatigue. There are three plots, one for each area identified on the legend. The markers representing the means of a particular condition and area are shifted on the x-axis for readability. The error bar represents the standard deviation from the mean.

J2.4 Gamma Band ANOVA Test 1 (Condition, Time) and Test 2 (Condition, Areas) Results

Factor	Epsilon Correction	F Statistic	P Value
Condition	Greenhouse-Geisser	1.027	0.355
Time	Greenhouse-Geisser	1.060	0.383
Condition * Time (Interaction)	Greenhouse-Geisser	2.219	0.140

Table J10: For the gamma band, the output of ANOVA Test 1 (condition, time).

Factor	Epsilon Correction	F Statistic	P Value
Condition	Greenhouse-Geisser	1.027	0.355
Areas	Greenhouse-Geisser	0.374	0.605
Condition * Areas (Interaction)	Greenhouse-Geisser	2.597	0.108

Table J11: For the gamma band, the output of ANOVA Test 2 (condition, areas).

Condition	Area	Mean	Standard Error
EC	ALL	0.166	0.010
	F-M	0.163	0.011
	PF-M	0.168	0.010
EO	ALL	0.154	0.011
	F-M	0.151	0.012
	PF-M	0.149	0.013
EX	ALL	0.152	0.008
	F-M	0.153	0.008
	PF-M	0.150	0.009

Table J12: For the gamma band for each level of each factor in Test 2 (condition, areas), the mean and standard error of the phase synchronization coefficients. The three conditions are represented by EC (eyes-closed), EO (eyes-open) and EX (exercise-until-fatigue). The three areas are represented by ALL (all pairs), F-M (frontal-motor pairs) and PF-M (prefrontal-motor pairs). The values are plotted in the graph below.

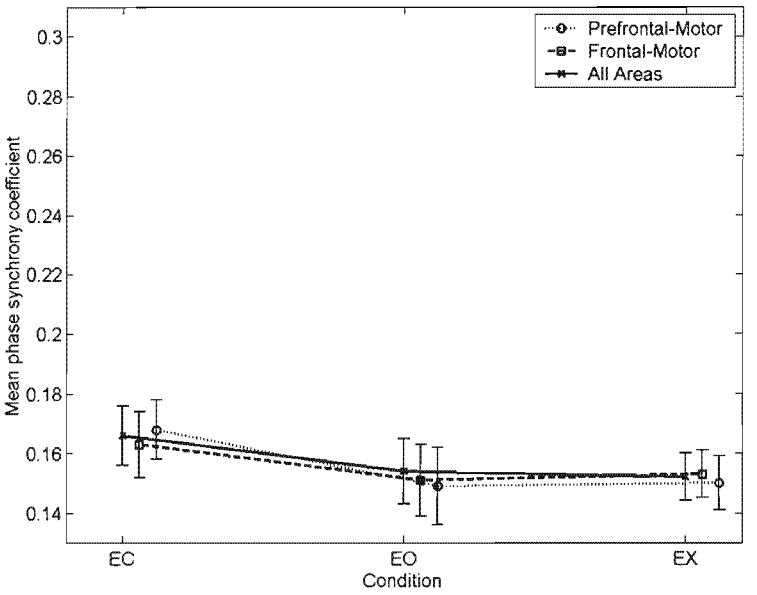

Figure J16: For the gamma band for each level of each factor in Test 2 (condition, areas), plot of the means of the phase synchronization coefficients. The y-axis represents the phase synchronization coefficients and x-axis represents conditions where EC stands for eyes-closed, EO stands for eyes-open and EX stands for exercise-until-fatigue. There are three plots, one for each area identified on the legend. The markers representing the means of a particular condition and area are shifted on the x-axis for readability. The error bar represents the standard deviation from the mean.

J2.5 Theta Band ANOVA Test 3 (Condition, Time) and Test 4 (Condition, Areas) Results

Factor	Epsilon Correction	F Statistic	P Value
Condition	Greenhouse-Geisser	1.051	0.352
Time	Greenhouse-Geisser	1.052	0.373
Condition * Time (Interaction)	Greenhouse-Geisser	1.696	0.202

Table J13: For the theta band, the output of ANOVA Test 3 (condition, time).

Factor	Epsilon Correction	F Statistic	P Value
Condition	Greenhouse-Geisser	1.051	0.352
Areas	Greenhouse-Geisser	.353	0.657
Condition * Areas (Interaction)	Greenhouse-Geisser	.072	0.918

Table J14: For the theta band, the output of ANOVA Test 4 (condition, areas).

Condition	Area	Mean (10^{-3})	Standard Error(10^{-3})
EC	ALL	-2.82	2.00
	F-M	-3.06	2.00
	PF-M	-2.75	3.00
EO	ALL	-0.18	1.00
	F-M	-0.32	1.00
	PF-M	-0.20	2.00
EX	ALL	2.56	3.00
	F-M	2.79	3.00
	PF-M	3.05	3.00

Table J15: For the theta band for each level of each factor in Test 4 (condition, areas), the mean and standard error of the differentiated phase synchronization coefficients. The three conditions are represented by EC (eyes-closed), EO (eyes-open) and EX (exercise-until-fatigue), and the three areas are represented by ALL (ALL pairs), F-M (frontal-motor pairs) and PF-M (prefrontal-motor pairs). The values are plotted in the graph below.

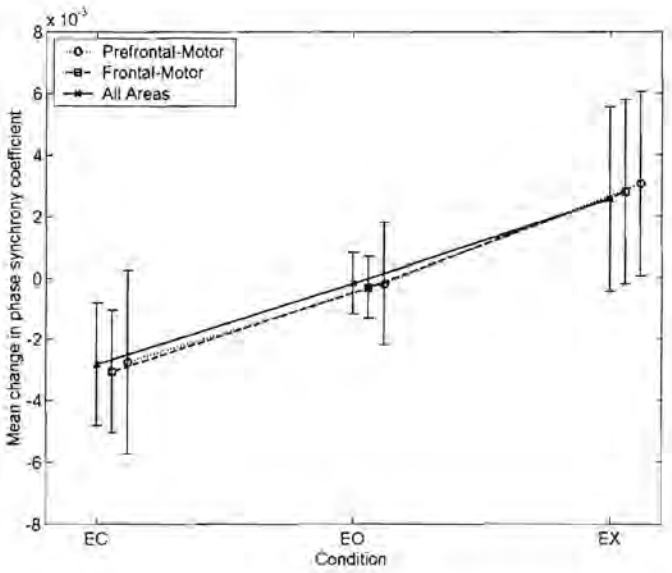

Figure J 17: For the theta band for each level of each factor in Test 4 (condition, areas), plot of the means of the differentiated phase synchronization coefficients. The y-axis represents the differentiated phase synchronization coefficients and x-axis represents the conditions where EC stands for eyes-closed, EO stands for eyes-open and EX stands for exercise-until-fatigue. There are three plots, one for each area identified on the legend. The markers representing the means of a particular condition and area are shifted on the x-axis for readability. The error bar represents the standard deviation from the mean.

a

Area	Epoch Change	Mean (10^{-3})	Standard Error (10^{-3})
ALL	1	-10.00	9.00
	2	-5.62	5.00
	3	4.32	4.00
	4	1.54	4.00
	5	-4.33	2.00
F-M	1	-9.31	10.00
	2	-7.93	5.00
	3	6.78	5.00
	4	-0.03	3.00
	5	-4.81	3.00
PF-M	1	-8.23	12.00
	2	-8.56	6.00
	3	6.53	6.00
	4	0.45	4.00
	5	-3.93	3.00

b

Area	Epoch Change	Mean (10^{-3})	Standard Error (10^{-3})
ALL	1	4.27	4.00
	2	-3.00	5.00
	3	3.70	5.00
	4	-4.27	3.00
	5	-1.59	5.00
F-M	1	3.03	5.00
	2	-1.98	5.00
	3	3.11	5.00
	4	-5.64	2.00
	5	-0.13	5.00
PF-M	1	8.41	8.00
	2	-4.07	7.00
	3	4.27	7.00
	4	-8.33	4.00
	5	5.60	7.00

c

Area	Epoch Change	Mean (10^{-3})	Standard Error (10^{-3})
ALL	1	-8.04	4.00
	2	6.26	5.00
	3	1.49	5.00
	4	15.20	7.00
	5	-2.10	4.00
F-M	1	-7.68	4.00
	2	5.49	5.00
	3	2.17	4.00
	4	16.60	8.00
	5	-2.59	4.00
PF-M	1	-8.84	5.00
	2	6.59	6.00
	3	0.62	6.00
	4	13.40	9.00
	5	3.45	5.00

Table J16: For the theta band, for the eyes-closed condition (a) the eyes-open condition (b) and the exercise-until-fatigue condition (c), for each epoch transition (1-5), for the 3 areas of the areas factor in Test 4 (condition, areas), the mean and standard error of the differentiated phase synchronization coefficients. The three areas are represented by ALL (ALL pairs), F-M (frontal-motor pairs) and PF-M (prefrontal-motor pairs). The epoch transitions are represented by the numbers 1-5. The values are plotted in the graphs below.

a

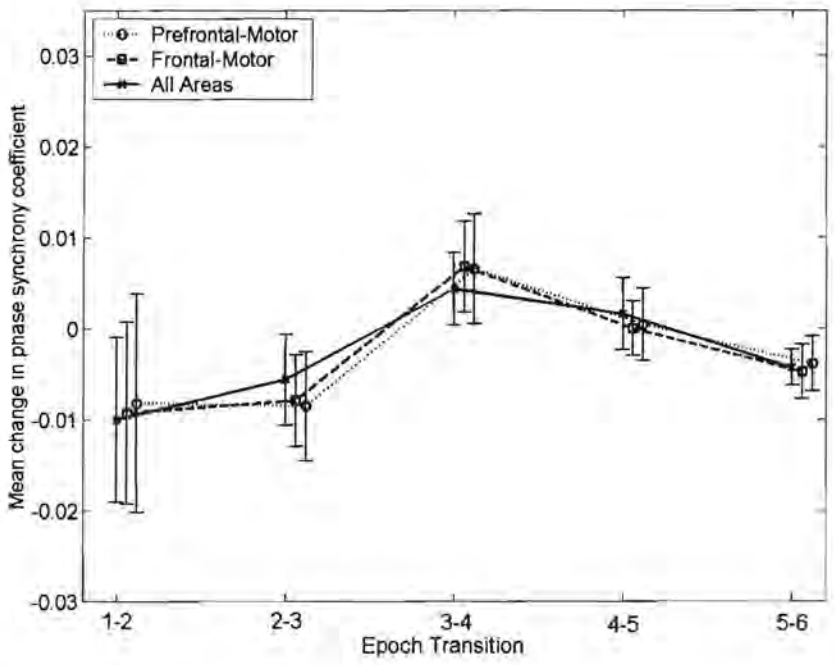
Prefrontal-Motor
Frontal-Motor
All Areas
Mean change in phase synchrony coefficient
0.03
0.02
0.01
0
-0.01
-0.02
-0.03
1-2
2-3
3-4
4-5
5-6
Epoch Transition

b

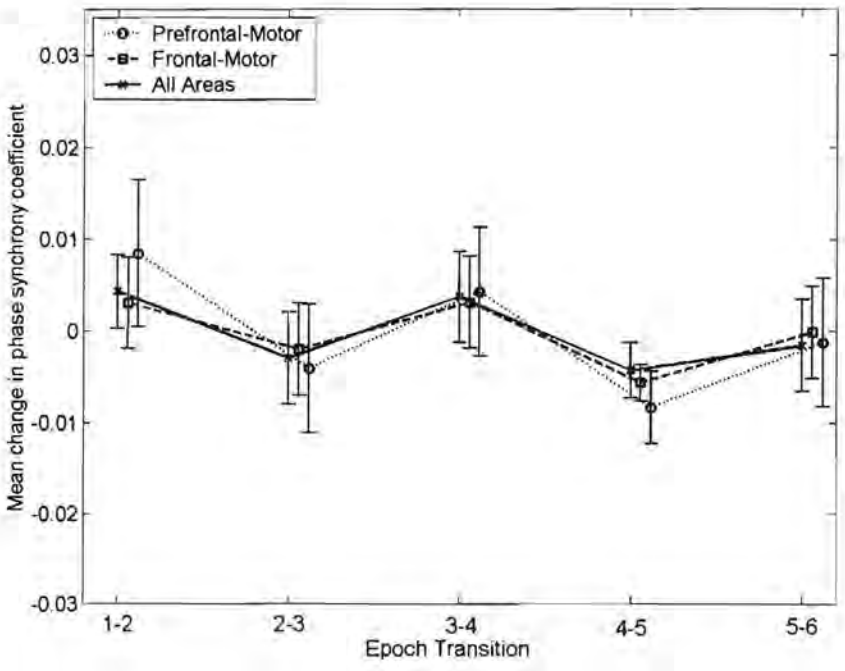
Prefrontal-Motor
Frontal-Motor
All Areas
Mean change in phase synchrony coefficient
0.03
0.02
0.01
0
-0.01
-0.02
-0.03
1-2
2-3
3-4
4-5
5-6
Epoch Transition

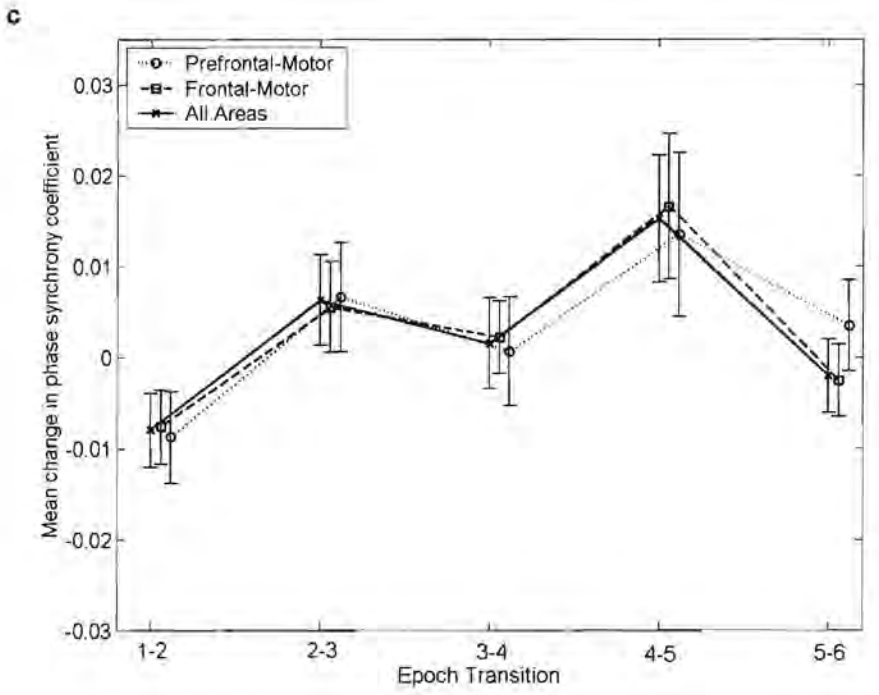

Figure J18: For the theta band, for the eyes-closed condition (a) the eyes-open condition (b) and the exercise-until-fatigue condition (c), for each epoch transition (1-5), for the 3 areas of the areas factor in Test 4 (condition, areas), the mean and standard error of the differentiated phase synchronization coefficients. The y-axis represents the differentiated phase synchronization coefficient and the x-axis represents epoch transitions. There are three plots on each graph (a) – (c), one for each area identified on the legend. The markers representing the means of a particular condition and area are shifted on the x-axis for readability. The error bar represents the standard deviation from the mean.

J2.6 Alpha Band ANOVA Test 3 (Condition, Time) and Test 4 (Condition, Areas) Results

Factor	Epsilon Correction	F Statistic	P Value
Condition	Greenhouse-Geisser	1.084	0.344
Time	Greenhouse-Geisser	.793	0.465
Condition * Time (Interaction)	Greenhouse-Geisser	1.032	0.398

Table J17: For the alpha band, the output of ANOVA Test 3 (condition, time).

Factor	Epsilon Correction	F Statistic	P Value
Condition	Greenhouse-Geisser	1.084	0.344
Areas	Greenhouse-Geisser	1.569	0.249
Condition * Areas (Interaction)	Greenhouse-Geisser	.029	0.968

Table J18: For the alpha band, the output of ANOVA Test 4 (condition, areas).

Condition	Area	Mean (10^{-3})	Standard Error (10^{-3})
EC	ALL	-4.13	3.00
	F-M	-3.63	2.00
	PF-M	-3.42	2.00
EO	ALL	-0.78	1.00
	F-M	-0.44	1.00
	PF-M	-0.15	1.00
EX	ALL	1.10	3.00
	F-M	1.33	3.00
	PF-M	1.70	3.00

Table J19: For the alpha band for each level of each factor in Test 4 (condition, areas), the mean and standard error of the differentiated phase synchronization coefficients. The three conditions are represented by EC (eyes-closed), EO (eyes-open) and EX (exercise-until-fatigue), and the three areas are represented by ALL (ALL pairs), F-M (frontal-motor pairs) and PF-M (prefrontal-motor pairs). The values are plotted in the graph below.

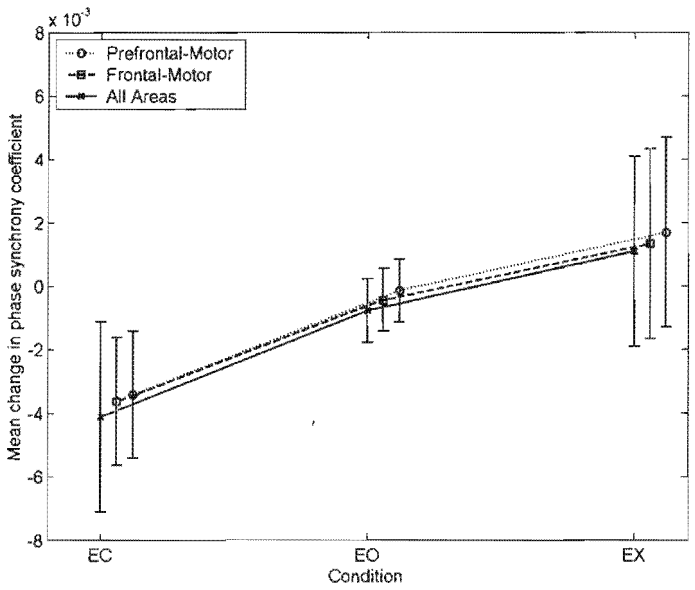

Figure J19: For the alpha band for each level of each factor in Test 4 (condition, areas), plot of the means of the differentiated phase synchronization coefficients. The y-axis represents the differentiated phase synchronization coefficients and x-axis represents the conditions where EC stands for eyes-closed, EO stands for eyes-open and EX stands for exercise-until-fatigue. There are three plots, one for each area identified on the legend. The markers representing the means of a particular condition and area are shifted on the x-axis for readability. The error bar represents the standard deviation from the mean.

a

Area	Epoch Change	Mean (10^{-3})	Standard Error (10^{-3})
ALL	1	-13.90	12.00
	2	1.35	6.00
	3	-2.05	6.00
	4	-1.99	7.00
	5	-4.02	6.00
F-M	1	-10.00	11.00
	2	-3.07	7.00
	3	1.20	5.00
	4	-2.52	5.00
	5	-3.75	7.00
PF-M	1	-7.23	10.00
	2	-7.30	6.00
	3	3.60	4.00
	4	0.55	5.00
	5	-6.73	5.00

b

Area	Epoch Change	Mean (10^{-3})	Standard Error (10^{-3})
ALL	1	3.04	4.00
	2	-3.13	6.00
	3	6.09	8.00
	4	-3.81	5.00
	5	-6.07	6.00
F-M	1	4.09	3.00
	2	-4.26	6.00
	3	8.99	7.00
	4	-5.06	4.00
	5	-5.95	6.00
PF-M	1	7.45	5.00
	2	-7.00	5.00
	3	8.26	7.00
	4	-5.71	5.00
	5	-3.76	6.00

c

Area	Epoch Change	Mean (10^{-3})	Standard Error (10^{-3})
ALL	1	-10.10	6.00
	2	6.18	7.00
	3	2.06	8.00
	4	11.80	5.00
	5	-4.45	5.00
F-M	1	-8.01	7.00
	2	4.65	6.00
	3	1.54	7.00
	4	11.50	6.00
	5	-2.97	5.00
PF-M	1	-5.92	5.00
	2	3.32	5.00
	3	-0.21	6.00
	4	14.30	7.00
	5	-3.03	5.00

Table J20: For the alpha band, for the eyes-closed condition (a) the eyes-open condition (b) and the exercise-until-fatigue condition (c), for each epoch transition (1-5), for the 3 areas of the areas factor in Test 4 (condition, areas), the mean and standard error of the differentiated phase synchronization coefficients. The three areas are represented by ALL (ALL pairs), F-M (frontal-motor pairs) and PF-M (prefrontal-motor pairs). The epoch transitions are represented by the numbers 1-5. The values are plotted in the graphs below.

a

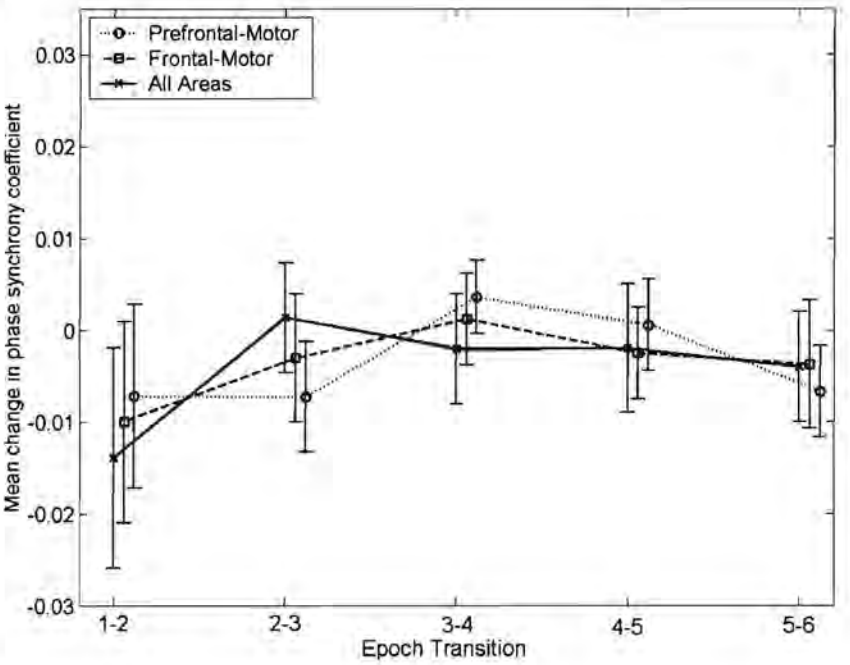
Prefrontal-Motor
Frontal-Motor
All Areas
Mean change in phase synchrony coefficient
0.03
0.02
0.01
0
-0.01
-0.02
-0.03
1-2
2-3
3-4
4-5
5-6
Epoch Transition

b

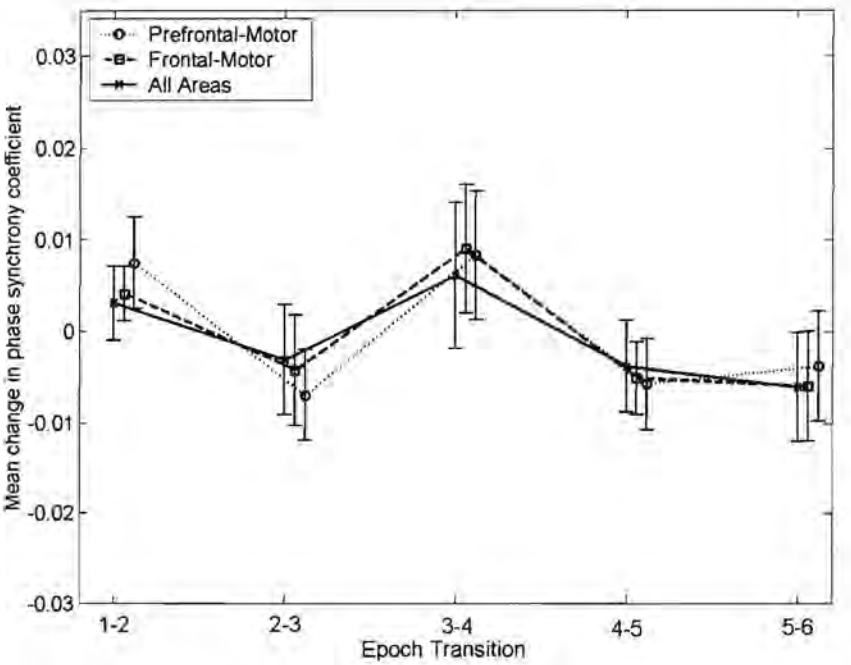
Prefrontal-Motor
Frontal-Motor
All Areas
Mean change in phase synchrony coefficient
0.03
0.02
0.01
0
-0.01
-0.02
-0.03
1-2
2-3
3-4
4-5
5-6
Epoch Transition

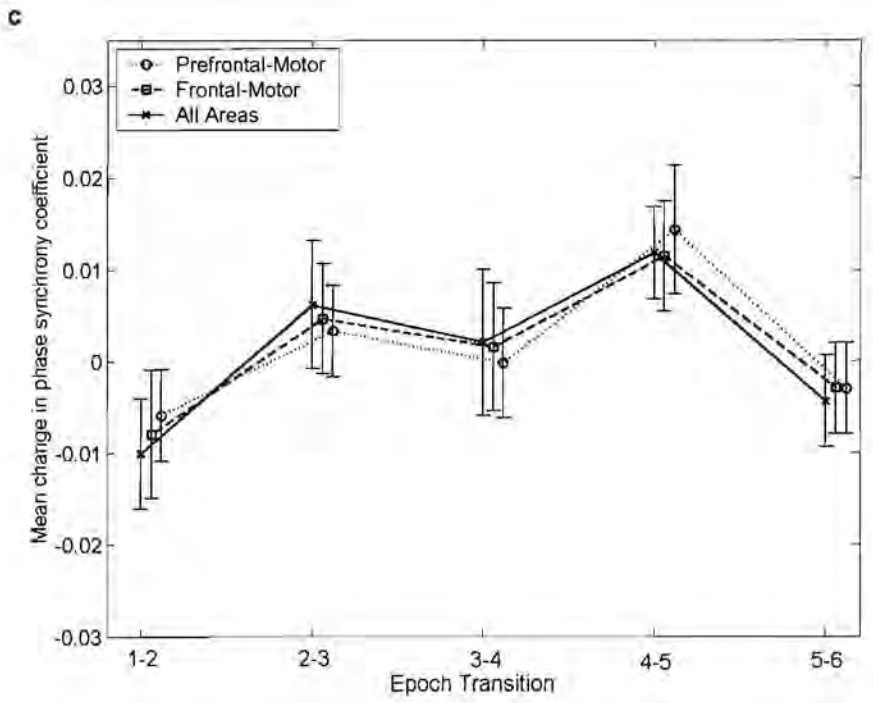

Figure J 20: For the alpha band, for the eyes-closed condition (a) the eyes-open condition (b) and the exercise-until-fatigue condition (c), for each epoch transition (1-5), for the 3 areas of the areas factor in Test 4 (condition, areas), the mean and standard error of the differentiated phase synchronization coefficients. The y-axis represents the differentiated phase synchronization coefficient and the x-axis represents epoch transitions. There are three plots on each graph (a) – (c), one for each area identified on the legend. The markers representing the means of a particular condition and area are shifted on the x-axis for readability. The error bar represents the standard deviation from the mean.

J2.7 Beta Band ANOVA Test 3 (Condition, Time) and Test 4 (Condition, Areas) Results

Factor	Epsilon Correction	F Statistic	P Value
Condition	Greenhouse-Geisser	1.254	0.310
Time	Greenhouse-Geisser	1.155	0.342
Condition * Time (Interaction)	Greenhouse-Geisser	.725	0.553

Table J21: For the beta band, the output of ANOVA Test 3 (condition, time).

Factor	Epsilon Correction	F Statistic	P Value
Condition	Greenhouse-Geisser	1.254	0.310
Areas	Greenhouse-Geisser	5.696	0.037
Condition * Areas (Interaction)	Greenhouse-Geisser	3.999	0.032

Table J22: For the beta band, the output of ANOVA Test 4 (condition, areas).

Condition	Area	Mean (10^{-3})	Standard Error (10^{-3})
EC	ALL	-2.88	2.00
	F-M	-3.01	2.00
	PF-M	-3.66	2.00
EO	ALL	-0.46	1.00
	F-M	-0.29	1.00
	PF-M	-0.66	2.00
EX	ALL	3.91	3.00
	F-M	2.12	3.00
	PF-M	-0.10	3.00

Table J23: For the beta band for each level of each factor in Test 4 (condition, areas), the mean and standard error of the differentiated phase synchronization coefficients. The three conditions are represented by EC (eyes-closed), EO (eyes-open) and EX (exercise-until-fatigue), and the three areas are represented by ALL (ALL pairs), F-M (frontal-motor pairs) and PF-M (prefrontal-motor pairs). The values are plotted in the graph below.

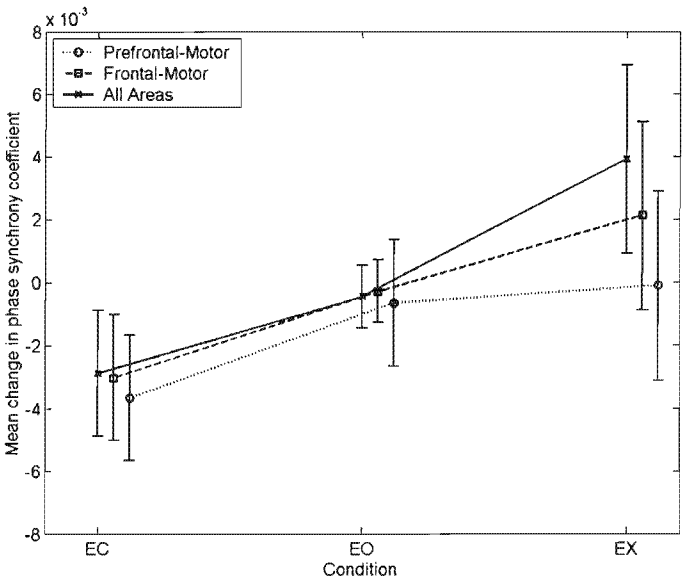

Figure J21: For the beta band for each level of each factor in Test 4 (condition, areas), plot of the means of the differentiated phase synchronization coefficients. The y-axis represents the differentiated phase synchronization coefficients and x-axis represents the conditions where EC stands for eyes-closed, EO stands for eyes-open and EX stands for exercise-until-fatigue. There are three plots, one for each area identified on the legend. The markers representing the means of a particular condition and area are shifted on the x-axis for readability. The error bar represents the standard deviation from the mean.

a

Area	Epoch Change	Mean (10^{-3})	Standard Error (10^{-3})
ALL	1	-9.78	7.00
	2	1.78	5.00
	3	-1.23	5.00
	4	-2.31	2.00
	5	-2.85	6.00
F-M	1	-10.60	8.00
	2	2.44	6.00
	3	-2.44	6.00
	4	-0.06	4.00
	5	-4.42	5.00
PF-M	1	-16.20	12.00
	2	6.25	8.00
	3	-3.06	9.00
	4	-3.98	6.00
	5	-1.37	7.00

b

Area	Epoch Change	Mean (10^{-3})	Standard Error (10^{-3})
ALL	1	-2.07	3.00
	2	-0.63	2.00
	3	6.91	6.00
	4	-3.12	4.00
	5	-3.37	4.00
F-M	1	-0.43	3.00
	2	-0.82	4.00
	3	6.21	6.00
	4	-0.85	4.00
	5	-5.54	6.00
PF-M	1	2.07	5.00
	2	-4.10	6.00
	3	9.32	9.00
	4	-1.78	5.00
	5	-8.79	8.00

c

Area	Epoch Change	Mean (10^{-3})	Standard Error (10^{-3})
ALL	1	-5.60	8.00
	2	2.63	6.00
	3	5.40	5.00
	4	10.70	7.00
	5	6.48	5.00
F-M	1	-9.53	7.00
	2	2.51	6.00
	3	5.17	6.00
	4	11.80	7.00
	5	0.68	5.00
PF-M	1	-12.60	9.00
	2	4.13	8.00
	3	3.33	8.00
	4	10.60	7.00
	5	-5.95	7.00

Table J24: For the beta band, for the eyes-closed condition (a) the eyes-open condition (b) and the exercise-until-fatigue condition (c), for each epoch transition (1-5), for the 3 areas of the areas factor in Test 4 (condition, areas), the mean and standard error of the differentiated phase synchronization coefficients. The three areas are represented by ALL (ALL pairs), F-M (frontal-motor pairs) and PF-M (prefrontal-motor pairs). The epoch transitions are represented by the numbers 1-5. The values are plotted in the graphs below.

a

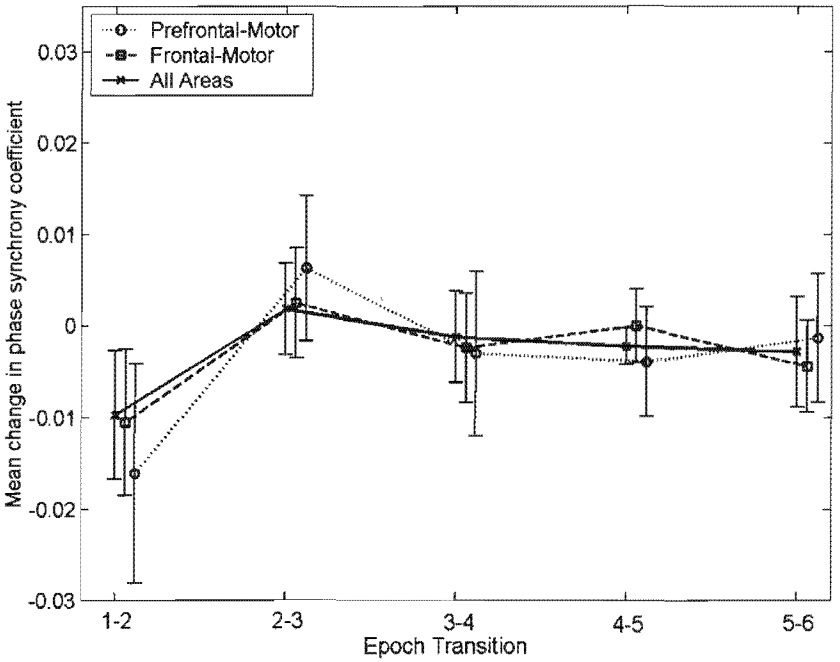
Prefrontal-Motor
Frontal-Motor
All Areas
Mean change in phase synchrony coefficient
0.03
0.02
0.01
0
-0.01
-0.02
-0.03
1-2
2-3
3-4
4-5
5-6
Epoch Transition

b

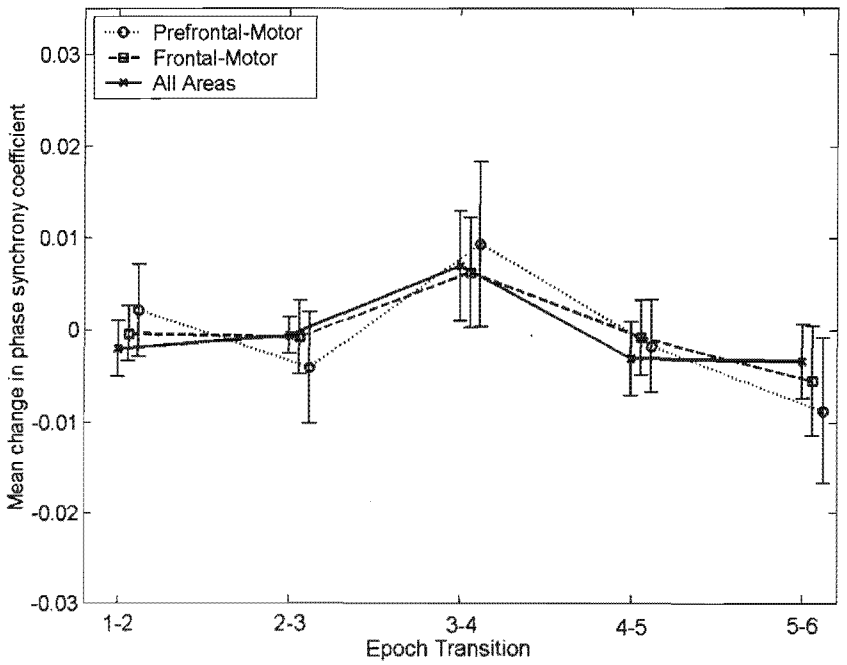
Prefrontal-Motor
Frontal-Motor
All Areas
Mean change in phase synchrony coefficient
0.03
0.02
0.01
0
-0.01
-0.02
-0.03
1-2
2-3
3-4
4-5
5-6
Epoch Transition

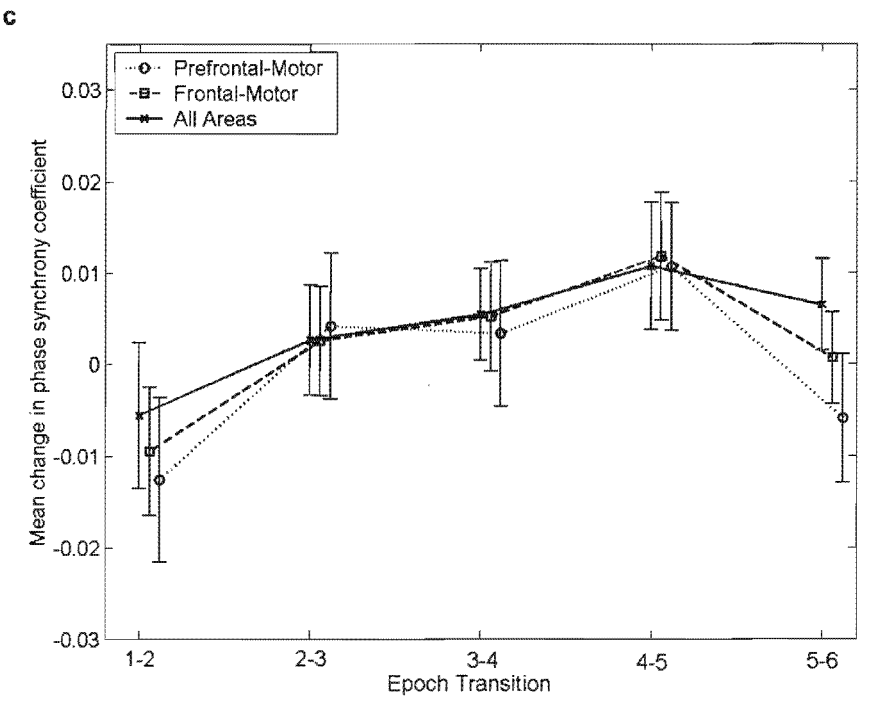

Figure J22: For the beta band, for the eyes-closed condition (a) the eyes-open condition (b) and the exercise-until-fatigue condition (c), for each epoch transition (1-5), for the 3 areas of the areas factor in Test 4 (condition, areas), the mean and standard error of the differentiated phase synchronization coefficients. The y-axis represents the differentiated phase synchronization coefficient and the x-axis represents epoch transitions. There are three plots on each graph (a) – (c), one for each area identified on the legend. The markers representing the means of a particular condition and area are shifted on the x-axis for readability. The error bar represents the standard deviation from the mean.

J2.8 Gamma Band ANOVA Test 3 (Condition, Time) and Test 4 (Condition, Areas) Results

Factor	Epsilon Correction	F Statistic	P Value
Condition	Greenhouse-Geisser	3.013	0.104
Time	Greenhouse-Geisser	.626	0.557
Condition * Time (Interaction)	Greenhouse-Geisser	.694	0.548

Table J25: For the gamma band, the output of ANOVA Test 3 (condition, time).

Factor	Epsilon Correction	F Statistic	P Value
Condition	Greenhouse-Geisser	3.013	0.104
Areas	Greenhouse-Geisser	.787	0.449
Condition * Areas (Interaction)	Greenhouse-Geisser	1.042	0.392

Table J26: For the gamma band, the output of ANOVA Test 4 (condition, areas).

Condition	Area	Mean (10^{-3})	Standard Error (10^{-3})
EC	ALL	-2.60	2.00
	F-M	-3.57	2.00
	PF-M	-3.08	2.00
EO	ALL	-0.52	1.00
	F-M	-0.11	1.00
	PF-M	0.28	1.00
EX	ALL	4.55	3.00
	F-M	4.60	3.00
	PF-M	4.79	3.00

Table J27: For the gamma band for each level of each factor in Test 4 (condition, areas), the mean and standard error of the differentiated phase synchronization coefficients. The three conditions are represented by EC (eyes-closed), EO (eyes-open) and EX (exercise-until-fatigue), and the three areas are represented by ALL (ALL pairs), F-M (frontal-motor pairs) and PF-M (prefrontal-motor pairs). The values are plotted in the graph below.

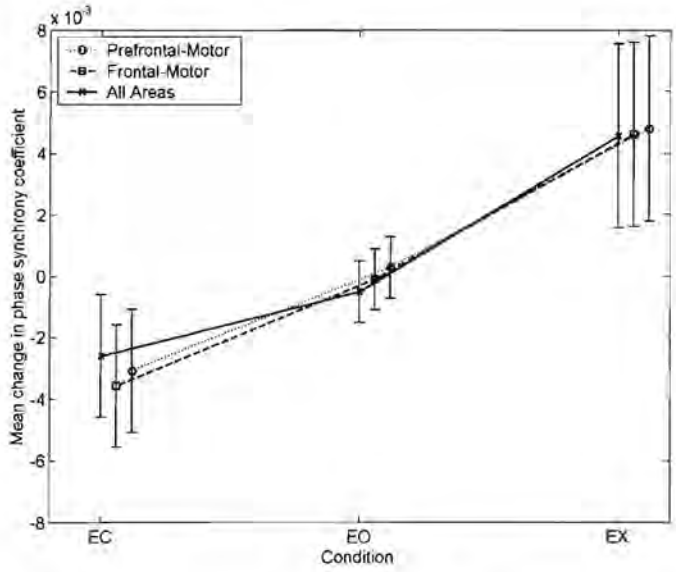

Figure J23: For the gamma band for each level of each factor in Test 4 (condition, areas), plot of the means of the differentiated phase synchronization coefficients. The y-axis represents the differentiated phase synchronization coefficients and x-axis represents the conditions where EC stands for eyes-closed, EO stands for eyes-open and EX stands for exercise-until-fatigue. There are three plots, one for each area identified on the legend. The markers representing the means of a particular condition and area are shifted on the x-axis for readability. The error bar represents the standard deviation from the mean.

a

Area	Epoch Change	Mean (10^{-3})	Standard Error (10^{-3})
ALL	1	-9.69	8.00
	2	1.06	5.00
	3	-3.41	5.00
	4	-0.76	2.00
	5	-0.19	6.00
F-M	1	-12.30	9.00
	2	3.18	4.00
	3	-4.34	5.00
	4	-1.83	3.00
	5	-2.59	7.00
PF-M	1	-9.58	10.00
	2	0.05	4.00
	3	-1.25	4.00
	4	0.08	4.00
	5	-4.69	8.00

b

Area	Epoch Change	Mean (10^{-3})	Standard Error (10^{-3})
ALL	1	-1.60	3.00
	2	-1.03	3.00
	3	6.62	6.00
	4	-4.04	4.00
	5	-2.52	4.00
F-M	1	-0.39	4.00
	2	-1.42	3.00
	3	3.73	5.00
	4	-2.83	4.00
	5	0.37	4.00
PF-M	1	4.29	3.00
	2	-5.07	3.00
	3	9.05	6.00
	4	-8.50	5.00
	5	1.63	3.00

c

Area	Epoch Change	Mean (10^{-3})	Standard Error (10^{-3})
ALL	1	-2.42	8.00
	2	1.33	5.00
	3	4.34	4.00
	4	11.20	8.00
	5	8.28	6.00
F-M	1	-2.35	9.00
	2	1.12	6.00
	3	7.05	5.00
	4	11.80	8.00
	5	5.37	6.00
PF-M	1	-2.74	11.0
	2	1.99	6.00
	3	4.61	4.00
	4	14.50	10.0
	5	5.60	7.00

Table J28: For the gamma band, for the eyes-closed condition (a) the eyes-open condition (b) and the exercise-until-fatigue condition (c), for each epoch transition (1-5), for the 3 areas of the areas factor in Test 4 (condition, areas), the mean and standard error of the differentiated phase synchronization coefficients. The three areas are represented by ALL (ALL pairs), F-M (frontal-motor pairs) and PF-M (prefrontal-motor pairs). The epoch transitions are represented by the numbers 1-5. The values are plotted in the graphs below.

a

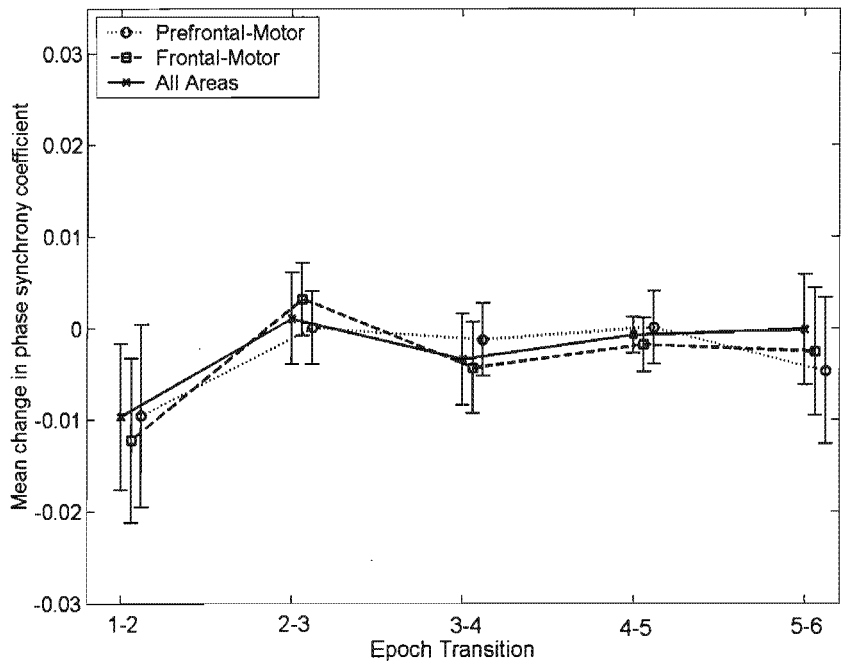
Prefrontal-Motor
Frontal-Motor
All Areas
Mean change in phase synchrony coefficient
0.03
0.02
0.01
0
-0.01
-0.02
-0.03
1-2
2-3
3-4
4-5
5-6
Epoch Transition

b

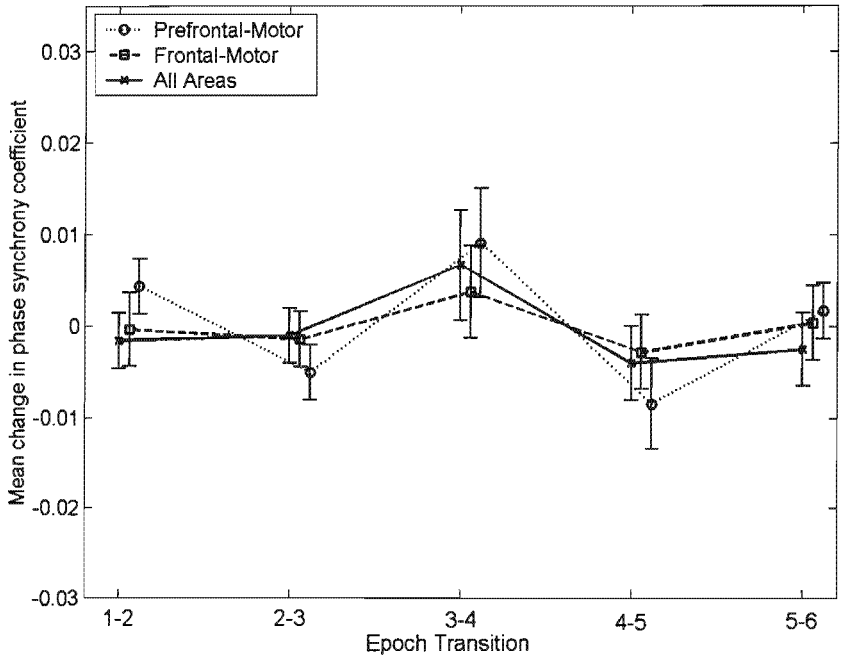
Prefrontal-Motor
Frontal-Motor
All Areas
Mean change in phase synchrony coefficient
0.03
0.02
0.01
0
-0.01
-0.02
-0.03
1-2
2-3
3-4
4-5
5-6
Epoch Transition

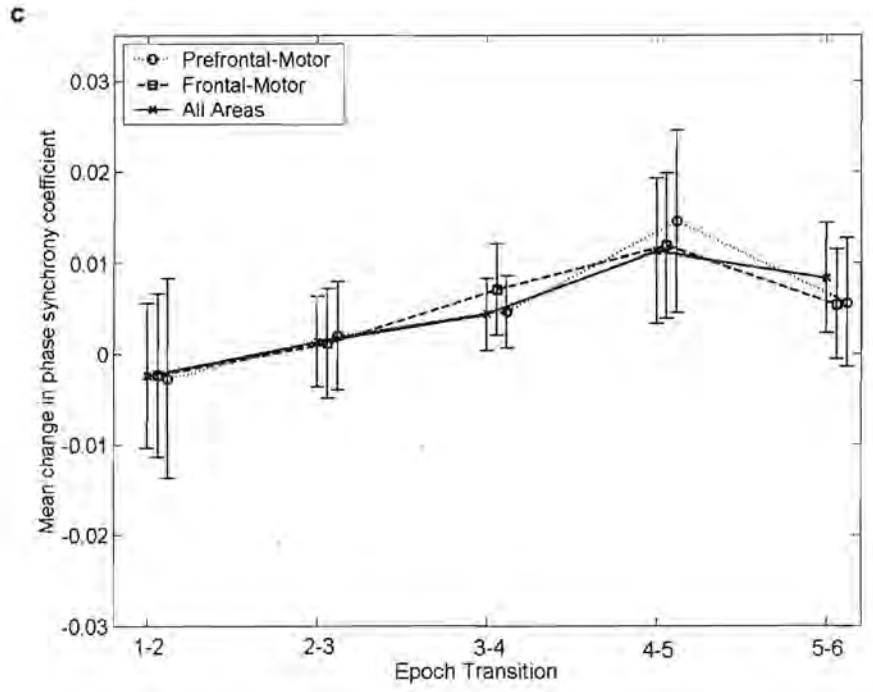

Figure J24: For the gamma band, for the eyes-closed condition (a) the eyes-open condition (b) and the exercise-until-fatigue condition (c), for each epoch transition (1-5), for the 3 areas of the areas factor in Test 4 (condition, areas), the mean and standard error of the differentiated phase synchronization coefficients. The y-axis represents the differentiated phase synchronization coefficient and the x-axis represents epoch transitions. There are three plots on each graph (a) – (c), one for each area identified on the legend. The markers representing the means of a particular condition and area are shifted on the x-axis for readability. The error bar represents the standard deviation from the mean.

Appendix K Generation of Surrogate Data

The EMSE software suite [123] was used to generate surrogate EEG data for this investigation. Surrogate EEG data is used to replace actual EEG recordings for purposes of a specific analysis, such as simulating experimental randomness or testing an EEG processing technique with controlled and well-defined data [21][76]. In this investigation it was used to test the phase synchronization quantification method on randomly generated data, between randomly selected epochs. The expected value of phase synchronization is low, with a small variance, which indeed was the case.

The surrogate data was generated using EMSE. EMSE generated EEG data by placing 32 dipoles current sources (as discussed in *The Generation of Voltages on the Scalp* in Section 3.1.1) within a 3-sphere head model, with parameters set to emulate how the dipole current sources propagate through the brain, surrounding tissues and skull, to the surface of the scalp. The dipoles were set to generate psuedo-random currents, thus essentially producing voltages that are EEG-like, but which have completely psuedo-random origins.

Appendix L Phase Synchronization Coefficient and Data Window Length Simulation

Introduction

The selection of the window length in this investigation was somewhat arbitrary and based primarily on criteria of ease of presentation and the assumption of stationarity of up to 10s. Furthermore, window lengths varied between subjects and conditions. In order to establish how window length affects the calculation of the phase synchronization coefficients, phase synchronization coefficients were calculated for windows of various lengths on the output of the Rossler system that was used to verify the phase synchronization coefficients in Section 5.2.2 (refer to this section for a description of the system). The system parameter C was varied such that 3 distinct cases were produced; no synchronization (case 1), near synchronization (case 2) and synchronization (case 3). The outputs of the coupled systems for each case 1 to 3 was analysed and the phase synchronization coefficient $\tilde{\rho}$ was calculated for window lengths that varied from 100 sample points to 20000 sample points, which was the length of the system output for each case. If the samples represent a signal sampled at 200Hz (the EEG recordings in this investigation were sampled at 200Hz) then the window lengths would vary between 0.5s and 200s. In this investigation the lengths of the windows varied between 2.2s to 6.14s, and after considering the additional averaging that was performed (reducing 50 epochs to 6 epochs) the maximum window length is about 10 times the largest resulting in a window length of 61.4s. Thus this simulation covers all the window lengths of interest.

The question is, how sensitive is $\tilde{\rho}$ to window length and does it make sense to first calculate $\tilde{\rho}$ on smaller window lengths before averaging to epochs of greater length, or should one simply calculate $\tilde{\rho}$ directly on epochs that are longer.

The results of the simulation are presented in Figure L1 and Figure L2 below.

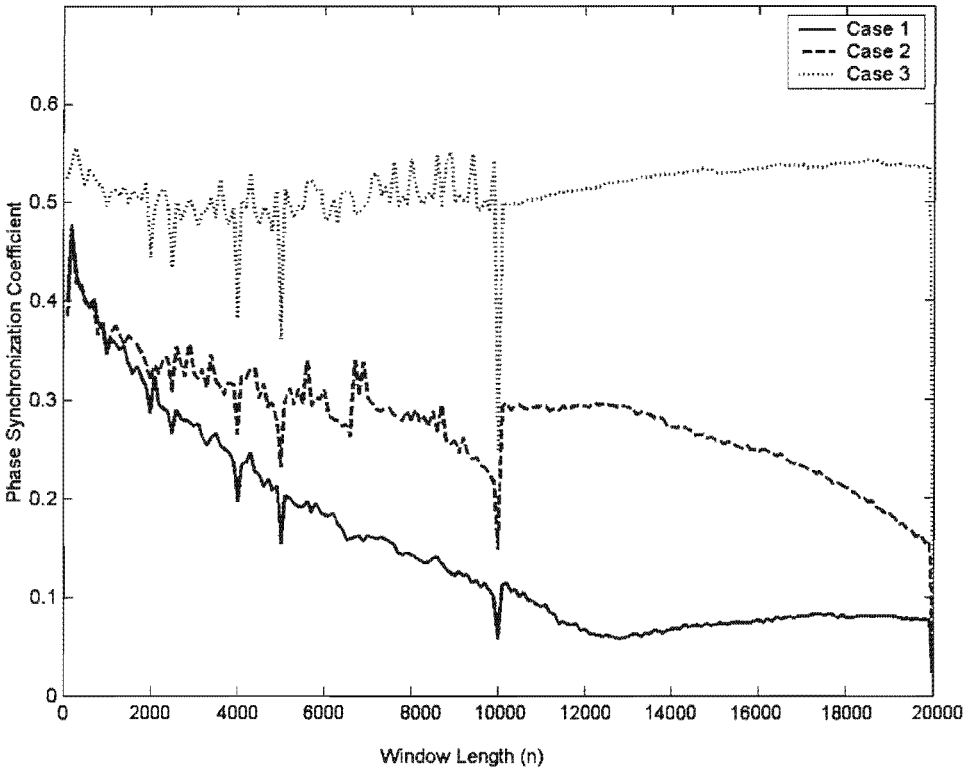

Figure L1: Mean Phase Synchronization Coefficient versus window length, for case 1 (no synchronization), case 2 (near synchronization) and case 3 (synchronization).

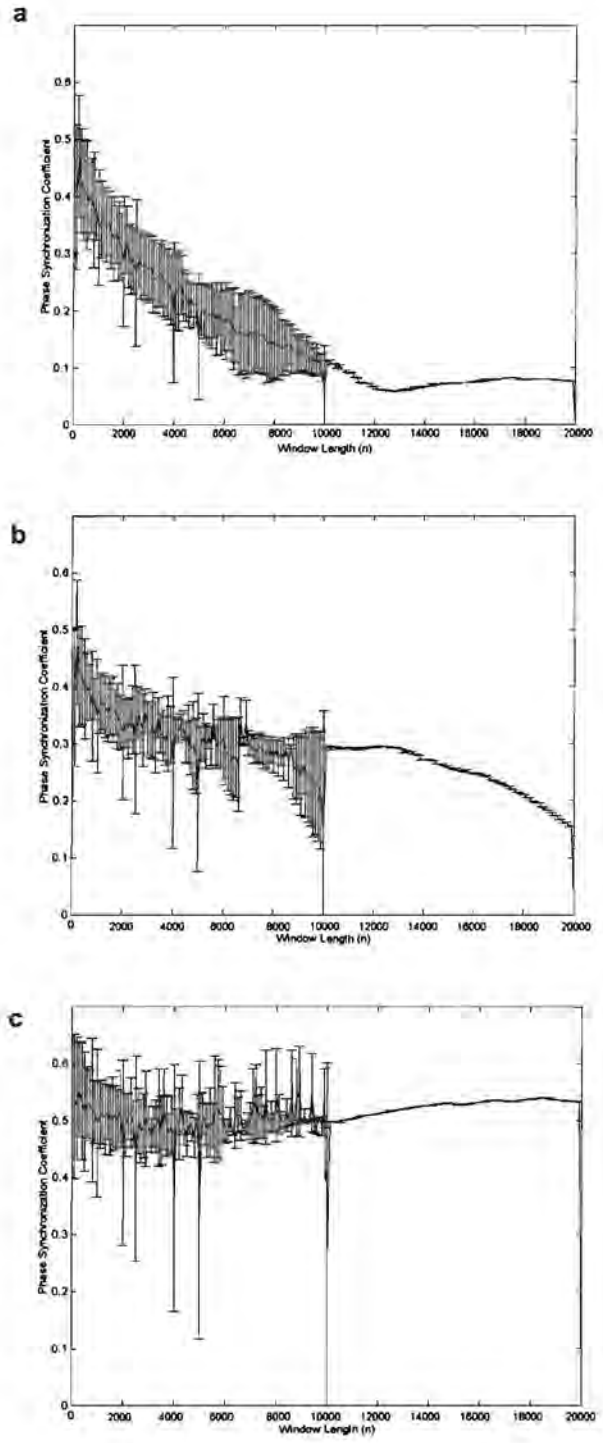

Figure L2: Mean and standard error of the Phase Synchronization Coefficient versus window length, (a) for case 1 (no synchronization), (b) case 2 (near synchronization) and (c) case 3 (synchronization).

Discussion

Figure L1 shows the mean value of $\tilde{\rho}$ for each case 1 to 3, for different window lengths. Of course, the number of individual $\tilde{\rho}$ values comprising the mean $\tilde{\rho}$ will vary depending on window length; the smaller the window length the larger the number of $\tilde{\rho}$. It can be seen that the mean $\tilde{\rho}$ does not change consistently with increasing window size across all 3 cases. In case 3 (synchronization) the value of the mean $\tilde{\rho}$ tends to remain constant, regardless of window length. As synchronization decreases (case 2 and 1 respectively), the mean $\tilde{\rho}$ increases with decreasing window size. In fact, the case 1 and 2 become indistinguishable at small window lengths.

Figure L2 represents the same data, except the means are plotted on separate graphs and the standard error is shown. This figure shows clearly how the variation of the $\tilde{\rho}$ values does not depend on window length and the variance itself displays great variance between different window lengths.

There is of course no variance after the maximum window length is reached, which is half the total data length (10000 in this case), but it is interesting to note that the single value of $\tilde{\rho}$ remains fairly constant as that single window length increases, and the 3 cases are clearly distinguishable from each other as seen in Figure L1 after window length 10000.

Since this investigation uses epochs that are fractions of the total lengths, it is interesting to note that at 1/50 of the total length represents a point close to the origin, and at 1/6 (the length of the longest window in this investigation), a point that is still highly variable, but which distinguishes the 3 cases better.

Conclusions

This simple experiment shows that smaller time windows used for calculating $\tilde{\rho}$ produce $\tilde{\rho}$ values that are larger than would be the case if larger time windows were used, and that this may blur the distinction between different levels of synchronization. More importantly it also shows that $\tilde{\rho}$ is highly variable at all window lengths. The difference between a window length of 1/10 and 1/50 may not be significant at first glance, but based on the variability of $\tilde{\rho}$, more sophisticated methods need to be devised to calculate window length.